Growth dynamics of braided gravel-bed river deltas in New Zealand

_____

A thesis
submitted in partial fulfilment
of the requirements for the Degree of
Doctor of Philosophy in Civil and Natural Resources Engineering

at

University of Canterbury

by

Michelle Anne Wild

_____

University of Canterbury
New Zealand

2013

ABSTRACT

Abstract of a thesis submitted in partial fulfilment of the
requirements for the Degree of Doctor of Philosophy

Growth dynamics of braided gravel-bed river deltas in New Zealand

by Michelle Anne Wild

This research has been undertaken to further our knowledge of decade-to-century timescale braided, gravel-bed river delta growth dynamics. The study included: a review of available literature; field studies; the development of microscale models for two study deltas; and the development of a simple numerical model incorporating movement of braided river channels across a delta topset (varying the location of sediment delivery to the delta).

Results from the microscale modelling showed that successful physical modelling requires well-defined fixed boundaries and, ideally, good historical aerial photography for the estimation of the model time scale. A complex braided gravel-bed river delta system composed of two merging deltas entering a deep, low-energy receiving basins was able to be successfully modelled to provide valuable information on delta growth dynamics. However, a microscale model of a delta prograding into shallow receiving basins, with a large supply of fine sediment, was more difficult to calibrate and assess (partly due to limited field data), and was considered less reliable.

The simple rule-based numerical model 'DELGROW', developed to simulate a braided river system entering a deep, low-energy body of water, requires a known sediment supply rate, as well as information on the braided river topography, submerged delta foreset, and lakebed bathymetry. Unlike simple 1-d width-averaged geometric models, DELGROW takes into consideration barriers (e.g. islands) as well as relatively complex converging braided river delta configurations. By changing the sediment supply, or modifying the river system, the response of the river system to various scenarios can also be assessed.

Microscale models and DELGROW appear to realistically simulate decade-to-century timescale growth of braided gravel-bed river deltas entering a deep, low-energy, receiving basin. Both of these modelling methods initially use the supplied sediment to try and eliminate any riverbed irregularities (e.g. low areas), before continuing to advance and deposit sediment in a more evenly-distributed manner, whilst taking into consideration irregularities due to barriers, and asymmetric sediment sources such as merging deltas. Neither model can reliably predict locations of bank erosion, or channel avulsions that divert flow and sediment outside of the fixed model boundaries.

Keywords: River delta, Braided river, Microscale model, Numerical model, Physical model

CO-AUTHORSHIP FORMS

Form 1

Please indicate the chapter/section/pages of this thesis that are extracted from co-authored work and provide details of the publication or submission from which the extract comes:

Chapter 3 (Section 3.2.5.3) includes text and figures also published in:

Wild, M., Cochrane, T., Davies, T. R., Hicks, D. M., Painter, D., & Palmer, G. (2008). Recent sedimentation rates for the Rees-Dart braided river delta. In J. Schmidt, T. Cochrane, C. Phillips, S. Elliot, T. R. Davies & L. Basher (Eds.), *Sediment Dynamics in Changing Environments* (IAHS Red Books Publ. 325 ed., pp. 312-315): Wallingford : IAHS Press, c2008.

Please detail the nature and extent (%) of contribution by the PhD candidate:

PhD candidate completed all data analyses and produced both draft and final reports (with technical guidance and recommendations from co-authors).

Please list the co-authors and the nature and extent of the contribution by each below:

Name:	*Dr Tom Cochrane*	Contribution:	*Technical guidance and review of draft paper*
Name:	*Dr Tim Davies*	Contribution:	*Technical guidance and review of draft paper*
Name:	*Dr Murray Hicks*	Contribution:	*Technical guidance and review of draft paper*
Name:	*Dr David Painter*	Contribution:	*Technical guidance and review of draft paper*
Name:	*Dr Gavin Palmer*	Contribution:	*Technical guidance and review of draft paper*

Certification by Co-authors:

The undersigned certify that:

- The above statement correctly reflects the nature and extent of the PhD candidate's contribution to this work and the nature and contribution of each of the co-authors
- In cases where the PhD candidate was the lead author of the co-authored work he or she wrote the text

Name:	*Dr Tom Cochrane*	Signature:		Date:	31 October 2012
Name:	*Dr Tim Davies*	Signature:		Date:	31 October 2012
Name:	*Dr Murray Hicks*	Signature:		Date:	31 October 2012
Name:	*Dr David Painter*	Signature:		Date:	31 October 2012
Name:	*Dr Gavin Palmer*	Signature:		Date:	31 October 2012

ACKNOWLEDGEMENTS

When I left my job to begin my postgraduate studies a work colleague said to me "Remember … it's a marathon not a sprint". Little did I realise how much of a marathon it would be, and how many people would become a part of it! As such there are many people I would like to gratefully acknowledge for their assistance, expertise and encouragement.

Firstly I would like to thank my supervisory committee of Dr Tom Cochrane (University of Canterbury), Dr Tim Davies (University of Canterbury), Dr Murray Hicks (National Institute of Water and Atmospheric Research Ltd, NIWA), Dr David Painter (DP Consulting Ltd) and Dr Gavin Palmer (Otago Regional Council) for collectively providing a large and complementary breadth of expertise during my studies. In particular, Dr Tom Cochrane who was always available to point me in the right direction - without applying too much pressure! The experimental component of my work required the additional expertise of Alan Stokes, Ian Sheppard and Kevin Wines in the Civil and Natural Resources Engineering (CNRE) Fluids Laboratory; CNRE students Luke van Bussel, John Langtry and Peter Cockrem also assisted with various aspects of the design, construction and initial operation of the microscale models. Both Alan Stokes and Ian Sheppard also went above and beyond the call of duty when given the task of constructing a microscale model in my garage at home, and Alan Stokes became my own personal 'MacGyver' with his solutions to the various problems (and earthquake repairs) required along the way. Without Alan's persistence and mindset to just 'get on with it' I would no doubt be still pottering along in the lab! Financial assistance for this study has been provided by an Otago Regional Council (ORC) studentship (including funding for laboratory experiments, data collection and field excursions) as well as the University of Canterbury (Department of CNRE and the University of Canterbury Summer Scholarships Scheme); Lincoln University also provided a sediment feeder and the sediment for the modelling. Hydrometric data for this project has been provided by ORC, NIWA, Contact Energy, Queenstown Lakes District Council (QLDC), M-co, Met Service, and the ReesScan Project. Many people within these organisations have also provided other valuable information including Mike Goldsmith, Richard Woods, Andrew Mackay, Kirsty Morris, Julie Allen, Pete Stevenson (all ORC), Kathy Walter (NIWA), Phil Barnes (NIWA) and Peter Silvester (Contact Energy). Sounding data collected by the ORC field team of Mike Anderson, Duncan Stewart, Peter Preston and Jeff Donaldson was also very valuable and much appreciated.

Finally, I would like to thank my family, friends and past and present work colleagues for their encouragement and welcome distractions from my studies. In particular my husband, Chris, for making the many sacrifices that have allowed me to return to my studies; my mother, Margaret, who also made it possible by committing to many years of childcare; and to Alex and Emily who always helped me keep it in perspective that there was much more to life than my laptop and the sandpit in the garage!

TABLE OF CONTENTS

LIST OF FIGURES

LIST OF TABLES

1 INTRODUCTION

In New Zealand there are many braided gravel-bed river systems. These river systems usually have an abundant supply of sediment generated by geologically-driven processes that cannot be reliably modified long-term (Davies & McSaveney, 2006). Where these braided gravel-bed rivers discharge into other rivers or lakes, inland braided gravel-bed river deltas can form. As these deltas prograde, the receiving basin (e.g. hydroelectric lake) is progressively infilled, and the delta topset aggrades to maintain the upstream river bed slope – causing aggradation to retrogress up the river.

Despite considerable research effort to better understand the processes occurring in deltas (e.g. Komar, 1973; Wright, 1977; Kostaschuk, 1985; Syvitski et al., 1988; Sohn et al., 1997; Swenson et al., 2000; Syvitski & Hutton, 2001; Sun et al., 2002; Kostic & Parker, 2003a, 2003b; Kleinhans, 2005a, 2005b; Swenson et al., 2005; Kim et al., 2006; Lai & Capart, 2007; Edmonds, 2009; Seybold et al., 2009; Reitz et al., 2010; Tomer et al., 2011; van Dijk et al., 2012), the temporal and spatial development of braided river deltas over the decade-to-century timescale is still not fully understood - largely due to the dynamic complexity of the braided river systems delivering the sediment to the delta.

Less emphasis has been placed on quantitatively simulating the growth processes that occur within active braided gravel-bed river delta systems over the decade-to-century timescale. This timescale is particularly difficult to simulate due to the relationship between the fluvial hydrodynamic processes of sediment deposition, generally studied at short time scales, and the resulting depositional characteristics of the prograding delta, generally studied on a medium to long time scale (e.g. Syvitski et al., 1988). Although some studies (e.g. Axelsson, 1967; van Maren, 2004) have combined both of these time scales, the majority appear to have focussed on one or the other. There is also limited knowledge of some processes occurring within these braided river and delta systems, including floodplain depositional behaviour (Fagherazzi & Overeem, 2007) and the impact of backwater effects on avulsion (Hajek & Wolinsky, 2011). Our scientific knowledge of the depositional behaviour of deltas formed by braided gravel-bed rivers is therefore far from complete.

In most cases this gap in knowledge of the growth dynamics of braided gravel-bed river deltas is of little concern. This is mainly because these deltas tend to form in rugged, remote, and relatively inaccessible areas. However, in the Otago region of New Zealand, information on the long term growth rate of these deltas is becoming increasingly important as it informs decisions on infrastructure development, land use, and hazard management in their vicinity.

The main methods currently able to be utilised to improve our understanding of the growth behaviour of braided gravel-bed river deltas are summarised below:

- small temporal and spatial scales

- modern field studies (i.e. measurements and observations of processes currently occurring)
- physical hydraulic models
- high-resolution process-based numerical models

- large temporal and spatial scales
  - ancient field studies (e.g. analysis of ancient delta deposits using exposed outcrops or core samples)
  - microscale models (i.e. very small scale physical movable bed models)
  - reduced-complexity and geometric numerical models

Intermediate temporal and spatial scales (e.g. time scale ~10^1 to 10^4 years) are difficult to study using many of the methods outlined. For example, there are physical scale limitations for hydraulic models, temporal scale limitations for field studies, and computational limitations for numerical models as both temporal and spatial scales increase.

Fortunately, even with limited field data, many physical modelling studies (including microscale modelling studies) have demonstrated that they are a valuable, and very capable, tool for simulating many aspects of braided gravel-bed river and delta dynamics over the intermediate temporal and spatial time scales. For instance Sheets (2002, p. 300) states that "despite scale differences, many of the basic mechanisms that fill sedimentary basins are present in experimental and natural environments". Microscale models are therefore able to provide an additional, often spatially and temporally continuous, source of data able to be used to develop and validate numerical models.

However, despite microscale models being used successfully to study many aspects of braided gravel-bed rivers, alluvial fans, fan deltas and, river deltas, there are no documented studies where:

- A braided gravel-bed river delta has been formed by the complex behaviour of two merging braided gravel-bed rivers. Unlike braided rivers, alluvial fans and some fan deltas (i.e. where delta deposition is more difficult to observe), the areal extent of sediment accumulating at a braided gravel-bed river delta can be relatively easily identified and quantified using geo-referenced aerial photography (e.g. Pelpola & Hickin, 2004; Wild et al., 2008); this information also has the potential to be used to assign a model reference time.

- A new delta has formed by, for example, the development of a hydro lake formed by drowning an existing braided river channel.

There also appear to be very few studies that have attempted to predict how braided gravel-bed river delta growth dynamics would be modified should engineering works change a delta configuration (Davies, 2007) or a seismic event generate a significant increase in sediment supply.

1.1 Thesis objectives

The main objective of this thesis is *to use information derived from field studies, quantitative microscale models, and a simple numerical model to advance our understanding of the dynamic processes involved in braided gravel-bed river delta growth over the decade-to-century timescale*.

An itemised summary of the research objectives and methodology for this thesis is given below.

1. **Use existing information to understand historic growth of braided gravel-bed river deltas.**

   This will be achieved by examining existing scientific literature, as well as analysing two braided gravel-bed river deltas (in the Otago region of New Zealand). The analysis of the two study deltas will include:

   a. Examination of recent delta growth using all available literature (e.g. flood and sedimentation study reports, cross section surveys, etc.) as well as GIS analysis of historic aerial photographs and bathymetric data.

   b. Identification of sediment sources and sinks (e.g. significant periods of gravel extraction) as well as the nature of sediment input to the river systems (e.g. local bank erosion, debris flows in upper catchment).

   c. Examination of the river system flow characteristics and the processes occurring in the delta receiving basin – in particular, during flood events when sediment is being fed into the delta system.

2. **Assess the feasibility of microscale models as a tool to examine historic and future braided gravel-bed river delta growth over the decade-to-century timescale.**

   This will be tested through:

   a. Construction of microscale models of the Rees-Dart and Clutha River/Mata-Au delta systems.

   b. Evaluation of the extent to which the Rees-Dart and Clutha River/Mata-Au microscale models are capable of simulating observed historic delta growth patterns.

   c. Prediction of future delta growth over the decade-to-century timescale.

d. A brief assessment of potential engineering solutions to modify the location of delta progradation (i.e. modifications to the upstream river system), as well as sensitivity of the river-delta system to increased sediment supply.

e. Identification of problems, limitations and potential further improvements for microscale modelling of braided gravel-bed river deltas.

3. **Develop a simple geometric numerical model to predict the growth of braided gravel-bed river deltas prograding into a low-energy basin over the decade-to-century timescale.**

   The development of this numerical model requires:

   a. Design and construction of a simple rule-based numerical model that simulates braided river delta progradation. The model should incorporate channel avulsion/switching to allow sediment delivery to the delta topset and foreset to vary laterally over time (i.e. not a 1-d width-averaged model).

   b. Validation of the model using the Rees-Dart delta.

   c. Identification of problems, limitations and potential futher improvements to the numerical model.

1.2 Thesis outline

To better understand the growth processes of braided gravel-bed river deltas, this thesis combines current knowledge of braided gravel-bed rivers and deltas (Chapter 2) with field studies (Chapter 3), microscale modelling (Chapter 4), and numerical modelling (Chapter 5).

In Chapter 3, two braided gravel-bed river deltas in the Otago Region of New Zealand are described including catchment, river and receiving basin features and delta growth processes; information was also derived for historic delta shoreline advance and sedimentation rates. Microscale models of both deltas used to simulate historic and future braided gravel-bed river delta growth over the decade-to-century timescale are described in Chapter 4. Based on the information gathered in Chapters 2 to 4, a relatively simple numerical model was developed to simulate braided gravel-bed river delta growth (including lateral delta growth due to braided river channel variability) over the decade-to-century timescale (Chapter 5). Conclusions and recommendations from the study are summarised in Chapter 6.

2 LITERATURE REVIEW

Over the past century there has been a growing research interest in deltas. This research is summarised below and includes: an introduction to braided gravel-bed rivers and deltas (Section 2.1), historic research trends (Section 2.2), field studies (Section 2.3), physical modelling (Section 2.4), and numerical modelling (Section 2.5). The emphasis of this review is on research related to braided gravel-bed river deltas. Descriptions of recent technological advances, and information on how this new technology is being applied to braided gravel-bed rivers and deltas, are also included.

2.1 Introduction to braided gravel-bed rivers and deltas

A river delta is an accumulation of sediment that forms where a river enters a downstream body of water that is not capable of transporting all of the supplied sediment further afield (e.g. a lake, ocean or river). This means that a river delta will only form and prograde when sediment is supplied to the water body more rapidly than the rate at which it is eroded by the receiving basin processes such as tides, currents and waves (e.g. Coleman, 1976, 1988).

For a delta of any significance to be produced, Coleman (1976) identified that a river system required:

- a large volume of available sediment,
- a high precipitation over the catchment (aiding erosion and transportation of sediment into the river system),
- a catchment capable of generating high river discharges (involving factors such as catchment climate, geology, topography and size).

A river-delta system can be divided into four parts as shown in Figure 2.1. In general, a drainage basin with a plentiful supply of sediment feeds sediment into an alluvial valley. Sediment is then transported along the valley until it is eventually dispersed and deposited on a deltaic plain prograding into a receiving basin (e.g. lake, river or ocean).

Deltas were originally characterised by alluvial and basinal process/response models, resulting in a classification as either a fluvial-, wave- or tide-dominated delta (Galloway, 1975). It was later noted (e.g. Syvitski & Farrow, 1983) that in some cases similar alluvial and basinal conditions did not produce similar delta characteristics so, over time, this relatively simple triangular classification was modified to incorporate other factors. These included the influence of sediment grain size (Orton & Reading, 1993) and the basinal water depth (Postma, 1990). The present study focuses on the growth of braided gravel-bed river deltas formed where the rivers enter non-tidal, freshwater lakes; fluvial processes are dominant rather than wave or tidal influences.

Both braided gravel-bed rivers and deltas are described below (Sections 2.1.1 and 2.1.2, respectively) since the growth dynamics of a braided gravel-bed river delta are dependent on the characteristics of the river system that is supplying the sediment to the delta (i.e. the fluvial processes of the river system determine where deposition will occur within the delta system). Therefore, understanding the complex processes occurring within the braided river system, and consequently the behaviour of the braided river as it interacts with the delta region and receiving body of water, is vital.

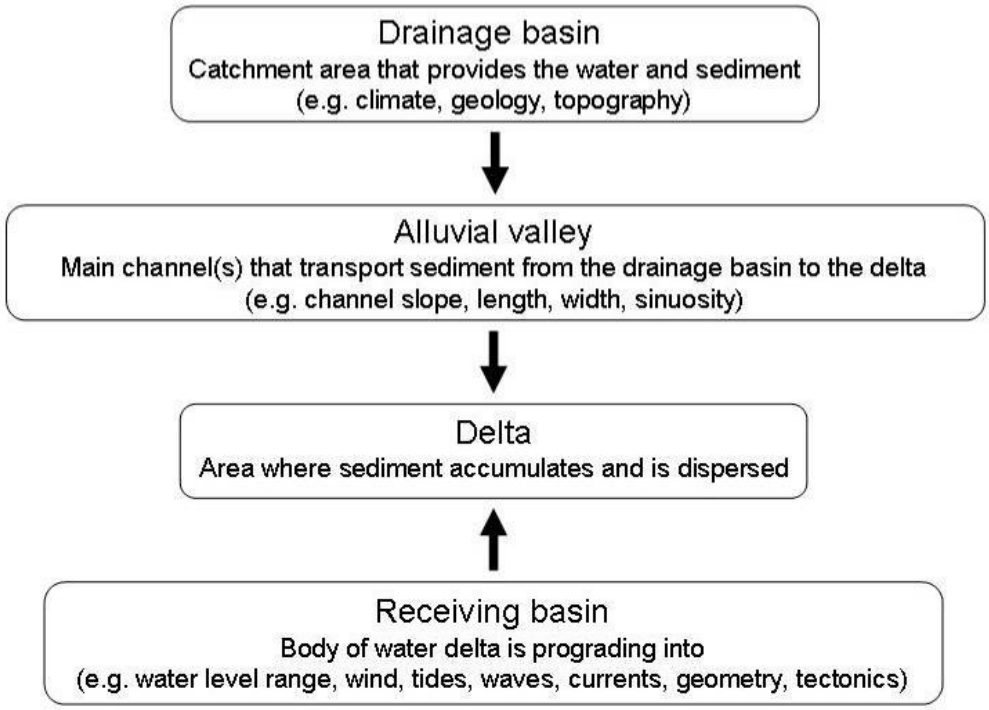

Figure 2.1: Components of a river system that interact to produce a delta (derived from Coleman (1976))

2.1.1 Braided gravel-bed rivers

A braided gravel-bed river generally has a high bedload transport rate and a highly variable discharge, and produces a dynamic and complex river system of continually changing geometry (Coleman & Wright, 1975). The individual river channels frequently alter course by the erosion of highly erodible river banks and channel sedimentation (Parker, 1979; Ferguson, 1987; Ashmore, 1991a). This leads to partial (or full) channel avulsions which divide the flow and produce the anastomosing channel formation characteristic of braided river systems (Bolla Pittaluga et al., 2003; Bertoldi et al., 2009b; Kleinhans et al., 2013 - review).

Such rivers also tend to have large differences between their relatively low base flows and much greater peak flood flows, resulting in the transportation of a relatively coarse mixture of poorly-sorted sediments (Coleman & Wright, 1975). Hicks etr al (2002) observed a range of gravel transport processes within a braided river system including within channel migrating lobes (for smaller flood

events and flood recessions) and gravel sheet flows (for bankfulll flood events). They also noted that any slightly elevated bars or mid-channel islands tended to be relatively stable compared to the adjacent low-lying braid belt. However, when a series of consecutive flood events occur, any erosional or depositional activity within the river system is likely to be exacerbated – including the migration of the main river thalweg and secondary channels (Williams et al., 2011). Over time, sediment transported by the highly mobile, and continually migrating, channels will be distributed relatively evenly across the entire width of the river system - and any downstream prograding delta (Postma, 1990).

If a steep, braided river was able to maintain a statistically constant flow and sediment input rate over the year-to-decade timescale, it is likely that the river would achieve a state of dynamic equilibrium with, for example, the mean bed slope adjusting so that the sediment transported through the river system is equivalent to the amount of sediment entering the river (Davies & McSaveney, 2006); total stream power for the river system would also be minimised in the equilibrium situation (Chang, 1982). Superimposed on this equilibrium state would be the smaller-scale temporal and spatial 'noise' of the constantly changing individual channel reach characteristics (e.g. channel orientation, size, number, slope and roughness) and flow characteristics (i.e. velocity and discharge) that can vary considerably (Pickup & Higgins, 1979). This stochastic behaviour in braided river systems has been likened to the stochastic nature of turbulence (Paola, 1976; Jerolmack & Paola, 2010), and has recently been referred to as "morphodynamic turbulence" (Jerolmack & Paola, 2010).

Unfortunately braided rivers are rarely in this equilibrium state over such time scales as both upstream river inflows and sediment inputs can vary significantly over short time periods. This leads to rapid erosion and deposition within the river system as channels migrate, divide and converge on the active braidplain. The spatial and temporal variability inherent within braided river systems, combined with potentially high flow velocities and coarse, poorly sorted sediments, also means that determining the hydraulic parameters required to predict sediment transport rates and future bed morphology is extremely challenging (Pickup & Higgins, 1979). To enable sediment transport rates to be determined, a compromise is often made where hydraulic parameters are averaged over the entire river system. This is likely to result in erroneous sediment transport rates (Davies, 1987), so it is important to emphasise that any sediment transport equations used to estimate sediment loads for such complex braided gravel-bed river systems need to be used with caution.

2.1.2 Braided gravel-bed river deltas

A typical vertical profile for a coarse-grained delta is shown in Figure 2.2. The main components of a coarse-grained delta are:

- Topset (or delta plain) – braidplain upstream of the lake.
- Foreset – steep sloping delta front.

- Bottomset – area in front of the foreset where the finer sediments are deposited.

A coarse-grained delta will usually have bottomset layers of fine sediment, gently sloping towards the receiving basin, overlain with considerably more steeply-sloping coarse layers that are parallel to the foreset. These layers are, in turn, overlain by coarse topset deposits parallel to the braided river channel slope (Gilbert, 1885; Le Blanc, 1975). Over time, the steeper foreset sediment layer progrades over the bottomset; the rate of delta shoreline migration is determined by the volume rate of sediment supplied to the delta and the foreset height, while the basin water level determines the delta thickness (Nemec, 1990).

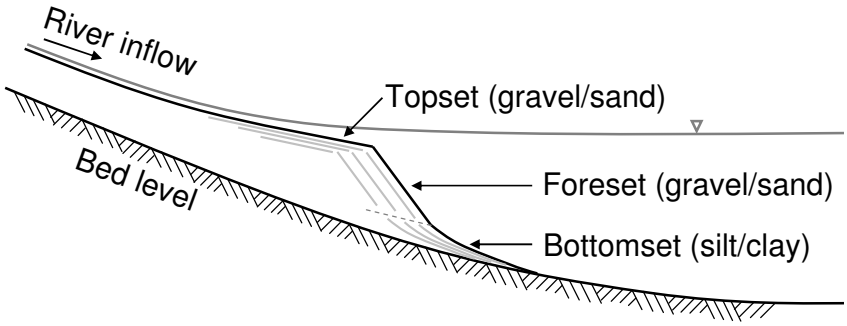

Figure 2.2: Schematic of a typical coarse-grained delta profile (from Parker, 2005)

The slope of a braided river delta topset is likely to increase slightly when sediment is stored (i.e. to compensate for temporarily not being able to transport all incoming sediment), and the slope will decrease slightly once the excess sediment is released and transported downstream to the delta shoreline (Kim et al., 2006). This autogenic behaviour has been linked to nonlinear sediment transport processes such as "transport thresholds and/or strongly nonlinear exponents in transport laws" (Paola et al., 2009, p. 21). In experiments where both flow and sediment supply remained constant, and subsidence (of the continental passive margin) and receiving basin water level changes were steady, Kim et al. (2006) observed fluctuating rates of laterally averaged shoreline migration. This was identified as being because the "fluvial system behind the shoreline acts as a kind of capacitor that alternately stores and releases sediment, thus varying the total sediment supply to the shoreline" (Kim et al., 2006, p. 4).

As sediment-laden braided river flows approach a receiving basin (e.g. a lake) the water decelerates, due to the backwater effect of the downstream body of water, and the coarsest material carried by the river flow can be deposited, forming a mouth bar (Olariu & Bhattacharya, 2006). As river water exits a confined river channel it also expands laterally and mixes with the downstream water body (Elliot, 1986). Where the receiving basin is relatively shallow, with a gentle slope, there will be a rapid deceleration of the river flow due to the bed friction of the shallower depth (Coleman & Wright,

1975). In this case, lateral spreading of the deposited sediment is likely to be significant (Coleman & Wright, 1975).

The density of the sediment-laden river water, relative to the density of the basin water, is one of the main factors that will determine how sediment is transferred from the river system onto the delta. If both bodies of water are of equal density (i.e. homopycnal flow) thorough mixing of the two bodies of water will occur and larger grains will be deposited near the river outlet while decreasing grain sizes tend to settle progressively further offshore. This results in the finer grains forming the bottomset in front of the prograding delta, and a typical Gilbert-type delta profile with an obvious slope break between the foreset and bottomset (Elliot, 1986; Lai & Capart, 2007). When denser, sediment-laden, river flood waters have sediment concentrations of approximately 1 kg/m^3, underflows or turbidity currents (i.e. hyperpycnal flows) may occur (Elliot, 1986). As the river flow enters the basin it plunges below the water surface and flows down the delta foreset, transporting both larger and smaller grains down the delta foreset and away from the river mouth (Lai & Capart, 2007). This produces a more gently curved foreset profile with a smooth, tangential, transition to the receiving basin floor (Lai & Capart, 2007). In other situations river water can form a buoyant plume at the water surface (i.e. hypopycnal flow); for instance, when the receiving body is relatively cold or a saltwater marine environment. For this scenario the coarser material is deposited near the channel mouth while turbulent mixing of the river and basin waters gradually allows the suspended sediment to settle out of the sediment plume onto the delta foreset and bottomset, with the progressively smaller grains settling out of the water column further away from the shoreline.

The delta foreset slope is usually at an angle that is equal to or less than the angle of repose for the submerged sediment, depending on the receiving basin characteristics (Gilbert, 1885; Le Blanc, 1975). Nemec (1990) noted that submerged delta foresets may have slopes of up to 24 to 27º, for sand, or 30 to 35º, for gravel. However, these slopes are likely to be reduced by external forcings such as turbidity currents (e.g. Kostic et al., 2002). Other processes within the receiving basin (e.g. waves, currents and localised foreset slope failures) may also have an impact on how the sediment is transported once it reaches the receiving basin.

Bedload deposition tends to produce localised oversteepening of the upper portion of the delta foreset, generally with the coarser grains from the supplied sediment. Prior & Bornhold (1988) showed that there are at least six different types of depositional systems of which the Bella Coola River delta represented a braided river delta plain with numerous delta front chutes on the delta foreset slope. These chutes were located immediately offshore from each braided distributary channel, and were likely to be due to “debris flows, liquefied sandflows, and turbidity currents” (Prior & Bornhold, 1988, p. 138) triggered by slope failures; this provided the sediment transport mechanism to transfer coarse sediment from the river channel to the lower slopes and bottomset, and hence, maintain the observed

2-15º delta foreset slope. Once sediment reached the base of a delta front chute it expanded laterally and was deposited (Prior & Bornhold, 1988).

If the sediment supplied to the delta contains a wide range of sediment sizes then, when grainflows (i.e. sediment mass transported downslope by gravitational forces) are initiated, 'kinematic sieving' occurs (Sohn et al., 1997; Kleinhans, 2005b). Kinematic sieving produces an inverse grading (i.e. finer layers of sediment overlain by larger sediment). During grainflows, the smaller grains 'drop' into the voids in the layer of sediment underneath. Meanwhile, larger grains tend to drift into the upper surface layer of the grainflow (Kleinhans, 2005b), and towards the front of the flow since the upper portion of the flow has higher velocities (Sohn et al., 1997). When the next grainflow occurs, the coarse surface layer of the previous grainflow deposit is likely to be entrained within the new grain flow, while the underlying, finer sediment of the previous grain flow deposit provides the less resistant failure surface. The resulting delta front has an upward fining pattern of coarser sediment on the lower delta slope and finer sediment near the topset (Kleinhans, 2005b).

During higher lake levels (e.g. floods), it has also been observed that sediment can be deposited in the lower reaches of river channels entering a basin; this sediment is transported from the channels, onto the delta foreset, once lake levels have lowered relative to the river levels (Gilbert, 1973, 1975). Progradation of the delta foreset and shoreline (at the mouths of the active river channels) lengthens the active channel and reduces the channel gradient; this triggers aggradation in the upstream channel (Elliot, 1986; Muto & Swenson, 2005). As the river channel continues to aggrade, channel avulsion and/or bank erosion will eventually encourage a new flow path to the receiving basin to form. As the braided river channels delivering sediment to the study deltas regularly change their outlet positions, deposition along the delta topsets and foresets is expected to be 'laterally non-uniform' (Kleinhans, 2005a, p 223). Although the pattern of upward fining of sediment on delta foreset slopes still exists, it is less prominent (Kleinhans, 2005a).

At present the effect of downstream basin levels on braided channel switching behaviour does not appear to be well understood, although recent studies of delta distributary channels have suggested that avulsion is influenced by both upstream aggradation and a downstream backwater (or "morphodynamic backwater") effect (Hoyal & Sheets, 2009).

Mass failure of delta foreset slopes has been observed in ancient delta deposits (e.g. Postma et al., 1988) as well as in recent times (e.g. Lindsay et al., 1984; Papatheodorou & Ferentinos, 1997; Schwab, 1999; Girardclos et al., 2007). These studies identify the following triggers: seismic activity; collapse (by slides or slumps) of an overloaded or oversteepened delta front (e.g. produced by rapid sediment accumulation during flood events); creep and deep-seated deformations due to high pore pressures which occur as a result of high sediment accumulation rates and waterlogged sediment deposits; and other external forces such as intense wave activity, rapid basin level changes or human

activity. However, the ~0.5 m tsunami that occurred in Lake Brienz in 1996 was likely to have been generated by a small slope failure that developed into a larger mass flow; in this event no specific initiating trigger was identified, and the cause was determined to be "normal sediment accumulation" (Girardclos et al., 2007).

2.2 Historic research trends

Historically, river deltas have provided important agricultural land for human populations (Coleman, 1976). In fact, the word 'delta' was one of the first geographical terms to be used when the similarities between the Greek letter delta (Δ) and the triangular-shaped formation at the mouth of the Nile River was noted (Celoria, 1966). Over time 'delta' became a general term used widely to represent other features similar in form to the Nile delta (Celoria, 1966).

The first study of modern deltas to be documented was published in German by Credner (1878). This paper 'discusses structure, form and distribution of several deltas of the world' (Le Blanc, 1975, Table 1) and 'alluded to rapid changes in sites of deposition through time, but he had little knowledge of sedimentation patterns' (Coleman, 1988, p 999). Documented research up until the 1930s (e.g. Gilbert, 1885; Johnston, 1921) tended to be mainly qualitative and/or speculative in nature, largely due to the lack of available technology and methodology to quantify delta growth dynamics. During the 1930s and 1940s delta research mainly focused on the growth dynamics of the Mississippi delta; the outcome of this work provided the fundamentals for future research applying newly-gained knowledge of modern delta growth dynamics to both ancient, observed, sequences of sediment deposition, as well as other deltas around the world (Coleman, 1988).

Delta research gained momentum in the 1950s and 1960s after the 1940s discovery of large deposits of oil, gas and coal in the sediments of many ancient deltas (Le Blanc, 1975; Elliot, 1986). This led to further research in the area of depositional processes as well as modern sediments in the Gulf of Mexico (more specifically the Mississippi delta). Research on other large deltas (e.g. Niger, Rhine and Rhone) followed. Around this time Bates (1953) also applied the principles of jet theory to delta formation, and Jopling (1965) used a small laboratory flume to examine the impact of various parameters (e.g. flow, sediment type, relative basin depths) on delta front profiles. Further information on early delta studies is summarised in Le Blanc (1975), Elliot (1986) and Coleman (1988).

In the 1980s research began to emerge in the areas of fan deltas (e.g. Nemec & Steel, 1988) and coarse-grained deltas (Colella & Prior, 1990). This was followed by research in the early 1990s that started to move from single channel meandering rivers to braided river studies (Best & Bristow, 1993; Sambrook Smith et al., 2006). In the past decade there have been considerable advances in all aspects of delta research including data acquisition, physical modelling and numerical modelling. This research is described below.

Demand for accurate field data, covering large temporal and spatial scales, appears to be increasing with the growing need for calibration and validation data for both physical hydraulic models and a wide range of emerging numerical models – especially those simulating complex braided river morphodynamics. This coincides with recommendations by Warburton et al. (1996, p. 299) that we require "integration of field, laboratory and theoretical approaches" to advance our understanding.

2.3 Field studies

Field studies of braided gravel-bed rivers and deltas generally take the form of either an intensive data collection exercise of an existing modern river-delta system or an analysis of ancient deposits via exposed outcrops, cores or surveys (e.g. ground penetrating radar). Examples of previous field studies of braided gravel-bed rivers, fan deltas, alluvial fans and deltas are summarised below.

2.3.1 Modern studies

2.3.1.1 Braided gravel-bed rivers

Field studies of 'modern' braided river environments are notoriously difficult. This is due to the complex nature of the constantly changing river channel networks – especially at high flows when turbid river waters often cover a wide spatial extent; are inaccessible; and/or are impossible to measure or observe. Initial attempts to quantify braided rivers included Fahnestock (1963) and Pickup & Higgins (1979), where variables such as water depths, discharge and slopes were measured. Mosley (1982) was able to undertake a unique field study (analogous to a 1:1 scale model) where the Ohau River flows were able to be controlled by the upstream power station on three separate occasions. This allowed the collection of water depths and velocities along the river at various known flows. Other braided river field studies that have attempted to quantify morphological changes (e.g due to flood events) have included:

- Measurement of flow, velocity, cross sections, bedload and various sediment characteristics in a small melt-water fed braided river reach over a 5 week period (Ashworth & Ferguson, 1986).

- Daily oblique photographs, and transects of the major channels of a 60 m braided river reach (at 10 metre spacings), completed for 25 days, including two periods where peak flows led to the "complete destruction and reconstruction of a large medial bar" (Goff & Ashmore, 1994, p. 199). This study also observed that sediment was sourced from both bank and channel bed erosion.

- A total station survey of a 350 m long by 50 m wide river reach, with an average point spacing of 2.1 to 3.0 m, surveyed on three separate occasions to cover two flood events (Eaton & Lapointe, 2001)

- A topographical cross section survey and planimetric digital photography analysis of a 1 km long by 850 m wide braided river reach over 1.5 years. Morphological changes for six flood events were observed (Bertoldi et al., 2010).

Oblique high angle photographs (e.g. Warburton, 1994), or cross section surveys (Ferguson et al., 1992), have also been used to assess changes in channel morphology. However, it is not possible to accurately quantify the full spatial extent of planform changes and/or the vertical changes due to degradation and aggradation with this information alone (Eaton & Lapointe, 2001). Previous river flow or velocity measurements also often required labour-intensive gaugings at a limited number of sites.

Fortunately new technological developments are allowing more detailed spatial and temporal data acquisition which will, in turn, allow closer analysis of the relationships between river flows, sediment transport and topography. For example, detailed digital elevation models (DEMs) can now be produced using the following methods:

- Real time kinematic (RTK) GPS surveys (Brasington et al., 2000).

- Digital photogrammetry or airbourne laser scanning (LiDAR – light detection and radar) combined with image analysis, which is used to generate water depths for the wetted areas by calibrating image colours to field data (e.g. Lane et al., 2003; Westaway et al., 2003; Legleiter, 2011).

- Terrestrial laser scanning (TLS), combined with empirical optical methods (for the submerged areas). By generating DEMs during the low flow periods, between successive floods, topographic changes for several successive flood events were quantified for a 2^{+} km long by up to 700 m wide braided river reach of the Rees River (Williams et al., 2011).

It is also now possible to measure three-dimensional flow fields, and changes in morphology, for large, braided channels using a combination of an acoustic Doppler current profiler (ADCP), an echo sounder and a differential GPS (DGPS) mounted on a boat (e.g. Richardson & Thorne, 2001). Other recent developments include through-water TLS which allows gravel bed surfaces to be scanned (tested at the patch scale) in water depths of up to approximately 200 mm (Smith et al., 2011); in the future this may eliminate the need for separate image analyses for submerged river channels.

Despite significant advances in airborne and terrestrial laser scanning, and in flow measurement methods, it is still difficult to develop technologies able to obtain accurate information regarding the varying riverbed surface composition over an entire study area. The composition of the sediment supply from upstream (especially during significant flood events when access and safety are also a consideration) is also difficult to quantify, although in-situ sediment deposits can be sampled between

flood events. Considerable errors in the application of surface-based transport models of gravel-bed rivers are therefore still likely (Wilcock, 2001).

2.3.1.2 Braided gravel-bed river deltas

As deltas usually have a distinctive profile, combined with relatively rapid delta progradation rates, measuring the accumulated deltaic sediment volume over a known time period provides a good estimate of average sedimentation and supply rates; bathymetric surveys of submerged deltas have been used for this purpose on several occasions (e.g. Thompson, 1985; Hickin, 1989). Gilbert (1975) also provided an estimate of long-term average sediment yield to Lake Lillooet based on maps, aerial photography, core samples and seismic profiling. A more recent field study also calculated sediment yields for a fan delta of a small river catchment using aerial photography, sonar bathymetry, GPR surveys and sediment sampling (Pelpola & Hickin, 2004).

The response of a braided gravel-bed river and delta to base level lowering was also able to be examined when the controlled Lake Benmore levels, at the downstream limit of the Ohau River and delta, were lowered by approximately 4 m for construction purposes (Mosley, 1984). Although it was expected that lake level lowering would produce an incised channel exiting into the lake (and channel degradation upstream), after the minimum lake level was reached aggradation occurred upstream of the delta and the single dominant channel was replaced by a network of distributary channels. This study reinforced the fact that unpredictable delta morphology can occur in the presence of several inter-related variables influencing delta progradation.

In the 1980s high-resolution acoustic surveys and sediment sampling enabled the dynamics of steeply-sloping, deep-water, gravel-bed river delta foreset slopes to be inferred (e.g. Prior & Bornhold, 1988). In spite of this, there still appear to be very few field studies that have completed an extensive data collection exercise for a modern braided gravel-bed delta due to the difficulty in obtaining data for modern delta foresets (e.g. submerged steep delta foresets in deep water, shallow water delta foresets smothered by aquatic weed, etc.). Nemec (1990) provides an overview of steep delta foreset processes based on available observations and emphasises the need for further information. Rojas & Le Roux (2005) also completed a two month study of a small (150 m by 200 m) Gilbert-type delta, with a water depth less than 30 m. For this study wind, wave, current and bed sample data were collected during the fair-weather periods (i.e. when field work was possible). No sediment movement was observed on the delta during these times - except for the action of bivalves on the delta slope (Rojas & Le Roux, 2005, p. 14). Conversely, during large storm events, a large portion of the ~30 m high delta (excluding the bottomset) was influenced by waves, currents and hyperpycnal flows.

2.3.2 Ancient delta studies

The study of ancient deltas began in the 1880s with the Lake Bonneville delta deposits (Gilbert, 1885; Gilbert, 1890). These delta deposits had steep foreset slopes, and are still known today as ‘Gilbert-

type' deltas. Recent studies have also examined the depositional processes occurring in the ancient deposits of Gilbert-type deltas (e.g. Sohn et al., 1997).

Generally, field studies of exposed ancient outcrops and core samples are problematic when attempting to interpret alluvial basin features. This is because they generally only have limited exposure and therefore do not provide full three-dimensional geometric data, or provide conclusive evidence of the dynamic processes that produced the preserved depositional features (Moreton et al., 2002). Ancient delta field studies, analysing facies and interpreting depositional architecture, are covered in many publications (e.g. Colella & Prior, 1990; Sohn et al., 1997; Fielding, 2010).

2.4 Physical modelling

As stated by Kleinhans (2010, p. 313) "Given the limited number of good data sets available, there is a clear role for experiments." Paola et al. (2009, p. 23) also state "… it is surprising how little attention deltas have received from experimentalists given the number of compelling motivations for studying them …". These comments are indeed relevant for braided gravel-bed rivers and delta systems where, until recent technological advances (as outlined in the previous section), it had proven to be extremely difficult or impossible to obtain accurate and detailed data sets of the dynamics of such systems over medium to large temporal and spatial scales.

The various types of physical models are described, along with advantages and limitations, in Section 2.4.1. Previous experimental studies (Sections 2.4.2 to 2.4.4) and scaling issues (Section 2.4.5) are also examined.

2.4.1 Description

A physical hydraulic model is a scaled representation of a full sized flow scenario (e.g. a hydraulic control structure, a natural phenomenon like an alluvial fan, or a proposed engineering work). For a physical model to exhibit similar flow conditions to the prototype, it requires:

> *Geometric similarity* – A similarity of form where the ratios of characteristic prototype lengths to model lengths are equal.
>
> *Kinematic similarity* – Flow paths are geometrically similar and there is similarity of motion (where the ratios of characteristic prototype velocities to model velocities are equal).
>
> *Dynamic similarity* - In addition to kinematic similarity, there must be similarity of masses and forces where the ratios of characteristic prototype forces to model forces are equal.

The reality of physical hydraulic modelling is that it is usually easy to achieve geometric similarity and kinematic similarity but extremely difficult to achieve full dynamic similarity. This is particularly

the case when the same fluid (i.e. the same fluid density and viscosity) is present in both the model and prototype as both Froude and Reynolds similarity criteria are not able to be satisfied simultaneously (Ashmore, 1991b). Therefore, when designing a physical hydraulic model with water as the model fluid, it is important to ensure that the dominant force acting in the prototype is modelled correctly, while the influence of the non-dominant forces is minimised (ASCE Committee on Hydraulic Research, 1942). When modelling movable-bed rivers, this often means the Froude number is scaled correctly while it is only necessary for the Reynolds number (Re) and grain Reynolds number (Re_*) to remain within the fully rough-turbulent flow regime, with $Re > 500$ and $Re_* > 70$ (Peakall et al., 1996). This type of model is referred to as a Froude scale model (or a 'generic' Froude scale model if a general geomorphic feature is being modelled). When the model scale is significantly reduced such that sediment transport is compromised, the slope of the model is often steepened to allow better transport of the bed material (Peakall et al., 1996). These models, that usually maintain Froude number scaling, are referred to as distorted Froude-scale models. In general, similarity of grain Reynolds number limits physical hydraulic models of rough-turbulent gravel-bed river flows to linear scales of 1:50 or so (Young &Warburton, 1996).

As it can be relatively costly to construct models of large geomorphic features, due to their reasonably large size and long length of model run times, the use of very small scale movable bed models, that may only adhere to *geomorphic similarity* (i.e. similarity of processes), have also been used. The requirements for geomorphic similarity are that (Hooke, 1968a, p. 392):

- gross scaling relationships be met (i.e. planform dimensions are scaled but the vertical scale is usually exaggerated to produce realistic behaviour).
- the model reproduces some morphologic characteristic of the prototype.
- the processes which produced this characteristic in the laboratory can logically be assumed to have the same effect on the prototype.

Physical hydraulic models that only adhere to geomorphic similarity generally examine a geomorphic process but not necessarily a specific prototype. For these models, Reynolds' number and Weber number generally do not fall within the same ranges for both model and prototype (resulting in laminar flows and surface tension effects in the models). However, Paola et al. (2009, p. 36) noted that "small-scale (laminar) flows are clearly and qualitatively different from large-scale turbulent flows, but the dynamics that matter – the relation between shear stress and topography, and that between shear stress and bedload flux – is similar enough that the morphodynamics is surprisingly consistent across this major, scale-dependent transition", and Malverti et al. (2008, p. 13) showed that "surface tension is important only if the microscale river width is on the order of or smaller than the capillary length" where the relatively small capillary length, ℓ_c, is defined as

$$\ell_c = \sqrt{\frac{\sigma}{\rho_L\, g}} \approx \quad 2.7mm \qquad \textit{(water at 25°C)} \tag{2.1}$$

Where: σ = surface tension between air and experimental fluid (kg/s^2)
ρ_L = density of experimental fluid (kg/m^3)
g = acceleration due to gravity (m/s^2)

As the processes examined in the small scale movable bed models are mainly dependent on inertial forces, geometry and gravity, ensuring similarity of only Froude number, relative depth and relative density has been considered acceptable (e.g. Davies & Korup, 2007). Similarity of these ratios can be relatively easily achieved by using fine sand (to maintain relative depth), together with water (to maintain relative density); similarity of Froude number is also likely to occur naturally at channel-forming flows (Grant, 1997; Davies et al., 2003). Such models (referred to in various texts as analogue process models, micro models, microscale models or hydraulic sediment response models) have been developed with horizontal length scales of the order of 1:2000, for alluvial fans (Davies et al., 2003; Davies & Korup, 2007), and as small as 1:20 000 for modelling river training works (Maynord, 2006). These small scale movable bed models will be referred to, hereafter, as microscale models.

Detailed descriptions of similarity theory, and similarity in sediment transport, can be found in several publications (e.g. ASCE Committee on Hydraulic Research, 1942; Graf, 1971; Yalin, 1971; Novak & Cabelka, 1981; Peakall et al., 1996; Chanson, 2004), while Young & Warburton (1996) provide a detailed overview applied to gravel-bed braided rivers.

The use of larger, physical models of braided gravel-bed rivers (that approximate dynamic similarity) has significant advantages and disadvantages as outlined in Mosley & Zimpfer (1978) and Young & Warburton (1996). As these models of braided gravel-bed rivers can usually not be smaller than a scale of approximately 1:50 (Young & Warburton, 1996), there are likely to be substantial costs involved in using them (e.g. construction and operation costs). Larger physical models are therefore usually only justified for expensive design projects, with complex flow conditions, where failure of the structure could be expensive or endanger human life (Gaines & Smith, 2002), and for research purposes.

Developments in numerical modelling, and in field data acquisition, mean that other options are often available for solving problems and designing engineering solutions for simple scenarios. Despite these developments, the complex behaviour of braided gravel-bed rivers makes it extremely difficult to obtain spatial and temporal estimates of sediment transport rates and hydraulic parameters in the field (e.g. Pickup & Higgins, 1979; Mosley, 1983), and numerical models may also be inadequate due to the complex nature of the river system being examined. Therefore the ability of some hydraulic

parameters to be controlled in a laboratory setting, and the reduced model time scales, offer many advantages.

As a result, microscale models have proven to be extremely useful for braided gravel-bed river studies as they provide information on general relationships as well as being able to provide context for an often limited range of field observations (given that geomorphic processes may require observations over a considerable period of time). The large deviations from similarity criteria have, on the other hand, generated some concern within the scientific community regarding microscale model capabilities, limitations and acceptable applications (e.g. Gaines & Maynord, 2001; Maynord, 2006). For instance, the steeper bed slopes, required for the operation of microscale models, mean that the sinuosity of the modelled channels is likely to be less than that of the prototype (Davies et al., 2003), and the vertical scale distortion also means that results need to be interpreted with caution, and should be interpreted qualitatively rather than providing "reliable quantitative data on geomorphic problems" (Hooke, 1968a, p. 393). Conversely, microscale modelling studies have been shown to be effective at simulating realistic areal extents of aggradation and degradation and relative rates of aggradation (Davies et al., 2003). It has also been noted that these models "produce spatial structure and kinematics that, although imperfect, compare well with natural systems despite differences of spatial scale, time scale, material properties, and number of active processes" (Paola et al., 2009, p. 1). Examples of models that have successfully simulated a range of complex and dynamic natural systems are described in Paola et al. (2009); braided river experiments by Rosatti (2002) also compared well with real braided rivers. The fact that these models have relatively low construction and operating costs, relatively quick run times, and make an excellent visual tool for demonstrating processes and communicating results to both a scientific and non-scientific audience (Max et al., 2002), mean they are an ideal tool for representing the growth of braided river deltas.

The application of microscale models to the simulation of braided gravel-bed river deltas is described further in Chapter 4. A general discussion of previous physical hydraulic modelling studies of braided gravel-bed rivers, fan deltas, alluvial fans and deltas is given below. Both narrow flume experiments (where lateral variability is eliminated or significantly reduced) and wider tank experiments (incorporating avulsion, channelization and other three-dimensional processes) are included.

2.4.2 Braided gravel-bed rivers

In the 1980s, scaled hydraulic models started to gain popularity as a tool for use in braided gravel-bed river research (e.g. Ashmore, 1982; Ashmore & Parker, 1983; Southard et al., 1984; Schumm et al., 1987; Ashmore, 1988; Davies & Lee, 1988). This was particularly the case in New Zealand, where a better understanding of braided river processes was required for several applications including the design of river control works (Warburton, 1996). Since that time, hydraulic models have been used to examine many facets of braided gravel-bed rivers in both two-dimensional (narrow flumes), and three-

dimensional (wider flumes where self-formed braided channels can develop without any lateral constraints). The two-dimensional models are generally used to study bedload transport while three-dimensional models can be used to study a wider range of braided river processes (Warburton, 1996). Some previous three-dimensional hydraulic modelling studies, usually 'generic' and at a scale of the order of 1:50 (to enable the formal model scaling techniques to be adhered to) have: identified the main braiding mechanisms (Ashmore, 1991b) and braided channel response to increasing discharge (Egozi & Ashmore, 2009); analysed the effect of braided channel width reduction on mean channel bed level (Davies & Lee, 1988); investigated relationships between bedload transport rates and stream power (Ashmore, 1988; Young & Davies, 1990); reproduced the stratigraphy of an aggrading coarse-grained braided river (Moreton et al., 2002), and examined the interaction between bedload transport and braided channel morphology (Hoey & Sutherland, 1991). Specific braided river processes, such as channel junction scour and mid-channel bar growth, have also been studied using physical hydraulic models (e.g. Leopold & Wolman, 1957; Mosley, 1976; Ashworth, 1996). However, despite many hydraulic models being developed, it appears that model runs are generally not replicated to observe the extent of variability possible for simulated braided river systems (e.g. Warburton & Davies, 1994).

Smaller scale, microscale, models of braided rivers have tended to be classified as alluvial fan models since they have mainly represented a reach of a braided river where the river is exiting a confined channel reach, and the channel width is expanding rapidly. Stream braiding has also been analysed using the 1:2000 scale microscale model of Hong & Davies (1979). This model study showed that, despite the braiding dynamics in their model differing to those observed in the field, a degree of geometric similarity existed between their model (with an exaggerated vertical slope of 4 to 10%), and the 1 km wide braided, gravel-bed Rakaia River in New Zealand; the number of braids in both the model and prototype were also able to be predicted successfully using Parker's (1976) stability analysis based only on stream slope, Froude number and width:depth ratio (Hong & Davies, 1979). Ashworth et al. (2004; 2007) also used microscale modelling to analyse the effect of increasing sediment supply rates on avulsion frequency in an unconfined braided river reach. Other recent microscale modelling studies of braided rivers have examined the effects of riparian vegetation on braided channel dynamics (e.g. Tal & Paola, 2010).

2.4.3 Braided gravel-bed fan deltas and alluvial fans

Like braided rivers, natural fans are most active during flood events when large volumes of sediment are transported (Parker et al., 1998). Although the behaviours of prograding alluvial fans and fan deltas appear to be very similar, due to their similar feeder systems, the obvious difference is that fan deltas prograde into a body of water while alluvial fans prograde over an alluvial plain. According to the narrow flume study by Postma et al. (2008), alluvial fans and fan deltas also have different stratigraphic behaviour with alluvial fans classified as being in the *start-up* stage (where all sediment is retained upstream of the base level as the fan progrades towards the base level location), while fan

deltas are classified as being in the *fill-up* stage (where the downstream body of water, i.e. base level, has already been reached with further aggradation occurring on the fan, along with the transportation of some sediment beyond the base level). While model studies of alluvial fan and fan delta evolution have both observed the fluctuating cycle of sheet flow and channelized flow (e.g. van Dijk et al., 2009; Clarke et al., 2010; van Dijk et al., 2012), Van Dijk et al. (2012) also found that these cycles were longer on fan deltas. This is due to the higher maximum fan delta slopes (and consequent greater slope variability) occurring due to fan deltas being in the fill-up stage. Higher slope variability resulted in deeper, incised, channels that required a longer period of time to fill before sheet flows commenced (van Dijk et al., 2012).

A summary of some of the microscale modelling studies of alluvial fans and fan deltas is given below, along with a summary of some of the scaling issues.

2.4.3.1 Alluvial fans

Three-dimensional alluvial fan behaviour has been extensively modelled using microscale models (e.g. Hooke, 1967, 1968b; Schumm et al., 1987; Koss et al., 1994; Zarn & Davies, 1994; Clarke et al., 2010; van Dijk et al., 2012). In each case, qualitative comparisons between 'generic' models and field-scale observations showed successful simulation of "depositional sequences and erosional features" (e.g. Koss et al., 1994, p. 96); descriptions of alluvial fan processes (e.g. alternating sequences of sheet flow and channelized braiding, channel entrenchment and aggradation, concave bank erosion and channel migration, etc.) are also provided by many authors (e.g. Zarn & Davies, 1994; Clarke et al., 2010; van Dijk et al., 2012). Microscale models have successfully simulated various external forcings on alluvial fans including the effects of: large, infrequent sediment pulses on fanhead morphology in a braided river (Davies & Korup, 2007); river training works, that confine the active braided river channel width, on aggradation of the river bed (Davies et al., 2003); varying flow, sediment feed rates, slope and subsidence on the distribution of surface flow and deposition dynamics (Cazanacli et al., 2002; Sheets et al., 2002); varying discharge (Milana & Tietze, 2002); a constant rate of increasing base level (Whipple et al., 1998); and sedimentation rates on avulsion frequency (Bryant et al., 1995).

Cazanacli et al. (2002) scaled up model results to field scale alluvial fans using distorted Froude modelling principles (e.g. Graf, 1971; Peakall et al., 1996); this provided an estimate of the reworking time which can potentially be used in assessing flood risk on alluvial fans. Using the same experimental data set, Sheets (2002, p. 300) observed that "established channels act largely as conduits for sediment, while overbank spills, flow expansions and failed avulsions all deposit a disproportionate amount of sediment". It was also noted that similar behaviour occurred in contrasting river environments, and therefore it was suggested that this behaviour "is a generic feature of channelized flow systems" (Sheets et al., 2002, p. 300); these findings were consistent with those of Ashworth et al. (2007). Sheets (2002, p. 288) also used the "stratigraphic integral scale" to scale up

experimental results for comparison with field studies (based on the time it takes for a certain amount of deposition to occur at the average aggradation rate).

The autogenic behaviour of evolving, and fully developed, alluvial fans has also been modelled by maintaining constant flows, sediment feed rates and base levels (Clarke et al., 2010). This study concluded that "Overall, the potential of physical models to provide rich data concerning the dynamic interaction between fan formation and flow configuration has been demonstrated" (Clarke et al., 2010, p. 285).

Although most early alluvial fan models provided only qualitative information, several model studies have also been used to provide data for numerical models (e.g. Parker et al., 1998).

2.4.3.2 Fan deltas

The morphology and dynamics of fan deltas have been modelled using narrow flumes exiting into larger, unconfined reservoir tanks (e.g. Chang, 1982; Schumm et al., 1987). Chang (1982) observed that channel adjustments favoured a return to an equilibrium fan system with total power within the system minimized; it was suggested that this was also applicable to alluvial fans.

Three-dimensional microscale models have also simulated various external forcings on fan deltas including the effects of: basin geometry and sediment supply (Smith, 1909); a constant rate of increasing base level (Kim & Muto, 2007); subsidence and varying base level (Kim et al., 2006); tectonic deformation representing a constant fault slip rate (Kim & Paola, 2007); a combination of four sediment point sources and laterally asymmetric subsidence (Connell, 2010), and various management options to control flow and sediment passing over a fan delta into a downstream river confluence (Davies, 2007).

Model studies have also been used to provide data for numerical models (e.g. Kim & Muto, 2007; Kim et al., 2011). Kim & Muto (2007, p. 12) note that for their one-dimensional geometric model "accounting for the relative importance of three-dimensional effects such as lobe switching is still problematic".

2.4.4 Braided gravel-bed river deltas

As mentioned earlier, there are significant difficulties in obtaining field data relating to delta foresets, so there has been relatively little research related to delta foreset processes. Recent physical modelling studies help to address this issue, mainly using narrow flumes to examine longitudinal profiles of deltas. Narrow flume experiments have examined various processes including: sediment deposition (e.g. Jopling, 1965; Kleinhans, 2005b, 2005a); the autogenic behaviour of deltas subjected to a constant rate of base level increase (Muto, 2001; Tomer et al., 2011) as well as various rates of base level decrease (Muto & Swenson, 2005); and the effect of turbidity currents (Kostic et al., 2002;

Kostic & Parker, 2003b; Toniolo & Schultz, 2005; Lai & Capart, 2007; Lai & Capart, 2009). A notable observation from turbidity current experiments was that the plunge point for the river flow corresponded to a point about a third of the distance down the delta foreset slope; turbidity currents also decreased the delta foreset slope and produced a bottomset deposit (Kostic & Parker, 2003b).

There have also been modelling studies of fine-grained deltas, representing river systems such as the Mississippi (e.g. Hoyal & Sheets, 2009), which are less relevant to the study of coarse-grained braided gravel-bed river deltas.

2.4.5 Scaling issues

Scaling issues identified as a result of physical modelling, and in particular microscale modelling of braided rivers, alluvial fans, fan deltas and braided river deltas, included: surface tension (Peakall & Warburton, 1996); potentially cohesive behaviour of fine sediments (Peakall et al., 1996; Whipple et al., 1998) as well as the potential effect of well-rounded sand grains with a limited size distribution not necessarily representing more angular gravel river beds (Ashmore, 1988; Church et al., 1991); reduced Reynolds number (Whipple et al., 1998); difficulty in relating model time to real time (Koss et al., 1994; Peakall et al., 1996; Davies, 2007); steep bed slopes and lower channel sinuosity (Davies et al., 2003; Davies, 2007); exaggerated local scour during localised turbulence (Davies, 2007); development of wider, shallow channels (rather than narrow, incised channels) during a period of aggradation (Davies & Korup, 2007); effect of vegetation (Peakall et al., 1996); effects of constant inflow hydrographs (Peakall et al., 1996); and "meander belts with clearly delineated floodplains", as well as other processes, not being replicated (Sheets et al., 2002, p. 291). As long as these limitations are taken into consideration, physical models can be usefully utilised for a variety of applications including those outlined above.

2.5 Numerical modelling

As stated by Gao (2007, p. 233) "… so far, high-resolution process-based morphodynamic models for sub-aerial delta evolution are few." Some of the currently available numerical models are discussed below, as well as being summarised in various publications (e.g. Overeem et al., 2005; Fagherazzi & Overeem, 2007).

2.5.1 High-resolution 1-d, 2-d and 3-d models

Physically-based numerical models of river and delta systems are based on the shallow water Navier-Stokes equations and are classified as being either 1-d (depth- and width-averaged), 2-d (depth-averaged or width-averaged), or 3-d. These models include various relationships for the simulation of sediment transport, and have either a fixed or movable bed (the latter being classified as a morphodynamic model).

2-d and 3-d morphodynamical numerical models of braided river and delta systems must deal with the complex processes of hydraulic and morphological interactions and feedbacks, and are therefore computationally-intensive. This is due to several factors including:

- the small time scales of the hydrodynamic processes (~ seconds to hours) mean the numerical models are required to also have a small timestep (Fagherazzi & Overeem, 2007).

- the topography and flow-field feedback (e.g. Ashworth & Ferguson, 1986) requires the bed surface and flows to be recalculated at each time step (Paola, 2000).

To improve the efficiency of models that require small time scales for some simulated processes, an event-based upscaling technique can be implemented (e.g. Storms, 2003). This involves using a smaller time step to capture large, low-frequency events (i.e. events that have a significant impact of morphology), and averaged values to simulate longer periods of smaller, high-frequency events.

A model that is currently being applied to various braided river and delta systems is Delft3D (Lesser et al., 2004). This model has the advantage of an improved calculation of sediment transport as it simultaneously determines sediment transport and morphological changes. River mouth and delta systems with river, wave, tide and wind influences have been successfully modelled using Delft3D in 2-d (e.g. van Maren, 2004; Dan et al., 2011) and 3-d (e.g. Edmonds & Slingerland, 2007; Geleynse et al., 2011). The effects of vegetation have also been modelled by instantaneously vegetating dry areas of a medium-sized river floodplain between flood events (Crosato & Saleh, 2011). This work may help address a limitation noted by Van Maren (2004) that the lack of roughness data for the subaerial floodplain compromises the quality of the flow routing. Model output may also be scale dependent (Passalacqua et al., 2006). For example, if the river channels are smaller than the grid cell size, the average value assigned to each grid cell is likely to produce a reduced channel density and, consequently, decrease the amount of transported sediment (Passalacqua et al., 2006)

Another physically-based 2-d or 3-d numerical modelling option is SEDFLUX (Syvitski & Hutton, 2001). SEDFLUX was developed from a 2-d process-reponse model (DELTA), that simulated a basin being filled by a prograding delta (Syvitski & Daughney, 1992), and combined with other process-based event models (Syvitski & Hutton, 2001). SEDFLUX delivers sediment to the delta via a single river mouth and distributes the sediment within the basin by several processes including bedload deposition near the river mouth, dispersion of suspended sediment plumes, and transfer of sediment further offshore via turbidity currents, debris flows, creep and slides (Syvitski & Daughney, 1992; Syvitski & Hutton, 2001). Stochastic delta switching, long shore transport, tectonics and sediment compaction can also be simulated over time scales of decades to 10 000+ years (Overeem et al., 2005). The 2-d SEDFLUX model has also successfully simulated a combination of hyperpycnal flows, subsidence and small and large flow pulses in a tank experiment (Kubo et al., 2005).

Unfortunately not all the governing equations required to model a 3-d sedimentary system are currently fully known (Paola, 2000; Bridge, 2009). For braided river systems this includes equations representing non-uniform sediment transport, channel processes, vegetation, bank erosion and accretion, near-bank flow pattern, and levee and overbank flow (Kleinhans, 2010), as well as the influence of mouth bar morphology on delta plumes (Overeem et al., 2005). As a result, existing morphological models capable of modelling the decade to century timescale still require averaging and/or a simplistic approach for some complex processes (Hardy, 2012). This usually means that physically-based morphological models, by necessity, incorporate various empirical equations (e.g. sediment transport equations with sediment classified by the fraction within each size range) and parameters (e.g. active depth in Exner equation).

Numerical models based on grid cells not only require averaging over each cell and time step but run into complications when defining moving boundaries such as bank erosion or accretion (Mosselman, 2012). By simplifying the processes within morphological models, the feedbacks into the model will also represent a simplified scenario (Hardy, 2012). Non-uniform sediment in gravel-bed rivers are also difficult to model since processes such as sediment entrainment, transportation and deposition are complicated by e.g. armouring, downstream fining, changes in gravel-bed porosity due to filling and emptying by finer sediment, and further complications relating to the dynamics of partially mobile river beds (Mosselman, 2012). It is also now common practise for additional processes to be coupled to existing fluvial-morphological models that have previously focussed on sediment transport. These processes (e.g. vegetation dynamics and bank erosion/accretion processes) still contain some simplifications within their own processes meaning the complex coupled models still requiring ongoing validation (Mosselman, 2012). Consequently, all of these factors contribute to the current inability to accurately predict braided gravel-bed river features such as complex systems containing bars, bifurcations and confluences (Mosselman, 2012: Kleinhans, 2010).

A further numerical modelling limitation is the substantial quantity of spatial and temporal field data required to build, calibrate and validate these complex models. For basin modelling the available data are usually inadequate (Paola, 2000; Overeem et al., 2005) - although rapid advances in technology are likely to make this more feasible in the future. Technical issues also arise regarding the representation of the model grid (i.e. regular rectangular versus curvilinear versus irregular unstructured); “complicated temporal and spatial variations in geometry, water and sediment supply” (Bridge, 2009, p. 100) also need to be addressed. For longer simulation run times (should these be computationally possible), small errors in the high resolution models may also be amplified if they are cumulative throughout the simulation, and other dynamics that occur over a longer temporal or larger spatial scale may not be accounted for (Fagherazzi & Overeem, 2007).

2.5.2 Reduced-complexity models (RCMs)

A more recent modelling development, requiring considerably less computational power than the more sophisticated 2-d and 3-d physically-based models, is that of reduced-complexity models or RCMs (e.g. McMillan & Brasington, 2007; Nicholas, 2009). RCMs allow greater spatial and temporal coverage, and include models which are based on the cellular automaton concept (Wolfram, 1984, 2002). The first cellular models of river channels consisted of a regular model grid where flow routing was based on a simple rule-based function of local bed slope, and sediment transport was determined from a simple stream-power relationship (Murray & Paola, 1994; Murray & Paola, 1997); the Cellular Automaton Evolutionary Slope and River (CAESAR) model (Coulthard et al., 2000; Coulthard et al., 2002), and other more sophisticated versions of these cellular models, have since been developed (e.g. Hodge et al., 2007; Nicholas, 2009).

Unfortunately, as these models are based on simplified flow routing, if the flow hydraulics are not parameterised adequately the results may differ significantly from those produced using more complex physically-based models (Nicholas, 2009). The parameterisation may also be dependent on scale and grid, and hence it may not be possible to scale to a specific prototype (Brasington & Richards, 2007). These models also tend to neglect or simplify the way they account for momentum balance (e.g. turbulence is not accounted for). As cellular models were initially developed with no consideration for potential backwater effects (i.e based on flow rather than water levels), subaqueous sediment transport on river deltas was not included (e.g. Sun et al., 2002). An exception is the recent cellular model developed by Seybold et al. (2007). In these models a downstream sea level or lake level is specified (providing a common base for the topography), and an erosion/deposition law (along with other parameters), is included to enable the simulation of different delta types and delta channel/lobe switching.

Overall, RCMs are more suited to understanding the governing physical principles, and obtaining a potential range of outcomes (based on the dynamics), rather than directly reproducing a specific prototype since quantitative comparisons are difficult (Brasington & Richards, 2007). In spite of this, Seybold et al. (2009) were able to use these models to simulate a bird-foot delta (i.e. river-dominated delta where the channels have levees and the main distributary channel(s) extend into the receiving basin as long narrow 'fingers'), and make a scaled comparison to the Mississippi River.

For RCMs Kleinhans (2010, p. 312) notes the importance of "evaluating model output quantitatively against real data" since there will always be some doubt as to whether a numerical model is successfully simulating a natural system when there has been any degree of simplification of the system processes. The accuracy of the field data must also be considered (Kleinhans, 2010) as well as other sources of human error possible when developing numerical models.

2.5.3 Geometric models

Geometric models are the simplest type of model. These models have at least one sediment surface that has a defined geometry, and they are capable of both conserving sediment mass and simulating varying sediment supply rates (Paola, 2000).

The advantages of these models include that they require considerably less computer power; are adaptable (Paola, 2000); are capable of simulating many of the dominant sedimentary features (Paola, 2000); and are able to simulate over considerable periods of time (Fagherazzi & Overeem, 2007). However, care should be taken when using these models since geometric models do not rely on process-based constraints so a process that is physically impossible may be simulated (Paola, 2000) and complications may arise from not being able to modify the fixed geometry (Fagherazzi & Overeem, 2007).

Geometric models have been previously used to simulate 2d (i.e. width-averaged) delta progradation. For example, Kenyon & Turcotte (1985) noted that, for the deltas they were studying, the foreset profiles maintained a similar profile over approximately a century of delta growth. The geometric model produced for these river-dominated deltas had an exponential delta foreset profile, advancing via slope-dependent bulk sediment transport (i.e. sediment redistribution by creep and small slides, but not turbidity currents) into a low-energy basin, with a constant water depth.

Gilbert-type delta growth has also been modelled by applying numerical heat transfer methods. These models assume all sediment delivered by the fluvial delta topset to the width-averaged delta foreset is deposited evenly over the delta foreset as it progrades onto a fixed or subsiding receiving basin floor (e.g. Swenson et al., 2000; Voller et al., 2004; Swenson et al., 2005); the shoreline is a moving boundary, flow and sediment fluxes are either constant or vary as a function of time, receiving basin water level elevation and delta foreset slope are usually constant, and the simulation run times are long relative to flood return periods and river avulsions. Capart et al. (2007) extended this method to include a topset that extended upriver, and Lai & Capart (2007) also incorporated hyperpycnal flows which were compared successfully to experimental results. Additional simulations of deltas formed by hyperpycnal flows passing over a fixed, bedrock bed were also modelled numerically and with microscale models (Lai & Capart, 2009). More recently a 3-d cone-shaped delta has been simulated with progradation onto a sloping bed with both offshore and onlap moving boundaries representing the extent of the delta growth (Voller, 2010).

A physically-based width-averaged moving boundary model has also been developed that combines a turbidity current model (forming the bottomset) with a fluvial delta model prograding the topset and foreset (Kostic & Parker, 2003a). This model has been tested against flume experiments simulating progradation of a delta composed of sand and mud (Kostic & Parker, 2003b).

Gerber et al. (2008) also modelled delta progradation under the influence of turbidity currents using a simple width-averaged morphodynamic model based on fluid, momentum and suspended sediment conservation. In this model the delta foreset slope and shape change over time as the following processes take place: 1) the delta foreset slope steepens as sediment accumulates, 2) the steeper slope favours generation of turbidity currents and transfer of sediment to the base of the foreset slope, and 3) additional sediment accumulates on the newly deposited sediment at the base of the foreset slope, prograding the entire foreset slope over time. This cycle is then repeated.

Other conceptual geometric models have also been developed, for example, to analyse rates of shoreline advance for the Changjiang delta (Gao, 2007). For this model a range of sediment discharge and water depth scenarios, as well as fixed rates of sea level rise and sea-bed subsidence, were used to determine rates of shoreline advance.

2.5.4 Miscellaneous models

Numerical models have also simulated various other aspects of delta growth. For example, a mathematical delta model has simulated delta growth where the river channel exits into a receiving basin that is influenced by wave action (Komar, 1973). For this model the redistribution of sediment along the adjacent shoreline determined the delta planform geometry.

Parker et al. (1998) also developed a simple theoretical numerical model that simulated (over a time scale greater than time taken to avulse across the full fan) mean bed slopes and elevations for alluvial fans formed by sheet and channelized flows. This model was tested using experimental data (Whipple et al., 1998).

2.6 Summary of relevant details from literature

The behaviour of braided rivers has been examined using field studies, physical models and numerical models. The following findings were of particular interest for this study:

- Slightly elevated bars or mid-channel islands tended to be relatively stable compared to the adjacent low-lying braid belt (Hicks et al., 2002).

- Over time, sediment transported by highly mobile, and continually migrating, braided river channels will be distributed relatively evenly across the entire width of any downstream prograding delta (Postma, 1990).

- As total flow increases, the 2 to 3 largest channels (out of the total of 7 to 8 braided channels) tended to carry an increased portion of the flow, while the flow in the other channels (whose location also changes with increasing flow) remained relatively constant (Mosley, 1982). A field survey of the Rakaia River in New Zealand by Mosley (1983) also showed that the

largest two braided channels carried the majority of the flow (with the largest channel carrying between 47 to 93% of the total flow, and the second largest channel between 3.3 to 39%). Using physical models, Egozi and Ashmore (2009) also noted that there was usually one main active channel transporting most of the bedload, while other channels mainly diverted flow into and out of this main active channel; for these experiments the braiding index for the active channels (i.e. with bedload transport occurring) was ~0.4 times the braiding index for the total number of channels carrying flow. The braiding index is defined as the number of river channels in a cross section. Field surveys have also shown that, within the 1 or 2 active channels, bedload transport is limited to only a small fraction of the total wetted width of each active channel (generally between 10 to 40%), with sediment transport increasing with increasing flow magnitude above the threshold for movement (Ashmore et al., 2011).

- There is a good relationship between peak flood water level, active width and mean bed elevation changes (Bertoldi et al., 2010). Note: active width was considered to be a better indicator than wetted width since observations showed that for bankfull flood flows ~40% of the braidplain experienced no significant morphological change.

- Flow pulses (events occurring on average 1^+ times per year) generally cause some bank erosion and tend to only affect a small number of active branches through sediment redistribution, while flood pulses (i.e. return periods of 2^+ years) are more likely to rework the entire braided network and include bifurcation and confluence dynamics (e.g. Bertoldi et al., 2010). Hickin (1989) noted that, for large flood events in the Squamish River (from 1956 to 1986), 18.5% of the annual sediment load tended to be transported over a total time period of less than ~18 hours (or 0.2% of the time).

- Riparian vegetation, that establishes itself on bars and other areas of the braidplain that are exposed during low flows (i.e. between flood events), has the ability to direct flood flows into the favoured/established main channel and slowly transform a braided river system into a single-channeled meandering river system (Tal & Paola, 2010); this newly-established meandering channel also develops a bankfull geometry by adjusting itself so that cyclic experimental flood flows are generally contained within the channel (Tal & Paola, 2010).

- During flood events, single-thread channels have been observed to widen, and 'temporarily' transform into braided river systems, in reaches where the river system is unconfined (Warburton, 1994). Braided river reaches tend to have a greater transport capacity, due to the greater shear stress variation (e.g. created by converging and diverging flows) and consequent migration of channel formations, whereas single-thread channels are more likely to have a more stable, armoured channel configuration (Warburton & Davies, 1994).

Several publications (e.g. Davies, 1987; Knighton, 1998; Robert, 2003; Kleinhans, 2010) provide further detailed descriptions of the fluvial processes and problems associated with the analysis of a braided, gravel-bed river. For braided river reaches bounded at the lower limit by a prograding river delta, the river system is also complicated by the fact that it is continuously adjusting to the progressive aggradation of the growing delta.

Some of the main findings for braided gravel-bed river deltas are also summarised below:

- The density of the sediment-laden river water, relative to the density of the basin water, is one of the main factors that will determine how sediment is transferred from the river system onto the delta.

- The delta foreset slope is at or less than the angle of repose for the submerged sediment, with delta slopes able to be reduced significantly by external forcings such as turbidity currents (e.g. Kostic et al., 2002).

- Even if river flows, sediment supply rates, and receiving basin levels remained constant, over short time periods the rate of delta progradation is likely to vary due to the fluctuating rate at which the braided river system and delta topset stores and releases sediment (Kim et al., 2006).

- When receiving basin levels are high during flood events, sediment is likely to be deposited in the lower reaches of the river channels approaching the receiving basin; this sediment is likely to be transported onto the delta foreset once receiving basin levels are low relative to the river levels (Gilbert, 1973, 1975).

- Deposition along braided gravel-bed river delta topsets and foresets is likely to be 'laterally non-uniform' due to frequent channel switching (Kleinhans, 2005a, p 223).

- The effect of downstream receiving basin levels on braided channel switching behaviour does not appear to be well understood, although it is likely that avulsion is influenced by both upstream aggradation and a downstream backwater ("morphodynamic backwater") effect (Hoyal & Sheets, 2009).

- Unpredictable delta morphology can occur when there is a change in one of the interrelated variables influencing braided gravel-bed river delta progradation. For example lowering the receiving basin water level (Mosley, 1984).

- The difficulties in obtaining field data for delta foresets means there has been relatively little research related to delta foreset processes. Recent physical modelling studies help to address this issue - mainly using narrow flumes to examine longitudinal delta profiles.

3 STUDY AREA

The Otago region of New Zealand is bounded by the Southern Alps mountain range to the west, and the Pacific Ocean to the east (Figure 3.1, insert). As a result, the Otago region has many steep, mountainous catchments subjected to high intensity rainfall. These mountainous catchments are capable of generating large volumes of coarse-grained sediments which are transported along braided river systems and deposited in downstream water bodies which include natural lakes, hydro lakes and larger river systems.

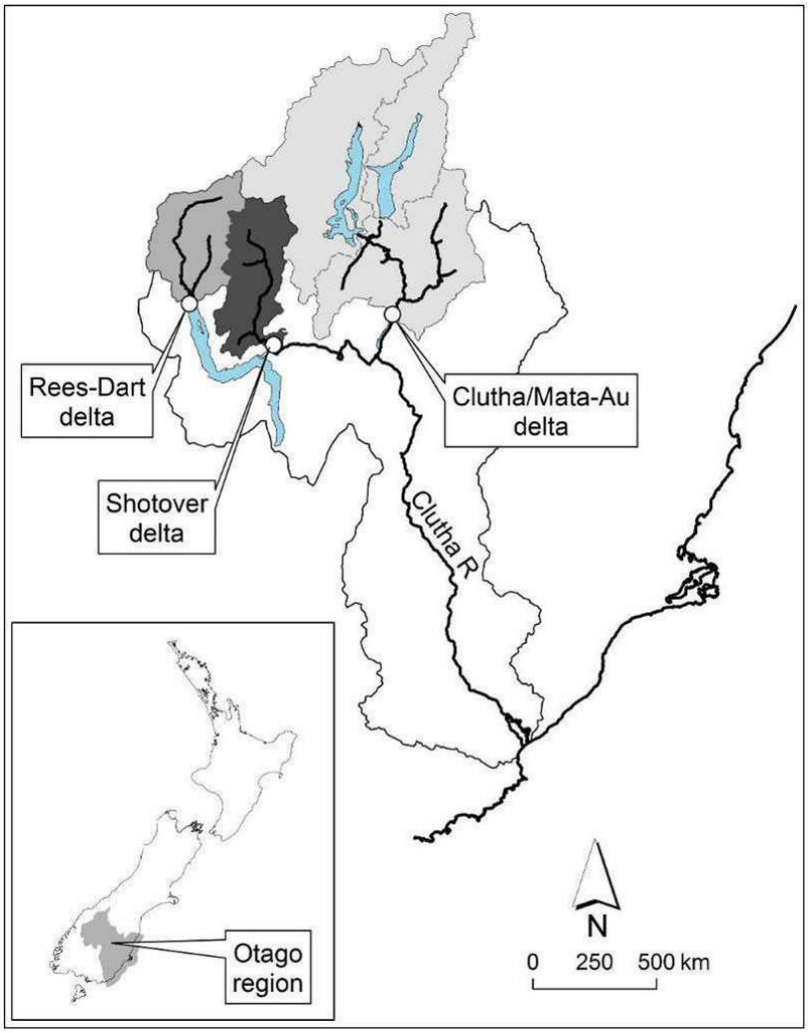

Figure 3.1: Location of Otago study deltas

The growth dynamics and management of several coarse-grained braided river deltas in the Otago region are of particular concern for local authorities due to the potential implications of land use, infrastructure development and hazard management. Figure 3.1 shows the location of three deltas (i.e. Rees-Dart, Shotover and Clutha River/Mata-Au) that are of particular interest at present. All of these

deltas lie within the Clutha River catchment, which has the largest river catchment area (20 582 km^2 at Balclutha) and largest mean flow (561 m^3/s between 1930-98) in New Zealand (Waugh et al., 2000). Despite all three deltas being located in the same area, the growth process of each delta is unique, allowing various aspects of delta growth to be examined. For instance, the receiving basin for the Rees-Dart delta is a deep natural lake, while the Clutha River/Mata-Au delta has formed in the Clutha riverbed (upstream of the recently constructed Clyde dam), and the Shotover delta has formed at the confluence with the Kawarau River. It should also be noted that, although the upstream catchments of each of these deltas produce large volumes of sediment, the Clutha River/Mata-Au delta lies downstream of two lakes that trap the sediment generated in the Southern Alps.

A detailed study of both the Rees-Dart and Clutha River/Mata-Au deltas is undertaken as part of this study analysing the growth dynamics of braided gravel-bed river deltas. Section 3.1 provides an overview of the Clutha catchment while Sections 3.2 and 3.3 give detailed information specifically for the Rees-Dart and Clutha River/Mata-Au deltas, respectively. A summary of estimated river characteristics for the Dart, Rees and Clutha rivers is summarised in Table 3.1, and Appendix A provides a location map for the relevant water level, flow and rainfall sites discussed in this chapter.

Table 3.1: Typical Otago river characteristics

Characteristic	Dart River	Rees River	Upper Clutha River
Mean channel bed slope, S (m/m)	0.003	0.003	0.002
Mean of annual maximum flood flow, Q_{mam} (m^3/s)	1000	310[1]	880[2]
Maximum recorded flow, Q_{max} (m^3/s)	1470	475	-
Mean water depth, h (m)	1-1.3	1-1.3	2
Mean channel width, W (m)	400	130	135
Mean grain size, D_{50} (mm)	13	13	24
Width:depth ratio (-)	300-400	100-130	68
Relative depth (D_{50}/h)	0.01	0.01	0.01
Mean velocity, v (m/s)	1.9-2.5	1.8-2.4	2.2
Chezy friction coefficient, C ($m^{0.5}/s$)	31-46	29-44	28
Froude number, Fr (-)	0.5-0.8	0.5-0.8	0.4
Shear stress, τ (Pa)	29-38	29-38	59
Shields Number, θ (-)	0.14-0.18	0.14-0.18	0.15
Backwater adaptation length[3], λ_{BW} (m)	60-110	60-100	120
Adaptation length of bed disturbance[3], λ_s (m)	300-400	300-400	500

[1] Calculated as being 0.31 * Dart flow
[2] Estimated by summing the Cadrona at confluence and Lindis at Peak flow records.
[3] For a summary of the equations used to calculate the adaptation lengths see Kleinhans & van den Berg (2011).

3.1 Clutha River catchment

Within the upper Clutha catchment there is a significant amount of schist bedrock. This material is easily weathered to form a thin layer of unconsolidated rock debris that, if saturated by high intensity rainfall, can lead to slope failures (e.g. landslides). This, in turn, can trigger debris flows in steeper tributaries. The bedload sediment input to the alluvial valleys is therefore likely to be in the form of 'pulses' (e.g. debris flows and landslides) rather than a continuous sediment supply (McSaveney & Glassey, 2002; Cui et al., 2003). For example, debris flows are likely to have occurred in over half of the upper Rees valley tributaries during a January 2002 storm. During this storm event, with a return period likely to be much greater than 5 years, high-intensity rainfall fell on an already saturated catchment (McSaveney & Glassey, 2002). As the Otago region is tectonically active, large earthquakes are likely to increase the sediment supply to catchments. Additional sediment is also supplied to the alluvial valleys and deltas from other sources including riverbank erosion and (historically) mining activity (Ministry of Works and Development, 1977b); gravel is also extracted from various riverbed locations for construction purposes.

Braided gravel-bed rivers store, transport, and rework sediment as it moves from the point of entry into the river system, downstream to the river delta. At the delta the upstream signal, from any bedload sediment pulse, is likely to be damped, while the input frequency of wash load from the catchment is still likely to be strongly observed at the delta (Murray Hicks, personal communication).

Upstream of both the Rees-Dart and Clutha River/Mata-Au deltas the river systems form braidplains while the Shotover delta has a fan delta configuration. Field observations of riverbeds, together with examination of photos taken during flood events, suggest that the sediment arriving at the study deltas consists of suspended sediment with a bedload of bimodally-distributed gravel (i.e. the gravel contains a high portion of both large cobbles and finer sand, but has a smaller proportion between these two sizes). Previous studies of New Zealand gravel-bed rivers (e.g. Clausen & Plew, 2004) have also shown that there is a good relationship between calculated bed-moving flows and recorded mean annual maximum flows (rather than smaller median or mean flows), suggesting that most bedload material is likely to be transported during flood events.

The largest flood events in the upper Clutha catchment tend to be created when there are strong north-westerly air flows preceding a frontal system (Waugh et al., 2000). These are often accompanied by 'a blocking anticyclone to the north or east of New Zealand, and frontal systems lying NNW to ESE across the southern part of the South Island' (Waugh et al., 2000, p8). For the November 1999 flood, a frontal system hovered over the Fiordland-Otago region for an extended period of time producing 72 hours of high-intensity rainfall centred on the area to the west and south of Lake Wakatipu (Waugh et al., 2000). This event also followed storms in mid-October and early November (Waugh et al., 2000). In general, the larger flood events tend to occur under these conditions when there is an extended

period of very heavy rainfall over the upper catchment areas combined with high antecedent lake levels and a series of storm events in close succession (Waugh et al., 2000); snow melt can also exacerbate the flooding. A detailed description of historic flooding in the Clutha catchment, including information on the largest flood events (e.g. September 1878, October 1978, January 1994, December 1994, November 1999, etc.) is summarised in Waugh et al. (2000).

A recent study, analysing historic precipitation trends and rainfall variability, has identified that between 1921 and 2003 there has been an increase in wet periods for the North, Westland and Southland regions of the South Island of New Zealand (Mojzisek, 2005). Future climate change impacts for the Clutha River have also been modelled (Poyck et al., 2011). Their study showed that modelled future scenarios (for 2040 and 2090) had an increase in annual precipitation and total streamflow volume over the Clutha catchment, while total snowmelt decreased. The combination of less precipitation contributing to snow accumulation (i.e. more precipitation directly contributing to streamflow), and an increase in winter and spring precipitation, is likely to result in a significant increase in winter and spring flows to the Rees-Dart, Shotover and Clutha River/Mata-Au deltas. Further downstream, at Balclutha, annual total streamflow increases are estimated to be ~6% (2040) and ~10% (2090). Given that a substantial proportion of the Rees-Dart, Shotover and Clutha River/Mata-Au delta catchments are predicted to have an increased precipitation of the order of 20 to 40% in winter and spring by 2090, these catchments are particularly susceptible to the increased streamflows at this time of year. Meanwhile, summer and autumn streamflows are likely to remain relatively unchanged throughout the catchment.

Deltas forming in deep, glacier-fed lakes are also of interest with regard to the stability of delta foreset slopes and the potential for a tsunami or water surface disturbance. For the Rees-Dart delta it has previously been observed that *'During the summer of 1937-38 a sharp earthquake shock was felt by a group on the Glenorchy wharf (Dr R. W. Willett, pers. comm.). Within minutes, the surface waters of the lake a few chains distant, over the delta edge, became violently turbulent and discoloured by sediment; the disturbed area was marked by extensive bubbling of gas. A slump had evidently been triggered by an earthquake'* (Brodie & Irwin, 1970, p. 492)). There are also several documented cases of large underwater landslides being generated by the failure of fan-deltas or river deltas. For example, in Canada, a 400 m by 60 m area of a fan-delta generated a ~3 million m^3 underwater landslide and a 2 m high tsunami in October 1998 (Schwab, 1999), and in April 1975 an 8.2 m high tsunami was measured after 25 million m^3 of material slumped along the lower Kitimat river delta.

By studying the varying drainage basin and receiving basin characteristics, the main factors controlling delta growth can be more easily identified and modelled. A description of the study deltas is given below.

3.2 Rees-Dart river delta

The Rees-Dart River delta lies at the head of Lake Wakatipu. The Dart and Rees braided river systems have catchment areas of 632 km^2 and 405 km^2, respectively. As these coarse-grained rivers approach Lake Wakatipu they form a river delta approximately 2.5 km wide with a foreset height of over 55 m in places (Figure 3.2 and 3.3).

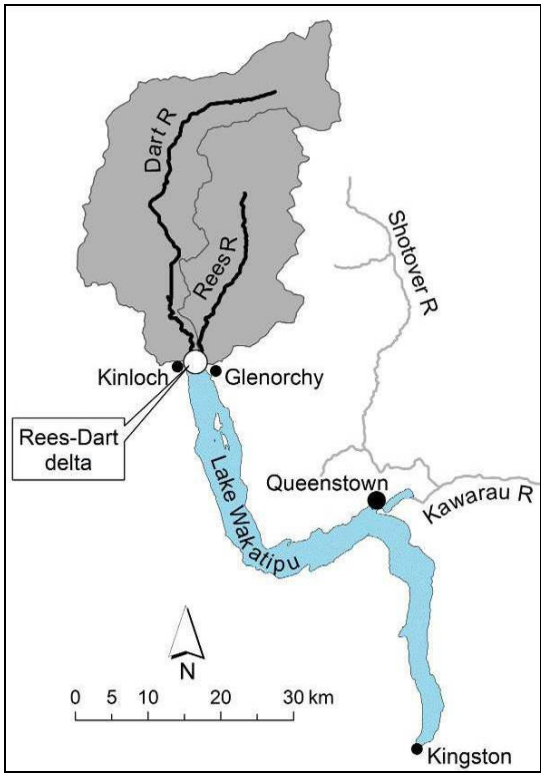

Figure 3.2: Location map for the Rees-Dart delta

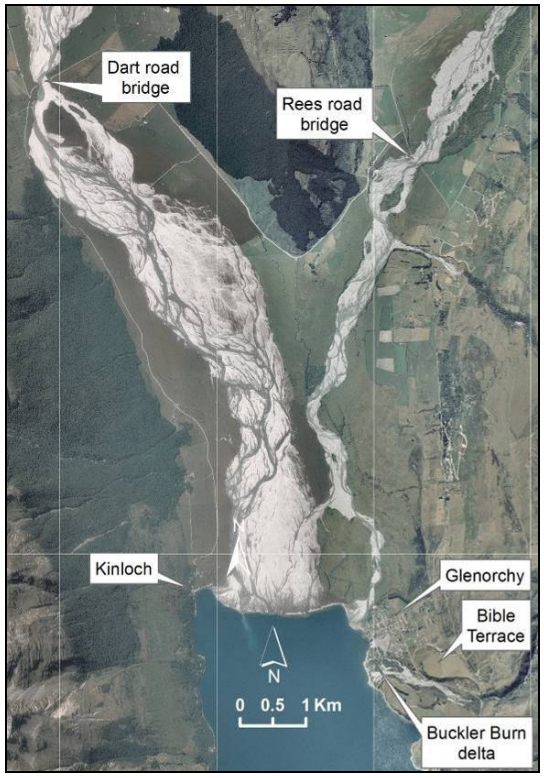

Figure 3.3: Aerial photography of the Rees-Dart delta in 2007

The headwaters of both rivers lie in the steep-sloped and tectonically-active Southern Alps. The combination of high-intensity rainfall, seismicity and foliated, highly erodible, fine-grained schist bedrock lead to high erosion rates and large volumes of sediment being transported along the river system to the Rees-Dart river delta.

Although the Rees and Dart catchments are relatively remote and 'untouched', there has been human activity in the area for some time. The first inhabitants of this rugged land at the head of Lake Wakatipu were West Coast Māori who used to undertake trips over the Southern Alps mountain range, to the Dart and Routeburn river valleys, in search of pounamu (a grey-green nephrite rock valued for carving ornaments, tools and weapons). Approximately 20 historic Māori camp sites have been

discovered beside the Rees and Dart rivers as well as on Pigeon Island, 7 km to the south of the Rees-Dart delta on Lake Wakatipu (http://www.glenorchyinfocentre.co.nz/history.html).

In the early 1860s European settlers moved into the Rees and Dart river valleys primarily to graze cattle. A series of mainly unsuccessful gold mining attempts closely followed in the Rees River, Buckler Burn and Precipice Creek river beds. In the 1880s underground mining in the upper Rees valley had some limited success, but a gold dredge in the Dart River (1890 to 1904) was not successful (URS, 2007). Scheelite (used in the production of tungsten) was discovered in the Richardson Mountains, behind Glenorchy, in the 1880s. It was mined at altitudes of up to 2000 m and then transported down to Wyuna Station where the scheelite was extracted (http://www.odt.co.nz/your-town/glenorchy/26979/scheelite-miners039-stories-told). This mining continued sporadically until the 1970s (URS, 2007).

In the late 1800s timber from the lower slopes of the Humboldt Mountains was milled and exported by steam ship to Queenstown (URS, 2007). At this time steam ships also brought tourists to Glenorchy and Kinloch to visit the Routeburn and Paradise valleys. In 1962 the road from Queenstown to Glenorchy was completed, improving access to this beautiful area that also acts as a 'gateway' to the Mount Aspiring National Park which was established in 1964. Spectacular scenery from the area is shown in the recent, high profile, movie 'Lord of the Rings' so this has also fuelled tourism in and around Glenorchy.

Unfortunately the small township of Glenorchy is 'sandwiched' between the Rees-Dart delta and the Buckler Burn delta (Figure 3.3). As the growth rates of these deltas are unknown, the time-frame in which they will have a significant impact on the local community and infrastructure, due to their inevitable progradation into Lake Wakatipu, is also unknown.

3.2.1 Geological setting

Suggate (1990) identified nine periods of glaciation for the South Island over the last 700 000 years. The extent of these glaciers decreased over time with the earlier glacier advances having an elevation of up to 1 km above the existing level of Lake Wakatipu compared to only 100 m above the existing lake level for the most recent glacial advance (Turnbull & Forsyth, 1988). The maximum advance of the most recent glaciation period ended about 18 000 years ago (Suggate, 1990). At this time glaciers along the Southern Alps extended down into the valleys and the schist bedrock and surface materials, deposited by earlier glacial and interglacial periods, had mainly eroded (Barrell et al., 1994). In the Wakatipu area, the Wakatipu Glacier extended to the area that Lake Wakatipu now occupies.

Approximately 14 000 years ago retreat of glaciers had begun and New Zealand moved towards a warmer interglacial period (Suggate, 1990). As the Wakatipu Glacier retreated, large volumes of gravel and sand accumulated in the Dart and Rees River valleys in the form of outwash plains

(Turnbull & Forsyth, 1988). Raised beach and delta deposits around Lake Wakatipu indicate that the lake originally formed with a water surface elevation considerably higher than it is today (Barrell et al., 1994). It appears that terminal moraine deposits initially held the lake at an elevation of 400 m asl, with the outflow route through the Kingston moraine gradually being incised until the schist bedrock was reached at an elevation of approximately 355 m (Barrell et al., 1994). The present lake level of ~310 m was reached after the Kawarau River outlet formed, providing a lower elevation outlet for the lake (Barrell et al., 1994). Evidence of this final fall in lake level is present in the Glenorchy area in the form of the Bible Terrace. As the lake level fell, the Buckler Burn adjusted its gradient by incising into the delta it had formed at the higher lake level (Barrell et al., 1994).

During periods of high-intensity rainfall large volumes of sediment are transported into the Rees-Dart river system by debris flows which are known to occur in the upper Rees and Dart catchment areas (McSaveney & Glassey, 2002). These debris flows occur when an accumulated layer of loose, eroded schist bedrock material (up to several metres thick), overlying a steep slope, becomes saturated. Initially a shallow landslide will form and accelerate rapidly along a preferential flow path. As it accelerates it is fed by additional water and debris resulting in a debris flow. Debris flows approximately 2 m high were observed in the Rees upper catchment in January 2002 (McSaveney & Glassey, 2002). Sediment is also transported into the river system by other processes including bank erosion.

Landslides also occur in the Rees and Dart catchments and may include anything from large blocks of schist bedrock through to highly eroded "chaotic debris" mobilised by "transitional slides, rotational slumps, rock flows, debris flows, and combinations thereof" (Barrell et al., 1994, p. 22). Rock avalanche events, capable of contributing large volumes of sediment (e.g. ~22.5×10^6 m^3), are known to have occurred as recently as several hundred years ago (McColl & Davies, 2011). In this particular event it is likely that the Dart River was temporarily dammed by the rock avalanche deposit.

3.2.2 Dart River system

3.2.2.1 Catchment

The Dart catchment is enclosed by the Humboldt Mountains to the west, and the Barrier and Snowdrift Ranges to the north. The Forbes Mountains also provide an eastern divide between the Rees and Dart catchments. Prehistoric glacial erosion in the westward-dipping schist bedrock of the catchment has resulted in a landscape that consists of 'slabby slopes on the eastern side of the valley, and steep cliffs on the western side' (Bishop & Forsyth, 1988, p. 30).

The source of the Dart River is the Dart glacier – a valley glacier surrounded by mountains at the head of the upper Dart valley. The 'outflow' from the glacier basin (or neve) is an icefall that passes the glacial material down the valley into the 0.5 km wide by 3 km long trunk section of the glacier, of which the lower portion is overlain by rock debris (Bishop & Forsyth, 1988). A major source of rock

debris for the Dart glacier is avalanches, which also add additional snow to the glacier. Other glaciers in the upper Dart catchment include the Whitbourn and Tyndall glaciers.

In 1986 the Dart glacier terminus (or snout) was located at an elevation of 1050 m above sea level (Bishop & Forsyth, 1988), with the Dart River flowing downstream from this terminal face. The 1850 terminal face was located approximately 5 km downstream from the 1986 location (Bishop & Forsyth, 1988), indicating a relatively rapid retreat of the glacier. If the Dart glacier continues to retreat with temperature rise, the glacier will not have the same ability to store water in the form of ice over the winter months and, consequently, there will be less ice-melt over the summer months; this will result in higher than usual river flows in winter and lower flows in summer (Bishop & Forsyth, 1988).

3.2.2.2 Rainfall

In the Dart catchment the only permanent rainfall recorder is the Dart at the Hillocks (Site 487302), located ~9 km upstream from Lake Wakatipu at the Dart road bridge. This site has been owned and operated by ORC since 21 August 1997. The maximum daily rainfall recorded at this site was 128.8 mm on 15 November 1999. The mean annual rainfall for the 1998 to 2009 time period was 1745 mm, and the maximum annual rainfall recorded was 2191 mm (in 1998). The Dart River is approximately 58 km in length but there are no raingauges located in the upper catchment where significantly higher rainfall can occur. An estimate of the maximum 24 hour rainfall total that is exceeded 20% of the time (i.e on average exceeded once in 5 years) has been derived for the Otago region as part of the "growOTAGO" Project (http://growotago.orc.govt.nz). The maximum 24 hour rainfall totals were derived for the summer (January to March), autumn (April to June) and spring (October to December) seasons but excluded winter due to complications arising due to the impacts of snow. Table 3.2 shows the area-weighted, 24-hour maximum, 5-year return period rainfall for the Dart catchment as derived by Srinivasan et al. (2007) using the growOTAGO data (based on regional climate data for the 1970 to 2001 time period).

Table 3.2: Dart catchment area-weighted, 24-hour maximum, 5-year return period rainfall (from Srinivasan et al., 2007)

	Summer (Jan – Mar)	Autumn (Apr – Jun)	Spring (Oct – Dec)
5-year return period rainfall	179	74	164

3.2.2.3 Water level/flow

In the Dart catchment the only permanent water level/flow record is the Dart at the Hillocks (Site 1075272), which is owned and operated by ORC. This site has only been operating since 12 June 1996 but the ORC archives also have a large number of gauging cards for the Dart River which could potentially be used to extend the existing Dart River flow record.

Between 12 June 1996 and 1 March 2012 the minimum and maximum flows (derived from the 15-minute instantaneous water level record) were 6 m^3/s and 1469 m^3/s, respectively. Figure 3.4 shows the seasonal variation in flows between July 1996 and June 2009. Generally, May through to September has smaller average monthly flows compared to flows recorded from November through to March. This coincides well with the trends in the seasonal 5-year return period rainfall data shown in Table 3.2.

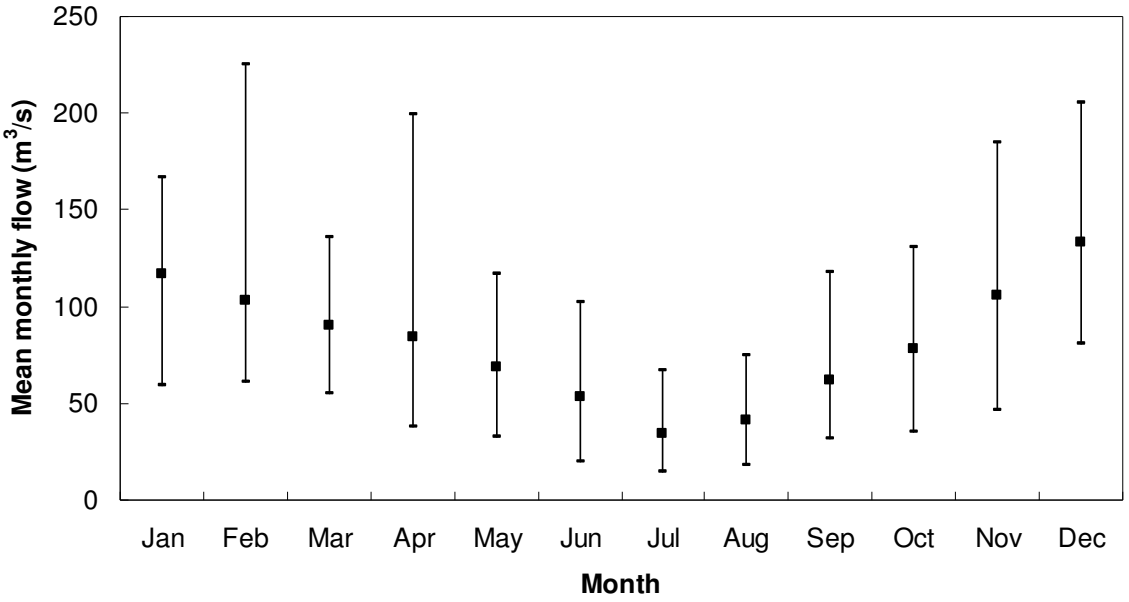

Figure 3.4: Dart River (Site 1075272) mean monthly flows for 1997 to 2011

Statistical analysis of the 16-year flow record estimated that the February 2011 peak flow of 1469 m^3/s had an annual exceedence probability (AEP) of between ~1.4% (Log-Pearson Type 3 distribution) and 5% (Gumbel distribution); the second largest peak flow of 1267 m^3/s, in April 2010, had a ~11 to 13% AEP for all of the main distributions.

3.2.2.4 Flood characteristics

During flood events the Dart River tends to rise rapidly from its baseflow to the flood peak within a period of approximately 12 hours. Meanwhile, Lake Wakatipu rises at a considerably slower rate. For example, during the November 1999 flood it took 90 hours for the lake to rise 2.25 m while the Dart River rose from 82 to 976 m^3/s over the first 13 hours of this same time period. This flood event maintained high Dart River flows for a considerable length of time but the peak lake level still occurred on the falling limb of the flood event at a flow of ~100 m^3/s.

Figure 3.5 shows 2-hourly averaged Dart River flows plotted against the Lake Wakatipu levels for 1999 (including November 1999 flood event) and 2006 (typical year). Both years clearly show the trend of the Dart River peak flow being reached during a period of relatively constant lake levels.

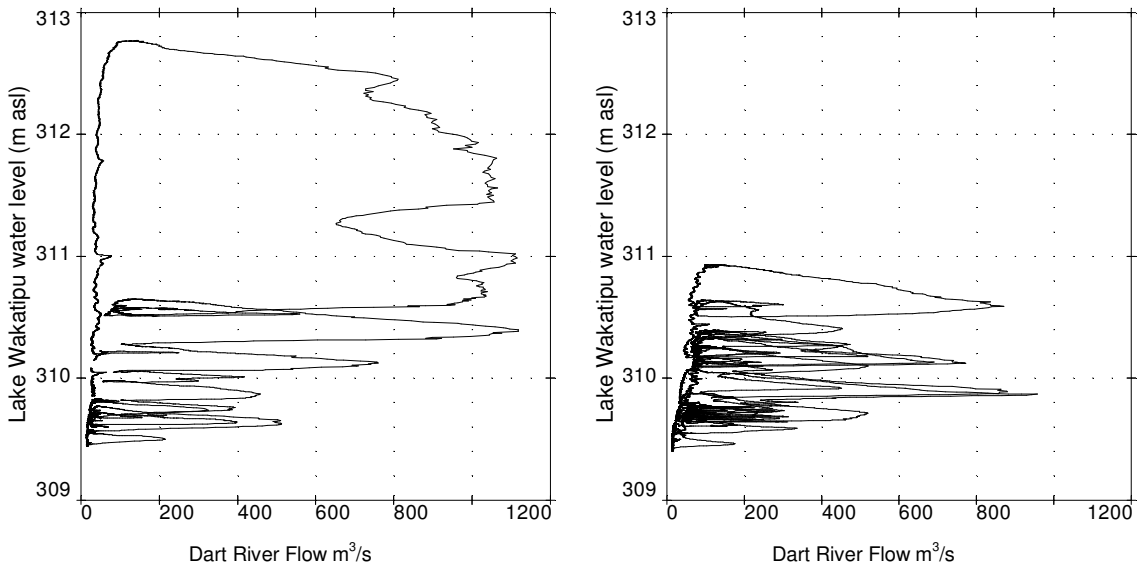

Figure 3.5: 2-hourly averaged Lake Wakatipu water level (m asl) versus Dart River flow (m^3/s) for (a) 1999 and (b) 2006

3.2.2.5 Riverbed sediment

Sediment samples from shallow pits, including both surface and subsurface material, were collected on 13th November 2007 from the Rees and Dart Rivers. These samples were collected at the road bridges (shown in Figure 3.7), and also at the Kinloch shoreline where the Dart River enters Lake Wakatipu. All samples were collected during a period of relatively low Dart River flows of between 75 and 79 m^3/s. The Rees River and Dart River (Site 1) samples were collected adjacent to the active river channel, while the Dart River (Site 2) sample was collected ~50 m from the waters edge on a slightly more elevated area of the riverbed. The median sediment size (D_{50}) for these road bridge samples ranged from 11 to 15.5 mm (Figure 3.6).

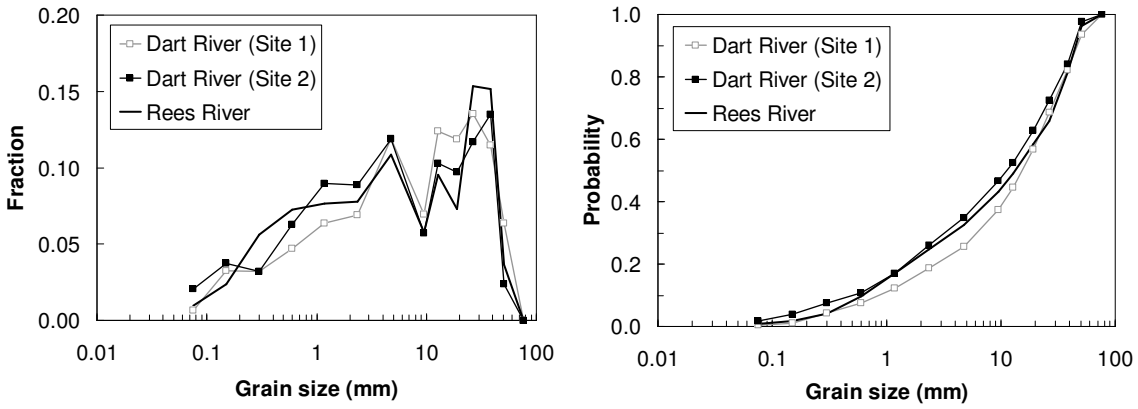

Figure 3.6: Dart and Rees riverbed sediment sample size distributions for road bridge sites

Further downstream at the Dart River delta, along the Kinloch shoreline at the end of the Kinloch 'spit', the delta sediment had a D_{50} of 2.3 to 3.3 mm. It should be noted that all of the sediment samples were only 5.8 to 13.1 kg. Given the relatively small size of the samples, and the relatively large size of some of the particles, the particle size distributions derived from them are only intended to be indicative rather than precise.

Gravel extraction occurs sporadically in both rivers, but the volumes extracted are considered negligible relative to the 1966 to 2007 estimated average annual rate of sedimentation at the Rees-Dart delta of $0.27 \pm 0.03 \times 10^6$ m^3/yr (Wild et al., 2008). As both the Dart and Rees Rivers deliver sediment to the portion of the delta referred to as the Dart delta (i.e. west of the grassed island), it is not possible to determine the individual sediment contribution of each river.

Although there does not appear to be any further information on the Dart River bedload characteristics, high spatial density terrestrial laser scanning (TLS) of a 2.5 km by 0.7 km reach of the Rees River has recently been captured upstream of the Rees River road bridge (Williams et al., 2011). This TLS data could be used to obtain further information on grain roughness and riverbed characteristics (Williams et al., 2011).

3.2.2.6 Suspended sediment and water temperature characteristics

Between February 1979 and June 1981 one litre samples of Dart and Rees River water were analysed to determine suspended sediment concentrations; water temperatures were also measured (Pickrill & Irwin, 1982). A 5-point moving mean showed the lowest suspended sediment concentrations for the Dart River occurred in the 1979 and 1980 winter period (June to August) while highest concentrations were recorded during the spring and summer periods (Pickrill & Irwin, 1982). Dart River suspended sediment concentrations were generally less than those measured for the Rees River with the exception of the months February to May (Pickrill & Irwin, 1982). During the peak of the 2-3 December 1979 flood, suspended sediment concentrations in both rivers reached approximately 2300 mg/L (Pickrill & Irwin, 1982). River water temperatures during the flood events that occurred were relatively constant, although the observed temperature varied between seasons. Winter river flood water temperatures were generally around 4-6 ºC while summer temperatures were slightly higher at 6-8 ºC (Pickrill & Irwin, 1982). At lower river flows water temperatures varied throughout the day, as well as seasonally, and summer temperatures reached as high as 20 ºC in January (Pickrill & Irwin, 1982).

3.2.2.7 Bank protection works

The earliest documented bank protection works for the Dart River date back to the 1950s. Bank protection works have mainly included 'log retard' protection structures and floodbanks along the true right bank (TRB) between the existing road bridge and the lake. These protection works were constructed to protect both leasehold river flat land and the Kinloch-Routeburn road. Although a 500 m long floodbank (on the TRB ~2.3 km downstream of the road bridge, Figures 3.7 and 3.9) has been

effective for current bed levels, Otago Catchment Board records indicate that earlier attempts to prevent farmland erosion in the lower reaches of the Dart River were eventually fruitless; bank protection works appear to have been regularly compromised or completely destroyed during flood events.

Post-1966 aerial photography (Figure 3.7) shows bank erosion has resulted in the loss of over 1.2 km^2 of farmland along the true right bank (TRB) of the Dart River over the 5 km immediately upstream of the lake – including the complete destruction of several bank protection works. Figures 3.10a to 3.10c show the erosion currently taking place along the Dart River TRB (in April 2011). Assuming an average erosion depth of ~1 m (estimated from LIDAR data), this represents ~10% of the total sediment deposited on the delta between 1966 and 2007.

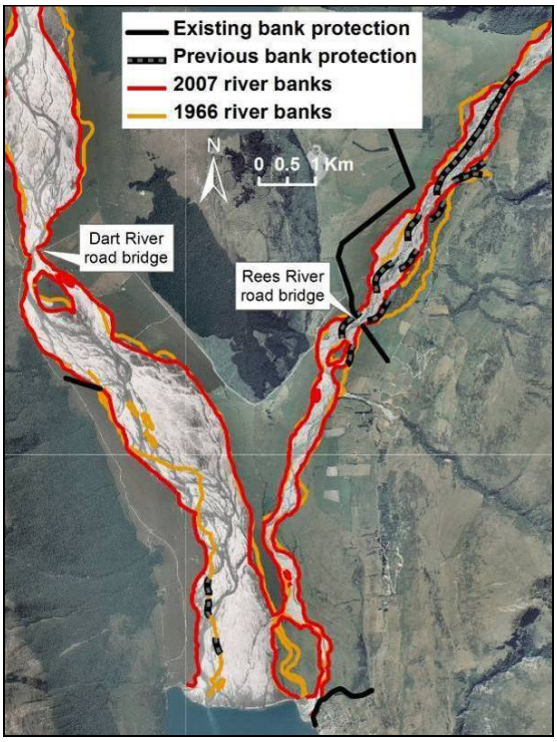

Figure 3.7: Dart and Rees River 'active' channels and flood protection works

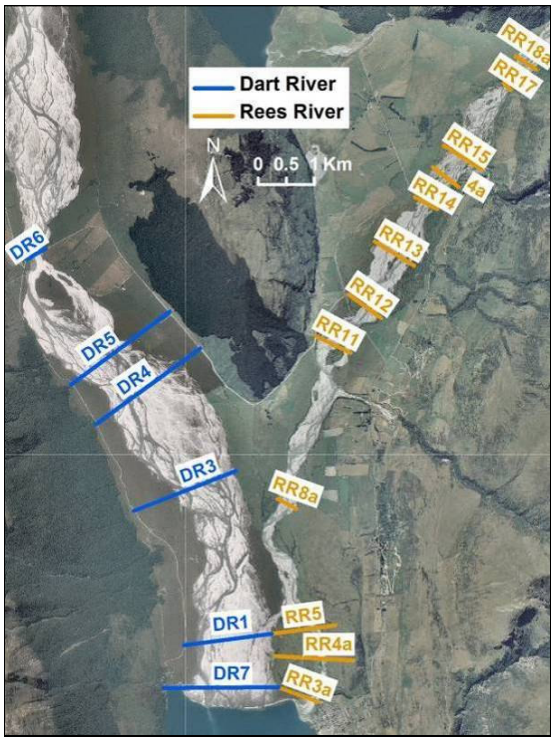

Figure 3.8: Dart and Rees River cross section survey locations

3.2.2.8 Cross section monitoring

In 1990 the Otago Regional Council (ORC) began monitoring cross sections on the Dart River between the road bridge (cross section DR6) and DR1 (Figure 3.8). In 2007 an additional cross section (DR7) was added closer to the lake but, with such a short record and sparsely placed cross sections, it is difficult to make any definitive conclusions regarding aggradation or degradation of the riverbed or delta topset. This information does provide some information about the relative river bed and bank levels though.

Figure 3.9: Landward face of Dart River floodbank located on the true right bank approximately 2.3 km downstream of the Dart road bridge

(a) Approximately 1.5 km upstream of the Kinloch waterfront, looking upstream at river banks 2^{+}m high

(b) Approximately 1.5 km upstream of the Kinloch waterfront, looking downstream at river banks 2^{+}m high

(c) Approximately 0.5 km upstream of the Kinloch waterfront, looking downstream at river banks 1^{+}m high

Figure 3.10: Bank erosion at various locations along the Dart River TRB

It should also be noted that an adjustment of +365.03 m has been made to the Dart local datum used for the surveys. This was determined by matching up points surveyed for both the Dart cross section (DR1) with points surveyed for the adjoining Rees River cross section (RR5).

3.2.2.9 Weed control

A programme to control weed growth (i.e. gorse and broom infestations) includes maintenance of 900 hectares of the Dart River between the road bridge and Lake Wakatipu (Landward Management Ltd, 2009). Along the true left bank (TLB) of the Dart River there are large, dense, infestations and regrowth is also present near the Kowhai and Turner Creek mouths on the TRB (Landward Management Ltd, 2009).

3.2.3 Rees River system

3.2.3.1 Catchment

The Rees catchment is bounded by the Richardson Mountains, to the east, and the Forbes Mountains to the west. At the upper limit of the catchment the Rees Saddle (1505 m above sea level) is the lowest point separating the upper Rees and Dart catchments.

Unlike the Dart River, the Rees River does not originate at a glacier (although there are several glaciers on the upper slopes of the Forbes Mountains, including the Earnslaw glacier). At an elevation of 464 m, the Rees Valley Station raingauge recorded minimum, mean and maximum annual rainfalls of 1203 mm, 1529 mm, and 1880 mm, between 1988 and 1998 (Devgun & Bowler, 1999). At present no raingauges have been installed at higher elevations in the upper Rees catchment where significantly higher rainfall can occur.

During periods of high-intensity rainfall, debris flows are known to have occurred in a significant number of the active channels in the upper Rees catchment. For example, on 3 January 2002 debris flows occurred in over half of the upper Rees River tributaries when shallow, rainfall-initiated landslides developed into debris flows (McSaveney & Glassey, 2002). Rainfall recorded at the near-by Dart Hut (approximately 3.3 km north of the observed debris flows) was 240 mm over the 24 hour period commencing at 8am on 3 January 2002. Although this is a volume of rain expected every 2 to 3 years at that site, the extent of the erosion in the upper Rees catchment suggested a similar storm had not occurred for much longer than a 5-year period (possibly even 50 to 100 years), and therefore a localised pocket of very high-intensity rainfall (possibly 10-minute rainfalls of 30-50 mm) may have occurred to cause such widespread debris flows (McSaveney & Glassey, 2002). Examination of sediment deposits after the 2002 event, showed a change in the composition of the flow to a much more diluted, hyper-concentrated flow downstream of the Cleft Peak tributary confluence; therefore the debris flows tend to be confined to the tributaries rather than continuing along the main channel (McSaveney & Glassey, 2002).

Aerial photographs of the Rees-Dart delta (Figure 3.11) show that ~1.4 km upstream of Glenorchy the river alternates between three possible flow paths. These flow paths are: an eastern route flowing along the northern side of Glenorchy, a western route directly onto the Dart braidplain, and a central route through the grassed island separating the eastern and western routes.

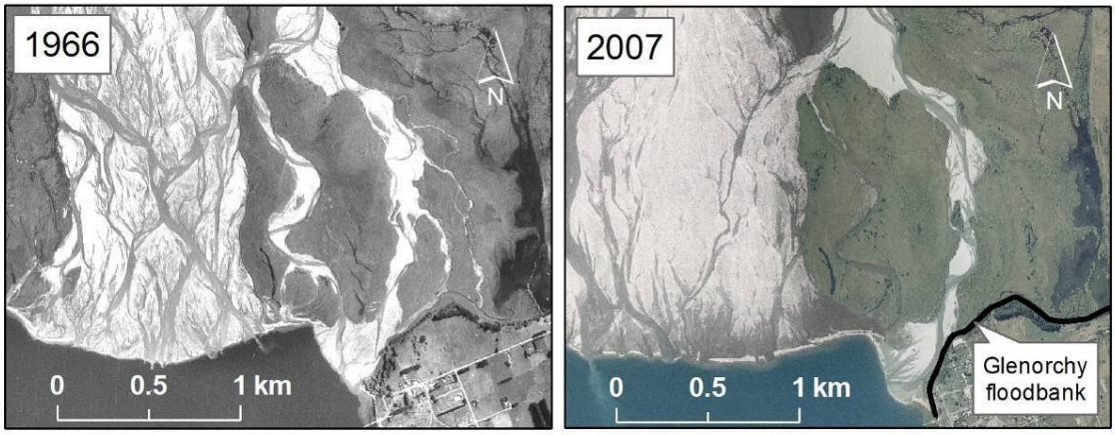

Figure 3.11: Rees-Dart delta and upstream grassed island in 1966 and 2007

3.2.3.2 Water level/flow

No permanent water level/flow recorders are located along the Rees River. However, for the recent ReesScan study (http://www.reesscan.org/) two continuous water level recorders were temporarily installed at the Rees road bridge, and at Invincible (near Invincible mine, approximately 7 km further upstream). Flows were then derived using stage-discharge ratings measured during flood events. Between 18 September 2009 and 25 March 2011 the Invincible site recorded a maximum flow of 475 m^3/s (6 February 2011), a minimum flow of 4 m^3/s (31 July 2010) and a mean flow of 20 m^3/s.

The ORC archives also hold one gauging card for *Rees River at above Invincible Creek* recorded on 21 March 1974. The measured flow, calculated by the slope-area method, was 17,500 cusecs (495.5 m^3/s).

3.2.3.3 Flood characteristics

A comparison between the permanent Dart flow record and temporary Rees at Invincible flow record (Figure 3.12) showed that the Rees River (at Invincible) tends to reach its peak flow approximately 1 to 2 hours before the Dart River peaks (at the road bridge). It can therefore be assumed that, like the Dart River, when a significant flood event occurs on the Rees River, the flow peak will pass relatively quickly - while Lake Wakatipu levels are still slowly responding to the increase in inflows.

Figure 3.13 shows the Rees and Dart peak flows (QP_{Rees} and QP_{Dart}, respectively) for the 5 largest flood events that occurred between 18 September 2009 and 25 March 2011. Although the Rees River flow record is only short, flood events occurred during the period of data acquisition. The best-fit line

for the data had an r^2 of 0.94 and gave a Rees River peak flow, QP_{Rees}, equal to $0.38*Q_{Dart}$ -76. A second best-fit line, forced through the point (0,0), had an r^2 of 0.91 and showed Rees River peak flows, QP_{Rees}, are ~$0.31* QP_{Dart}$ (or QP_{Dart} ~$3.2* QP_{Rees}$). This second relationship appears to be a better fit to the largest Dart River peak flow but, given the limited data, both relationships should only be used as a guide. An earlier statistical scaling analysis, completed as part of a flow-frequency decomposition (using only flow data up until 15 January 2010), resulted in a lower scaling of 1.9 to 2.4 being indicative of the range of runoff events experienced in the catchment (James Brasington, personal communication, 5th May 2011). The more recent, and larger flood flows have therefore tended to produce higher Dart River flows relative to the Rees River flows.

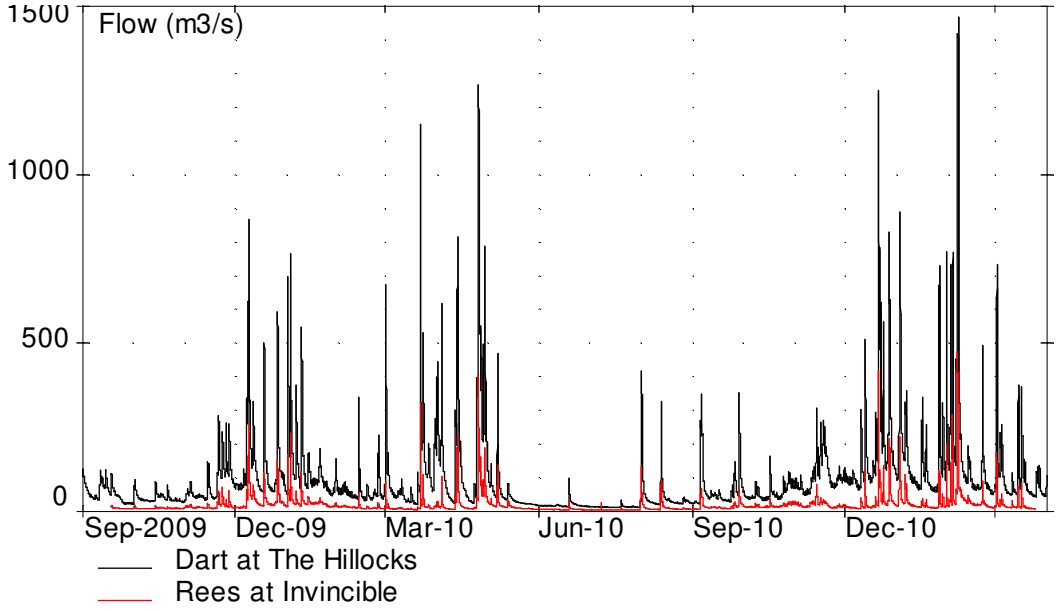

Figure 3.12: Comparison of Dart and Rees River flows [Source: ORC & ReesScan project]

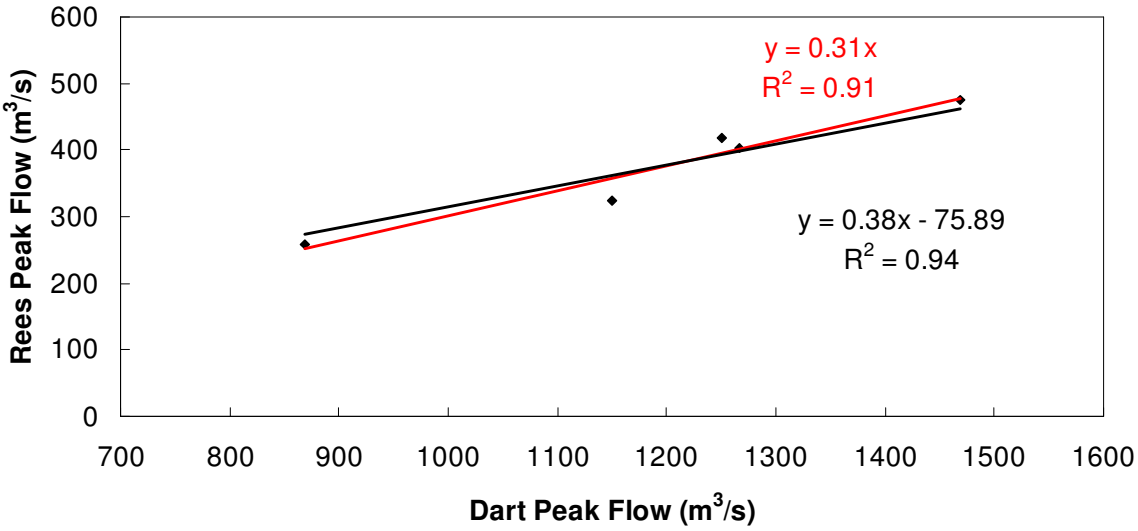

Figure 3.13: Relationship between peak flood flows on the Dart and Rees Rivers for 5 largest events in Figure 3.12 [Source: ORC & ReesScan project]

3.2.3.4 Bank protection works

A relatively small flood in the Rees River in May 1999 produced river levels in the eastern route, ~400 m upstream of the lake adjacent to Glenorchy, that were over 1 m higher than the lake level. This was attributed to the main flood channel passing along the northern boundary of Glenorchy, rather than flowing via the western outlet onto the Dart braidplain (Otago Regional Council, 1999). As a result of this flooding, and concerns for future flooding, a floodbank was constructed in 2000 along the northern boundary of Glenorchy (Figure 3.11). This floodbank is approximately 1400 m long, up to 1.5 m high, and 3 m wide across the crest.

Various other river training and bank protection works have also been undertaken on the Rees River to prevent bank erosion and the reoccupation of old river channels. One of the biggest flooding concerns for the Rees River is on the true right bank immediately upstream of the road bridge as flooding prior to 1984 resulted in sections of the original Glenorchy-Paradise Road being washed away. 1n 1984/85 a 4 km long floodbank (Figures 3.7 and 3.14) was built from the upstream boundary of the Rees road bridge along the upstream side of the rerouted Glenorchy-Paradise Road (Otago Catchment Board, 1985). This floodbank is approximately 1.5 m high and is protected along its upstream face by willows in the section closest to the river. Changes in the river meander patterns have, on several occasions, resulted in repairs to the floodbank being required (Otago Catchment Board, 1987). Three rock groynes were also constructed for additional floodbank protection in this area (Otago Regional Council, 1990).

Figure 3.14: Upstream limit of the 4 km long floodbank located upstream of the current Rees road bridge, on the true right bank

3.2.3.5 Cross section monitoring

Regular monitoring of cross sections in the Rees River delta area commenced in May 1999. Other sites further upstream have been surveyed as far back as 1978 (Otago Regional Council, 2008a). Although it is difficult to make any definitive conclusions regarding aggradation or degradation with short records, and sparsely placed cross sections, it does appear that most cross sections have observed net aggradation since surveying commenced. It has also been noted that river activity has tended to

remain within the confines of the active river channel banks over the survey time period (Otago Regional Council, 2008a).

A drawing from the ORC archives entitled "*Proposed new bridge Rees River, Lake County Council* (Job No. 1878/2)" has also been digitised to provide ground level and bridge elevations for the existing Rees Bridge whose site was surveyed c. 1953. Anecdotal information suggested that historically tractors were able to pass under this bridge. However, given that most of the cross section would have always had less than 2 m clearance, this perception may be incorrect and may be the result of reworking of the braided river channel. Figure 3.15 shows the digitised c. 1953 bridge cross section with an assumed datum.

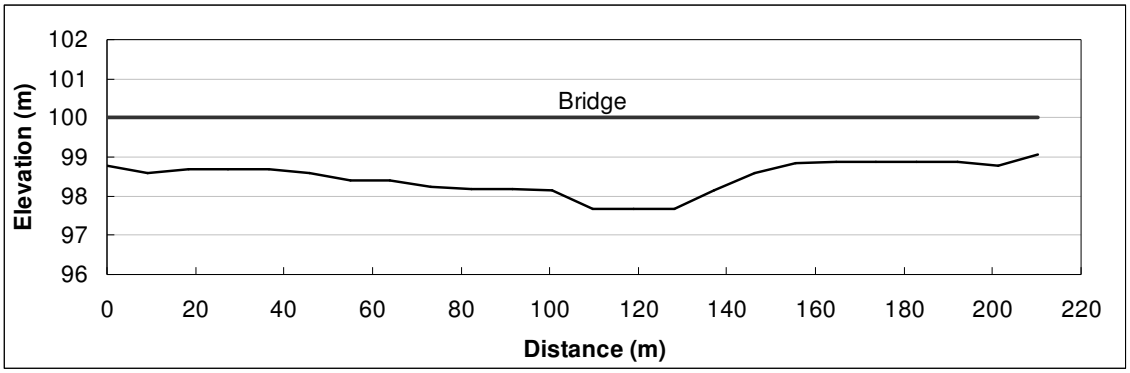

Figure 3.15: Rees River and road bridge elevations digitised from c. 1953 proposed bridge drawings

3.2.3.6 Weed control

A programme to control weed growth (e.g. new seedling growth on islands and riverbanks) includes maintenance of 600 hectares of the Rees River between the Ox Burn confluence and Glenorchy (Landward Management Ltd, 2009). New areas of infestation have been observed on the Rees River true right bank upstream of the grassed island near Glenorchy (Landward Management Ltd, 2009).

3.2.4 Lake Wakatipu

Lake Wakatipu is the third largest lake in New Zealand with a surface area of 291 km^2 and a surface elevation of approximately 310 m above sea level. The plan view of Lake Wakatipu is shown on Figure 3.2. From the Rees-Dart delta the 2.5 km wide lake increases in width to 6 km before narrowing back to a width of 2.9 km at a distance of 29 km south of the delta (average bearing of approximately 169º). The lake then makes a sharp turn and is orientated in an east-north-east direction (with a bearing of approximately 68º) for a further 17 km to the township of Queenstown, and the Frankton Arm/lake outlet, on the northern side of the lake. The last section of Lake Wakatipu is orientated in a south-east (bearing of 135º) direction for 9 km before the lake orientates almost directly south for the final 25 km.

Lake Wakatipu has formed in an abandoned glacial trough and is surrounded predominantly by steep, mountainous valley slopes which continue below the lake surface.

3.2.4.1 Bathymetry

The lake bed between the Rees-Dart delta and the southern limit of Pigeon Island (located 7.4 km to the south) appears to be relatively uneven. Brodie and Irwin (1970) suggest this is likely to be due to the geological relief (e.g. rocky outcrops that have been more resistant to previous glacial erosion processes). Beyond Pigeon and Pig Islands, the lake bed is mainly flat with a gentle slope for the next 20^{+} km down the lake. The following section of lake, approximately 15 km either side of Queenstown, is predominantly flat and is also the deepest section of the lake with depths of up to 380 m (Brodie & Irwin, 1970). As Kingston is approached, in the south, the water depth again gradually decreases.

A bathymetric survey of Lake Wakatipu undertaken in June and December 1968 used an echo sounder to collect over 450 km of soundings. The data collected in this survey are shown and discussed in Brodie & Irwin (1970) and includes a full description of a series of sublacustrine channels - including two channels which originate at the head of the lake on the foreset slope of the Rees-Dart delta. This network of channels travels down the lake beyond the sharp bend in the lake to where the lake bed is approximately horizontal. These steep-sided and flat-bottomed channels are up to 200 m wide and 30 m deep, with levees (Brodie & Irwin, 1970). Similar sublacustrine channels have also been observed in nearby Lake Wanaka (Irwin, 1980).

Another series of bathymetric surveys, undertaken by Department of Scientific and Industrial Research (now NIWA), were completed in the Rees-Dart delta area on 5 and 17 February 1988 (Contract CR5201), 11 June 1991 (Contract CR5220) and in March 1993 (Contract CR5222). Figure 3.16 shows the bathymetry derived from this data set, which also includes sublacustrine channels.

3.2.4.2 Water temperatures

Recorded Lake Wakatipu water temperatures, at all depths, do not fall below approximately 8.7ºC, while Rees and Dart River temperatures can fall as low as 6ºC (Brodie & Irwin, 1970). At water depths greater than 150-200 m water temperatures remain constant all year at around 8.5 to 9ºC, while surface temperatures reach 15-16.5 ºC between January and March, reducing to 12 ºC in May, 10ºC in July, and 8.7ºC in August (Pickrill & Irwin, 1982).

3.2.4.3 Water levels

Continuous Lake Wakatipu levels have been recorded since 28 November 1962 at *Lake Wakatipu at Willow Place* (Site 75277); a site jointly funded by Contact Energy (Contact), Foundation of Research Science and Technology (FRST), Queenstown Lakes District Council (QLDC) and The Marketplace Company Ltd (M-co). Figure 3.17 shows that the lake level is usually lower in the winter months and higher in spring and summer with lake levels remaining relatively constant all year - within a 1.6 m

range (309.4 m to 311.0 m above sea level) approximately 98% of the time between 1962 and 2010. The maximum recorded Lake Wakatipu level is 312.78 m (on 18 November 1999) and the mean lake level is approximately 309.95 m.

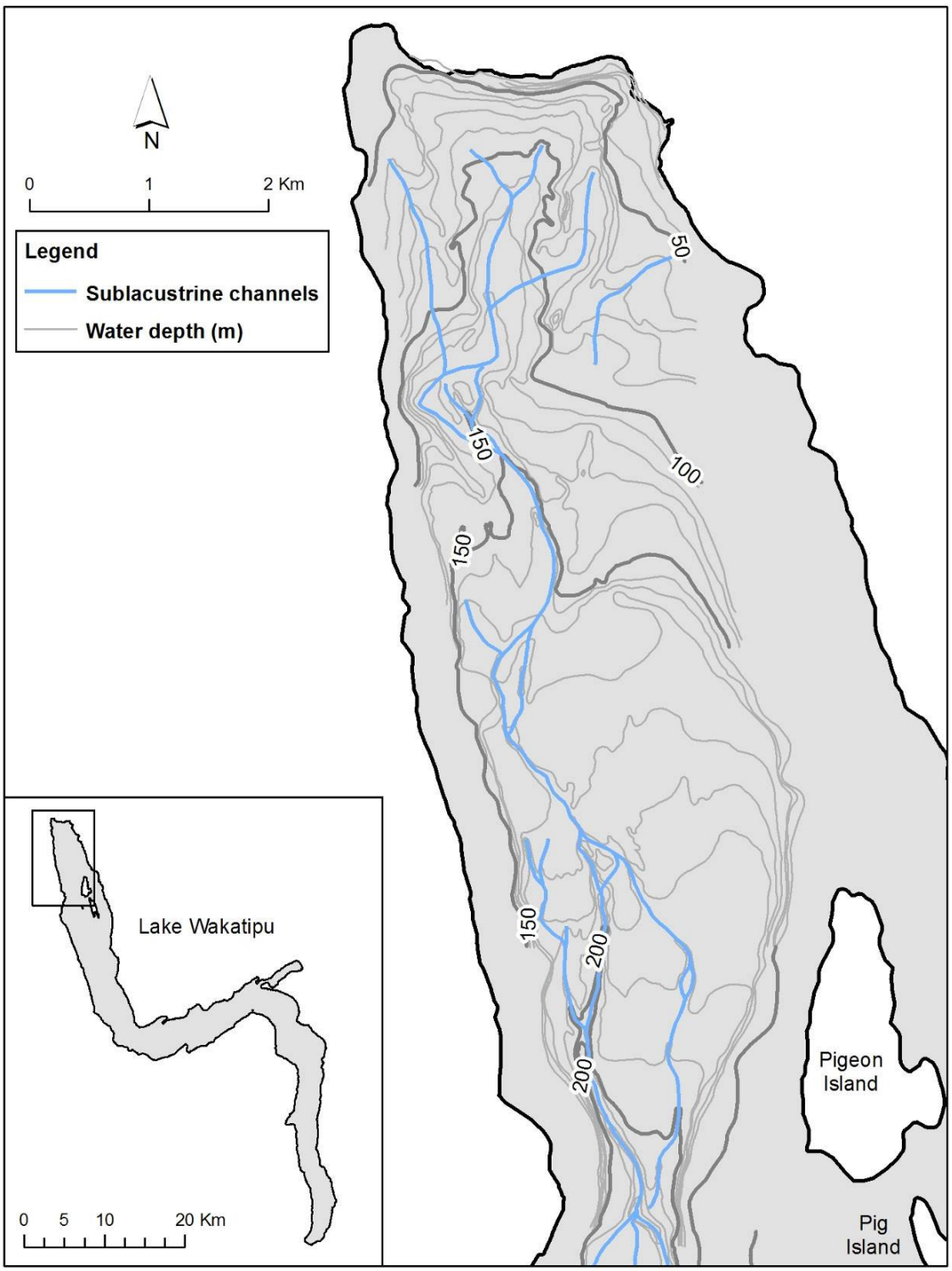

Figure 3.16: Wakatipu bathymetry and submarine channel network [Source: NIWA]

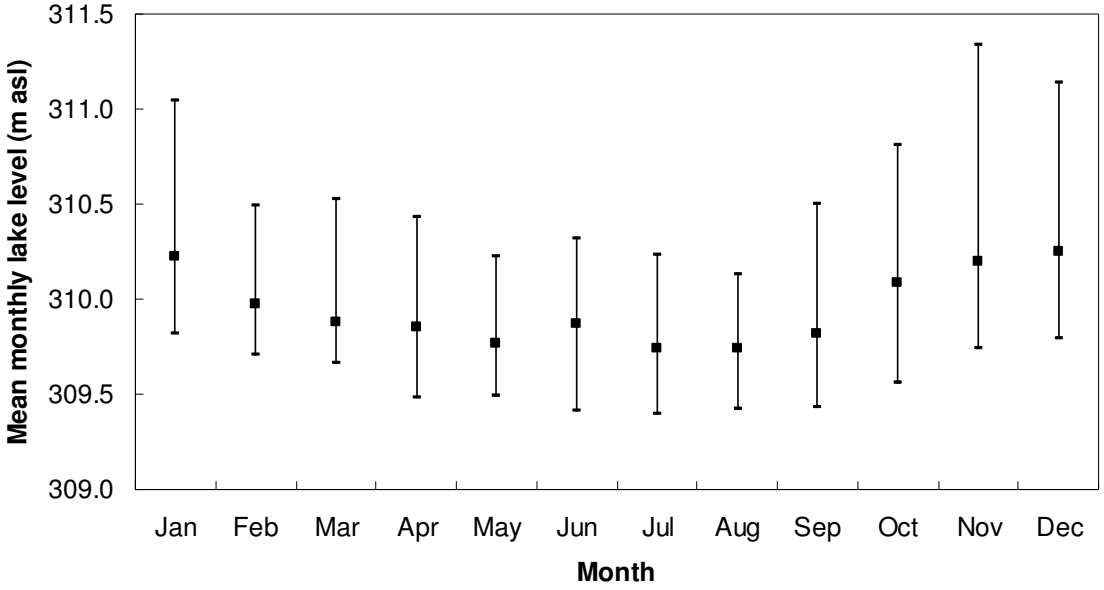

Figure 3.17: Lake Wakatipu (Site 75277) mean monthly lake levels between 1 January 1986 and 31 December 2009

Several previous studies of Lake Wakatipu water levels (e.g. Heath, 1975) have also observed regular seiching in the lake with periods of oscillation of 52 minutes and 27 minutes (also 18.5, 15 and 10 minutes for higher modes of oscillation). Long-term records show that, like Lake Wanaka, Lake Wakatipu maximum annual levels have been gradually increasing over the past century or so (Figure 3.18).

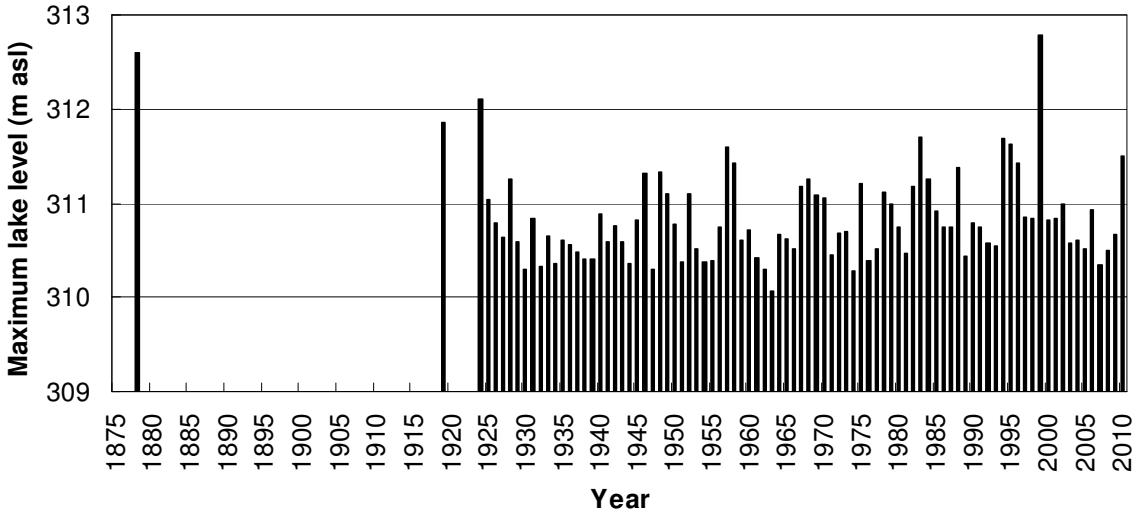

Figure 3.18: Maximum yearly Lake Wakatipu levels (1875 to 2010)

3.2.4.4 Historic flooding

The current warning levels for flooding around Lake Wakatipu are:

- 310.8 m - First warning level
- 311.1 m - Standby level

- 311.3 m - Low lying Queenstown streets start to flood via the stormwater system. There is a 13% chance that this level will be exceeded in any year, and a 75% chance that this level will be exceeded during any 10 year period [Source: ORC].
- 311.6 m - Level equivalent to the Steamer Wharf deck. There is a 6% chance that this level will be exceeded in any year, and a 45% chance that this level will be exceeded during any 10 year period [Source: ORC].

In November 1999 the Queenstown central business district (CBD), located on the Lake Wakatipu waterfront, received substantial damage from flood waters that exceeded 311.3 m for 15 consecutive days (peaking at 312.78 m). At this time properties in Glenorchy (Figure 3.19) and Kingston were also affected by the high lake levels. Lake levels of greater than 312 m have also been observed previously for significant flood events in 1878 and 1924, even though regular records of lake level were not collected until 1924 (Figure 3.18).

Figure 3.19: Flood inundation at Glenorchy during the November 1999 flood [Source: ORC]

3.2.4.5 Outflows

Prior to 1926 Lake Wakatipu outflows passed over a natural outlet control into the Kawarau River. Since 1926, water flowing out of Lake Wakatipu has passed into the Kawarau River through a gated weir structure with an average sill level of 308.83 m (mean sea level datum) and an effective total width of 110 m (Webby & Waugh, 2006). Although this structure was originally constructed to control downstream flows, for gold mining in the Kawarau River, the gates now only operate occasionally in times of low lake levels when minimum lake levels need to be maintained for environmental and navigational purposes (Webby & Waugh, 2006).

The hydraulic characteristics of this outlet are quite complex. Approximately 3 km downstream from the gated structure, the Shotover River delta protrudes into the Kawarau River providing a constriction to the river flow. On 26 occasions between 1963 and 2004 a combination of the Shotover River delta constriction, a Shotover River flood peak preceding the Lake Wakatipu peak, and the negligible slope between Lake Wakatipu and the Shotover River delta, has led to a backflow of Shotover River water into Lake Wakatipu (Webby & Waugh, 2006).

3.2.5 Rees-Dart delta

Coarse bedload from the Rees and Dart Rivers travels along the braided river system and, on entering Lake Wakatipu, forms a steep sand/gravel delta with slopes approaching the angle of repose (Pickrill, 1987). Brodie & Irwin (1970) describe the Rees-Dart delta foreset slope as being steep and 'only slightly convex in plan'. The delta topset is mostly visible as the steeply sloping delta foreset starts almost immediately beyond the shoreline where the 'beach' drops away steeply.

Over time, a sloping wedge of coarse sediment can accumulate on the upper foreset slope with measured slopes of up to approximately 30º. Once sufficient sediment has accumulated, slope failure is likely to occur resulting in a decreased delta foreset slope (Kleinhans, 2005b). For example, for the Rees-Dart delta, slide failures have been shown in seismic reflective profiling (Pickrill, 1987). Such slope failures are likely to be exacerbated by Rees and Dart River underflows that occur when denser (i.e. cooler and/or laden with suspended sediment) river water enters Lake Wakatipu and plunges and flows along the lake bed. In high river flows, sediment-laden flood waters can form turbidity currents that accelerate downslope and entrain additional sediment. These turbidity currents are capable of travelling at over 20 cm/s for over 60 km along the lake (Pickrill & Irwin, 1982) in sublactustrine channels formed by the intermittent turbidity currents (Brodie & Irwin, 1970). Interflows (i.e. underflows in a stratified lake that become neutrally buoyant above the lake bed) and overflows (i.e. lower density river water that tends to travel across the lake surface) are also known to occur as part of a daily cycle in summer. These interflows and overflows are also likely to revert back to being turbidity currents during flood events with high suspended sediment concentrations (Pickrill & Irwin, 1982). Figure 3.20 shows underflows occurring during the November 1999 flood events. At this time turbid waters are observed up to 300 m offshore. Beyond this distance the lake waters remain clear, indicating the position of the plunge line (i.e. where the river water sinks and flows along the delta foreset/lake bottom).

Coriolis forces in the Southern Hemisphere also deflect incoming river flows to Lake Wakatipu in a clockwise direction (Pickrill & Irwin, 1983). This is likely to result in higher sedimentation rates along the TLB of the Dart and Rees Rivers as they enter Lake Wakatipu. For example, the Rees River outflows and sediment should favour the Glenorchy waterfront - which appears to be the case in Figures 3.20 and 3.24. Figure 3.21 also shows 2001 and 2007 Dart River flows entering Lake

Wakatipu and flowing towards the east - indicative of a clockwise circulation of water within Lake Wakatipu. Although strong underflows are likely to overpower the Coriolis force during flood events (Pickrill & Irwin, 1982), sedimentation rates measured along the eastern side of nearby Lake Tekapo (due to Godley River inflows at the northern end of the lake) are higher indicating that Coriolis forces are an important consideration (Pickrill & Irwin, 1983).

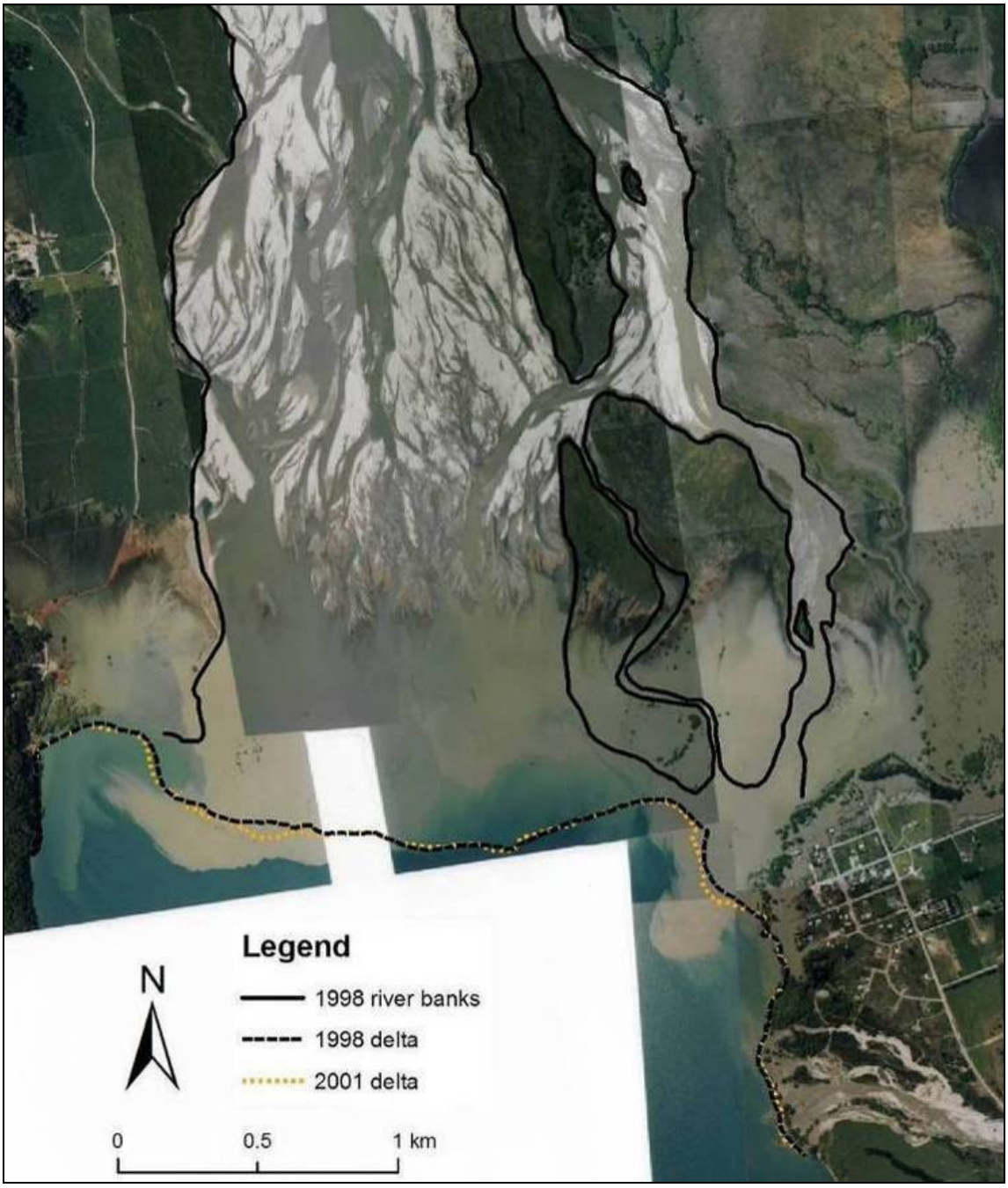

Figure 3.20: Geo-referenced photograph mosaic of the Rees-Dart delta in flood on 22 November 1999 [Source: ORC]

(a) 19 February 2001 (b) 17 February 2007

Figure 3.21: Aerial photographs showing Dart River sediment plumes moving in an easterly direction [Source: ORC]

Rees-Dart river delta growth between 1966 and 2007 has been quantified using geo-referenced historic aerial photographs (Section 3.2.5.1) and sonar data (Section 3.2.5.2). Rees-Dart delta sedimentation rates are calculated in Section 3.2.5.3, and the estimated portion of the sediment expected to be provided by the Rees versus Dart River systems is determined in Section 3.2.5.4. This relative proportion is used later for the microscale physical modelling (Section 4.3). A recent 2011 Lidar survey also provides additional information on the Rees-Dart delta behaviour (section 3.2.5.5).

3.2.5.1 Aerial photography

Historic black and white photographs from as far back as the 1880s, showing scenery, people and ships around the Rees-Dart river delta, are available in photographic collections from various sources including the MacMillan Brown library, Hocken Library, Glenorchy museum, Te Papa museum, Settlers museum, and Lakes District Museum. Although these photographs often show the delta in the background, there is not enough information to precisely define the historic delta location. Some of these historic photographs are also published in several books (e.g. Muir & Moody (1904), Davies (1922), McKenzie (1973), Meyer (1980)). Historic maps from this time period also tended to be more like schematics/sketches and were therefore more indicative than accurate (Figure 3.22).

Fortunately full or partial aerial photograph coverage of the Rees-Dart delta and catchment has been captured on several occasions since the first aerial photographs of Glenorchy and the Rees River were taken in 1937. The most recent aerial photographs, showing the full Rees-Dart river delta and catchment, were taken in 2007, with the oldest set of aerial photographs taken in 1966. The 2007 orthorectified colour aerial photographs have been provided by ORC and have a ground sampling distance of 0.6 m. A summary of the aerial photographs used in this study is given in Table 3.3.

Lake Wakatipu at Willow Place (Site 75277) recorded water levels were used to check that lake levels were comparable for each aerial photograph (Table 3.4). This resulted in the 1988 aerial photograph being excluded from the delta growth analysis as lake levels were over 1 m higher than the 1966 levels and some of the delta features were submerged. Initially the aerial photographs were geo-referenced

using the co-ordinates of various 'permanent' landmarks in the vicinity of the delta (Figure 3.23). These 'permanent' landmark co-ordinates were obtained in November 2007 using a portable GPS unit with an accuracy of approximately ±2 m in the mode used for the survey. 'Permanent' landmarks included the corners of old (& in some cases derelict) buildings, jetties and bridges.

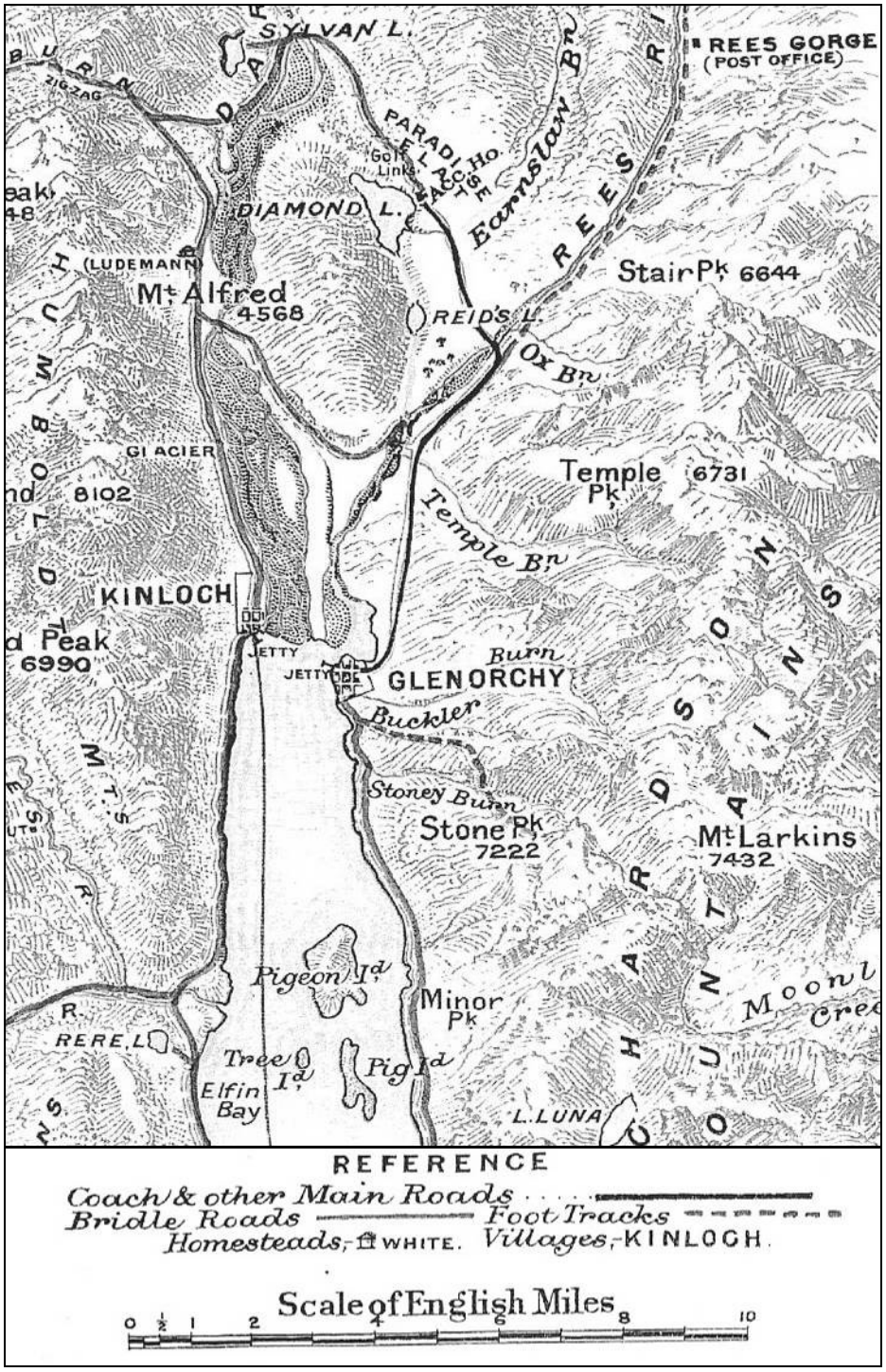

Figure 3.22: New Zealand Department of Tourist and Health Resorts c.1904 map of the Rees-Dart delta (Deverell, 1904) [Source: Unknown]

Table 3.3: Rees-Dart delta aerial photograph coverage

Survey	Date	Scale	Colour	Source	Coverage
SN40	1\04\37	1:8000	No	ORC	Glenorchy and Rees River only.
SN2016	12\03\66	1:75 000	No	ORC	3985/23 = Rees-Dart delta
SN5062	12\02\77	1:25 200	No	NZAM	A/10 = Rees-Dart delta.
SN8996	15\12\88	1:50 000	No	ORC	E/18 = Rees-Dart delta in flood.
SN12325	27\11\98	1:50 000	Yes	ORC	P/7 = Rees-Dart delta
-	22\11\99 (2:30-5pm)	~1:9000	Yes	ORC	Mosaic - Rees-Dart delta in flood
SN25055c	19\2\01	1:50 000	Yes	NZAM	1/109 = Rees-Dart delta
SN50556c	17\2\07	1:40 000	Yes	ORC	Rees-Dart catchment and delta orthorectified

Table 3.4: Rees-Dart aerial photograph lake level and photograph resolution information

Year	Lake Wakatipu level (m)	Difference to 1966 level (m)	Photo scale	Ground sampling distance (m)
1966	309.85	0	1:75 000	2.0
1977	310.19	+0.34	1:25 000	0.4
1998	309.92	+0.07	1:50 000	0.8
2001	309.78	-0.07	1:50 000	0.8
2007	309.83	-0.02	1:40 000	0.6

At a later date the orthorectified 2007 aerial photographs were provided by ORC and the aerial photographs were geo-referenced again using the 2007 photographs as the 'base'. This had the advantage of having a larger number of features that could be geo-referenced (e.g. more inaccessible landmarks) but this did not change the delta front locations significantly.

Figure 3.24 shows the digitised Rees-Dart delta shoreline derived from the 1966, 1977, 1998, 2001 and 2007 geo-referenced aerial photgraphs. During the 1966 to 2007 time period the Dart River has predominantly transported sediment into Lake Wakatipu near the true right bank (TRB), advancing the delta front by up to 210 m. Meanwhile the Rees River has advanced the delta by up to 120 m and the total surface area of the Rees-Dart delta grew by ~203 000 m^2 (or 4951 m^2/yr) along the lake shoreline.

Given that ~1.2 km^2 of farmland along the Dart River TRB has been lost to the river between 1966 and 2007, some of the recent delta growth is likely to be derived from this sediment source. Assuming an average erosion depth of ~1 m (estimated from LIDAR data), this represents ~10% of the total sediment deposited on the delta between 1966 and 2007.

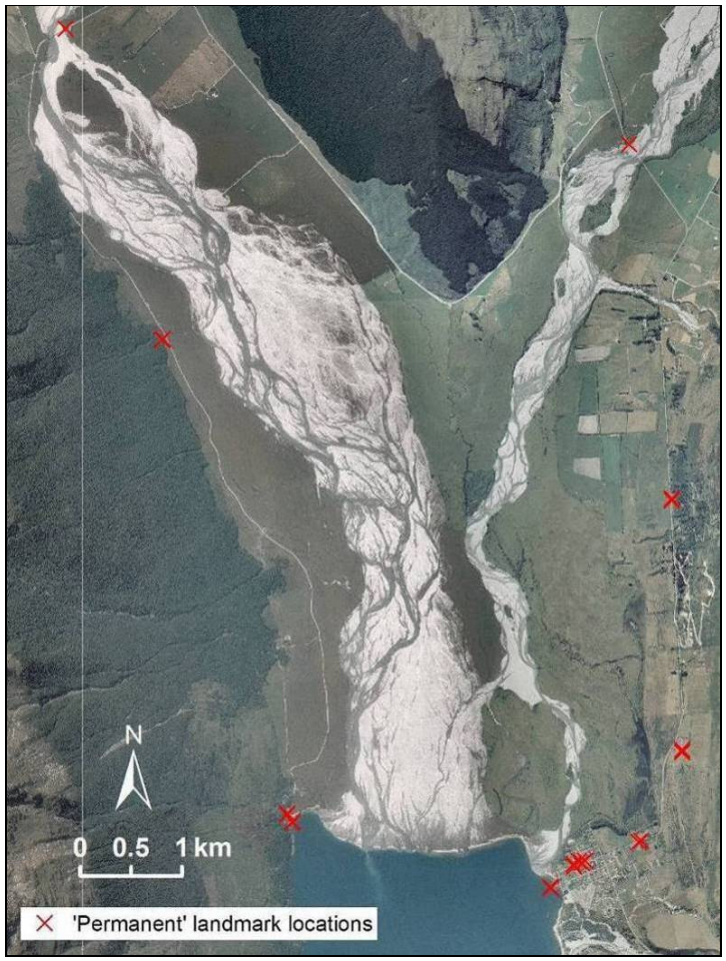

Figure 3.23: Location of GPS 'permanent' landmarks

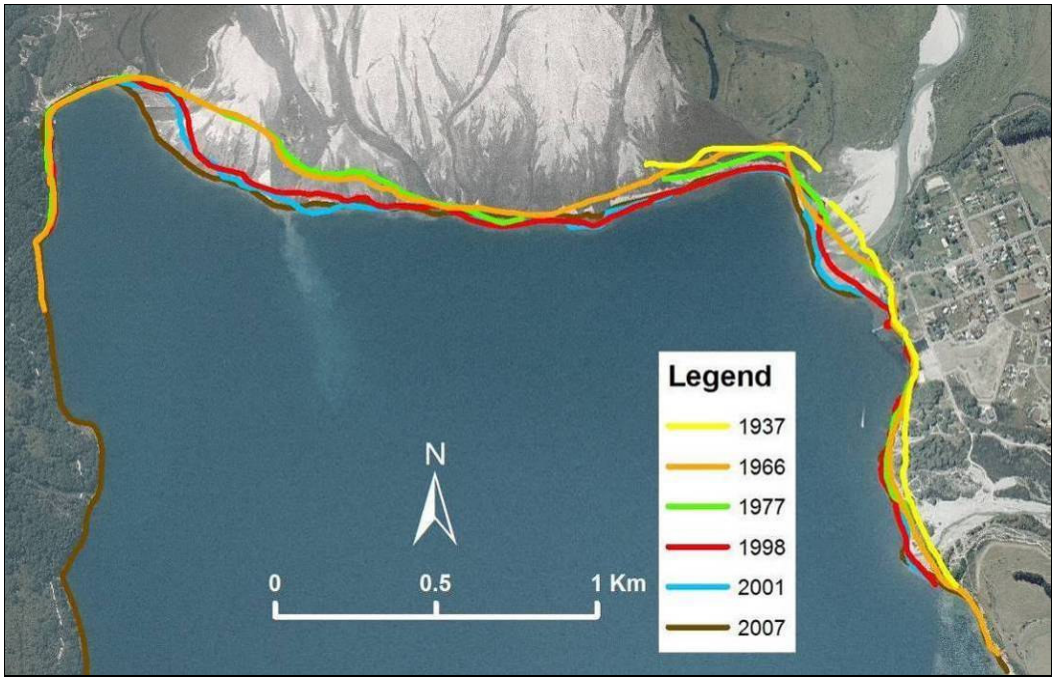

Figure 3.24: Rees-Dart delta shorelines for 1937 to 2007 shown on 2007 aerial photography

3.2.5.2 Sonar data

Historically bathymetric data for Lake Wakatipu were collected by dropping a weighted line and recording manually the location and depth of the measurement. More recently sonar (echo sounding) units have become a much more efficient method for measuring bathymetry, allowing a large number of depths to be recorded in a considerably shorter time frame. Further developments have seen global positioning systems (GPS) built into the sonar units. 3-d swath mapping is also available, with latest technology combining multibeam sonar (high quality bathymetry) and sidescan sonar (backscatter/imagery data). The cost of acquiring 3-d bathymetric swath data prevented this technology being used in this study but future delta studies may be able to make use of this technology.

Sonar units, generally mounted on the hull of a boat, have a transmitter that emits a frequent electrical pulse or 'ping' (several times per second) which is transformed into a sound wave by the transducer. This sound wave then travels through the water body until it is obstructed by a 'solid' object (e.g. lake bed). The wave is reflected back, via the transducer, to the sonar receiver where the signal is amplified and the distance to the obstruction (i.e. water depth) is calculated from the wave speed and time of travel for the reflected wave. The location of the measured depth is simultaneously determined by a GPS unit. At least three satellites need to be within signal range for the position of the GPS unit to be determined; four satellites can enable position and elevation of the GPS unit to be calculated. GPS units emit high frequency signals so locations can only be determined if the GPS to satellite 'line of sight' is not obstructed by trees, structures, etc..

For this study sonar surveys were considered to be a quick, cost-effective option for data acquisition as the ORC field services team already had a "Lowrance fish-finding sonar and mapping GPS" unit (model LMS-527cDF iGPS) hull-mounted on a small motorboat. This sonar unit was set to a 200 kHz frequency and had a built-in GPS unit. Soundings were measured every 3 to 6 m (depending on the speed of the boat) with the accuracy of the GPS and sonar data noted as having an accuracy of within 10-20 m horizontally and 2-3 m vertically in the Lowrance manual (http://www.lowrance.com/upload/Lowrance/Documents/Manuals/LMS527-522_0152-181_120406.pdf). However, the results obtained seemed considerably more accurate than this. For instance, when sonar data points were overlain on geo-referenced aerial photographs the boat was accurately placed at both the jetty and passing out the narrow entrance of the boat harbour (the accuracy of the sonar data will be discussed later in this section).

The Lowrance sonar signal produces a stronger signal when it reflects off a harder (i.e. more dense) lake bed compared to when the lake bed is a softer mud or vegetated surface. The SonarViewer program distinguishes between the different surfaces by colouring harder surfaces with a wider "reddish yellow to bright yellow" colour, and softer, less dense surfaces with a narrower "dark blue with less prominent red or yellow" colouring. Harder surfaces are also more likely to generate a

'second bottom' signal which is represented by a second signal at double the actual depth. A weaker signal may also represent areas where there has been some shadowing (e.g. if there is a steep drop in the profile in the same direction that the data are being collected). Figure 3.25 shows a typical Rees-Dart delta profile (profile 5-6, Figures 3.27 and 3.30) along the lake bed and up onto the delta front using the SonarViewer software package.

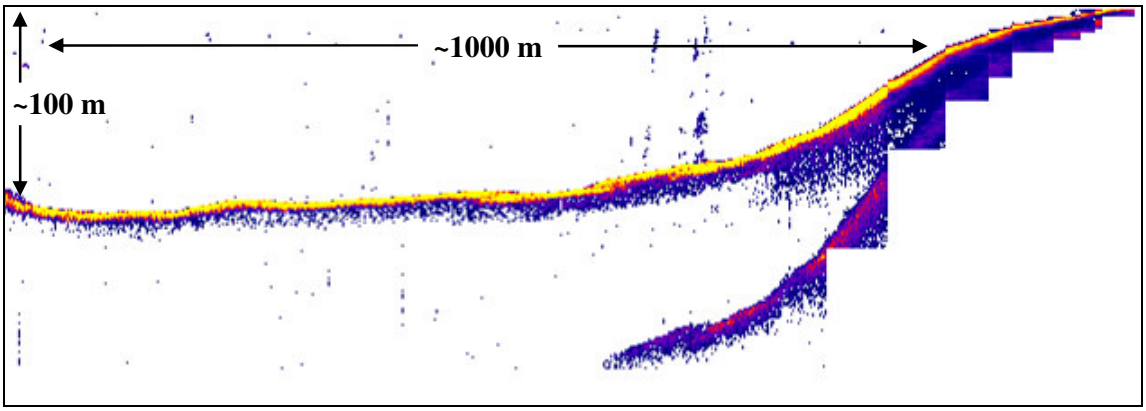

Figure 3.25: Sonar data profile (profile 5-6, Figures 3.27 and 3.30) along the lake bed and up onto the Rees-Dart delta foreset on 19 November 2007

The first sonar survey for this study was completed on 12 and 19 November 2007 (Figure 3.26). Two additional sonar surveys were completed on 30 November 2010 and 1 June 2011, following a similar set of reference lines but only in the vicinity of the delta (Figure 3.27).

For the June 2011 sonar survey a second GPS unit (Trimble ProXL) simultaneously recorded the location of the sonar instrument at 5 second intervals. This second GPS unit had the antenna mounted on the boat directly above the Lowrance sonar instrument whereas the Lowrance GPS antenna was mounted in the cabin of the boat, approximately 2.82 m from the Lowrance sonar instrument. Figure 3.28 shows that, with the exception of profiles 17-18 and 16-17, the Lowrance fish-finding GPS consistently recorded coordinates that were offset from the Trimble ProXL GPS by a mean distance of between 1.4 and 3.8 m, with 95% of the data points generally lying within ±2 m of the mean. During this survey the Trimble ProXL GPS has Position Dilution of Precision (PDOP) values between 1.8 and 2.8, which indicate a good level of precision for the GPS positions (i.e. 95% confidence of 1-3 m accuracy).

For each sonar survey it was envisaged that the same delta profiles would be measured. In practice this was hard to achieve since there are no fixed reference points on the water. The delta profile locations therefore had to be determined solely from specified waypoints and real-time readings from the Lowrance GPS unit. Figure 3.29 shows the mean offset distances (perpendicular to the reference lines shown in Figure 3.27) for June 2011 delta profiles. Most delta profiles were within ~15 m of the reference line 95% of the time.

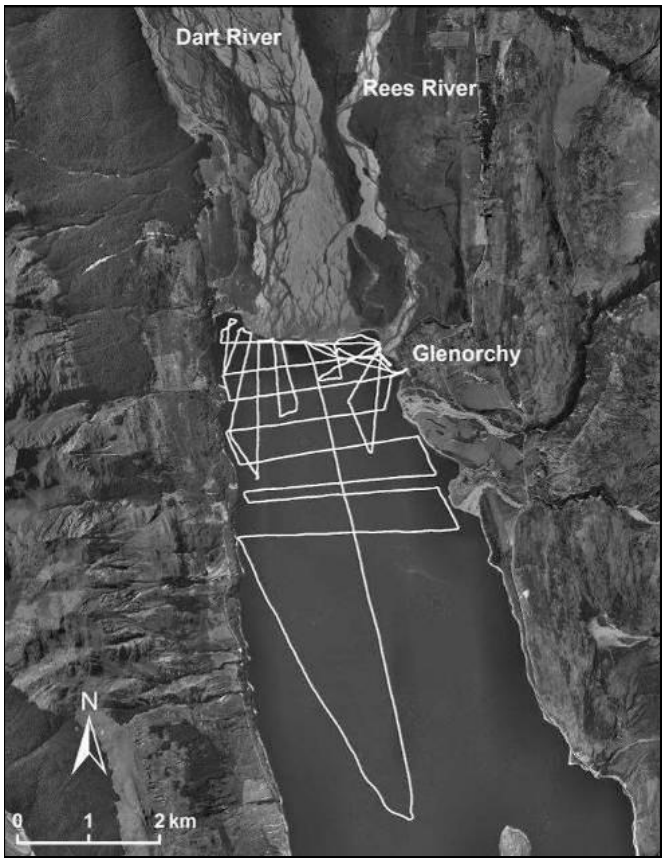

Figure 3.26: Sonar data for Lake Wakatipu (12 and 19 November 2007)

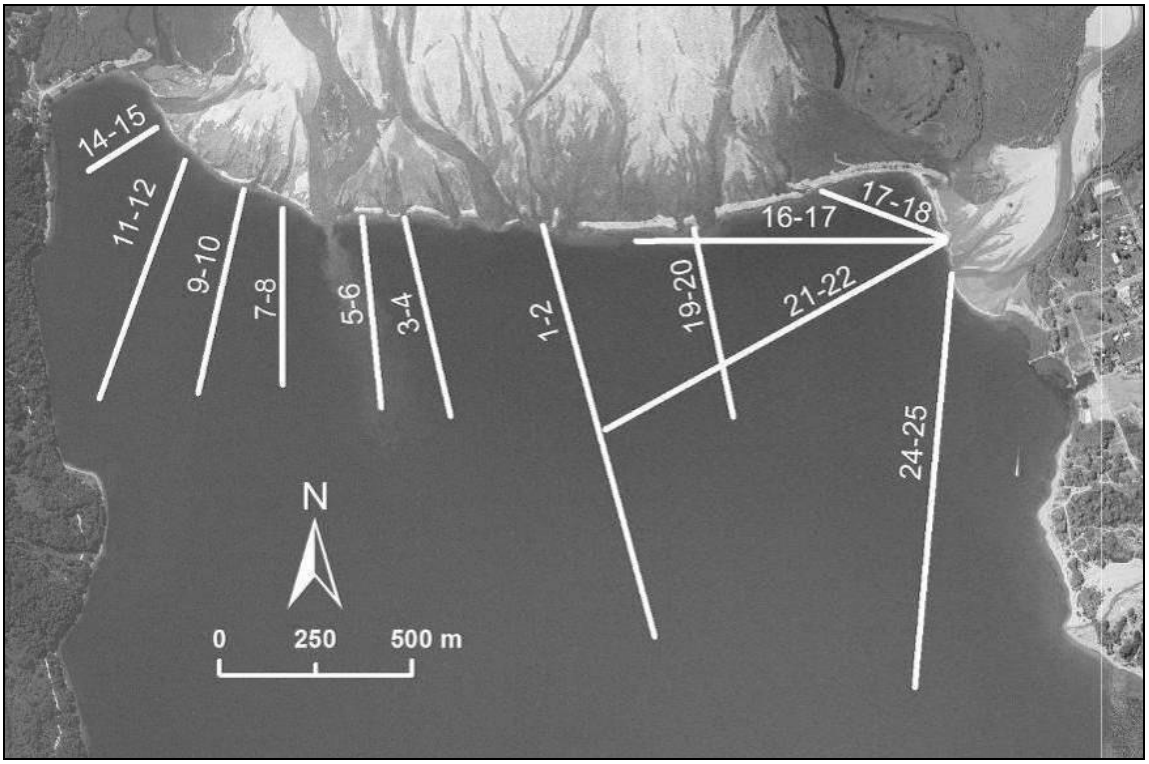

Figure 3.27: Reference lines for the Rees-Dart delta sonar surveys (for 2007, 2010 and 2011)

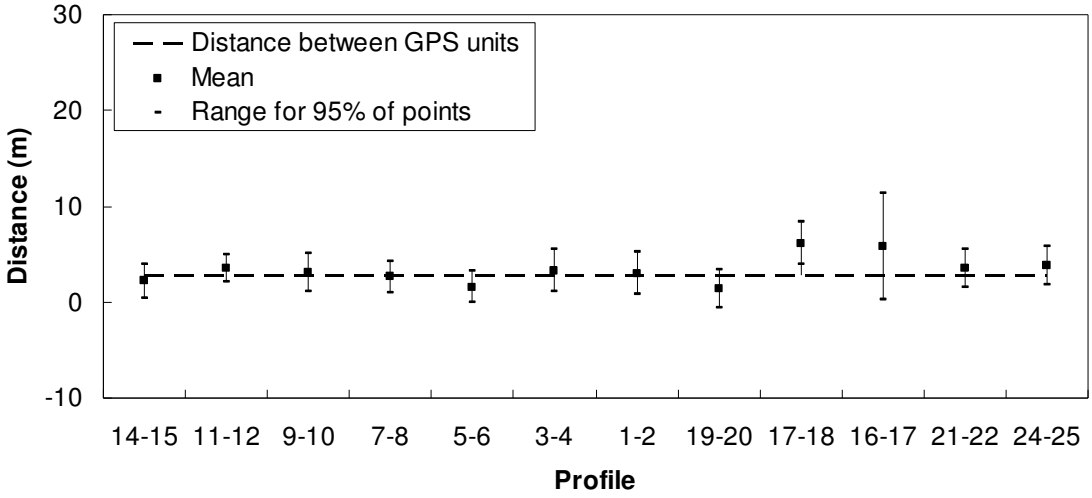

Figure 3.28: Recorded distance between the two boat-mounted GPS units (located 2.82 m apart), for each delta profile during the June 2011 sonar survey

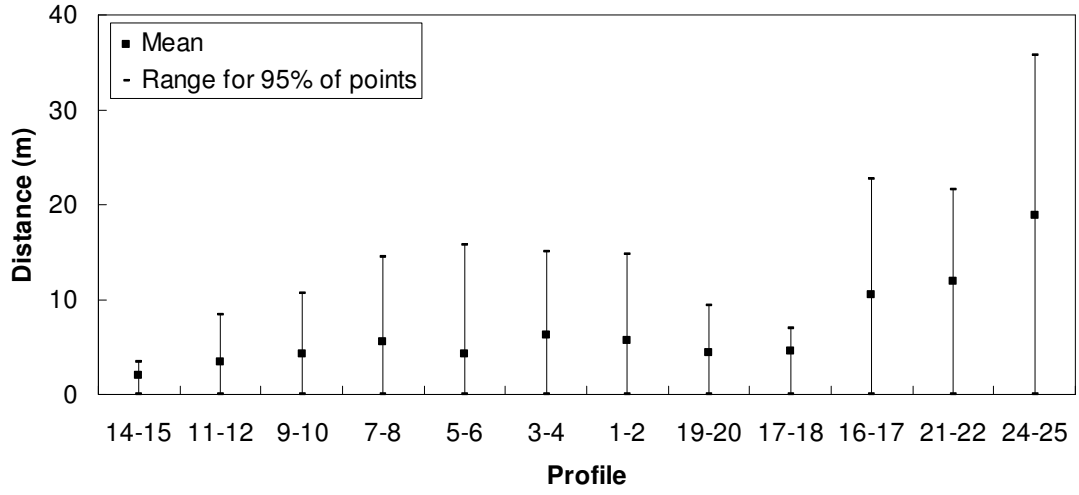

Figure 3.29: Perpendicular offset from the sonar reference line to the recorded location for each delta profile in the June 2011 sonar survey

Figures 3.30 and 3.31 also show this offset distance (d) plotted for the sonar surveys. From these comparisons it can therefore be concluded that, for the sonar data collected in this study, the Lowrance GPS is likely to be recording to a similar level of accuracy as the Trimble ProXL although several periods of time did show larger variations. These variations may be due to there temporarily being less satellite coverage due to the position of the satellites (which seemed to occur early to mid-afternoon) and/or reduced satellite coverage due to interference from the screen on the boat. More importantly, the most significant source of error with regard to location is the actual offset from the delta reference lines due to navigational difficulties (possibly exacerbated during times of low satellite coverage by less accurate real-time GPS readings). There is also an offset of 2.82 m between the location of the sonar reading and the GPS coordinate for the 2007 and 2010 sonar surveys. Since this distance is relatively small (and the boat followed a similar route for all three surveys), the delta profiles plotted in Figures 3.30 and 3.31 are still comparable.

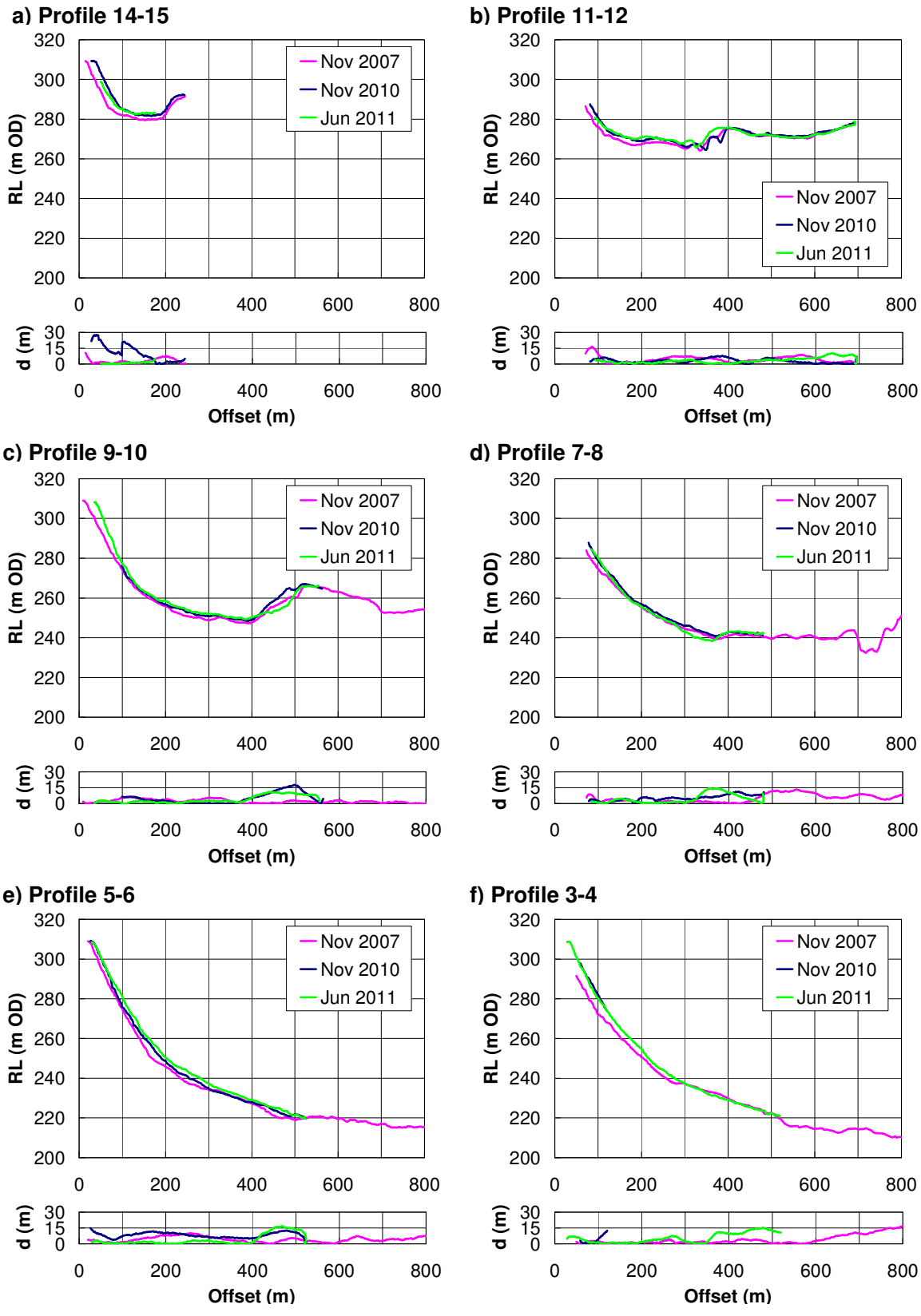

Figure 3.30: **Rees-Dart delta sonar survey profiles 14-15 to 3-4 from 2007 to 2011 (d=perpendicular offset from reference line)**

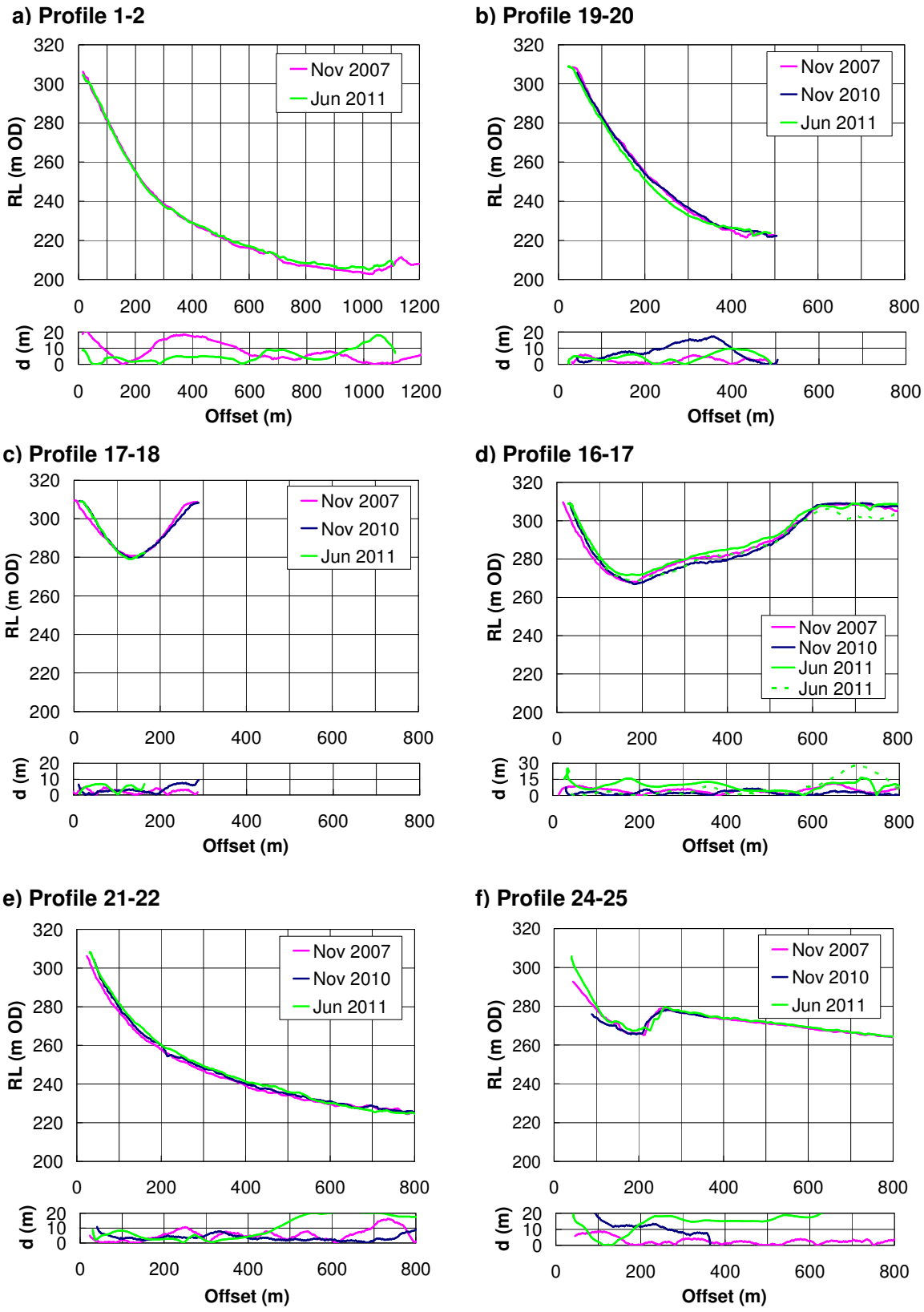

Figure 3.31: Rees-Dart delta sonar survey profiles 1-2 to 24-25 from 2007 to 2011 (d=perpendicular offset from reference line)

The easiest, but most expensive, option to improve the spatial coverage (and also temporal coverage) of the submerged delta profile would be to carry out multibeam sonar swath surveys which produce continuous coverage of the lake bed. Using the existing methodology, the best way to increase the accuracy of future sonar surveys, and also identify delta growth behaviour, is to:

- add extra waypoints along the reference lines, and place temporary markers on the shoreline, to assist the boat navigator when trying to follow the correct path along the reference lines.

- mount a GPS unit at a known fixed location (e.g. jetty) for comparison and corrections to the boat-mounted GPS unit (i.e. differential GPS).

- gather a series of sonar points around the main river exits to try and identify the delta profile at these locations (i.e. the locations of current and/or very recent delta progradation).

When sonar surveys are undertaken, simultaneous aerial photograph coverage would be useful for identifying the active river channels and the location of upstream river channels. This information would help identify areas where it is thought that the delta foreset slope will steepen (as sediment is delivered to the delta foreset) and/or reduce in slope (as sediment-laden turbidity currents transport foreset sediment away from the delta). For the June 2011 survey the location of the river outlets was noted using the boat-mounted GPS unit. However, it was difficult to identify which river channel flows were the largest at the time; this information also doesn't provide the location of the actively prograding river outlets to the lake during previous flood events occurring between sonar surveys. It should also be noted that, as the river outlets regularly change position, it is not realistic to expect the prograding delta locations to always (or even regularly) coincide with the survey reference lines.

Despite the limited spatial coverage, and difficulties in precisely maintaining a boat course along the reference lines, several observations can be made:

- Within ~20 m of the shoreline (at ~308.5 m asl) the submerged and gently sloping delta topset rapidly changes to a considerably steeper foreset slope of 15 º to 30º. It should also be noted that, although the delta slope was calculated for each reference line, it is difficult to identify whether this measured the maximum foreset slope since the alignment of the reference line may not capture the steepest slope.

- The steeply sloping Rees River delta foreset varies linearly with depth until a level of 275 to 285 m asl. Beyond this point the foreset slope has a concave profile (bottomset) that forms a smooth transiton to the lake bed.

- The steeply sloping Dart River delta foreset varies linearly with depth until a level of 285 m asl (Kinloch) to 250 m asl (near centre of lake). Beyond this point the foreset slope has a concave profile that forms a smooth transiton (bottomset) to the lake bed.

- Steepening of the delta foreset slopes does appear to be occurring at some locations (e.g. profiles 3-4 and 9-10, Figure 3.30, and profile 17-18, Figure 3.31).

- No delta foreset steepening or growth is observed at profile 1-2 (Figure 3.31) which is located in the central, currently less-active, portion of the Dart River delta.

- Dart River delta profiles 19-20 (Figure 3.31) and 17-18 (offset ~200 to 300 m, Figure 3.31) show the upper portion of the delta foreset slope retreating slightly. This may be due to survey inaccuracies but, given both these profiles are in the currently less-active portion of the Dart River delta, it may also be possible that during some flood events there is a net transfer of sediment away from this area of the delta foreset (e.g. by turbidity currents). For example, Figure 3.20 shows that during the November 1999 flood the delta topset upstream of profile 19-20 is 'drowned' and the relatively clear water suggests that there is not a significant volume of sediment reaching this portion of the delta foreset.

3.2.5.3 Sedimentation rates (1966 to 2007)

Due to the confined nature of the sediment accumulating on the Rees-Dart delta, as well as the rapid, observable rates of delta progradation, sedimentation rates for the Rees-Dart river delta over the 1966 to 2007 time period were calculated using a combination of the geo-referenced historic aerial photographs (Section 3.2.5.1) and the 2007 lake bathymetry derived from sonar data (Section 3.2.5.2). Similar methods of differencing bathymetric surveys has previously been used successfully to determine sedimentation fluxes (e.g. Hickin, 1989).

Methodology

The volume of sediment accumulating at the Rees-Dart delta was estimated using the GIS software program ArcGIS. Initially the November 2007 sonar data (Figure 3.26) and 2007 delta front location (Figure 3.24) were combined to generate a 25 m raster grid surface of the lake bed, up to and including the delta front. This grid was converted to a set of 5 m contours (Figure 3.32).

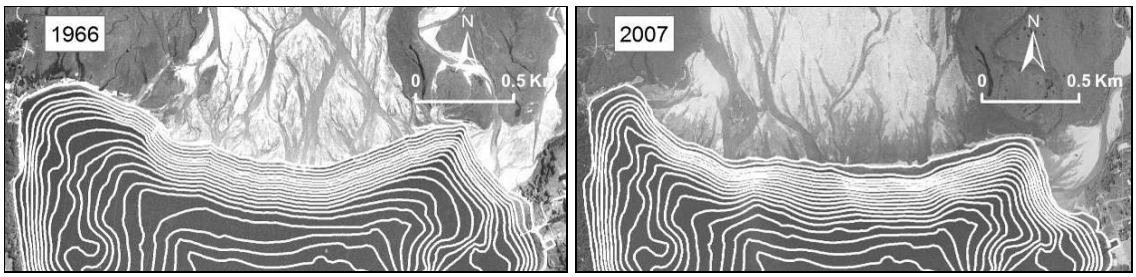

Figure 3.32: Estimated Rees-Dart delta 5 m contours in 1966 and 2007

The 1966 and 1998 lake bed contours were then estimated by modifying the 2007 contours in the vicinity of the delta, using the 1966 and 1998 delta front locations (shown in Figure 3.24), and assuming that the delta front remains at approximately the 2007 slope (as measured near the centre of the Dart and Rees rivers at the delta shoreline). The 2007, 1998 and 1966 contours were then converted into raster grid surfaces, and volumetric sedimentation rates were determined by differencing the grid surfaces.

Calculated sedimentation rates

Figure 3.33 shows the derived sediment accumulated at the Rees-Dart delta between 1966 and 2007. From Figure 3.33c it can be seen that during this time the western side of the Dart River delta, near Kinloch, has accumulated sediment ≥35 m deep in places.

A summary of the calculated Rees-Dart delta sedimentation rates, calculated from the GIS volumetric analysis, is given in Table 3.5. Interestingly, the 1999 to 2007 average annual rate of sedimentation is estimated to be over double the rate for the previous 33 years. This indicates that the large flood event that occurred in November 1999 (Figure 3.34) is likely to have had a significant influence on sedimentation rates.

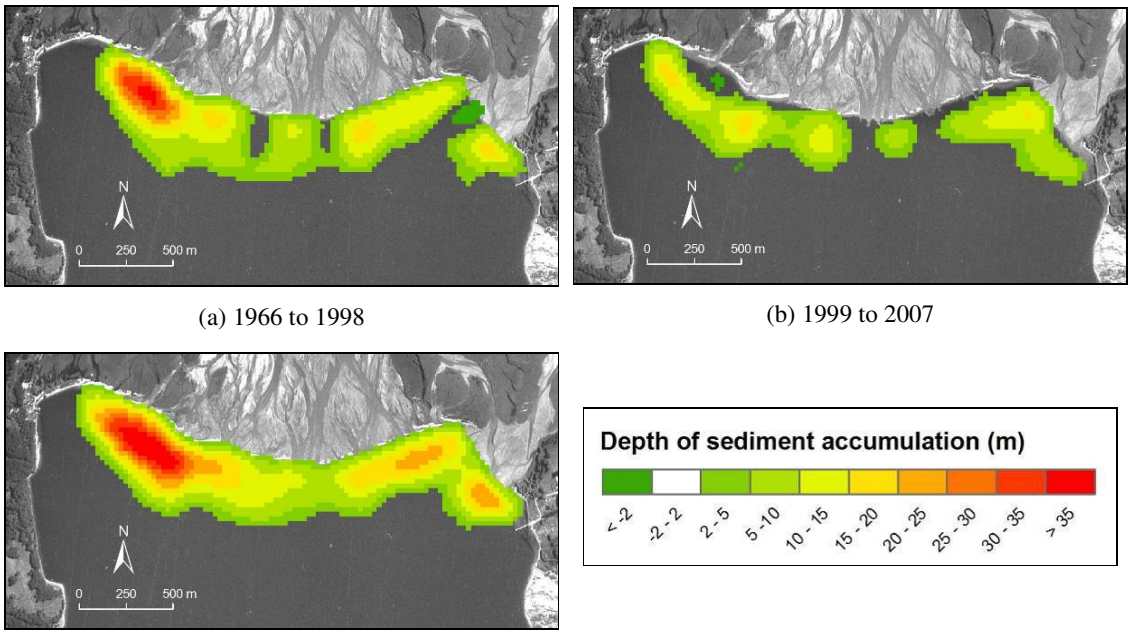

(a) 1966 to 1998

(b) 1999 to 2007

(c) 1966 to 2007

Figure 3.33: Location and depth of sediment accumulated on the Rees-Dart delta for various time periods

Comparisons can also be made with the adjacent Shotover River catchment which has an area of 1088 km^2, compared to the 1037 km^2 Rees-Dart catchment. The Shotover documented bedload estimate of 0.263×10^6 t/year for the period 1967 to 1999 (Hicks et al., 2000) converts to a volumetric rate of 0.15

$\times 10^6$ m^3/year (assuming a bulk density of 1.8 t/m^3). This is of the same order of magnitude as the Rees-Dart volumetric rate (which will have some suspended sediment load trapped along with the bedload) of 0.22×10^6 m^3/year for 1966 to 1998.

Table 3.5: Estimated sedimentation rates for the Rees-Dart delta

Time range	No. of years	Volume of sediment ($\times 10^6$ m^3)	Average annual rate of sediment accumulation ($\times 10^6$ m^3/year)
Mar 1966 to Nov1998	33	7.2	0.22 ± 0.04
Nov 1998 to Feb 2007	8	4.1	0.51 ± 0.18
Mar 1966 to Feb 2007	41	11.3	0.28 ± 0.03

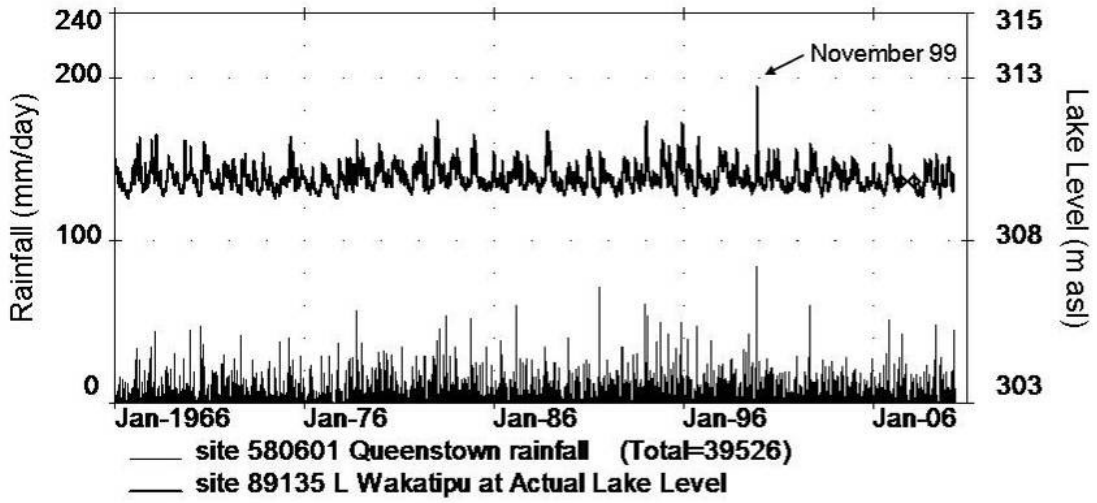

Figure 3.34: Rainfall (mm/day) and Lake Wakatipu levels (m above msl) for 1966 to 2007

Estimated sedimentation rates for the Rees-Dart delta between 1966 and 2007 are equivalent to a 0.3 mm/year average catchment denudation rate. A recent study by Beavan et al. (2010), based on 10 years of GPS measurements and modelling, estimates that present-day uplift rates of up to ~5 mm/year occur across the Southern Alps. This is in agreement with documented long-term uplift rates for the Rees-Dart catchment produced by Tippett and Kamp (1993), and indicates that there are likely to be significant volumes of additional sediment stored in the catchment (e.g. aggrading riverbed) and/or transported away from the delta (e.g. suspended sediment depositing further offshore, turbidity currents, etc.).

This methodology has several limitations. Firstly, an assumption is required that the delta foreset slope for each time period is similar to the data from the 2007 sonar survey. In addition, the aerial photos are limited to a ground sampling interval of 0.4 to 2.0 m, and the geo-referenced location of the delta shoreline also has errors associated with the GPS survey, since the delta topset is a dynamic

environment with no permanent landmarks that can be geo-referenced (i.e. survey points were located beyond the delta and river bed). There is also the possibility that a recent flood event, prior to aerial photographs being flown, may have reworked part of the topset and/or mouth bars so that an area of prograded delta that was previously above the lake water level may partially erode and become submerged (even though the majority of the sediment is still in-situ). This would result in progradation rates being underestimated or it may appear that the delta has even retreated. Sensitivity tests have shown that the overall accuracy of the derived sediment volumes, calculated for each time period, is likely to be approximately $\pm 1.4 \times 10^6$ m^3. This is equivalent to 0.3 to 1.8×10^5 m^3/year (using the average annual sedimentation rates in Table 3.5).

Catchment sedimentation rates calculated using this method will provide more accurate estimates for catchments where sediment transport is bedload-dominated. This is because finer material may be removed from the delta area as suspended sediment or in turbidity currents. Sedimentation rates are also likely to be under-estimated if delta topset sedimentation is excluded (as in this case here since there is a lack of historical topographical and cross sectional information for the Rees and Dart rivers); this will become more important the more the delta progrades (and consequently, the more the delta topset aggrades). The recent 2011 acquisition of LiDAR data for the Rees-Dart delta has provided some detailed topographical information (see Section 3.2.5.5). From these data the Dart and Rees River bed slopes have been estimated to be ~0.3% and ~0.23%, respectively. This means that a Dart River delta shoreline progradation distance of 200 m would increase the upstream bed level (i.e. topset) by ~0.6 m. Although it is difficult to define the upstream extent of topset aggradation occurring between 1966 and 2007, if it is assumed that the topset extended as far north as the upstream extent of the grassed island (near Glenorchy), the combined topset aggradation for both the Dart and Rees Rivers would be ~0.9×10^6 m^3. This is less than 10% of the volume of sediment estimated to be deposited on the delta foreset between 1966 and 2007 (Table 3.5)

3.2.5.4 Sediment contributions from the Rees River versus Dart River

Given the limited hydraulic data, and our specific interest in bedload sediment transport along a braided river system, the relative contribution of sediment for each river was determined using a stream power relationship (e.g. Bagnold, 1980; 1986) as in previous studies (e.g. Gomez & Church, 1989; Young & Davies, 1990; Martin & Church, 2000) in which bedload transport rate is proportional to (excess stream power)$^{1.5}$. Assuming both the Dart and Rees Rivers have similar hydraulic characteristics (i.e. grain sizes, flow depths, slope, q_o, etc.), the following relationship follows

$$\frac{i_{b(\text{Dart})}}{i_{b(\text{Rees})}} \propto \left[\frac{(\omega-\omega_o)_{\text{Dart}}}{(\omega-\omega_o)_{\text{Rees}}}\right]^{1.5} \propto \left[\frac{(q-q_o)_{\text{Dart}}}{(q-q_o)_{\text{Rees}}}\right]^{1.5} \quad \textbf{(3.1)}$$

Where: i_b = transport rate per unit width (kg/m-s)

ω = ρSq = stream power per unit width (kg/m-s)
ω_o = threshold stream power per unit width (kg/m-s)
ρ = water density (kg/m^3)
S = channel slope (m/m)
q = channel flow per unit width (m^2/s)
q_o = threshold channel flow per unit width (m^2/s)

Recent studies (e.g. Bertoldi et al., 2009a; Ashmore et al., 2011) have also shown that

$$\frac{b_a}{b_w} \alpha \frac{Q S'}{b_w \sqrt{g \Delta D_{50}{}^3}} \quad \textbf{(3.2)}$$

Where:
b_a = active channel width (m)
b_w = wetted channel width (m)
Q = discharge (m^3/s)
S' = longitudinal free water surface slope (m/m)
g = acceleration due to gravity (m/s^2)
Δ = relative submerged density
D_{50} = mean grain size (m)

For a fixed surface slope, and mean sediment size, b_a is proportional to Q. The ratio of total bedload transport rate (I_b, kg/s) for the Dart and Rees Rivers can then be estimated as

$$\frac{I_{b(\text{Dart})}}{I_{b(\text{Rees})}} = \frac{i_{b(\text{Dart})}}{i_{b(\text{Rees})}} \times \frac{b_{a(\text{Dart})}}{b_{a(\text{Rees})}} \approx \left(\frac{Q_{\text{Dart}} / b_{w(\text{Dart})}}{Q_{\text{Rees}} / b_{w(\text{Rees})}} \right)^{1.5} \times \frac{b_{a(\text{Dart})}}{b_{a(\text{Rees})}} = \left(\frac{Q_{\text{Dart}}}{Q_{\text{Rees}}} \right)^{2.5} \times \left(\frac{b_{w(\text{Dart})}}{b_{w(\text{Rees})}} \right)^{-1.5} \quad \textbf{(3.3)}$$

Based on hydraulic geometry, b_w for a braided river can be approximated as $b_w = aQ^{0.5}$ (Leopold & Maddock, 1953; Hey & Thorne, 1986) and the following bedload transport relationship can be derived

$$\frac{I_{b(\text{Dart})}}{I_{b(\text{Rees})}} \approx \left(\frac{Q_{\text{Dart}}}{Q_{\text{Rees}}} \right)^{1.75} \quad \textbf{(3.4)}$$

Based on this relationship, Q_{Dart}/Q_{Rees} ratios ranging from 1.9 to 3.1 ($I_{b(Dart)}/I_{b(Rees)}$ ~3.1 to 7.2), and an average total sediment supply rate of 0.28 ± 0.03 x 10^6 m^3/yr, the Rees and Dart River average sediment supply rates are estimated to be of the order of 0.03 to 0.07 x 10^6 m^3/yr and 0.18 to 0.27 x 10^6 m^3/yr, respectively.

3.2.5.5 LiDAR data

Light Detecting and Ranging (LiDAR) data are ideal for identifying the features of braided river systems since large quantities of high-density topographic data can be acquired over short periods of time. This method of data collection has been made possible in the past 30 years due to the development of global positioning system (GPS) technology. During LiDAR surveys, GPS units located on both the aircraft and ground determine the aircraft location. Simultaneously, an aircraft-mounted inertial navigational system (INS) and LiDAR instrument (i.e. high frequency infrared laser beam) determine the location of the ground features relative to the aircraft. Further information on LiDAR is available from many internet sources as well as reference texts (e.g. Paine & Kiser, 2012).

Between 30 September and 3 October 2011 LiDAR topographic data were collected for the Rees-Dart delta. During the data collection period the lake level was ~309.6 m asl (i.e. a lower than average winter lake level prior to the higher lake levels that occur in spring and summer). The lower lake level was an advantage since more of the Rees-Dart river delta topset, including river mouth bar formations, were able to be observed. Figure 3.35 shows detrended LiDAR data with a slope of 0.28% (i.e. average riverbed slope) removed from the original LiDAR data.

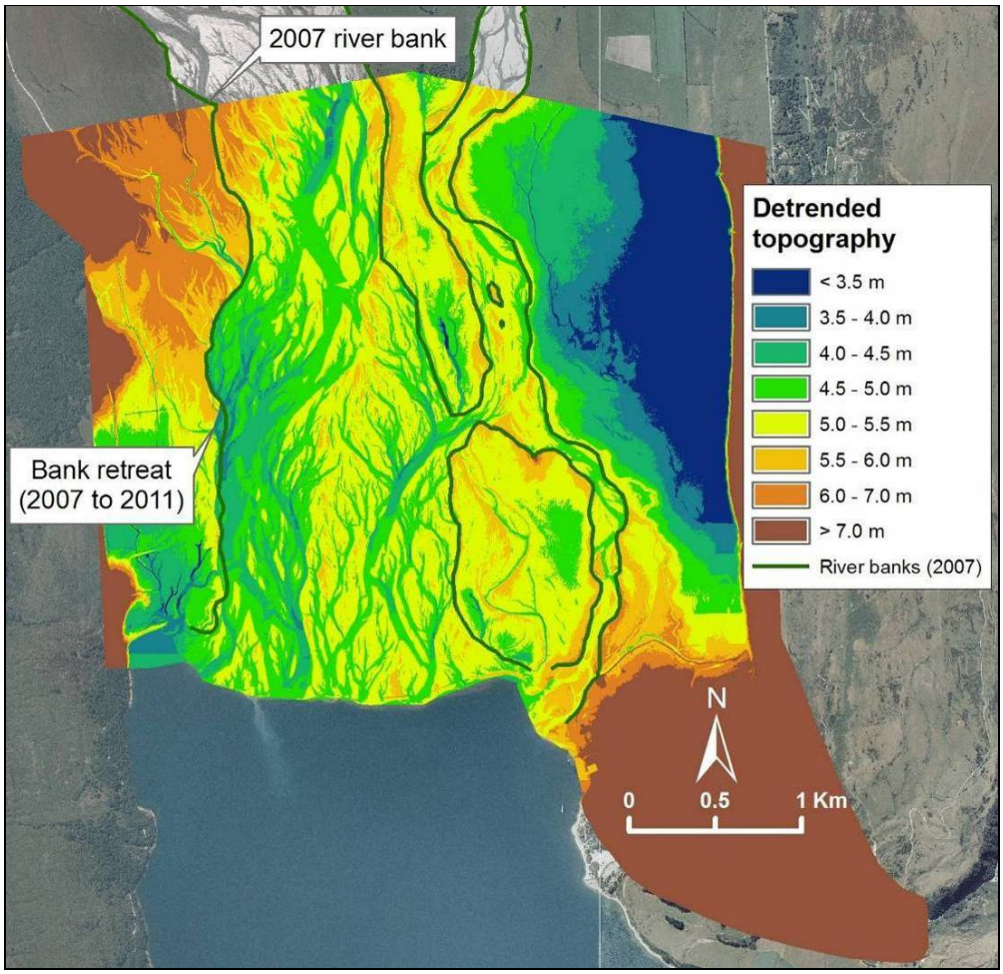

Figure 3.35: Detrended 2011 LiDAR data for the Rees-Dart delta and river system

The 2007 river bank location has also been added to Figure 3.35, showing that between 2007 and 2011 bank erosion has continued on the Dart River TRB with an additional ~0.06 km^2 of farmland lost to the river. Assuming an average depth of 1 m for the eroded banks, this would supply an estimated additional 0.6 x 10^5 m^3 of sediment to the delta in the vicinity of Kinloch.

Approximately 1.5 km upstream of the lake the river bank has retreated by up to 70 m since 2007, placing some sections of the road to Kinloch within 150 to 170 m of the Dart River TRB. Continued bank erosion in this area will inevitably result in the Dart River finding the shorter and steeper route to the lake via the lagoon at Kinloch (rather than the existing route to the lake via the currently prograding and aggrading delta).

Other observations from Figure 3.35 include:

- River bed levels in the Rees River near the lake are similar to levels in the north-western portion of Glenorchy.
- Natural levees appear to have formed along much of the Rees River (e.g. between the Rees River TLB and the lagoon to the east) as well as along the banks of the grassed island to the north-west of Glenorchy.

At present, under normal flow conditions a natural, elevated, "levee-type" formation divides the active Dart River flow from the active Rees River flow (channel passing flow onto the Dart River floodplain upstream of the grassed island).

Observations from the LiDAR data are consistent with the experimental observations of Sheets et al. (2002, p. 300) where "established channels act largely as conduits for sediment, while overbank spills, flow expansions and failed avulsions all deposit a disproportionate amount of sediment".

3.2.5.6 Rees-Dart river mouth processes

The 2011 LiDAR data have also been used to examine the Rees-Dart delta near the shoreline (Figure 3.36). One of the main observations that can be made from Figure 3.36 is that the least active areas of the delta have more prominent mouth bar formations shown in brown by the 310.5 m contour. This is due to the limited exposure these areas have had to reworking by the braided river flows since their creation. It is therefore likely that the Kinloch waterfront and the eastern Dart River have had the lowest rates of recent delta progradation, while the western Dart River and Rees River will have experienced more rapid rates of delta progradation – which is in agreement with the observations in Figure 3.24. Closer inspection of the river mouth bar formations shows that they tend to attach themselves to the shoreline in the east, with the river flowing into the lake to the west of the mouth bar.

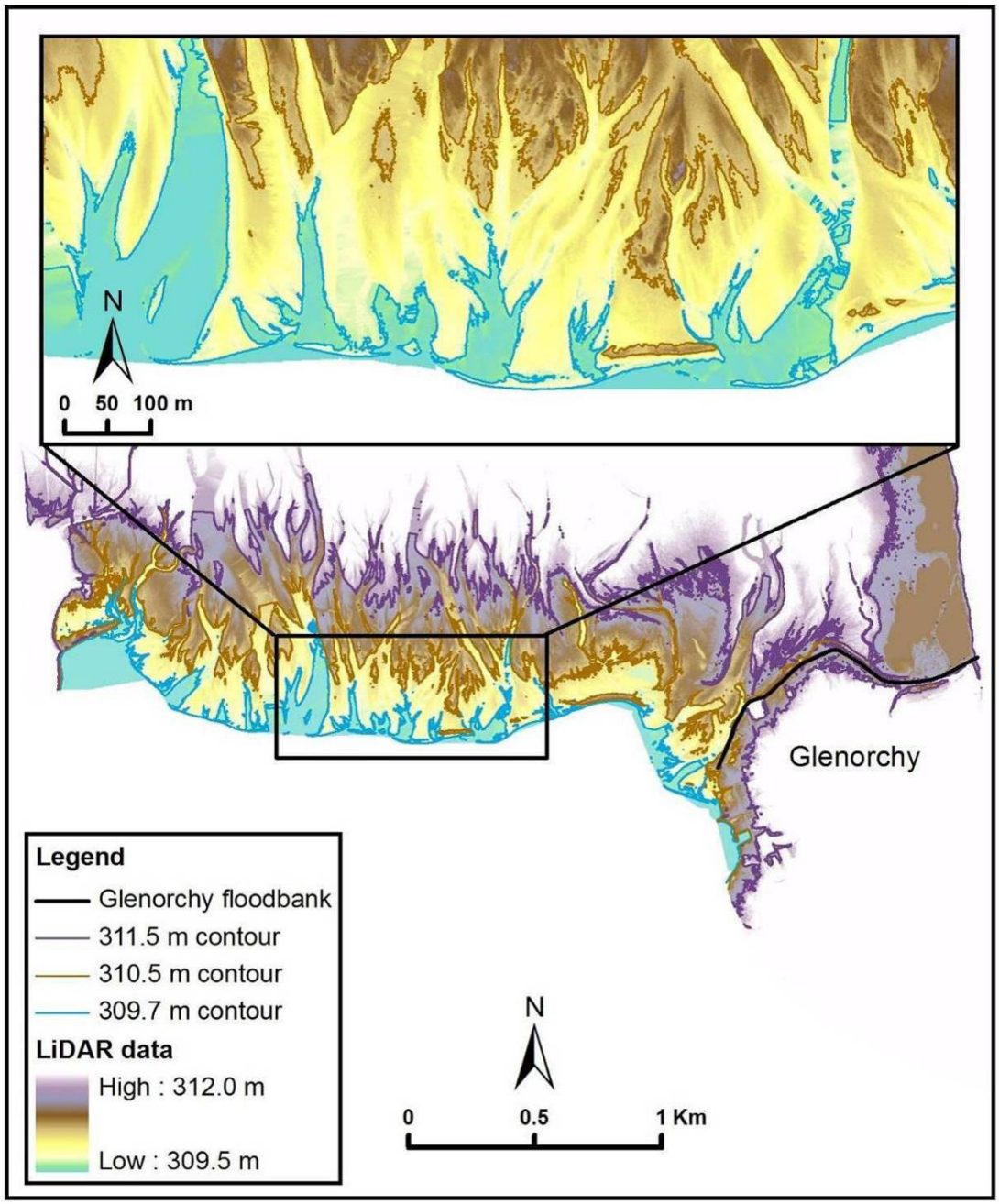

Figure 3.36: 2011 LiDAR data showing Rees-Dart shoreline features

Although changes in channel locations are rarely noticed or documented, Dart River mouth activity in February/March 2008 was monitored for several weeks as the river channel near Kinloch gradually changed course before "a sudden change in direction caused 15 m of land to disappear alongside the Kinloch Foreshore Reserve near Glenorchy and the Department of Conservation closed a part of the popular camping and swimming area" (http://www.odt.co.nz/your-town/glenorchy/1616/threat-reserve-subsides). In this 6th March 2008 newspaper (Otago Daily Times) article it was also reported that "despite fears wet weather would make the situation worse, the heavy rain over the weekend caused the river to resume its previous course" (http://www.odt.co.nz/your-

town/glenorchy/1616/threat-reserve-subsides). The Dart at the Hillocks flow record (Figure 3.37) shows that the first rapid change in channel course was likely to be due to flows of up to 625 m^3/s on 24th February 2008, while the flows of up to 774 m^3/s on 1st March 2008 led to the channel switching back to its previous course. Flows of this magnitude or greater have occurred ~0.5% of the time since the flow record began in 1996.

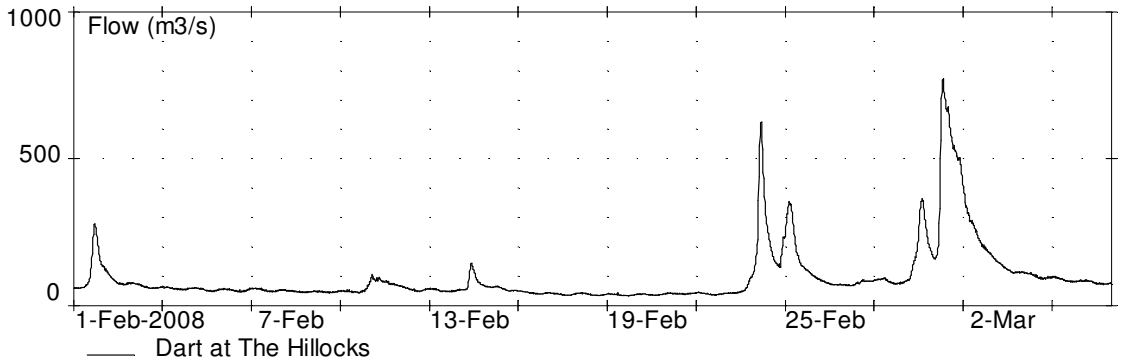

Figure 3.37: Dart at the Hillocks river flows from 1 February to 6 March 2008

Figure 3.38 shows the maximum monthly Dart River flows, and Figure 3.39 compares 2007 aerial photographs of the Kinloch Foreshore Reserve to 2011 LiDAR data - showing the erosion and delta progradation that has taken place over this time period. Between the February 2007 aerial photographs and the September/October 2011 LiDAR survey, 4 of the 5 largest recorded flows occurred with peak flows reaching between 1150 and 1469 m^3/s. The largest two events had return periods of 10+ years while the smaller two events had return periods of 3 to 4 years.

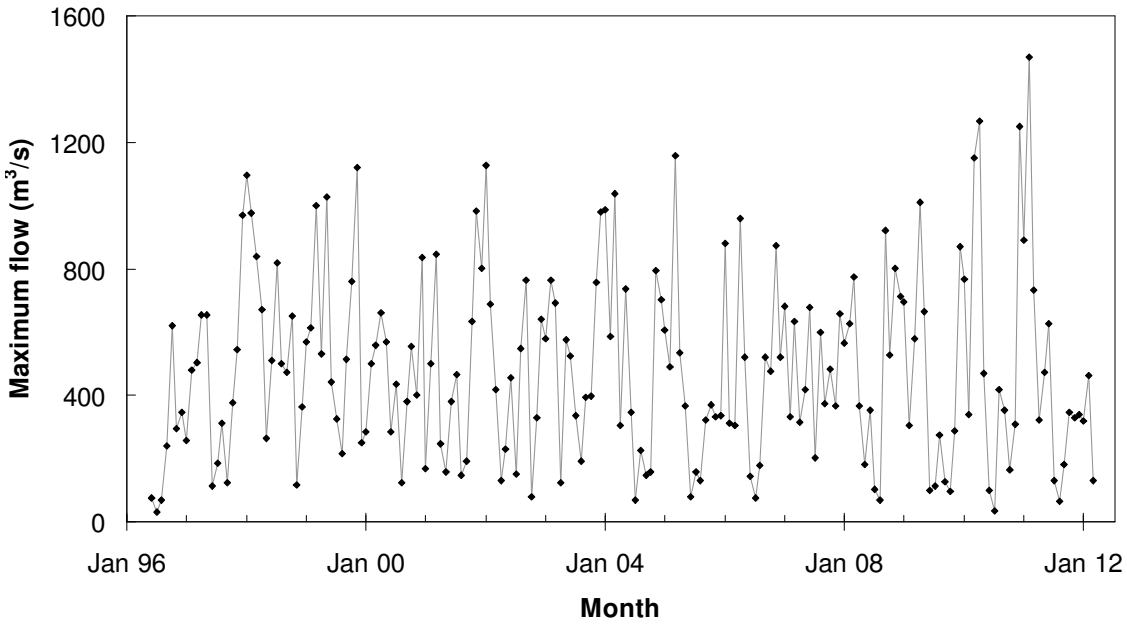

Figure 3.38: Dart at the Hillocks maximum monthly river flow

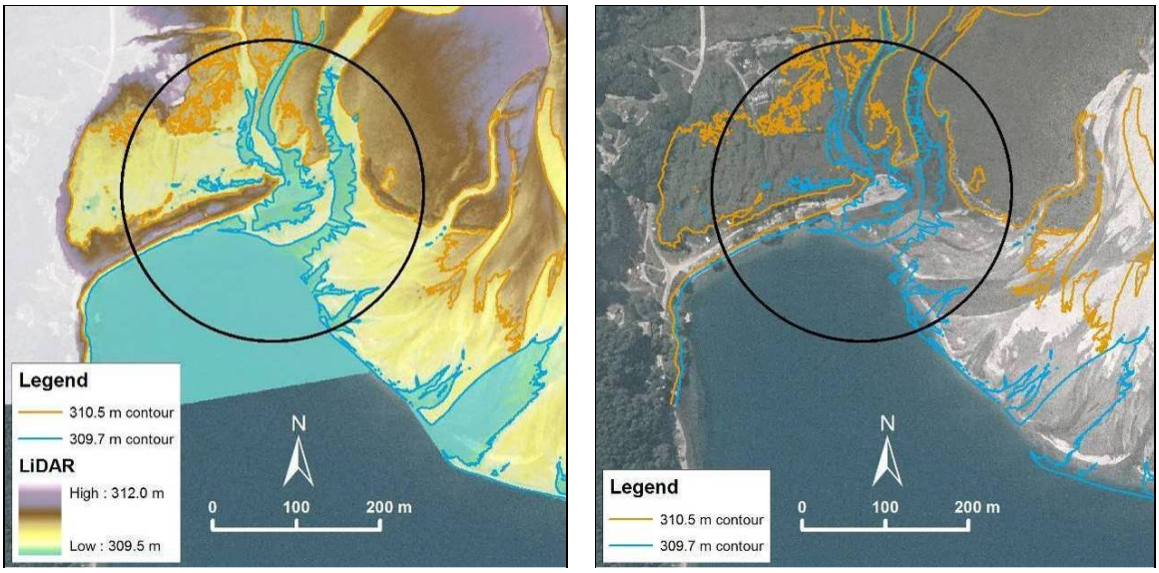

a) 2011 LiDAR data b) 2011 LiDAR contours on 2007 photograph

Figure 3.39: Rees-Dart delta at Kinloch comparison between a) 2011 LiDAR data, and b) 2007 aerial photography

The resulting delta progradation between February 2007 and September/October 2011 is shown in Figure 3.40 (for shoreline contour levels of 309.8 m asl) and equates to an increase in delta surface area of ~34 100 m^2 (or 6820 m^2/yr) over ~5 years. This is 1.4 times the average rate of surface area increase between 1966 and 2007 (4951 m^2/yr), and raises the mean rate of increase in surface area between 1966 and 2011 to 5154 m^2/yr.

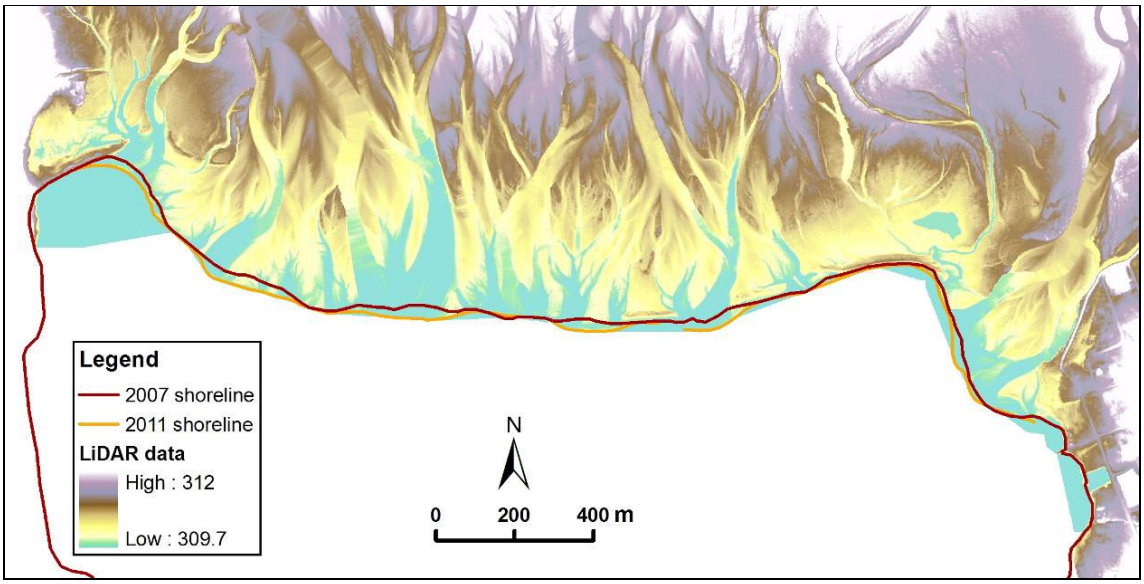

Figure 3.40: Rees-Dart delta growth between February 2007 and October 2011

Delta growth over the 2007 to 2011 time period produced 'bulges' in the shoreline where the channels exited into the lake depositing sediment (Figure 3.40). The sediment was distributed over ~200 to 320

m lengths of the shoreline as the mobile, braided river channels altered course due to a combination of natural braided river processes and the influence of the lake backwater effects. As the Dart and Rees rivers have an estimated backwater adaptation length of flow, λ_{BW}, of ~100 m and an adaptation length of a bed disturbance, $\lambda_{S,}$ of ~300 - 400 m (Table 3.1), at distances greater than 400 m upstream of the shoreline braided river processes are likely to have more of an influence on flow behaviour than the lake backwater effects.

In places the Dart River delta shoreline has advanced by up to 35 m horizontally between 2007 and 2011; less obvious advances were observed for the Rees River delta suggesting that a large portion of the Rees River sediment was probably passing onto the Dart River delta during this time.

3.3 Clutha River/Mata-Au delta

Little is known about the growth of the relatively new Clutha River/Mata-Au delta that has formed since the construction of the Clyde Dam, and filling of Lake Dunstan in September 1993 (Figures 3.41, 3.42 and 3.43). As this delta progrades along the 'drowned' river channel, there will be significantly less storage capacity for accumulating sediment compared to, for example, the Rees-Dart delta that is prograding into a deep lake. Fortunately a substantial portion of the catchment runoff passes through Lake Wanaka or Lake Hawea which attenuates flood flows and 'traps' incoming sediment – reducing the amount of sediment supplied to the Clutha River/Mata-Au delta.

The growth of the Clutha River/Mata-Au delta is of interest as delta progradation will lead to reduced storage capacity within Lake Dunstan, possible increased abrasion on downstream power station turbines and additional aesthetic and recreational issues relating to the growth of aquatic plants in shallow, silty lake areas where the prograding delta material deposits (Ministry of Works and Development, 1976). Growth of the delta will also lead to aggradation in the river channels upstream of the delta which will potentially increase flooding risk to the adjacent and upstream land that is currently under pressure to be developed.

The Clutha River/Mata-Au delta is located in a wide, shallow valley formed during Late Quaternary glacial advances and retreats from the upstream Lake Wanaka and Lake Hawea catchments (Ministry of Works and Development, 1977a). As the glaciers advanced and retreated the Clutha River aggraded and degraded, forming various glacial gravel outwash terraces in the valley (Ministry of Works and Development, 1977a). These alluvial terraces and fans line both sides of the valley, upstream of the delta, as well as the western side of Lake Dunstan; the Dunstan Mountains (up to 1700 m) follow the eastern side of Lake Dunstan, and the relatively steep rock slopes of the Pisa Range (up to 2000 m) rise beyond the alluvial terraces and fans to the west of the river. During the cold winters snow accumulates along these ranges; in spring-summer warm, heavy north-westerly rainfalls can rapidly melt this snowpack exacerbating any flood flows (Waugh et al., 2000). The steep rock slopes, and

most of the baserock within the valley, also consists of quartzofeldspathic schist (Ministry of Works and Development, 1977a) which rapidly erodes by physical and chemical weathering in this environment.

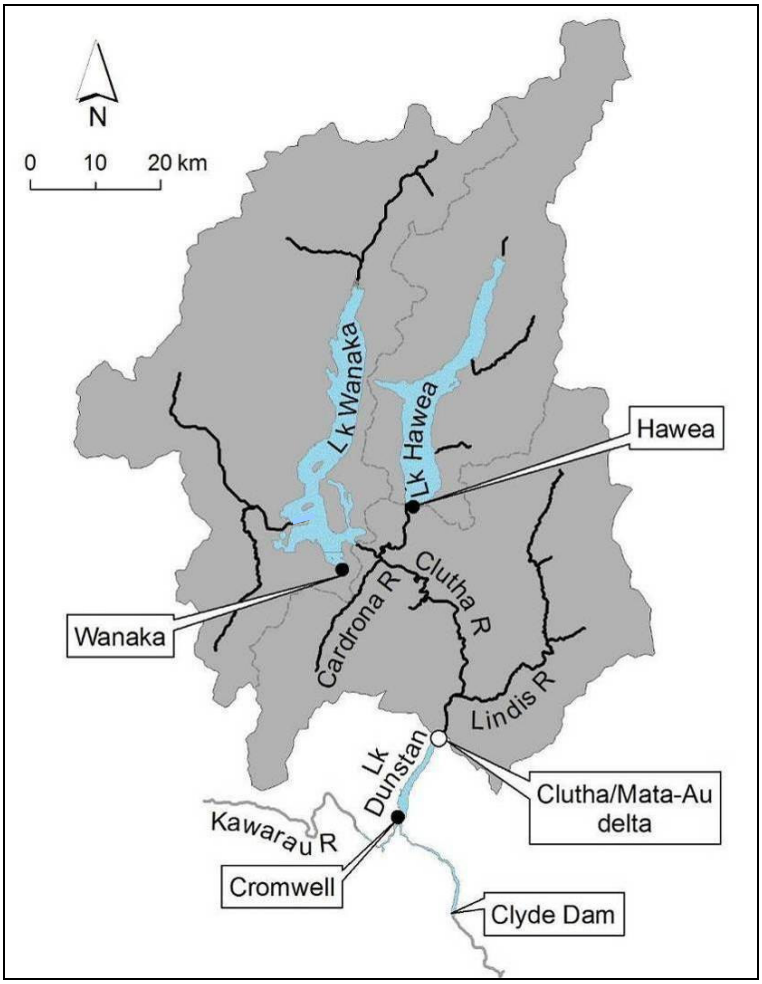

Figure 3.41: Upper Clutha River/Mata-Au location map

Figure 3.42: Clutha River/Mata-Au delta on 17 March 2010 [Source: Contact Energy Ltd]

Figure 3.43: Aerial view of the Clutha River/Mata-Au delta in 2009 [Source: Contact Energy Ltd]

3.3.1 Upper Clutha River system

Upstream of the Clutha River/Mata-Au delta 67% (4012 km^2) of the catchment area passes flow and sediment directly into Lakes Wanaka and Hawea where sediment is trapped and flood flows are attenuated and/or controlled. The remaining 2002 km^2 of the catchment, which provides the sediment that is accumulating at the Clutha River/Mata-Au delta, includes the Lindis River, Cardrona River, Hawea River, and other minor tributaries. As such a large proportion of the mean flow entering the Clutha River is free of sediment, the river should have sufficient capacity to transport all suspended sediment that does enter the river (Ministry of Works and Development, 1976). A brief description of the lakes and rivers feeding into the Clutha River/Mata-Au delta are summarised below.

3.3.1.1 Lake Wanaka

Lake Wanaka is a natural, uncontrolled lake with a catchment area of 2628 km^2. This lake has formed in a deep glacial basin with a mainly natural upper catchment vegetated with native forests, scrub, tussocks, etc. (Waugh et al., 2000). Nor-westerly storms tend to provide the most substantial flood events for Lake Wanaka – especially in spring and summer when rapid snow melt can exacerbate flood flows (Waugh et al., 2000).

3.3.1.2 Lake Hawea

Lake Hawea is a deep glacial lake with a catchment area of 1384 km^2, and controlled lake levels to provide additional storage. Before the dam was constructed, Lake Hawea had a mean level of 327.61 m; the current minimum and maximum control levels are 338.0 and 346.0 m, respectively, although under extreme conditions the lake can be lowered to 330.0 m (Waugh et al., 2000).

Hawea Dam was constructed between 1954 and 1958, and filled in 1959. The four sluice gates control outflows into the Hawea River, and allow Lake Hawea to provide additional storage for Roxburgh power station which was completed in 1956 (Waugh et al., 2000). In the unlikely event that the lake level reaches 350.5 m, the Gladstone Gap Emergency Spillway (constructed in 1956) is designed to be overtopped and eroded away to allow flood waters to pass along the old river channels and rejoin the river downstream (Waugh et al., 2000). The combined flood capacity of the four sluice gates and the Gladstone Gap is 730 m^3/s, although the normal operating maximum discharge is limited to 200 m^3/s to prevent erosion in the Lower Hawea River. The normal operating minimum flow release to the Hawea River is 6 m^3/s, which is the minimum operational flow for the control structure. At present Contact Energy has resource consent to install a 17.2 MW hydro-generation facility in this control structure. Should this project be undertaken it is not expected to have any long-term impacts on the river environment (http://www.odt.co.nz/your-town/hawea/193439/contact-vies-more-time-establish-hydro-scheme).

The south shore of Lake Hawea experienced accelerated rates of erosion from 1960, when the operation of the lake was modified to allow for the storage of summer flows for winter release (Ministry of Works and Development, 1976). Substantial volumes of glacial till (including 30 000 tonnes of gravel) passed downstream into the Clutha River via the new lake outlet while the area adjusted to the new operating regime (Ministry of Works and Development, 1976).

3.3.1.3 Cardrona River

The Cardrona River flows in a northwest direction along a steep, narrow river valley and joins the Clutha River/Mata-Au at Albert Town, which is approximately 37 km upstream of Lake Dunstan and 4 km downstream of Lake Wanaka. The 346 km^2 Cardrona catchment is bounded by the Criffel Range, to the east, and the Crown Range, to the south and west. In the mountain ranges located in the upper catchment the median annual rainfall is 1250 to 1500 mm, while the lower catchment only receives 650 to 700 mm (Otago Regional Council, 2007).

The upper catchment vegetation is mainly tussock and pasture used for sheep and beef farming. More productive pasture, deer farming, and tourism are other land uses found in the lower catchment (Otago Regional Council, 2007).

Over the summer period low rainfall and high evapotranspiration rates lead to a moisture deficit. There are also river abstractions for irrigation up to a maximum consented take of approximately 2.8 m^3/s (Otago Regional Council, 2007). Abstractions from the Cardrona River, together with groundwater losses, mean that most summers the lower reach of the Cardrona River can dry up. However, by the time the river has reached the Clutha confluence, groundwater and excess irrigation water usually allow the river to regain some flow (Otago Regional Council, 2007).

Figure 3.44 shows the 1979 to 2001 flow record for the Cardrona River at Albert Town (Site 75290). The highest Cardrona River flows tend to occur during the months of September and October, during the spring melt. Figure 3.45 shows that flows from the Cardrona River will exceed 20 m^3/s approximately 1% of the time, and 10 m^3/s approximately 3% of the time. At this site the river is estimated to have a suspended sediment yield (SSY) of 159 $t/km^2/yr$ (Hicks et al., 2011), and bed-moving flows of 1.3 and 3.9 m^3/s for the d_{50} (24.3 mm) and d_{84} (78 mm) bed materials, respectively (Clausen & Plew, 2004).

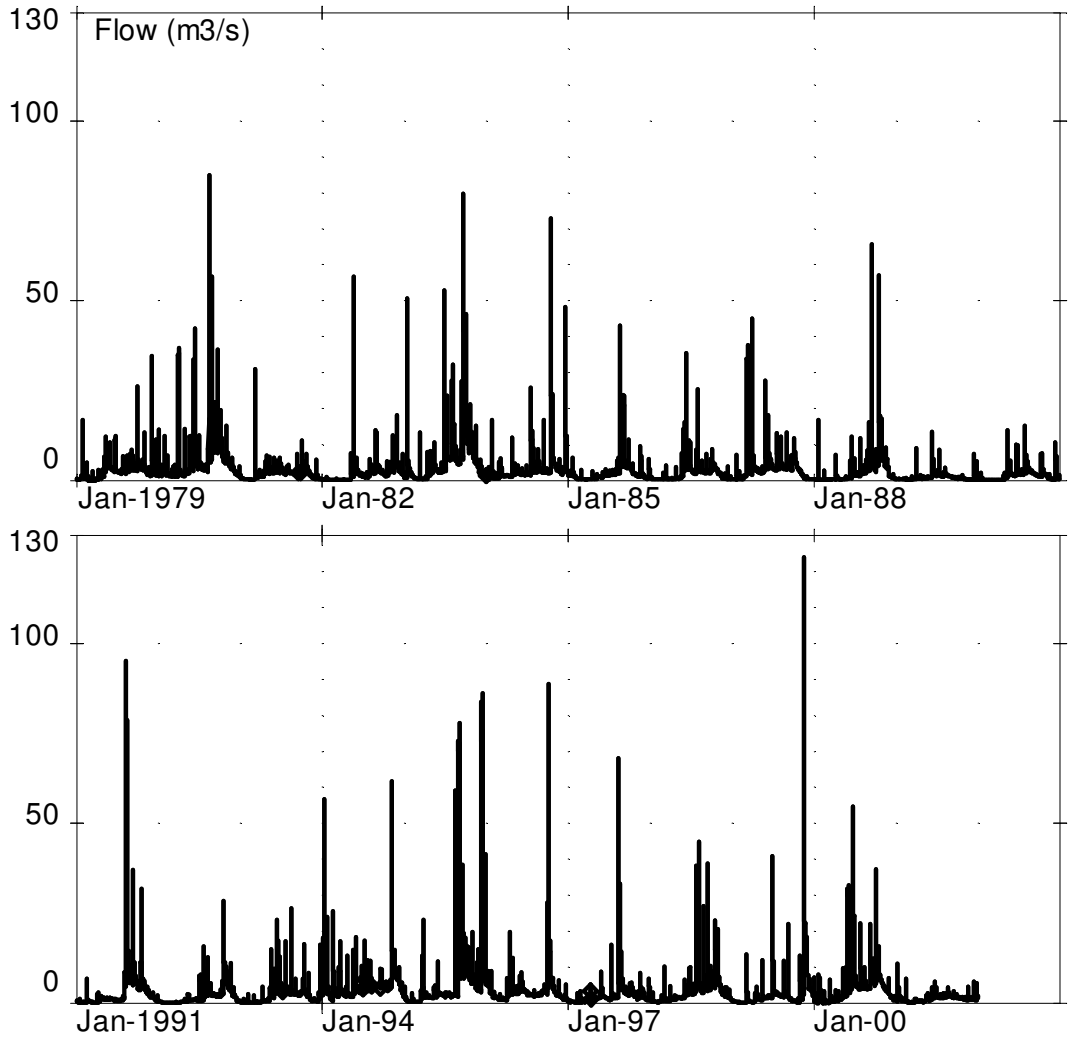

Figure 3.44: Cardrona at Albert Town flow record (1979 to 2001)

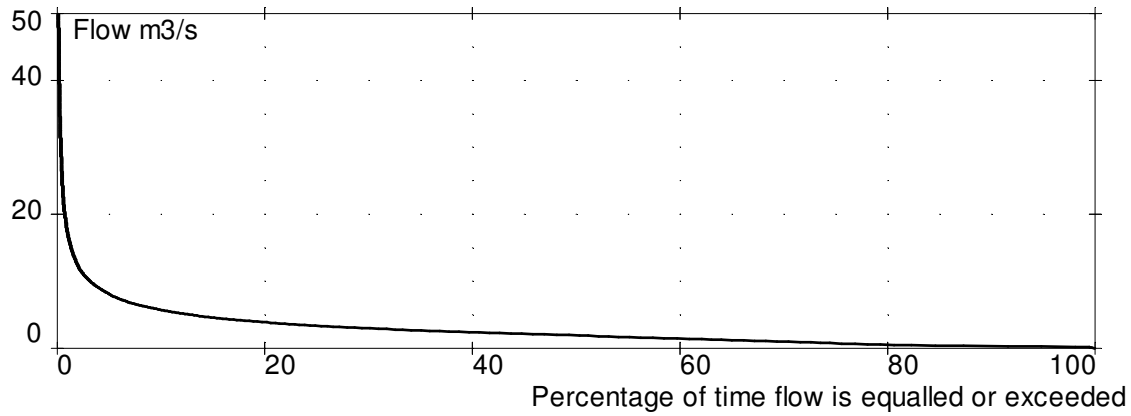

Figure 3.45: Cardrona at Albert Town flow distribution plot (1979 to 2001)

3.3.1.4 Lindis River

The Lindis River flows along a steep river valley and joins the Clutha River/Mata-Au approximately 6 km upstream of Lake Dunstan. The 1050 km^2 Lindis catchment receives high rainfall in the upper catchment during winter and spring, which can lead to high flows during the spring melt. In contrast, the lower catchment receives very little rainfall during the summer months and is part of the very dry Central Otago zone.

The upper catchment vegetation is mainly tussock and pasture for sheep and beef farming. More productive pasture and viticulture are the main land uses in the lower catchment (Otago Regional Council, 2008b).

Between October and April, water abstractions take place in the middle to lower Lindis catchment resulting in flows in the upper catchment (Lindis at Lindis Peak, Site 75219) that are up to 3 m^3/s greater than at those recorded further downstream (Lindis at Ardgour Road, Site 1075253). Outside of this abstraction period (May to September) the Ardgour Road flows tend to show the same trends as the upstream site, and are generally higher than the Lindis Peak flows – except for the peak flood flows for which Lindis Peak flows tend to also be higher (Figure 3.46). A map showing the recorder sites is provided in Appendix A (Figure A1).

Otago Regional Council (2008b) observed that, around February, flows at Lindis at Crossing Bridge (Site 75218) dropped below the flows recorded 3 km further upstream at Ardgour Road, and remained lower for several months. This was assumed to be due to losses to groundwater when recharge levels are low over the summer period since the abstractions are further upstream. It is also likely that during extremely dry summers the Lindis River will naturally dry up around the Clutha River/Mata-Au confluence for some period of time (even if no abstractions were allowed). As the availability of water for the existing water scheme (that abstracts water from the Lindis River) is unreliable, and it is likely that when the existing water rights expire in 2021 they will only be renewed for a reduced rate of water abstraction, it has been proposed that water for the Tarras Water Scheme (TWS) be abtracted

from the Clutha River/Mata-Au instead (Aqualinc, 2009). The proposed TWS would pump a maximum total flow of 4.5 m^3/s from two infiltration galleries on the Clutha River/Mata-Au TLB (located ~9 km upstream and ~0.2 km downstream of the Lindis River confluence). The environmental impacts of this proposed Clutha River/Mata-Au water abstraction are considered negligible, and the reduced rate of abstraction from the Lindis River is considered beneficial (Aqualinc, 2009).

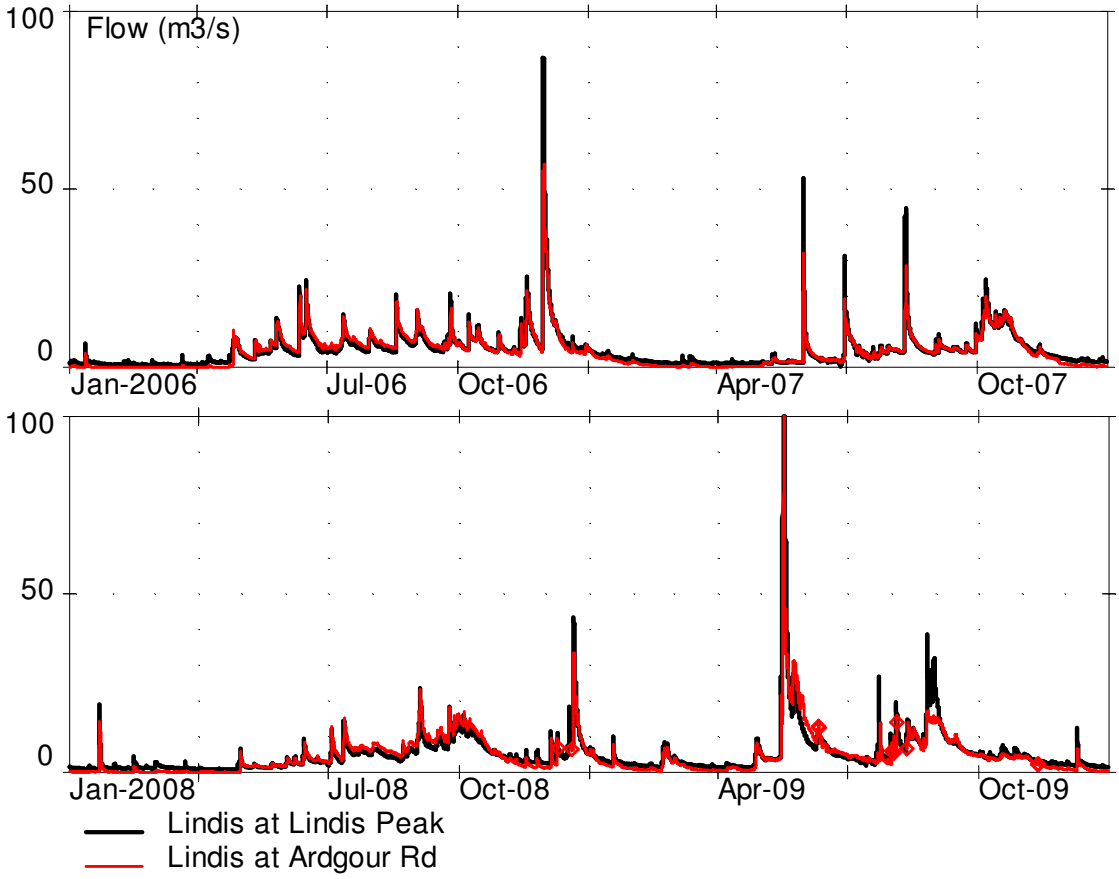

Figure 3.46: Comparison of Lindis at Lindis Peak and Lindis at Ardgour Road flows (2006 to 2009). Note: Peak flows recorded on 17 May 2009 were 263 m^3/s (Lindis Peak) and 106 m^3/s (Ardgour Road)

Assuming that the peak flood flows at Ardgour Road are similar to those at the Clutha River\Mata-Au confluence, flow contributions from the Lindis River will exceed 20 m^3/s approximately 1 to 2 % of the time and 10 m^3/s approximately 10% of the time (Figure 3.47). The estimated average annual suspended sediment yields for the Crossing Bridge and Lindis Peak sites are 77 and 106 $t/km^2/yr$, respectively (Hicks et al., 2011), although the Crossing Bridge site used less than 3 years of data and 10 gaugings.

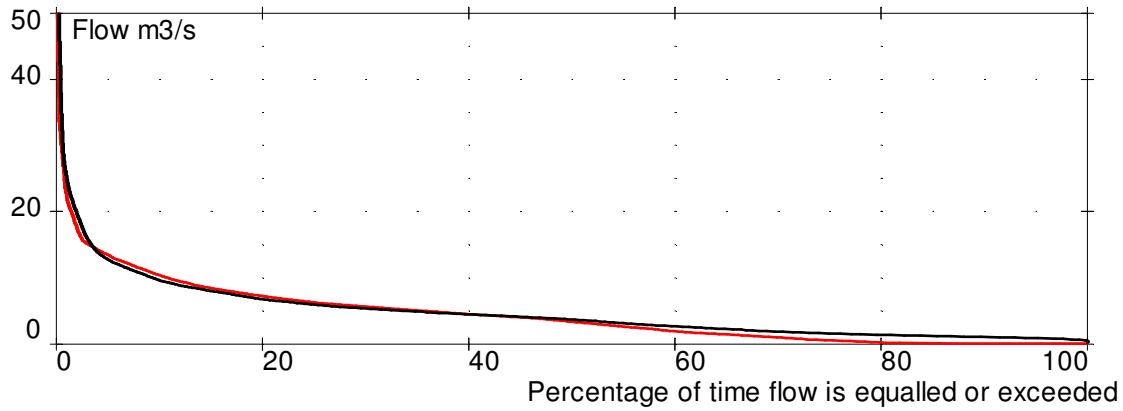

Figure 3.47: Comparison of Lindis at Lindis Peak (black) and Ardgour Road (red) flow distributions plots (2006 to 2009). Note: Peak flows are not shown for clarity

3.3.1.5 Upper Clutha River

Approximately 4 km downstream of Lake Wanaka, the Clutha at Cardrona confluence site (Site 75282, Appendix A, Figure A1) measures the combined Lake Wanaka and Hawea outflows together with the Cardrona River flows. The mean monthly flow data for this site show that the largest flows in the upper Clutha River/Mata-Au occur over the November to January period, although there is also a slight increase in flow in June/July (Figure 3.48).

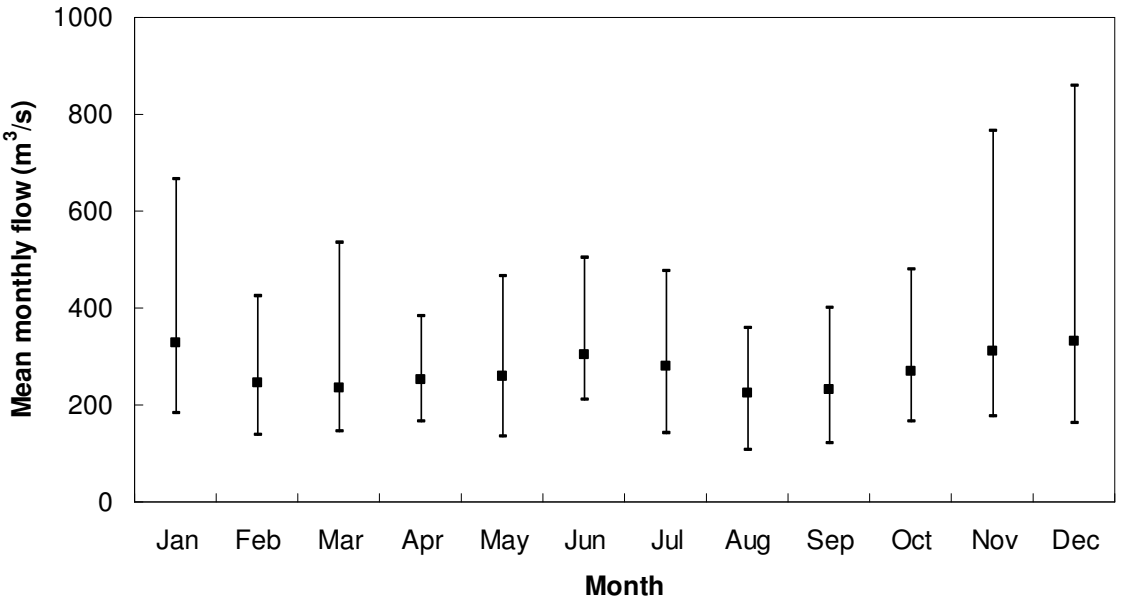

Figure 3.48: Clutha at Cardrona confluence mean monthly flows (1993 to 2009)

The natural landscape along the upper Clutha valley is predominantly vegetated with tussock grasslands (Waugh et al., 2000). Pastoral land and stone fruit orchards have also recently started to compete with viticulture and other more intensive land uses. The presence of a large, wild, rabbit population is also obvious; these pests were introduced in the 1800s and have been a problem ever since. Fortunately the land occupied for these uses does not coincide with the areas producing the

main sediment supply to the Clutha river system and, therefore, do not have a detrimental impact on sediment supply (Hicks et al., 2000). Further information on the sediment supplied to the upper Clutha River/Mata-Au (i.e. from tributaries and bank erosion) is provided in Section 3.3.3.5.

Air temperatures around Cromwell and Lake Dunstan tend to be hot and dry in summer and cold in winter, with summer temperatures generally reaching 30^{+} ºC and winter temperatures falling to around -6 ºC. The diurnal air temperature range is large and evening cooling rates are rapid.

3.3.1.6 Upper Clutha River: Lindis River confluence to Lake Dunstan

Previous (post-lake-filling) studies have identified that, even during large flood events, the main Clutha River/Mata-Au river channel transports most of the flood waters (Department of Conservation, 1992). The upper Clutha River/Mata-Au confluence with the Lindis River (a significant sediment source) is approximately 9 km upstream of Lake Dunstan, and 7.5 km upstream of the Bendigo Wildlife Reserve (Figure 3.49). The Bendigo Wildlife Reserve and the Clutha River/Mata-Au (between the Lindis River confluence and Lake Dustan) are described below.

Bendigo Wildlife Reserve

The Bendigo Wildlife Reserve has been developed on part of the Clutha River/Mata-Au delta at the upper limit of Lake Dunstan (Figure 3.49). This reserve was established to provide a shallow water refuge and breeding area for wildlife.

Prior to lake filling, vegetation clearance in the reserve area was limited to the removal of vegetation not likely to survive inundation, removal of any dead trees, and clearance of the four flood channels (Paine, 2009). This was less extensive clearance than the requirements set out in the Water Right for Clyde Dam (i.e. total clearance of vegetation in the upper 7 m of the lake) as it was considered more beneficial for the wildlife.

Under flood conditions on the Clutha River the Bendigo Wildlife Reserve is mainly submerged, and for large events (even prior to lake filling) the adjacent low-lying farmland is also inundated (Stewart, 1992). For example, during the December 1984 flood (which was estimated to have a 75-year return period), flows peaked at 1600 m^3/s on the Clutha River/Mata-Au at Lowburn (upstream of the Kawarau River confluence). During this event the proposed Bendigo Wildlife Reserve was completely submerged (Department of Conservation, 1992).

The impact of the Bendigo Wildlife Reserve and Clutha River/Mata-Au delta on flood levels, over the first 30 years post-lake-filling, was considered likely to be negligible, as long as the main flood channels remained clear of vegetation; it was also assumed that vegetation would re-establish itself in the area over time, and the main flood channels would also migrate at an undetermined future date (Stewart, 1992).

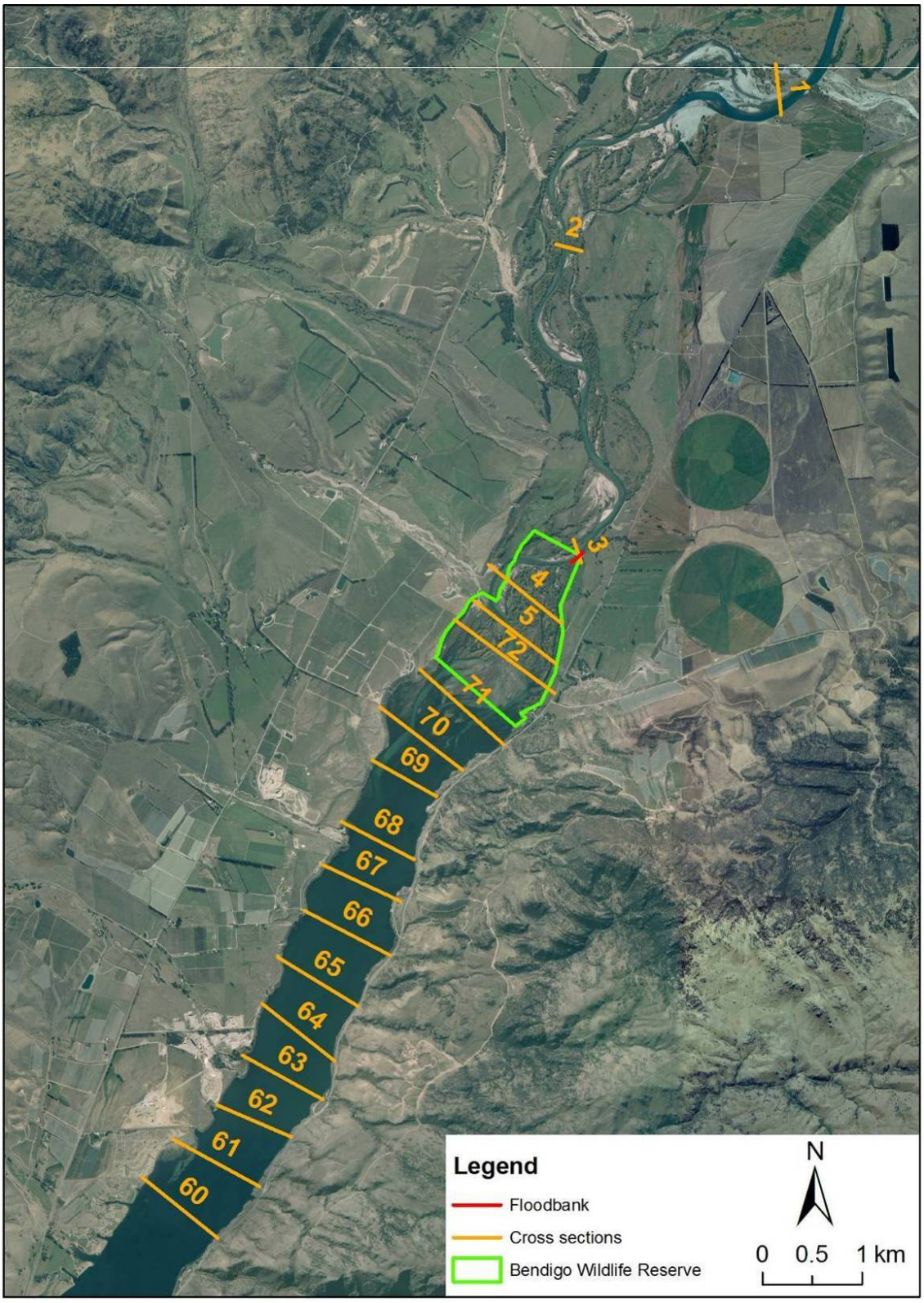

Figure 3.49: Clutha River/Mata-Au delta location map

During periods of time when no significant floods occur, new vegetation tends to establish on the exposed bars and islands in the Bendigo Wildlife Reserve area. When these areas become inundated

during flood events the vegetation is likely to obstruct flows and trap sediment (Paine, 2009). These conditions, combined with the aggrading main river channels, are likely to increase water levels upstream. At the north-eastern boundary of the wildlife reserve a floodbank was also constructed across a side channel on the TLB of the Clutha River (Figure 3.49). This floodbank was designed to reduce flooding of farmland to the east of the wildlife reserve, and to discourage the main Clutha River channel from changing course by moving further east (Stewart, 1992).

Cross section monitoring

Five cross section monitoring sites were established in May 1995 between the Lindis River confluence and Lake Dunstan (1 to 5, Figure 3.49). These cross sections were established to monitor delta sedimentation, and any other potential increase in flooding risk due to the Bendigo Wildlife Reserve and the formation of Lake Dunstan. Regular surveying of these cross sections in May 1995, July 1997, September 1999, January/February 2000 and September 2008 allowed areas of aggradation and degradationed to be identified and data acquisition and accuracy issues to be described (Paine, 2009).

Figures B1 and B2 (Appendix B) show the cross section profiles comparing 1995 to 2008 and 1999 to 2000 (i.e pre- and post- November 1999 flood), respectively. Despite some potential accuracy issues with the data (e.g. alignment of cross section survey lines), Figures 3.50 and 3.51 show that, since the filling of Lake Dunstan, there appears to be a general trend of aggradation downstream of cross section 2 (BXS2). These data are also summarised in Tables B1 and B2 (Appendix B).

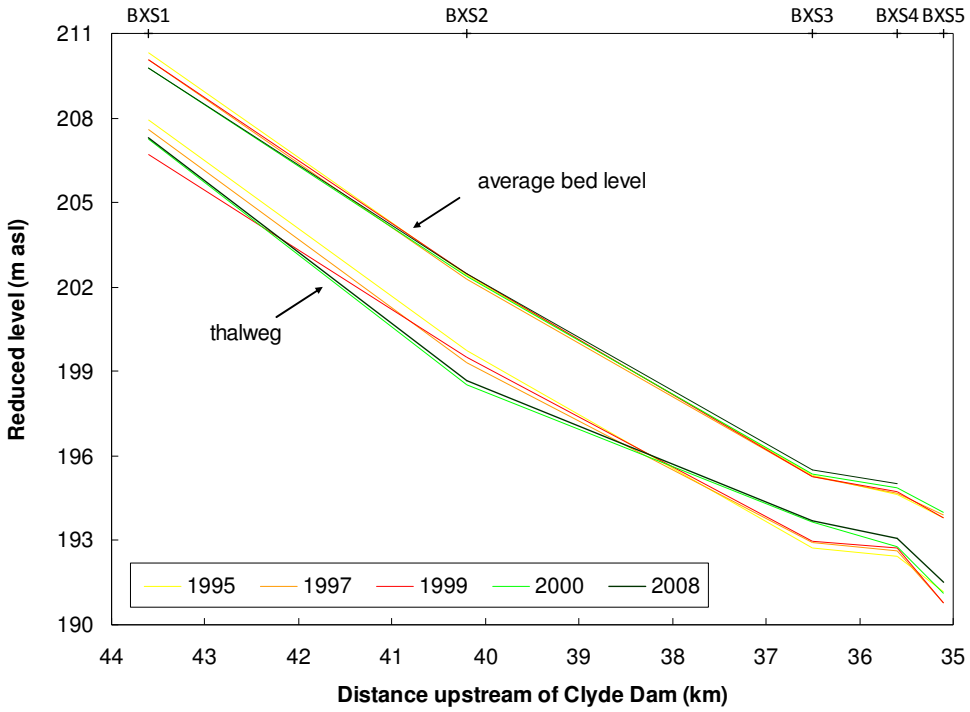

Figure 3.50: Thalweg and average bed levels for surveyed cross sections BXS1 to BXS5 between 1995 and 2008

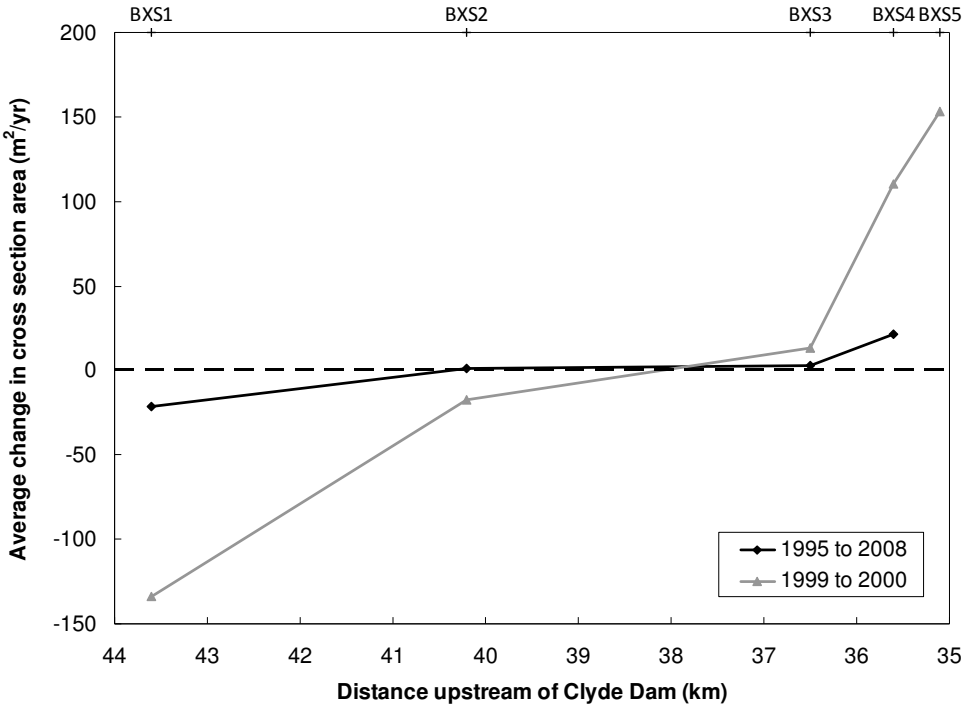

Figure 3.51: Average change in cross section area for surveyed cross sections BXS1 to BXS5 between 1995 and 2008 (negative number represents erosion and/or degradation)

Of particular note is the ~70 m of bank erosion of the Clutha River/Mata-Au TLB immediately downstream of the Lindis River confluence at cross section 1 (or BXS1). This bank erosion is responsible for the considerable increase in cross section area at this site (as shown in Figure 3.51). Cross section 5 (BXS5) was also unable to be completed in 2008.

All of the cross sections have remained relatively stable since Lake Dunstan was filled, although some bank erosion and aggradation has occurred. It would also appear that most sediment deposited in the channels during floods is reworked downstream to the delta over time (Paine, 2009). Despite the cross section data only covering a 14-year period, the average longitudinal bed level slope and thalweg slope appear to be decreasing as bed levels upstream of the Clutha River/Mata-Au delta increase.

Using the equations summarised in Kleinhans and Vandenberg (2011), the Clutha/Mata-Au River has an estimated backwater adaptation length of flow, λ_{BW}, of ~100 m and an adaptation length of a bed disturbance, $\lambda_{S,}$ of ~500 m (Table 3.1). Although there are only limited cross sections upstream of Lake Dunstan, this backwater effect is likely to explain the aggrading bed levels at Cross sections 4 and 5 (BXS4 and BXS5, Figures 3.50 and 3.51).

Aerial photography

Figure 3.52 shows aerial photography from 1949, 1984, 1996/98 and 2007 for the upper Clutha River from the Lindis River confluence downstream to Lake Dunstan. Further information, and aerial photographs of the Clutha River/Mata-Au delta, is provided in Section 3.3.3.2.

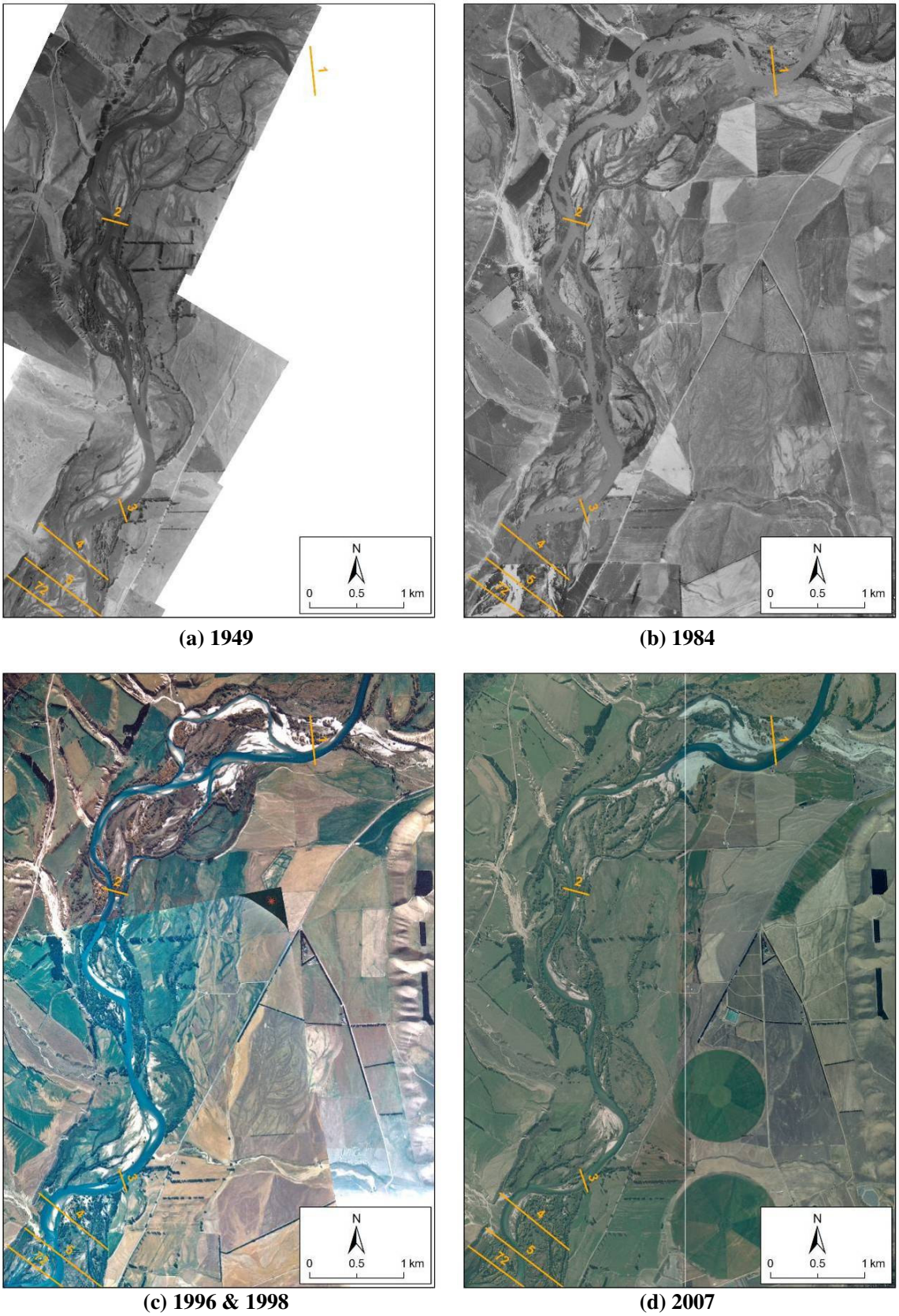

(a) 1949 (b) 1984

(c) 1996 & 1998 (d) 2007

Figure 3.52: Aerial photographs of the Clutha River from the Lindis River confluence to the Clutha River/Mata-Au delta between 1949 and 2007

Like the cross section data, these aerial photographs show the relatively stable nature of the surveyed cross section locations. They also show that the main channels for the surveyed cross section locations, as well as the reaches between the cross sections, have pretty much maintained their current location as far back as 1949 (i.e. cross sections 2 and 3, and the reach between these two sections), and since at least 1984 (i.e. cross sections 1, 4 and 5, and most of the river reaches downstream of cross section 2) with mainly minor migration of the main channel meanders.

The most significant change in the main river channel course appears to have occurred in the 1.6 km river reach downstream of cross section 1. Between 1984 and 1998 a second Clutha River/Mata-Au channel has formed further south - taking a shorter, less sinuous, route downstream – while the rest of the flow still passes along the more northern river branch. This highlights the fact that there may be aggradation and more significant channel changes occurring within the system that will not be observed in the current cross section monitoring program.

As the main river channel course changes are significantly further upstream than the backwater effects of Lake Dunstan, they are likely to be the result of natural braided river processes adjusting to the influx of sediment from the Lindis River (and other upstream sources) as well as the past change over to controlled outflows from Lake Hawea. Previous studies (e.g. Gilvear, 2004) have also noted accelerated rates of aggradation downstream of tributaries, when the upstream main river flow has been regulated. This is because the regulated flows usually reduce the magnitude and/or duration of flood peaks - channels then need to compensate for the reduced flow capacity (e.g. by adjusting course or narrowing in width, both of which can be observed in Figure 3.52 for the Clutha River/Mata-Au).

3.3.1.7 Rainfall

Rainfall in the upper Clutha catchment varies considerably with ~8000 mm/yr in the north-western alpine regions, and 406 mm/yr in Cromwell (Waugh et al., 2000). For the December 1995 flood, over 200 mm of rain fell in 48 hours in the headwaters of the lakes adjacent to the Southern Alps (Waugh et al., 2000). Over 150 mm of rain also fell in the upper Clutha catchment area that included the Lake Wanaka and Hawea headwaters, Wanaka township, and the Lindis Valley (Waugh et al., 2000). Approximately 5 days prior to this flood event a storm had already passed through the area raising lake levels and wetting the catchment. Fortuitously, heavy rainfall warnings also allowed Lake Hawea to be lowered to create additional storage capacity (Waugh et al., 2000).

3.3.1.8 Flood characteristics

At Roxburgh power station, located downstream of Clyde power station and Lake Dunstan, the largest percentage of floods (~63%) occur in Spring-Summer (October to January) during the spring melt. Only ~11% of floods occur during Winter (June to September), when precipitation is stored in the snowpack (Waugh et al., 2000), although this does include the very large September 1878 flood. During flood events (e.g. December 1995) recorded Lake Dunstan outflows were slightly smaller than

the inflows, indicating that the lake storage capacity does attenuate flood peaks to some degree (Waugh et al., 2000).

The severity of the flood events occurring at the Clutha River/Mata-Au delta appears to be dependent on the antecedent lake levels for Lakes Wanaka and Hawea, and recent storm activity wetting the catchment. For example, although Lake Wanaka inflows were significantly higher for the October 1978 flood, compared to the December 1995 and November 1999 floods, the inflows into Lake Dunstan were disproportionately lower for October 1978 due to the available storage within Lake Wanaka (Waugh et al., 2000).

Figure 3.53 shows the Clutha at Cardrona confluence (Site 75252) and Lindis at Lindis Peak (Site 75219) flow records between 1992 and 2011. During this time period the largest flood events passing the Clutha at Cardrona confluence occurred on 17 November 1999 (1620 m^3/s), 13 August 1995 (1263 m^3/s) and 24 January 1994 (1092 m^3/s). Over the same time period the largest flows passing the Lindis at Lindis Peak site occurred on 13 December 1995 (322 m^3/s), 17 November 1999 (286 m^3/s), 17 May 2009 (263 m^3/s) and 9 January 1994 (218 m^3/s). This information shows that since the November 1999 flood event this river system has had relatively few flood events – especially between 2003 and 2008.

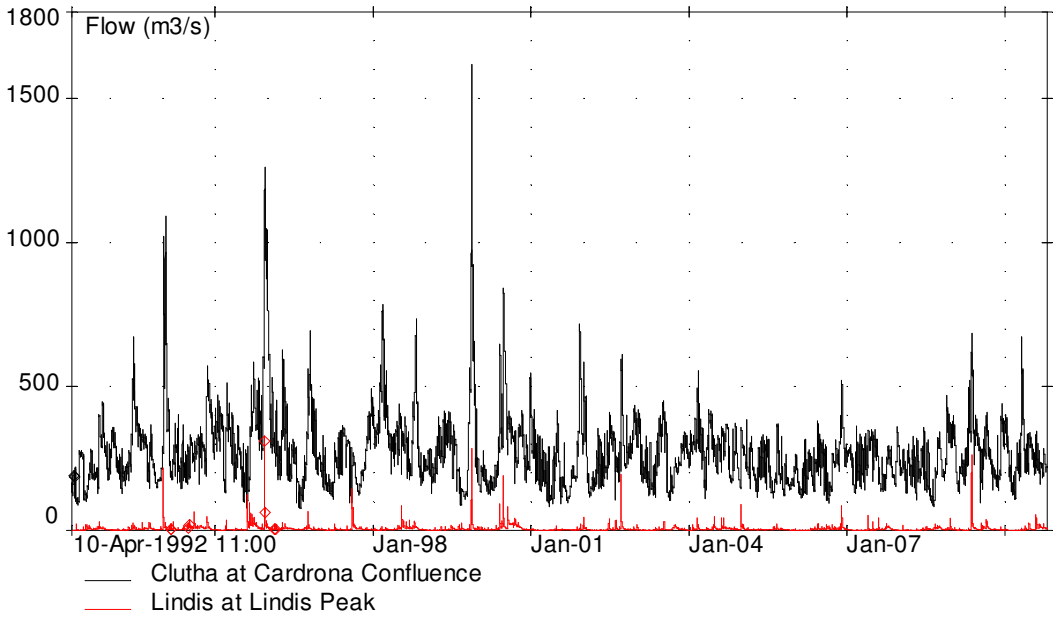

Figure 3.53: Clutha River and Lindis River flows between 1992 and 2011

3.3.1.9 Sediment yields

Large areas of dredge tailings, some now submerged in Lake Dunstan, were formed along the Clutha River during the 1890s to 1950s, and again in the 1980s, when gold mining was popular within the Otago region (Waugh et al., 2000). It is estimated that "gold mining activities during the late 19th Century probably increased sediment supplies to the Clutha River by about 50 % for several decades,

but it is expected that this 'slug' of excess sediment has long since worked its way downstream to the coast" (Hicks et al., 2000, Executive Summary).

The volume of suspended sediment and bedload transported along the Clutha river system can vary considerably for each flood event – even for the same recorded flow at a given point along the Clutha River (Jowett & Hicks, 1981). This is due to the spatial variation of the storm precipitation as well as the catchment antecedent conditions (e.g. if a large rainfall event follows a dry period, upstream lake levels and outflows may be low but the tributaries may have high flows and sediment loads, while a smaller rainfall event that follows a wet period may produce higher outflows from the lakes but smaller flows and sediment contributions from the tributaries).

Based on a suspended sediment sampling program in the upper Clutha catchment between April 1978 and June 1979 (Jowett & Hicks, 1981):

- 91% of the sediment at the Kawarau River-Clutha River confluence is derived from the Kawarau River (predominantly from the Shotover tributary), while only 9% (or 0.31 Mt) is derived from the Clutha River.

- The largest particles carried as suspended load in the Clutha River at Clyde (for location see Site 9120, Appendix A, Figure A1) are 0.2 to 0.25 mm.

- Bedload makes up 10 to 30% of the total sediment load in the Clutha River system. Larger particles are transported as suspended load in the steeper tributaries compared to the main river system, resulting in a smaller percentage of the total sediment load consisting of bedload whilst being transported in the tributaries. For example, the Shotover River at Bowens Peak (Site 75276, Appendix A, Figure A1) bedload provided 14% of the total sediment load (transporting particles coarser than 0.3 mm), while further downstream in the Clutha River at Clyde bedload provided 23% of the total sediment load (transporting particles coarser than 0.14 mm). Note: these particle sizes of 0.3 mm (Shotover River) and 0.14 mm (Clutha River at Clyde) represent the average $d_{90\%}$ for which 90% of the depth-integrated suspended sediment samples by weight are finer. This $d_{90\%}$, which represents the transition from bedload to sediment load in this study, reduces to 0.10 mm downstream of Alexandra (but still upstream of the backwater effects from Lake Roxburgh).

- In Lake Roxburgh 67% of the deposited sediment is finer than 0.10 mm, and likely to be delivered as suspended sediment. The other 33% of the sediment is likely to be transported to the lake as bedload.

A more recent study by Hicks et al. (2000) used turbidity data (together with suspended sediment samples collected adjacent to the sensor site) to determine suspended sediment concentration (SSC)

versus turbidity relationships at several sites along the Clutha river system, including on the Clutha River at the Bendigo Wildlife Reserve (i.e. at the Clutha River/Mata-Au delta). The edited turbidity record was used to produce a continuous SSC record from which event yields could be calculated. Suspended sediment yields for ungauged tributaries were also estimated using relationships derived for the gauged catchments for suspended load, basin rainfall and geology. Figure 3.54 shows the Clutha River/Mata-Au delta event yields for the 10 largest events occurring over the 1995 to 1999 period (excluding the November 1999 event due to a lack of data). The average annual suspended sediment yield over this time period was also determined to be 0.21 Mt/yr for the Clutha River\Mata-Au delta (Hicks et al., 2000), and is shown as a dashed line in Figure 3.54.

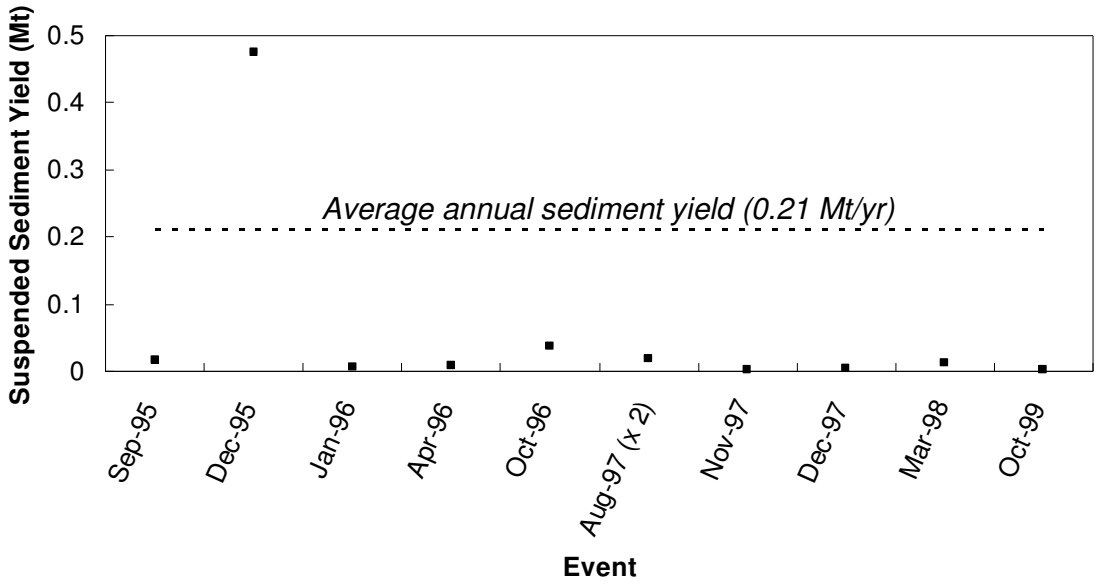

Figure 3.54: Clutha River\Mata-Au delta event yields for September 1995 to November 1999 (Hicks et al., 2000, p. 40, Table 5.4)

The suspended sediment size grading for each tributary was usually found by averaging all available grading data produced from the particle size analyses of the depth-integrated samples at each site (Hicks et al., 2000). For the Lindis at Lindis Peak (site 75219) 6 particle size analyses were averaged to produce the representative particle size distribution shown in Figure 3.55. This particle size distribution was assumed to be representative of the suspended sediment passing the Clutha River/Mata-Au delta site (given that the Lindis River is the largest upstream tributary). Using the approach of Jowett and Hicks (1981), the transition from bedload to suspended sediment transport (i.e. average $d_{90\%}$ for which 90% of the depth-integrated suspended sediment samples by weight are finer) for the Lindis River is therefore approximately 0.19 mm post-lake-filling (Figure 3.55).

Hicks et al. (2000) also estimated that the bedload for the Shotover River was approximately 20 % of the suspended sediment load, and applied this ratio to the other Clutha tributaries when estimating bedload. The Shotover River at Bowens Peak (Site 75276) bedload particle size distribution was also

considered representative of the other tributaries (Hicks et al., 2000). Estimates of the amount of bedload undergoing abrasion (i.e. the increase in volume of suspended sediment, and decrease in bedload, as the sediment travels downstream) were also calculated in Hicks et al. (2000).

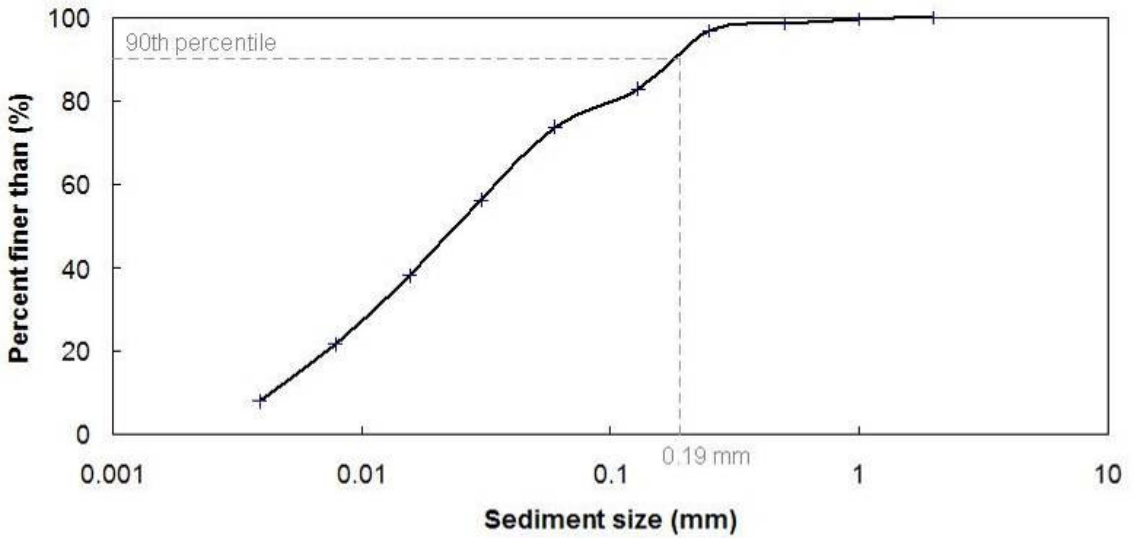

Figure 3.55: Lindis at Lindis Peak (Site 75219) average particle size distibution for September 1995 to November 1999 (Hicks et al., 2000, p. 42, Table 5.5)

3.3.2 Lake Dunstan

Lake Dunstan was formed when Clyde Dam (Site 9120, Appendix A, Figure A1) was constructed near the township of Clyde at the downstream limit of Cromwell Gorge. Construction of the concrete gravity dam took place between 1978 and 1990 (Waugh et al., 2000). Lake Dunstan was then filled in three stages commencing on 22 April 1992 and finishing in September 1993 (Devgun & Bowler, 1999). Lake Dunstan has a volume of 343.6 x 10^6 m^3 at a lake level of 193.5 m, and a volume of 368.4 x 10^6 m^3 at a lake level of 194.5 m (Freestone & Payne, 2000).

3.3.2.1 Water levels

The operating range for Lake Dunstan is 193.5 to 194.5 m msl Dunedin (at Clyde Dam) for power generation purposes (Devgun & Bowler, 1999). When the lake is in the flood range of 194.5 to 195.1 m a stringent relationship between lake level and flow rates is followed, to accommodate flows up to 3,200 m^3/s (Freestone & Payne, 2000).

As the Clutha River/Mata-Au delta is approximately 36.4 km upstream of Clyde Dam, the lake level in the vicinity of the delta is higher than at Clyde Dam during flood events. This difference is due to constrictions, such as Cromwell Gorge (downstream of the Kawarau River confluence), causing a backwater effect. Further increases in water level also occur at the Clutha River/Mata-Au delta due to local sediment deposition. Webby et al. (2009) simulated 2007 water levels for Lake Dunstan using the 2007 cross section survey and MIKE-11 hydraulic modelling software. Figure 3.49 shows the

location of the 2007 surveyed Lake Dunstan cross sections in the immediate vicinity of the Clutha River/Mata-Au delta (i.e. XS60 to XS72). Table 3.6 summarises the model scenarios and simulated Lake Dunstan water levels at selected cross sections. This shows that for an Upper Clutha River/Mata-Au flow of ~300 m^3/s, the difference between Lake Dunstan water levels at the Clutha River/Mata-Au delta compared to at Clyde Dam are negligible despite there being an increase in water level elevation of 0.15 m between cross sections 68 (XS68) and 72 (XS72). For a very large flood flow of 1760 m^3/s in the Upper Clutha River/Mata-Au predicted water levels downstream of the delta (i.e. downstream of XS60) would be approximately 0.36 m higher than the Clyde Dam water levels, while XS72 water levels would be approximately 0.55 m higher than XS60 and 0.91 m higher than Clyde Dam.

Table 3.6: Simulated Upper Clutha Arm water levels for 2007 (Webby et al., 2009)

Cross section	Scenario 1 $Q_{Upper\ Clutha}$ = 291.5 m^3/s $Q_{Kawarau}$ = 238.5 m^3/s $RL_{Clyde\ Dam}$ = 194.50 m asl	Scenario 2 $Q_{Upper\ Clutha}$ = 1100 m^3/s $Q_{Kawarau}$ = 900 m^3/s $RL_{Clyde\ Dam}$ = 194.83 m asl	Scenario 3 $Q_{Upper\ Clutha}$ = 1760 m^3/s $Q_{Kawarau}$ = 1440 m^3/s $RL_{Clyde\ Dam}$ = 195.10 m asl
XS72	194.66	195.43	196.01
XS68	194.51	194.99	195.51
XS60	194.51	194.98	195.46

Once sedimentation from the Kawarau River (shown on Figure 3.41) starts to significantly increase downstream of the Kawarau River-Lake Dunstan confluence, water levels at the Clutha River/Mata-Au delta will also start to rise due to this backwater effect along the upper Clutha arm. Predicted water levels for 2023 (using the same boundary conditions as modelled for 2007) are summarised in Table 3.7. This indicates that lower flows will not cause increased water levels upstream of the Clutha River/Mata-Au delta. However, water levels upstream of the Clutha River/Mata-Au delta are likely to increase by a further 0.09 m and 0.44 m for Upper Clutha River/Mata-Au flood flows of 1100 m^3/s and 1760 m^3/s, respectively. Although the results in Table 3.7 were provided in Webby et al. (2009), there are no details of the assumptions made when modelling these scenarios.

Table 3.7: Predicted Upper Clutha Arm water levels for 2023 (Webby et al., 2009)

Cross section	Scenario 1 $Q_{Upper\ Clutha}$ = 291.5 m^3/s $Q_{Kawarau}$ = 238.5 m^3/s $RL_{Clyde\ Dam}$ = 194.50 m asl	Scenario 2 $Q_{Upper\ Clutha}$ = 1100 m^3/s $Q_{Kawarau}$ = 900 m^3/s $RL_{Clyde\ Dam}$ = 194.83 m asl	Scenario 3 $Q_{Upper\ Clutha}$ = 1760 m^3/s $Q_{Kawarau}$ = 1440 m^3/s $RL_{Clyde\ Dam}$ = 195.10 m asl
XS72	194.66	195.52	196.45
XS68	194.56	195.29	196.27
XS60	194.56	195.28	196.24

The Lake Dunstan (Clutha arm) at Crippletown (Site 75266, Appendix A, Figure A1) water level recorder is located adjacent to the Clutha River/Mata-Au delta at Lake Dunstan. Between 1994 and 2009 the average water level for this site was 194.23 m, with a maximum level of 195.47 m recorded on 17 November 1999. The lowest recorded level post-lake-filling was 193.49 m on 8 April 1994.

A comparison between Lake Dunstan water levels at Crippletown (i.e. at the Clutha River/Mata-Au delta) and another water level recorder further downstream at Cromwell (Site 75267) show that the difference in lake level is usually negligible, with water levels at Crippletown slightly higher during flood events. Figure 3.56 shows a comparison of the 3-hourly average Lake Dunstan water levels in 1999 for both sites. During the large December 1999 flood event the Crippletown water levels were up to 57 mm higher than Cromwell water levels.

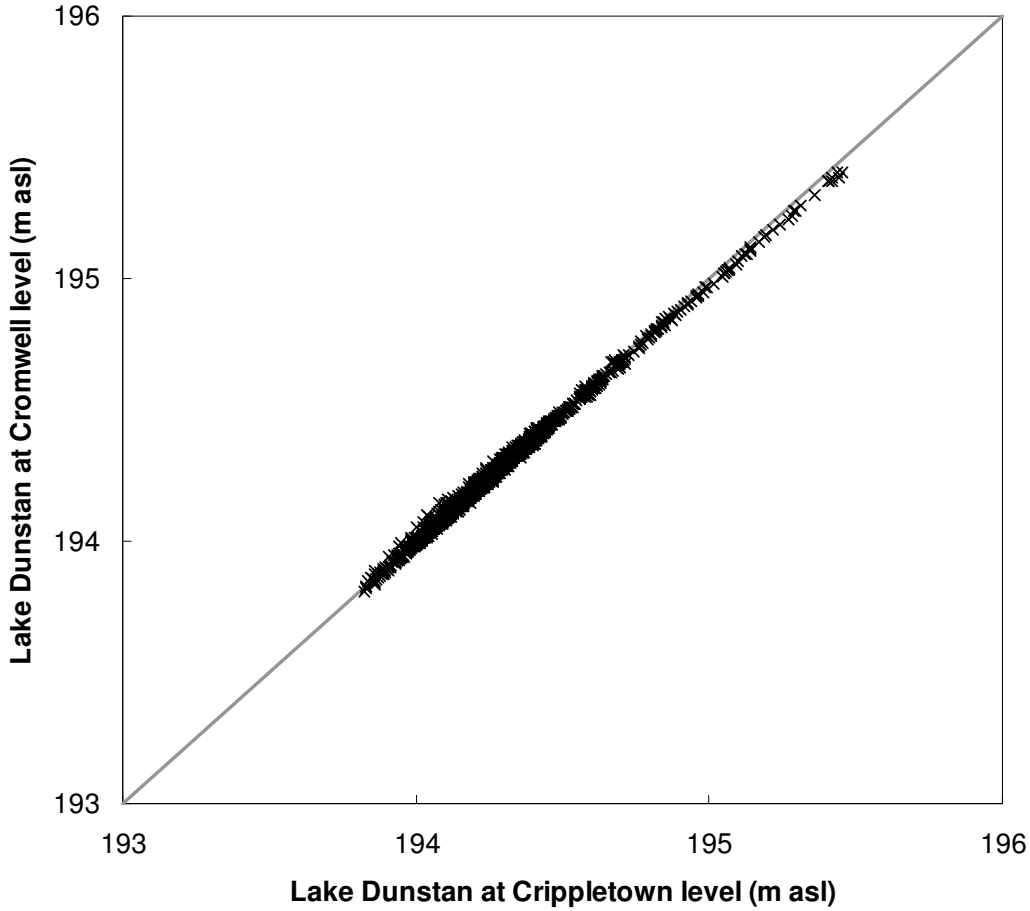

Figure 3.56: Comparison of 3-hourly averaged Lake Dunstan water levels at the Clutha River/Mata-Au delta compared to at Cromwell for 1999

3.3.2.2 Outflows

The outflows from Lake Dunstan pass through the Clyde Power Station (Site 9120), which has four turbine generators capable of generating a total of 432 MW (Waugh et al., 2000). Excess water and flood flows pass over the four 14.3 m high by 10 m wide spillway gates (Waugh et al., 2000).

3.3.2.3 Vegetation

Prior to lake filling, the Water Right for Clyde Dam required the clearance of vegetation from the upper 7 m of the lake, to prevent fouling of the lake. However, as was expected, the relatively stable lake level has significantly increased the habitat available for aquatic plants. *Lagarosiphon*, an aquatic plant species recognised as a pest plant, is the main aquatic plant located in the 2-4 m deep lake zone. Due to the steep sides of the lake this results in the most prolific growths being found in the shallow delta, beach, fan head and ridge areas around the lake (Otago Regional Council, 2002).

Other plants found along the river, and on islands within the river system, include willows and poplars (planted to stabilise banks), as well as infestations of gorse, broom, sweet briar and hemlock (Department of Conservation, 1992).

3.3.3 Clutha River/Mata-Au delta

When the water level in Lake Dunstan was raised, sediment that would usually be transported along the Clutha River/Mata-Au instead entered a stationary body of water. This led to the development of a relatively fine-grained delta with coarser sediment being deposited near the entry point of the lake while finer sediment was transported further into the new lake. As the delta progrades, extending the river system further into the lake, finer deposits of sediment are overlain with coarser sediment which can now be transported further into the lake by the prograding river system/delta.

Over time, the river channels upstream of the delta will also aggrade resulting in a decrease in the bed slope and energy gradient upstream of the aggradation. This will cause the zone of deposition of coarse sediment to extend gradually upstream, raising the bed of the original river (Otago Regional Council, 2002).

Unfortunately the growth of this delta is complicated by the dynamic nature of the river system during flood events, as well as the effects of the established vegetation and smaller tributary inflows. This makes it difficult to predict the behaviour of the Clutha River/Mata-Au delta and upstream reaches both before and after lake filling. Further information related to the behaviour of the Clutha River/Mata-Au delta is given below.

3.3.3.1 Cross section monitoring and sedimentation rates

A series of cross sections is regularly surveyed along both the Kawarau River and upper Clutha River/Mata-Au arms of Lake Dunstan. The upper Clutha River/Mata-Au arm of Lake Dunstan was surveyed in April 1994, September 1999 and July 2007. The cross sections immediately downstream of the Clutha River/Mata-Au delta (i.e. cross sections 63 to 72) are shown on Figures B3 and B4 (Appendix B) with the location of the cross sections shown earlier on Figure 3.49. Like the Bendigo Wildlife Reserve cross sections surveyed further upstream (Section 3.3.1.6), access to the cross sections in the vicinity of the Clutha River/Mata-Au delta has become more difficult over time for

these surveys and in 2007 cross sections 71 and 72 were unable to be surveyed for this reason; the 1999 survey of cross section 72 was also incomplete.

Observations from the cross section surveys include:

- The channel adjacent to the eastern bank remains relatively stable between 1994 and 2007, with the exception of cross section 68 where aggradation occurs.

- Significant aggradation occurs as far downstream as cross section 66 for both the main channel (flowing near the western bank), as well as in the central portion of the submerged cross section, with most aggradation occurring between 1999 and 2007 (i.e. most likely as a result of the 1999 flood event).

- Any significant aggradation downstream from cross section 66 appears to be largely due to tributary and bank contributions (e.g. along the western bank at cross section 63 as shown in Figure 3.57 and in Appendix B, Figure B4). The large volume of sediment deposited at cross sections 68 and 67 may also be partly due to the tributary entering between these cross sections (Figure 3.57 and Figure B3 and B4, Appendix B).

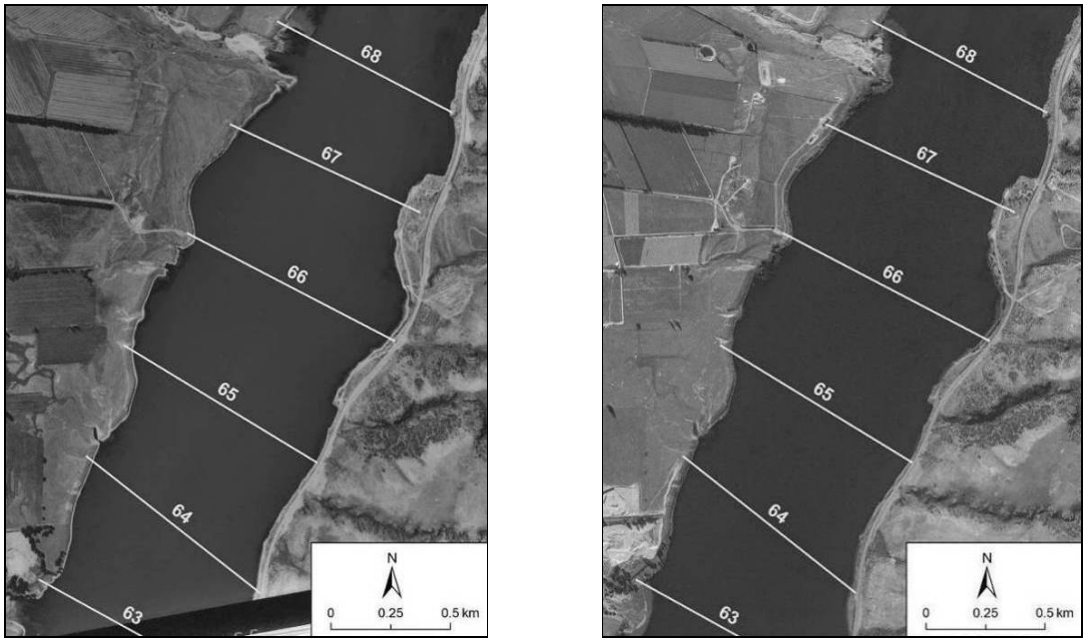

(a) 1996 **(b) 2007**

Figure 3.57: Location of tributary sediment sources on the western shore of Lake Dunstan (i.e. immediately downstream of cross sections 68 and 63)

The average and minimum bed levels for cross sections 72 to 61 are shown in Figure 3.58 and summarised in Table B3 (Appendix B). As expected, all cross sections aggrade between 1994 and 2007. The largest increases in average bed level occurred in the vicinity of cross sections 71 and 68.

The change in average bed level tended to decrease in a down lake direction (except near cross sections 68 and 63). The 2007 average bed levels show that there are relatively high average bed levels at cross sections 63 and 68 compared to the adjacent cross sections. The minimum bed levels upstream of cross section 67 also increase - indicating the likely spatial extent of infilling due to the deposition of coarse-grained material at the Clutha River/Mata-Au delta.

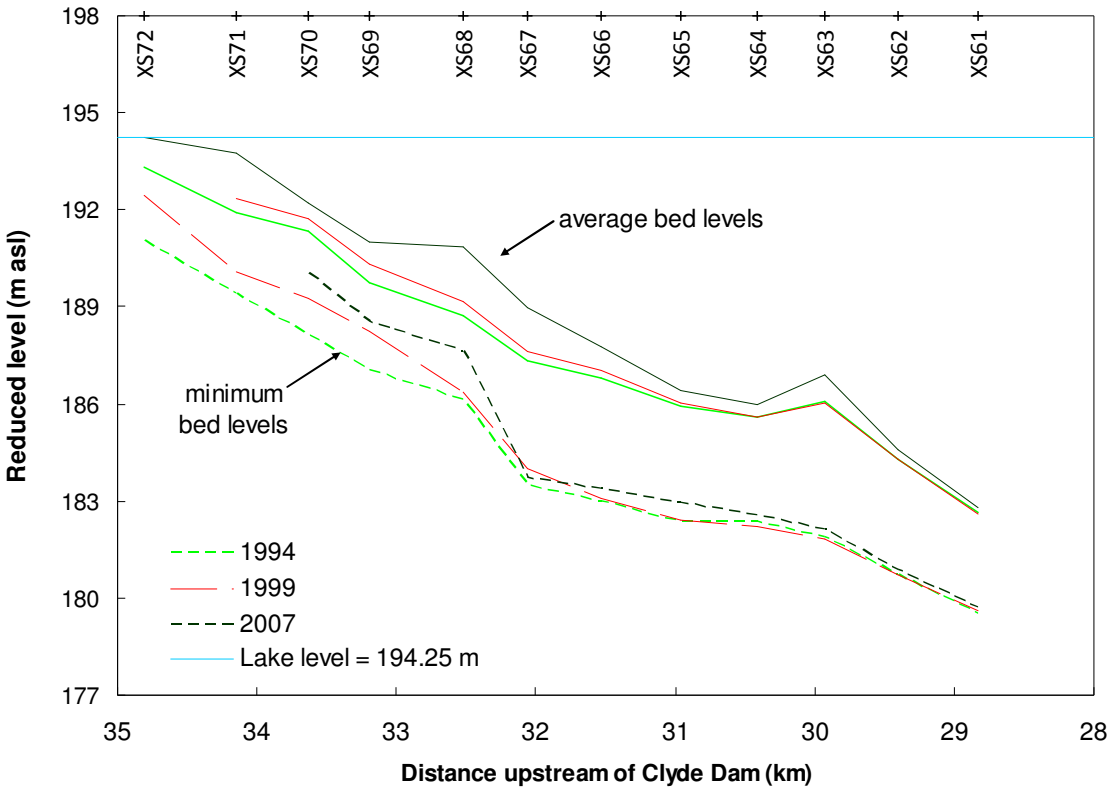

Figure 3.58: Average and minimum bed levels for Lake Dunstan cross sections 72 to 61 in April 1994, September 1999 and July 2007

The total increase in cross section area due to aggradation was calculated by multiplying the average change in bed levels between surveys by the width of the cross section. Figure 3.59 and Table B3 (Appendix B) show that between 1994 and 1999 the change in cross sectional area due to sedimentation decreased from 435 m^2 at cross section 71 to ~0 m^2 by cross section 64.

For the 1999 to 2007 time period, including the November 1999 flood event, the increase in cross sectional area due to sedimentation increased significantly for most cross sections – but in particular cross sections 71, 68/67 and 63 where the cross sectional area increased by 740 to 1350 m^2 (accounting for 76 to 100% of the total increase in cross sectional area between 1999 and 2007). This indicated that the large November 1999 flood event provided a large influx of sediment to this area and that the sediment was likely to have been supplied by both the upper Clutha River/Mata-Au and the tributaries that enter Lake Dunstan near cross sections 68 and 63.

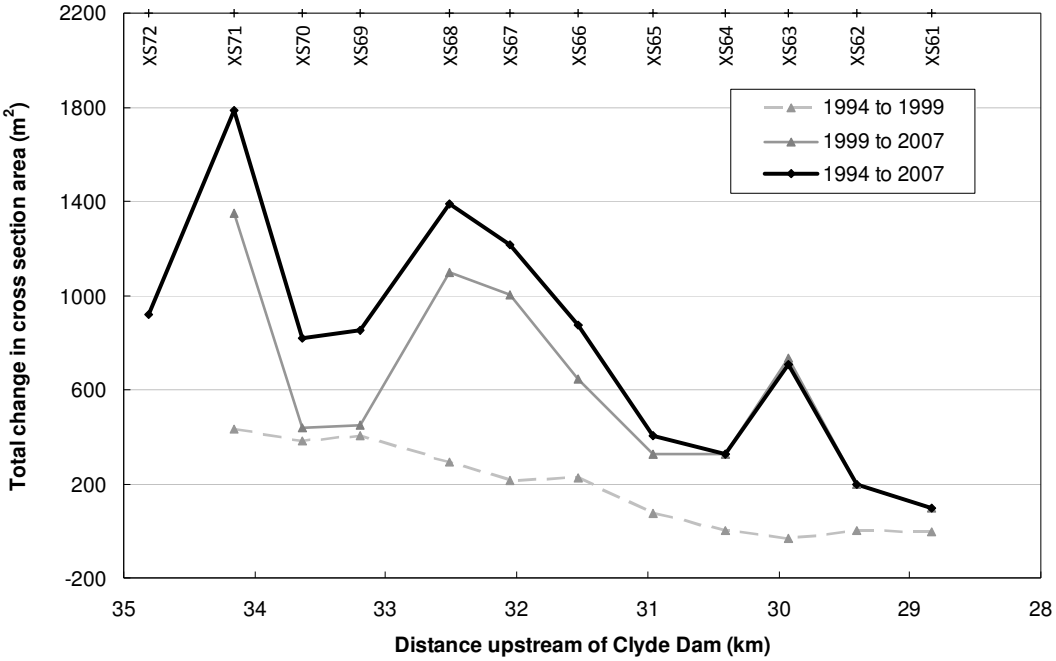

Figure 3.59: Total change in the area of Lake Dunstan cross sections 72 to 61 in April 1994, September 1999 & July 2007

By contrast, cross sections 70 and 69 had very similar increases in cross sectional area for both the 1994 to 1999 and 1999 to 2007 time periods. This may be due to the November 1999 flood flows (and other periods of high flow) transferring sediment from these cross sections further down lake (i.e. reducing the volume of sediment stored at these sections and increasing the volume stored further downstream); otherwise these cross sections may be further down lake from the area where the Clutha River/Mata-Au delta is actively prograding – or the delta has already prograded beyond this area and the bed has adjusted to a more efficient slope to transfer a larger portion of the sediment supply further down lake. More detailed bathymetric data (e.g. multibeam sonar swath mapping) would potentially provide this information.

Using the available cross section data, the volume of sediment deposited in the upper Clutha Arm was estimated, for the April 1994 to September 1999 time period, to be 0.9 million m^3 or 0.17 million m^3/yr (Opus, 2000). This estimate increased to approximately 0.23 million m^3/yr when the November 1999 flood event was included (Opus, 2000). Webby et al. (2009) provided a more recent estimate of up to 5 million m^3 (or up to 0.38 million m^3/yr) of sediment being deposited between cross sections 72 and 60 between April 1994 and July 2007.

In an attempt to identify the sediment contribution due to the upper Clutha River/Mata-Au (compared to the local tributary contributions at cross sections 67/68 and 63, and immediately upstream of cross section 71), the total change in cross section area for these cross sections was reduced (pink line,

Figure 3.60 and Table B3, Appendix B). This was based on the assumption that the 'spikes' observed could be due to the tributary sediment inputs.

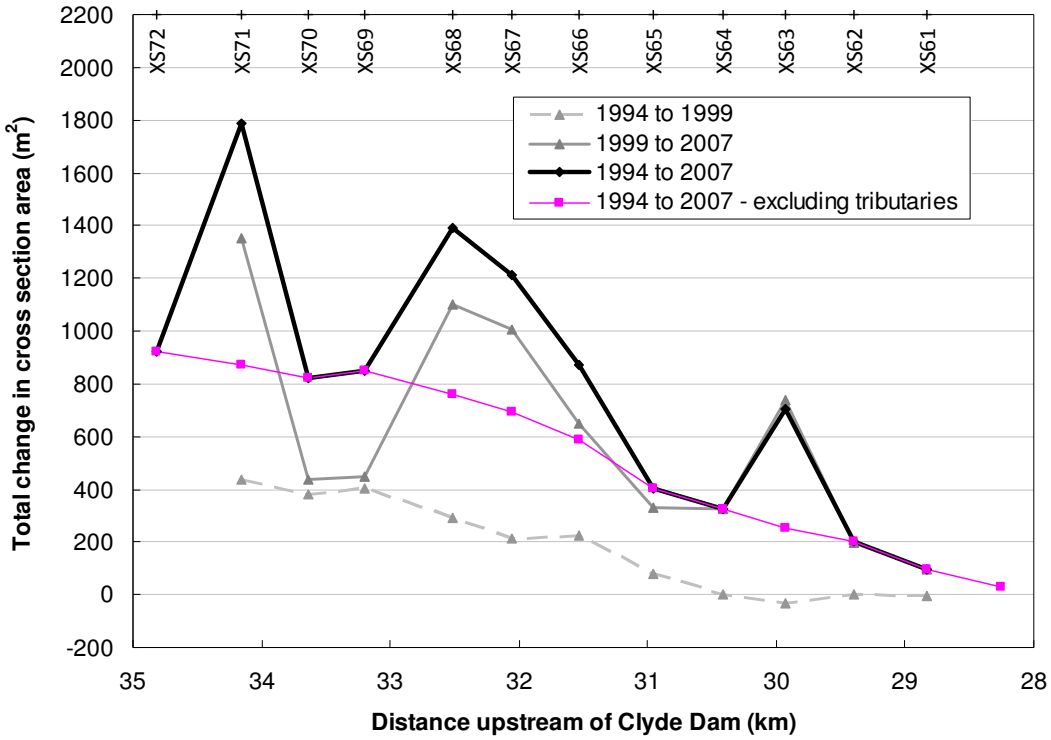

Figure 3.60: Total change in the area of Lake Dunstan cross sections 72 to 61 in April 1994, September 1999 & July 2007 including 1994 to 2007 values modified to exclude 'potential' tributary sediment sources

The 'potential' volumes of sediment attributed to the tributary sources in the vicinity of cross sections 71, 67/68 and 63 were calculated by subtracting the modified total change in cross section values from the original values and multiplying by the distance between cross sections. This reduced the total volume of sediment deposited between cross sections 72 and 60 (from further upstream Upper Clutha River and Lindis River sources) by 1.54 million m^3 with 0.23 million m^3 attributed to the cross section 63 tributary source, 0.77 million m^3 from the cross section 67/68 tributary source, and the other 0.54 million m^3 from the tributary sources immediately upstream of cross section 71. Table B3 (Appendix B) shows that between 1994 and 2007 the Clutha River/Mata-Au sediment contribution to the area between cross sections 72 and 60 would therefore be reduced to ~3.48 million m^3 (or 0.27 million m^3/yr) compared to 1.54 million m^3 (or ~30%) being provided by local tributaries.

Figure 3.61 shows estimates of sediment contributions provided by the WRENZ model (http://wrenz.niwa.co.nz/webmodel/) and, although these results should be used with caution due to the inbuilt assumptions made to extend this model to cover the entire country, it would tend to suggest that the relatively small local tributaries would not be capable of generating all of the deposited sediment.

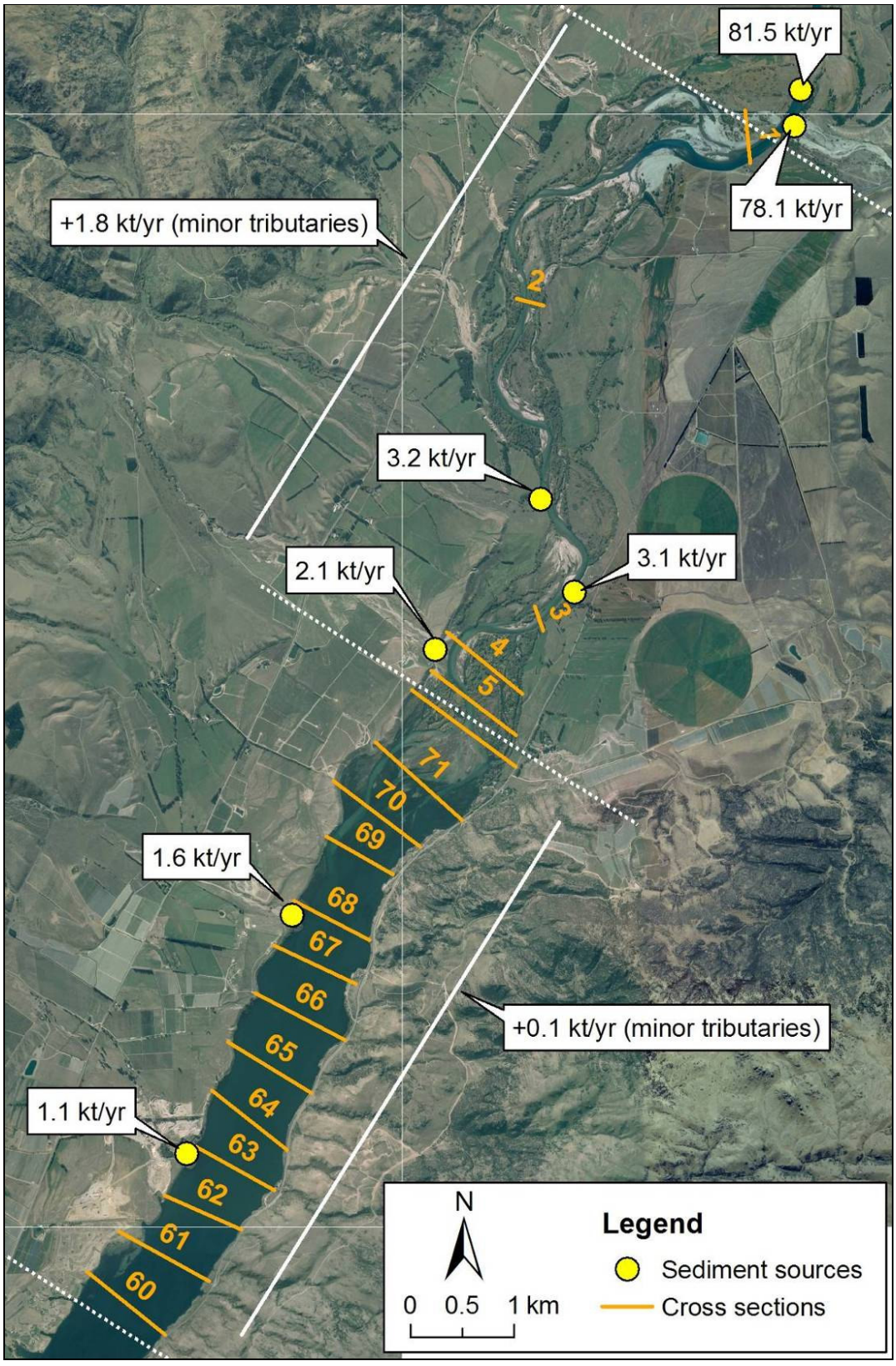

Figure 3.61: Estimates of sediment contributions from the major tributaries along the Clutha River/Mata-Au [Source: WRENZ, http://wrenz.niwa.co.nz/webmodel/]

For instance, assuming the deposited sediment density is 1.8 t/m^3, the estimated 1.6 kt/yr of sediment supplied by the cross section 67/68 tributary source would be equivalent to ~890 m^3/yr. This is considerably less than the 0.77 million m^3 (or 59 230 m^3/yr) measured above. Therefore, it can not be assumed that the increase in sediment deposition volumes observed around cross sections 67/68 and 63 are due to tributary sources, although they may contribute larger volumes than those estimated using WRENZ due to the extremely large flood event that occurred in November 1999.

3.3.3.2 Aerial photography

Aerial photographs of the Clutha River/Mata-Au delta and catchment are available for several dates both pre- and post- the 1992/93 formation of Lake Dunstan (Table 3.8).

Table 3.8: Clutha River/Mata-Au aerial photograph information

Survey	Date	Scale	Colour	Source
SN533	9\03\49	~1:8000	Black & White	Otago Regional Council (ORC)
SN8436	31\12\84	1:50 000	Black & White	New Zealand Aerial Mapping (NZAM)
SN12324	7\03\96 & 22\4\98	1:27 500	Colour	Otago Regional Council (ORC)
SN12780	Feb\Mar 2003	1:50 000	Colour	Land Information New Zealand (LINZ)
-	14\4\2005	-	Colour	GoogleEarth
SN50556c	26\3\2006	1:40 000	Colour	Otago Regional Council (ORC)
-	16\2\2007	-	Colour	GoogleEarth
-	2009	-	Colour	Contact Energy (Contact)

The most recent aerial photographs of the entire Clutha River/Mata-Au delta and catchment were taken in 2006, while the oldest set of aerial photographs of the river were taken in 1949. Aerial photographs of the delta area have also been taken as recently as 2011 (on GoogleEarth but with cloud cover). The 2006 orthorectified colour aerial photographs have been provided by ORC and have a ground sampling distance of 0.7 m.

Geo-referenced aerial photographs of the Clutha River/Mata-Au delta and Bendigo Wildlife Reserve are shown in Figures 3.62 and 3.63, covering the 1949 to 2009 time period. These photographs show that:

- Between 1949 and 2009 the main Clutha River/Mata-Au channel feeding the delta area (i.e. channel at north-east corner of each photograph) remains in the same approximate location with some shifting of the main meander in an easterly direction. The TRB in this area remains unvegetated suggesting that overbank flow occurs often during flood events.

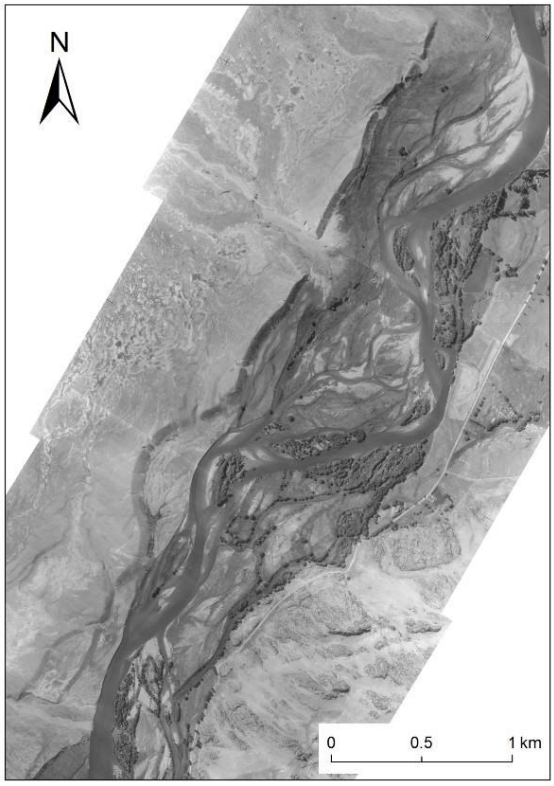

(a) 1949 [Source: ORC]

(b) 1984 [Source: NZAM]

(c) 1996 [Source: ORC]

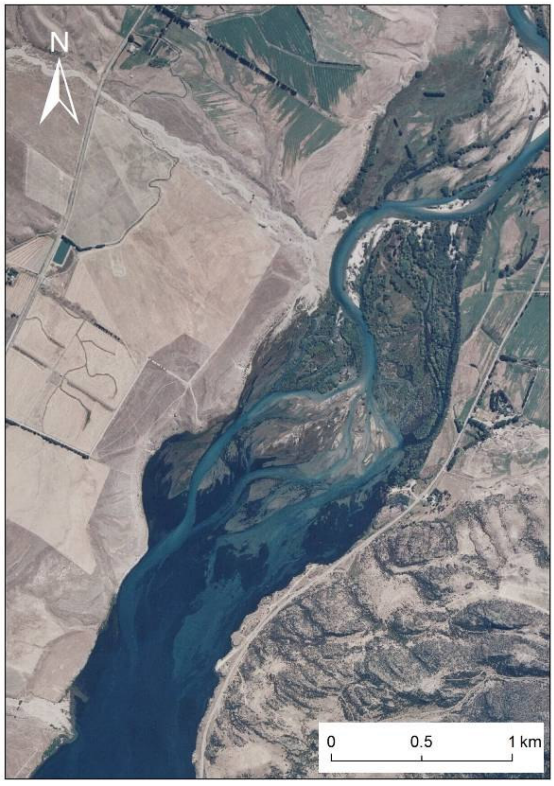

(d) 2003 [Source: LINZ]

Figure 3.62: Historic aerial photographs of the Clutha River/Mata-Au delta pre- and post-filling of Lake Dunstan (1949 to 2003)

(e) 2005 [Source: GoogleEarth]

(f) 2006 [Source: ORC]

(g) 2007 [Source: GoogleEarth]

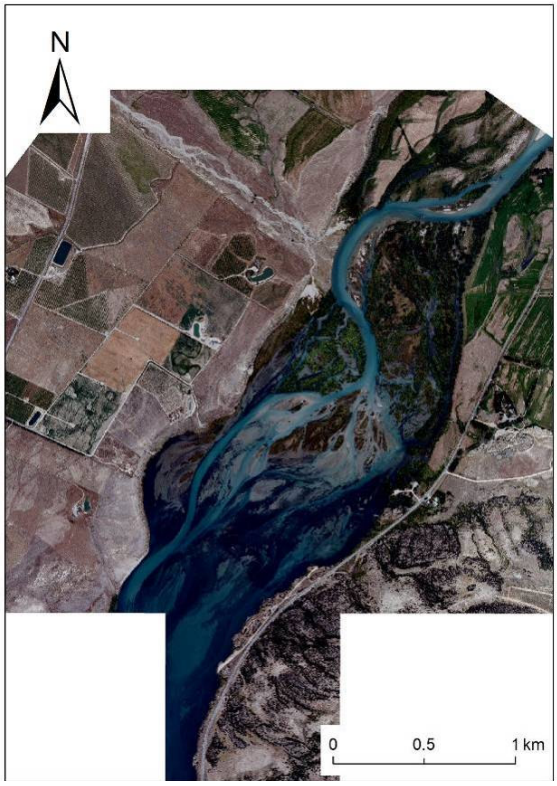

(h) 2009 [Source: Contact Energy]

Figure 3.63: Historic aerial photographs of the Clutha River/Mata-Au delta post-filling of Lake Dunstan (2005 to 2009)

- From 1984 through to the formation of Lake Dunstan (and beyond lake filling until at least 1996), the main river channel maintained a similar course with mainly minor meander shifts.
- By 2003 a sufficient volume of sediment had deposited at the river-lake boundary, such that a river bifurcation developed to transport river flows and sediment around the newly created delta formation; the location of this bifurcation has remained stable between 2003 and 2009.
- The delta bar formations that are now above lake level have become progressively more vegetated over time.

3.3.3.3 Contour data for Bendigo Wildlife Reserve

In the Bendigo Wildlife Reserve 2 m contours have previously been derived for Contact Energy by New Zealand Aerial Mapping (Figure 3.64). These relatively recent contours show that cross section 72 is largely at or above a level of 194 m and cross section 71 is mainly below 194 m. This ties in well with the assumptions made by Webby et al. (2009) that the sediment at cross section 72 filled the cross section to the water surface, and cross section 71 was filled with sediment to within 0.5 m of the water surface – where the water level was 194.25 m.

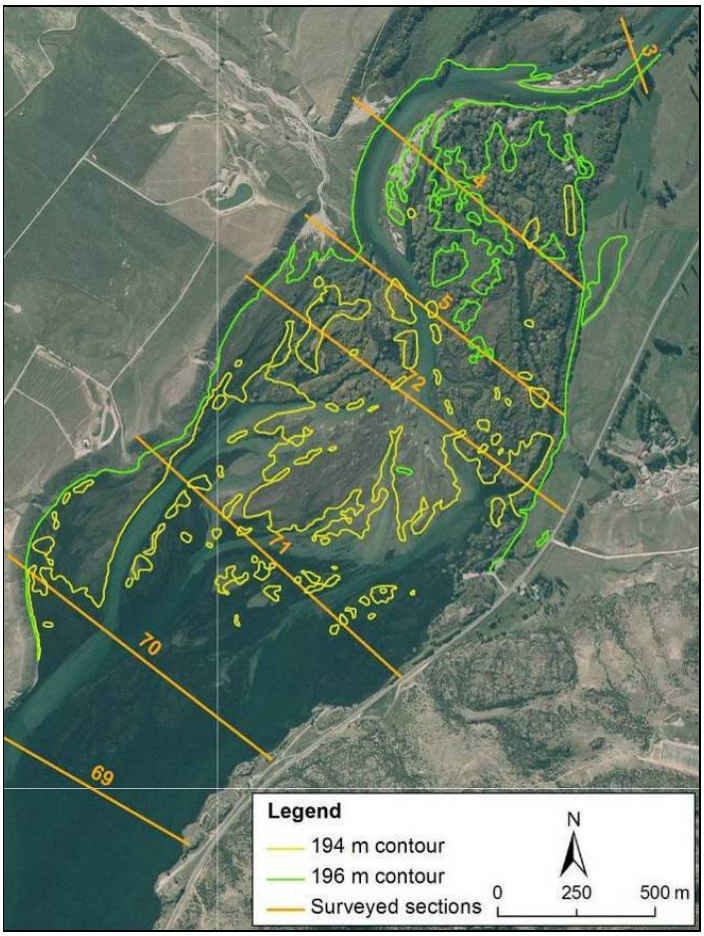

Figure 3.64: Recent (date unknown) contour information for the Clutha River/Mata-Au delta. [Source: Contact Energy]

3.3.3.4 Sonar data

For this study a sonar survey was considered to be a quick, cost-effective option to obtain data for the navigable parts of the delta as the ORC field services team already had a "Lowrance fish-finding sonar and mapping GPS" unit (model LMS-527cDF iGPS) hull-mounted on a small motorboat; this survey method had also proven to be successful for the Rees-Dart delta (Section 3.2.5.2).

For the initial 31 May 2011 survey the sonar unit was set to a 200 kHz frequency. Soundings were measured every 3 to 6 m (depending on the speed of the boat) with the accuracy of the GPS and sonar data noted as having an accuracy of within 10-20 m horizontally and 2-3 m vertically in the Lowrance manual (http://www.lowrance.com/upload/Lowrance/Documents/Manuals/LMS527-522_0152-181_120406.pdf). As observed for the Rees-Dart sonar survey, the data captured seemed considerably more accurate. For instance, when sonar data points were overlain on geo-referenced aerial photographs the boat was accurately placed at the boat ramp and in the navigable channel (Figure 3.65a).

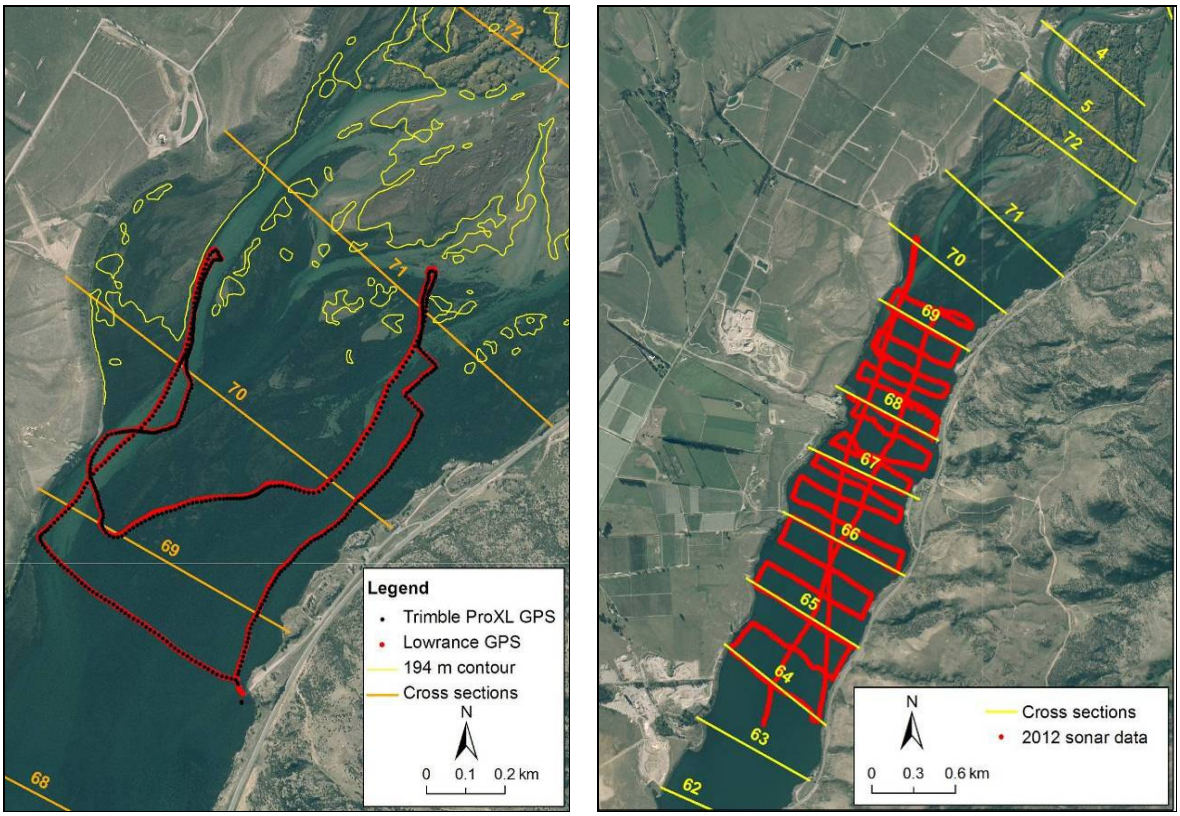

(a) Comparison of Lowrance and Trimble ProXL GPS locations for May 2011 sonar survey (with 2009 194 m contour)

(b) September 2012 sonar survey

Figure 3.65: Sonar data from May 2011 and September 2012

The short sonar survey tended to follow the main channels, and travelled as close to the delta as practically possible, given the shallow water and submerged weeds. A second boat-mounted GPS unit

(Trimble ProXL) simultaneously recorded the location of the sonar instrument at a 5 second interval. This second GPS unit antenna was mounted directly above the Lowrance sonar instrument whereas the Lowrance GPS antenna was mounted in the cabin of the boat, approximately 2.82 m from the Lowrance sonar instrument. Recorded sonar survey locations for both GPS instruments are shown on Figure 3.65. During this survey the Trimble ProXL GPS has Position Dilution of Precision (PDOP) values between 2.6 and 5 (with an average value of 3.1), which indicate a good level of precision for the GPS positions (i.e. 95% confidence of 1-3 m accuracy). A second sonar survey was completed on 18 September 2012 to more closely examine the lake bathymetry. The sonar data collected in September 2012 are shown on Figure 3.65b.

As the sonar data are collected as a series of points, rather than producing a 3-d surface, it is difficult to determine the exact bed profile (e.g. the longitudinal channel gradient varies depending on whether the boat is travelling along the deepest part of the channel or nearer the bank), as well as which bed profiles are caused by sedimentation versus pre-lake-filling natural topographic features. Areas of sedimentation could potentially be determined by carrying out a series of sonar surveys, at the same locations, over time. However, given the difficulty of maintaining a boat on a given course, as well as the rapidly changing bed levels over short distances (e.g. due to channels and existing bathymetry), it would be difficult to use this method to obtain precise measurements of sedimentation, or to interpolate an accurate 3-d surface of the delta.

Consequently, it has proven to be difficult to identify the extent of the sumerged Clutha RiverMata-Au river delta. At the upstream extents of the 2011 sonar survey, and in the central portion of the lake between cross sections 69 and 70, water depths rapidly decreased to 0.5 to 0.8 m (reduced levels of ~193.0 m to 193.3 m asl) and the sonar survey boat needed to retreat downstream. This may mark the location of a relatively shallow and short delta foreset boundary (i.e. identify the location of the deposition of coarse bedload at the Clutha River/Mata-Au delta), although further field measurements in this area would be required to confirm this.

Other jet boat operators that regularly travel along this reach of the Clutha River/Mata-Au (in jet boats with a draft of about 200 mm) have also observed “it is shallowest from about half way between sections 71 and 72 to just upstream of section 72. By section 5 you are definitely in a deeper faster flowing river channel … the preferred route heading upstream or downstream is the channel on the true right *(Figure 3.66)*. As long as you stay in the channel the boat does not hit the bottom. A guy here has boated up and down the other 2 channels you can see but touched the bottom in places” (Peter Silvester, Contact Energy Ltd, personal communication, 5th July 2012).

The September 2012 sonar data followed a similar track as the established cross section monitoring program, as well as collecting additional cross section profiles between these sites (see Appendix B, Figures B5 and B6). This set of sonar data has been compared to the 1994, 1999 and 2007 cross

section data (Appendix B, Figures B3 and B4); where the 2011 sonar survey data intersected the cross section monitoring sites, the sonar survey bed levels were also shown.

Figure 3.66: Oblique aerial photograph of Clutha River/Mata-Au delta looking downstream [Source: Contact Energy]

A raster grid surface of the lakebed was generated in ArcGIS by fitting a hydrologically correct surface (Topo to Raster interpolation method) to a combination of the 2012 sonar point data and a digitised 194 m asl shoreline (Figure 3.67). Contour lines were then generated in ArcGIS using the derived lakebed raster grid surface (Figure 3.67).

These contours show that the channels are not always clearly defined between the measured cross sections when limited spatial data are available. However, by analysing the contours (Figure 3.67) in conjunction with all available cross section information (Appendix B, Figures B3 to B6), it can be observed that:

- Although there are some discrepancies in the data (potentially due to lakebed vegetation and/or sediment movement between surveys), there appears to have been significant aggradation from cross section 69 downstream to cross section 66 between 1999 and 2007 (and 2012), with less aggradation upstream (cross sections 71 and 70) and downstream of cross section 66.
- The lakebed levels change quite abruptly in the vicinity of cross section 67. This is likely to represent the downstream limit of the delta foreset. See Figures B4 and B5 in Appendix B for

cross section information from the 2012 sonar survey at locations immediately upstream (cross section 67_68c) and downstream (cross section 66_67a) of cross section 67.

- Downstream of cross section 67 the main sublacustrine channel flows along the eastern shoreline, whilst upstream of cross section 67 sublacustrine channels are observed near both shorelines.
- There is a high point near the centre of the lakebed at cross section 68 that extends both upstream and downstream in the 2012 sonar data. This feature also appears in the 2007 cross section survey at cross section 68 but is not observed in the earlier surveys.

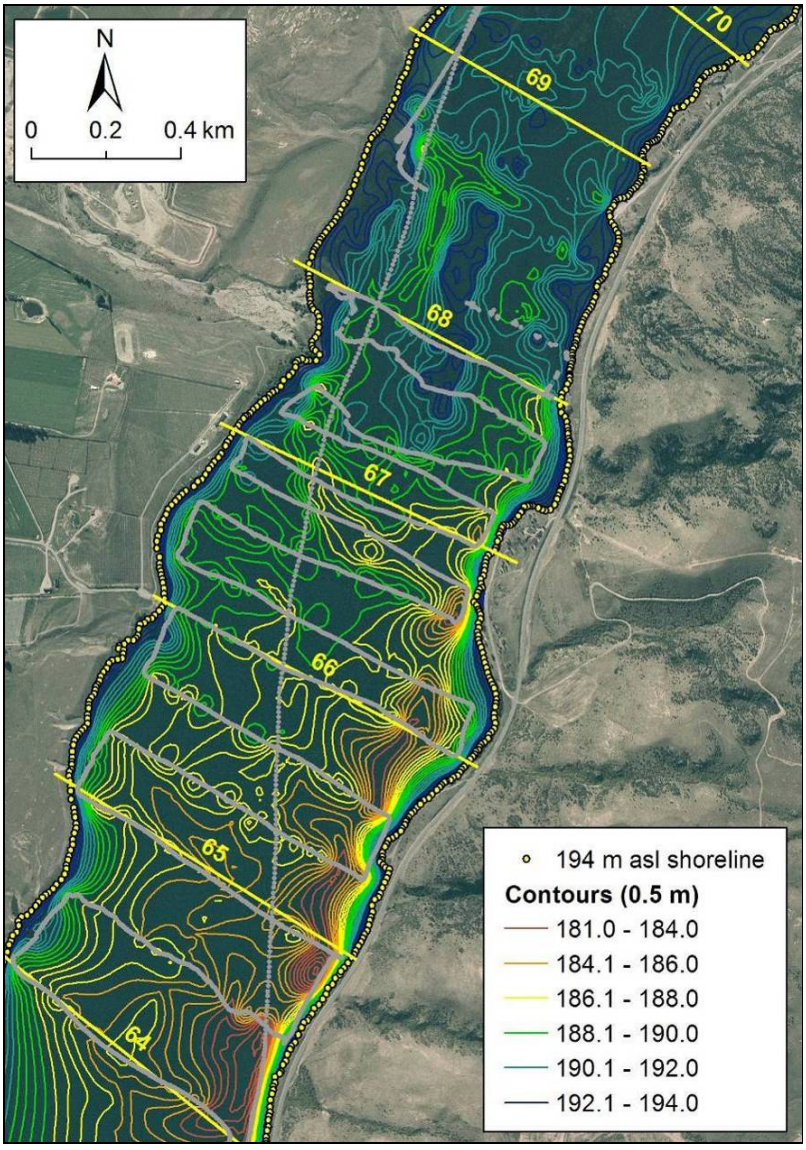

Figure 3.67: Derived contours (0.5 m interval) for the Clutha River/Mata-Au, within Lake Dunstan, between cross section 69 and 64. Contours were derived by fitting a surface to the 2012 sonar data (grey lines). Cross section monitoring sites are shown as yellow numbered lines

Therefore, despite the additional acquisition of the 2012 sonar data, there are still many unanswered questions regarding data discrepancy (potentially caused by vegetation) and the complex delta geometry as it interacts with the lakebed bathymetry.

3.3.3.5 Sediment and flow contributions from the Lindis River versus Clutha River

Along the upper Clutha River/Mata-Au the main sediment sources include the Cardrona River, Lindis River, other minor tributaries and material eroded from the river banks. Figures 3.68a and b show the erodible materials that form the river banks and Table 3.9 summarises the Clutha River/Mata-Au delta suspended sediment sources and yields, as derived by Hicks et al. (2000).

(a) Upper Clutha River\Mata-Au between Lake Wanaka and Albert Town

(b) Upper Clutha River\Mata-Au approximately 22.5 km upstream of Lake Dunstan

Figure 3.68: Photographs of upper Clutha River/Mata-Au river banks

Table 3.9: Clutha River/Mata-Au delta suspended sediment sources (Hicks et al., 2000, p. 14, Table 3.4)

Sediment source	Area (km^2)	Bulk suspended sediment load (kt/y)
Cardrona River	346	53.0
Lindis River	1050	70.0
Other small tributaries	1056	68.5
Abrasion in upper Clutha River		15.9
Sum to Clutha River/Mata-Au delta		207.4
Clutha River/Mata-Au delta – Lindis River		137.4

This shows that the Lindis River provides approximately a third of the suspended sediment load at the Clutha River/Mata-Au delta. Assuming that a similar ratio of bedload is transported by each river, it can be assumed that the Lindis River will provide approximately a third of the total sediment load to the Bendigo Wildlife Reserve, and consequently to the Clutha River/Mata-Au delta. The ratio of total bedload transport rate (I_b, kg/s) for the Clutha River/Mata-Au and Lindis Rivers can therefore be estimated as

$$\frac{I_{b(\text{Clutha})}}{I_{b(\text{Lindis})}} \approx 2 \quad \textbf{(3.5)}$$

As the most substantial proportion of the sediment deposited at the Clutha River/Mata-Au delta has been deposited during large flood events (i.e. the November 1999 and December 1995 flood events), 'typical' flows for large flood events have been assumed when determining the relative flow contributions for the Lindis River versus Clutha River/Mata-Au flows. As Lake Hawea outflow is controlled, and the outflows from both lakes are largely dependent on antecedent conditions for any given flood event, many different flow scenarios could be considered to be 'typical' flood events.

Table 3.10 summarises the 'typical' flood flows used in this study to produce relative flood flow contributions for the Lindis River and Clutha River/Mata-Au. The Clutha River/Mata-Au flow (Q_{Clutha}) contribution at the Clutha River/Mata-Au delta is the sum of all of the 'typical' flows in Table 3.10 excluding the Lindis River flow (Q_{Lindis}). This combined flow (Q_{Clutha}) is divided by the Lindis River flow (Q_{Lindis}) to give the flow ratio

$$\frac{Q_{\text{Clutha}}}{Q_{\text{Lindis}}} \approx 3.5 \quad \textbf{(3.6)}$$

This Clutha River/Mata-Au to Lindis River flow ratio (Equation 3.6) is used as a guide for the Clutha River/Mata-Au microscale modelling in Section 4.4.

Table 3.10: Clutha River/Mata-Au delta flood water sources

Water source	Area (km^2)	'Typical' flood flow (m^3/s)	Data source
Lake Wanaka	2515	544	Flow exceeded for 1% of flow record (1934 to 2010, inclusive)
Lake Hawea (controlled outflows)	1389	10	Typical flood flow
Cardrona River	346	162	1% AEP (WRENZ)
Lindis River	1050	288	1% AEP (WRENZ)
Other small tributaries	1056	289	Scaled by comparison with Lindis River catchment
Sum to Clutha River/Mata-Au delta		1293	
Clutha River/Mata-Au delta – Lindis River		1005	

WRENZ = Water Resources Explorer New Zealand (http://wrenz.niwa.co.nz/webmodel/)

3.4 Recommendations for future delta field work

To better understand the growth dynamics of braided gravel-bed river deltas, more detailed and accurate spatial and temporal data are required. This includes simultaneous information (ideally pre- and post- flood events) for both submerged delta\lakebed bathymetry, and the braided gravel-bed river system in the reach immediately upstream of the shoreline. This would improve our knowledge of sediment deposition volumes (and locations of deposition), as well as providing information on braided river delta growth dynamics for individual events – including feedbacks between delta deposition and braided river avulsions. Fortunately, advances in airborne and terrestrial laser scanning (Section 2.3.1) and sonar technology (e.g. 3-d bathymetric swath mapping combining multibeam sonar and sidescan sonar) will make these data-intensive field studies progressively more practical and feasible in the future.

To obtain better field data on the delta growth dynamics for newly-formed deltas, it is recommended that LiDAR data are obtained immediately prior to the river system being 'drowned' (and the lake formed). This would provide valuable information on the scale of riverbed and floodplain features (including remaining structures and vegetation) as well as providing a base ('pre-delta sedimentation') for future calculations of sediment deposition. As multibeam sonar (bathymetric) swath mapping technology becomes more widely available it will become progressively more cost-effective to determine sedimentation rates by simply subtracting newly obtained lakebed surfaces from the initial LiDAR data.

4 MICROSCALE MODELLING

4.1 Overview

Microscale models are very small scale movable bed models (MBMs) that can be used as a tool to predict river morphology (Maynord, 2006). The degree to which these models adhere to similarity criteria determines the extent to which they can be used for quantitative and/or qualitative comparisons with the prototype. In general, the greater the extent of scaling in the model, the more difficult it is to mobilise and transport the sediment. Additional forces (to mobilise and transport the sediment) are therefore provided by several means including increasing flow, modifying sediment properties and increasing the slope of the bed (Gaines & Smith, 2002).

For this study two movable bed microscale models were constructed to simulate the historic and future growth of existing river deltas in the Otago region of New Zealand. They were:

- A 1:2000 scale model of the Rees-Dart river delta system consisting of two braided, alluvial river systems delivering sediment to a combined delta prograding into a deep lake.

- A 1:1500 scale model of the Lindis River and Clutha River confluence and the Clutha River/Mata-Au delta, located approximately 9 km downstream at Lake Dunstan. Lake Dunstan is a relatively new man-made hydropower storage lake which was formed between 1992 and 1993, after the construction of the Clyde Dam.

These microscale models used constant flows and sediment feed rates rather than hydrographs. The constant flows represent "a continuous series of channel-forming discharges" (Ashmore, 1982, p. 203), and represent the conditions under which most significant changes to channel morphology occur. The flows were adjusted as part of the calibration process since it is not possible to directly scale between the model and prototype to determine specific flows (Gaines & Maynord, 2001). Vertical datums are also adjusted as part of the calibration, so there may be significant vertical distortion of modelled delta and upstream riverbed elevations (Gaines & Maynord, 2001). When this is the case, the information may be used to identify *relative* trends between separate model run scenarios.

The construction of the microscale models is discussed in Section 4.2 while the Rees-Dart river delta and Clutha River/Mata-Au delta microscale models are described in Sections 4.3 and 4.4, respectively.

4.2 Microscale model construction

Max et al. (2002) discuss the calibration and operation of microscale models and emphasise the importance of a correctly constructed and calibrated model to enable valid results to be produced. A

description of the steps involved in the development of a microscale model is outlined below. This is adapted from Max et al. (2002), and other authors where stated, to be specifically relevant for alluvial fans and braided river delta modelling.

1. Complete a thorough review of the study reach. This should preferably include a site visit and analysis of any historic data (e.g. aerial photos/photos, hydrographic surveys, etc.). Of particular interest, with regard to the modelling of a braided river delta, are any physical obstructions in the river reaches upstream of the delta (e.g. floodbanks or rock outcrops).

2. Determine the horizontal and vertical scale of the microscale model. The horizontal scale is based on the areal extent of the study reach to be modelled, the space available for the construction of the model, and any other 'economic' restrictions. Recent microscale models of alluvial fans (Davies et al., 2003; Davies, 2007; Davies & Korup, 2007) have used horizontal scales of the order of 1:1000 to 1:3333. The slope of the microscale models also deviates from the prototype to enable appropriate sediment movement to occur for the relatively small model flows. An arbitrary model base slope of 10% was used successfully in the above mentioned models.

3. Construct model. A simple, yet effective, method is to construct a flat, waterproofed, platform and use high-density polystyrene (glued to the platform) to provide the outer lateral extents of the movable bed reaches. The downstream boundary of the model can be modelled as a horizontal free overfall if the downstream boundary of an alluvial fan model is assumed to be fairly constant over time (Davies et al., 2003), or if the location and elevation of a fan toe is required to be constant (Davies & Korup, 2007). A downstream free overfall has also been used to model an alluvial fan at the confluence with another major river (Davies, 2007). However, a free overfall is not appropriate when modelling a prograding braided river delta; instead, a waterproof tank with a fixed overfall to a receiving basin of arbitrary depth is used. A steady rate of sediment can be delivered to the model via a sediment feeder that consists of a rotating, sloping, cylindrical pipe connected to a reservoir of dry sand. The water flow to the model is usually either a steady flow (e.g. delivered by a small pump) or a recurring hydrograph (e.g. created by supplying a steady flow to an automatic siphon and reservoir tank, or by using an automated flow valve). It is important that the sand and water mix before entering the model bed (to prevent sand from floating on the water surface tension), and care also needs to be taken to prevent localised scouring at the inflow location.

4. Run model to produce dynamic equilibrium. The basic underlying theory, with regard to microscale models, is that given a certain set of input variables (i.e. flow, lateral boundary extents and sediment characteristics) the bed slope will adjust to an equilibrium state (Max et al., 2002). At this point there should be no significant aggradation or degradation within the

system. If the microscale model has a free overfall as a downstream boundary, equilibrium will be achieved simply by running the model for a sufficient length of time (Davies et al., 2003; Davies, 2007; Davies & Korup, 2007); When there is a prograding delta at the downstream boundary, the only way to achieve dynamic equilibrium is to continually remove the sediment from the downstream limit of the prograding delta, or initially run the model with a free overflow to achieve equilibrium and then attach the downstream tank to simulate delta progradation. To achieve a suitable dynamic equilibrium the following variables can usually be easily adjusted: flow, sediment feed rate, platform slope, and downstream control level (Max et al., 2002). The degree to which these variables are adjusted, and the resulting steady volume of sediment transport, will vary according to the perception of individual modellers (Gaines & Smith, 2002). Ideally, the riverbed or alluvial fan slope needs to be reasonably parallel to the model platform base so that sediment is not scoured to expose the platform base nor aggraded to the point that the lateral boundaries are overtopped. The resulting model bed profile, in dynamic equilibrium, is often referred to as the 'base' model. Once the model reaches dynamic equilibrium the topography developed by the microscale model should fairly accurately represent that of the prototype. Although this comparison is often made qualitatively, Gaines & Smith (2002) recommend quantitative comparisons be made between the model and the prototype for thalweg location, cross section area, water surface width, hydraulic depth and ratio of width/depth to ensure morphologic similarity exists. Once morphologic similarity exists, the next step is to examine the impact of changes to this model.

5. Make adjustments to the model and run new scenarios (e.g. proposed engineering works, impact of landslide-induced sediment pulse on an alluvial fan, growth of a river delta). Adjustments are made to the 'base' model or input variables before running the model again to obtain a new equilibrium condition or, in the case of a scenario where equilibrium will not be achieved (e.g. a prograding delta), a suitable amount of change over time has occurred. By using a laser scanner to measure the bed profile at various run times, the differences between various scenarios and the initial 'base' model can be observed. At this stage it is important to note that because of scale effects (i.e. the lack of dynamic similitude between the prototype and these very small scale microscale models) the data acquired from microscale models must be used with caution. Rather than providing precise, quantitative information, these microscale models are better suited to identifying relative trends between various scenarios. With regard to alluvial fans and braided river deltas this generally means identifying the areal extent and relative rate of aggradation and/or degradation (Davies et al., 2003; Davies, 2007; Davies & Korup, 2007).

Sections 4.2.1 to 4.2.8 describe the various components required to successfully construct and operate the microscale models.

4.2.1 Model platform

The structural support for the model platforms was provided by steel box section framework. Steel brackets, welded to the box sections, allowed wooden and/or metal support beams to be bolted or welded to the steel framework. The fibreboard platform was screwed onto the framework and was painted with a water-based paint to prevent any moisture damaging the structural integrity of the fibreboard.

The platform was initially tilted to a 10% slope and a waterproof base for the platform was formed from offcuts of a flexible, waterproof, synthetic butyl rubber membrane, known as Butynol® or Butylclad. This membrane was primed then glued together along seams 50 to 100 mm wide using an ADOS F2 contact adhesive. To improve the water tightness of the butyl rubber, these seams were glued so that the upstream piece of rubber butyl overlay the more downstream piece. The rubber membrane was then stapled to the external edges of the platform – except along the downstream edge where it was glued into the waterproof 'lake' tank of the model.

4.2.2 Lake tank and sump

The lake tank and sump for both models are constructed from 12 mm thick plywood board with joins that have been routed, glued and screwed together to make the tanks watertight. All tanks have been painted and have outlet valves near the base of the tanks to allow water to drain from the tanks when required.

An outlet from the lake tank (e.g. adjustable weir or valve) controlled water levels in the lake and flows into the sump. The water pumps, submerged in the sump, provide the inflows for the microscale model. Figures 4.1a and 4.1b show the weir and overflow structures used in the Rees-Dart microscale model.

(a) (b)

Figure 4.1: Rees-Dart lake outlet control structure: (a) adjustable perspex overflow weir and (b) wooden spillway from the lake tank to sump

4.2.3 Polystyrene model boundaries

Fixed boundaries for the microscale model, representing the outer limits of the braided river, delta and lake, were created as an ArcGIS shape file. The boundary shape file was then converted into an AutoCAD (*.dxf) file which was compatible with software used by an automated laser cutter that was able to produce the scaled boundaries in shaped, polystyrene blocks. High density (H grade) polystyrene was chosen for the boundaries as it is light, easily-modified and relatively watertight. The 50 to 100 mm thick polystyrene blocks were glued to the butyl rubber membrane using ADOS Styrobond; where higher boundaries were required additional shaped polystyrene sheets were glued onto the initial layer of polystyrene. Once the polystyrene blocks were glued in place, heavy weights held the blocks in place until the adhesive had dried. The butyl rubber/polystyrene and butyl rubber joins were also sealed using an acetic, fast curing, silicone sealant (Silaflex® RTV). Two coats of white paint were applied to make the polystyrene watertight.

4.2.4 Sediment feeders

A combination of three sediment feeders (Figures 4.2a, b and c) was used to provide a steady supply of sediment to the upstream limits of the river. Although the sediment feeders were not identical, they were all of a similar design with a motorised rotating, circular tube transferring sediment from the storage reservoir into the model; the sediment feed rates were calibrated by adjusting the slopes of the tubes. All sediment feeders had a reliable and consistent feed rate of within ± 2% of the specified feed rates throughout the duration of each experiment.

(a) Rees & Lindis (b) Dart (c) Clutha

Figure 4.2: Sediment feeders used for microscale modelling

4.2.5 Sediment

A fine-grained, silica sand originating from the Mt Somers silica sand quarry was used in all microscale model runs. The sediment was originally used in a physical hydraulic model at Lincoln University and was kindly donated for this project. The sediment was initially sieved to remove all material (both coarse grains and debris) greater than 560µm. The grain size distribution of the sediment used in the microscale model runs is shown in Figure 4.3. The sediment has an arithmetic mean, D_{mn}, of 0.22 mm and a standard deviation, σ, of ~0.07 mm.

Once the microscale models were fully constructed, a 3 cm thick layer of sand was placed over the entire platform. A metal bar with two thin 3 cm long metal vanes (Figure 4.4) was used to smooth the sand and ensure a relatively even layer of sand.

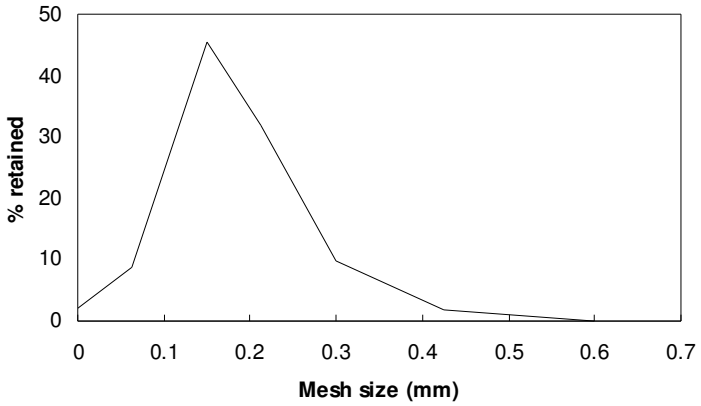

Figure 4.3: Grain size distribution for microscale model sediment

Figure 4.4: Sand 'smoother'

4.2.6 Water pumps

Pumps (Figure 4.5) were used to transfer water from the sump to the upstream inflow locations for the rivers (i.e. the same input location as the sediment).

Figure 4.5: Rees-Dart water pumps in sump

Initial testing of the pumps showed they pumped 0.12 to 0.16 l/s (i.e. 7.2 to 9.6 l/min). To reduce the flow rate to the flows required to model the rivers, the flow from each pump was split near the pump outlet; one hose led to the upstream limit of the microscale model, where another butterfly valve controlled the flow into the model, while the other shorter hose led to another butterfly valve that released the excess water back into the sump. Any changes to the flows were made by adjusting the butterfly valves. Inline flow meters were also installed between the pump and the model inflow to provide a continuous measurement of the flow for all model inflows, except for the smaller Rees inflow which was measured by filling a measuring jug over a known time interval.

For a required flow of 1.5 l/min the actual flow varied by up to 0.1 l/min (± 7 %), while at a lower flow of 0.4 l/min the actual flow varied by up to 0.05 l/min (± 12%). The flows appeared to be sensitive to several factors including the water level in the sump, water temperature, and length of operation of pumps.

4.2.7 Laser scanner and trolley

An instantaneous-profile laser scanner (Darboux & Huang, 2003) was used to measure the surface profile for the braided river and delta progradation zone at various times throughout the model runs. This allowed the delta profile, river system, and volumes of accumulated sediment to be quantified. The laser scanner, consisting of two lasers and a camera mounted on a carriage (Figure 4.6a), was moved up to 3 m along a carriageway by a stepper motor. The single carriageway was attached to a trolley structure with wheels that was able to be moved upstream from the lake tank along two rails parallel to the 10% slope of the model platform. To ensure the scans were made at the same location each time, a measuring tape was attached to the steel box sections that the trolley ran along, and pointers were attached to the trolley frame on both sides of the model (Figure 4.6b).

The width of the scan was determined by the height of the camera from the surface being scanned (i.e. the larger the distance from the camera to the surface, the wider the swath being scanned).

For accurate surface profile acquisition the model runs needed to be temporarily halted, and the water in the lake tank drained; this was because the water would have refracted the laser light and given false spatial information. Prior to the start of the experiment, and at any time during the course of the experiment that the angle of the camera or position of lasers was changed, the laser scanner also needed to be calibrated.

The laser scanner was calibrated using the calibration frame and lightbar shown in Figure 4.7. The lightbar consisted of a black, rectangular bar with light-emitting diodes (LEDs) spaced at even intervals along its length. This lightbar slotted into the calibration frame at 2.5 cm vertical spacings; during calibration the lightbar was scanned in each slot that was within the vertical range for the delta and river surface that needed to be scanned.

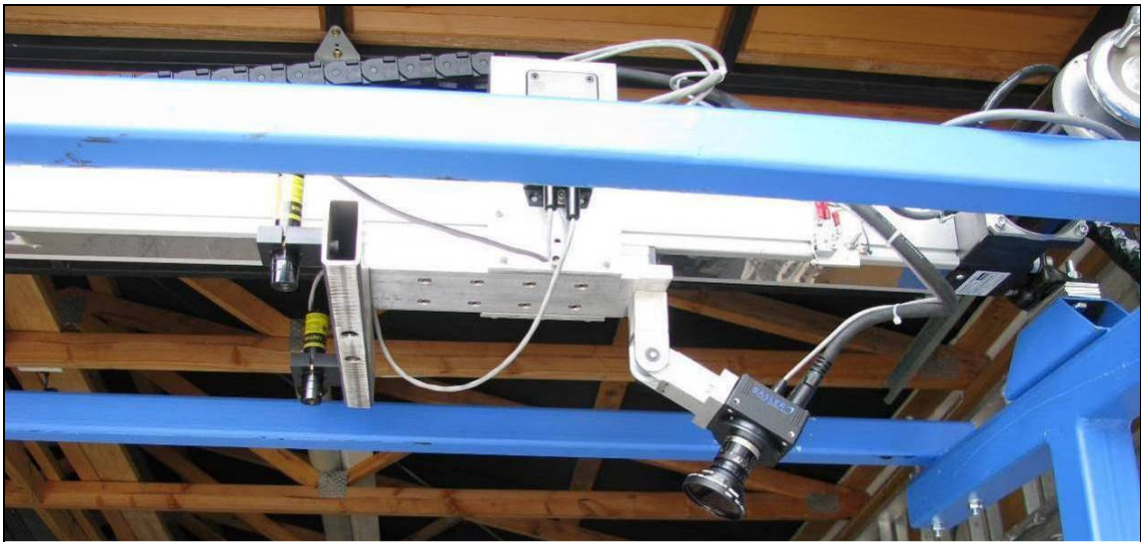

(a) Laser scanner carriage with 2 lasers and camera

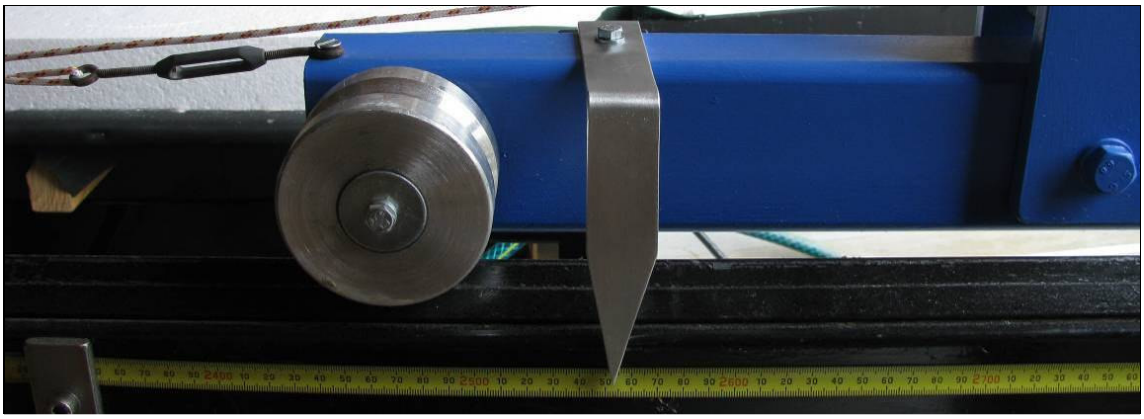

(b) Laser scanner trolley pointer

Figure 4.6: Laser scanner and trolley

The vertical and positional accuracy of the scanned data are approximately ±0.5 mm (Darboux & Huang, 2003). However, the scanner used for this study did, at an irregular interval as it crossed the carriageway, record levels that were around 2 mm lower than the actual recorded values at the point 1 mm before and after. There was no obvious reason for this (e.g. loose connections), and the scanner ran smoothly along the carriageway. Therefore, as the main data required from the model was the delta front location (rather then sediment volumes), the laser scanner accuracy was considered adequate for the needs of this experiment.

4.2.8 Webcams

Two 2-megapixel webcams with autofocus (Logitech QuickCam Pro 9000, Figure 4.8) were used to capture the prograding delta profiles. Photographs were taken at regular intervals (usually every minute) using Flix software (http://www.nimisis.com/projects/flix.php). At the end of each model run Flix software generated time-lapse videos from the photograph sequences.

The photograph sequences were usually produced using with a resolution of 960 x 720, although some sequences used a coarser resolution of 680 x 480.

Figure 4.7: Laser scanner calibration frame and LED lightbar

Figure 4.8: Logitech QuickCam Pro 9000 webcam mounted on ceiling beam

4.3 Rees-Dart microscale model

A 1:2000 scale microscale model of the Rees-Dart delta (Figure 4.9) was constructed to examine the braided river delta growth processes of the Rees and Dart rivers as they prograde into Lake Wakatipu. The model configuration, methodology and results are summarised below.

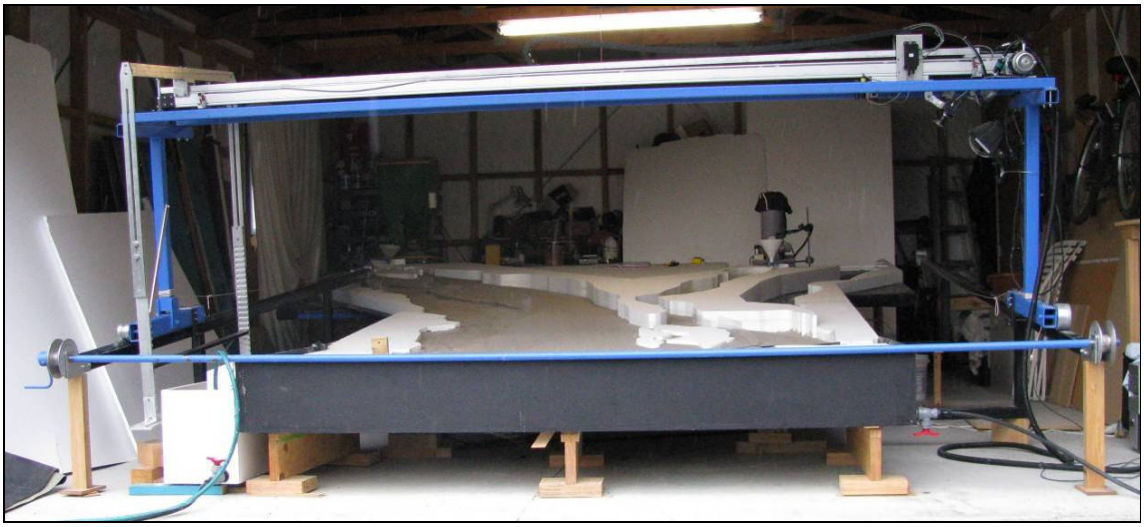

Figure 4.9: Microscale model of the Rees and Dart rivers and delta

4.3.1 Model configuration

Figure 4.10 shows a schematic of the Rees-Dart microscale model. The microscale model was constructed on a 2.44 m to 4.0 m wide by 4.0 m long platform set to a 10% slope as used successfully in previous microscale models (e.g. Davies et al., 2003).

The design of the platform support was such that the platform slope could be increased or decreased by pivoting the platform about the mid-point (Figure 4.11a), if required. The lower end of the platforms rested on wooden and/or metal blocks (varying in size so that small adjustments can be made). The upper limit of the platforms was supported by height-adjustable struts (Figure 4.11b) and wooden props were also used to support the platform where the weight of sand on the platform caused minor bowing.

The lower edge of the platform was attached to a 2.4 m wide by 0.93 m long 'lake' tank with an adjustable false floor and adjustable overflow weir set to 100 mm and 191 mm, respectively, above the base of the tank. The overflow weir maintained a constant water level and passed the excess water back into a sump (0.970 mm long by 276 mm wide by 336 mm deep). From the sump, two water pumps recirculated water to the upstream limits of the model (i.e. Dart and Rees road bridge locations) where the water was combined with dry sediment (in a funnel) and fed into the model. The dry sediment was supplied by sediment feeders with motorized, rotating, circular tubes that transferred the sediment from a dry storage reservoir into the model at a steady feed rate.

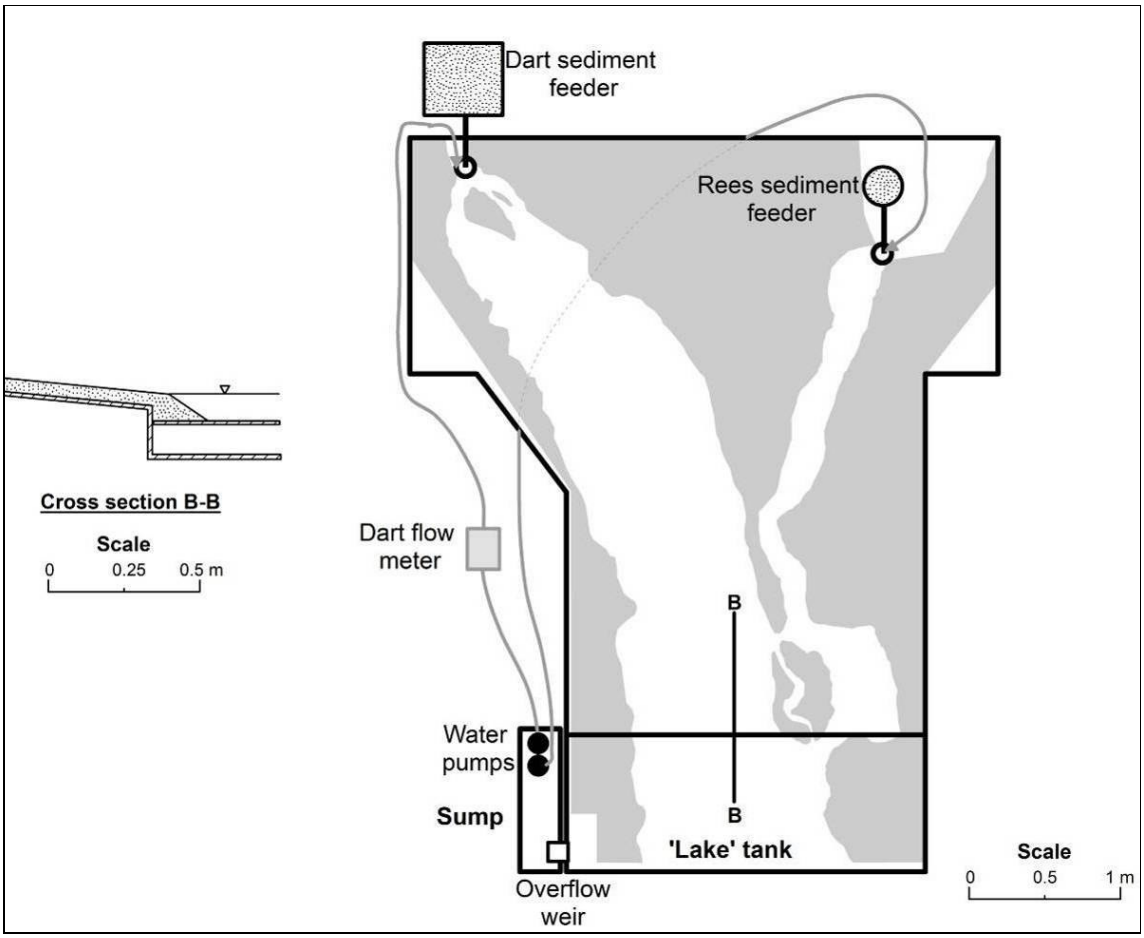

Figure 4.10: Schematic of the Rees-Dart microscale model with final model boundaries

(a) Pivot support (b) Strut

Figure 4.11: Rees-Dart microscale model platform structural supports

High density expanded polystyrene was used to form the fixed boundaries of the river and lake. The initial fixed boundaries for the microscale model were derived from 5 m contours created using ArcGIS, and a 25 m DEM of New Zealand generated by Landcare Research (Barringer et al, 2002). The DEM was produced using Land Information New Zealand (LINZ) digital topographic data which are stated as having a planimetric (x,y) accuracy where "90 percent of well-defined points are within ±22 metres", and a vertical (z) accuracy where "90 percent of well-defined points are within ±10 metres" (http://www.nztopoonline.linz.govt.nz/about/data-details/index.html).

The Landcare Research DEM has been derived placing most importance on the generated 25 m cells being consistent with LINZ spot height and 20 m contour information. Although the spatial accuracy of different landforms in the derived DEM varies, most landforms having a RMS error of 5-8 m; valley floors tend to be less accurately represented with RMS errors of ~15 m (Barringer et al, 2002).

For the model fixed boundaries, the lower reaches of the converging river system and delta were bounded by the 320 m contour while the middle and upper reaches of both rivers were bounded by the 340 m and 360 m contours, respectively. This represented the boundary between the steeply rising mountains and the gently sloping valley floors. Using these contour boundaries, and the model platform extent (scaled up to represent the prototype area), an ArcGIS shape file was generated of the model boundary regions. This is referred to as the initial model boundary and is shown in Figure 4.12.

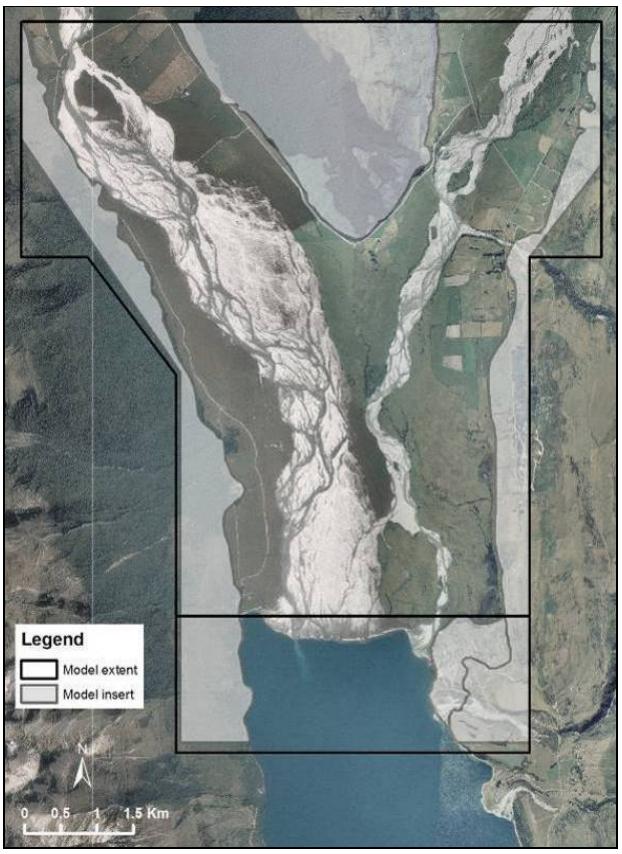

Figure 4.12: Rees-Dart microscale model *initial* fixed model boundaries

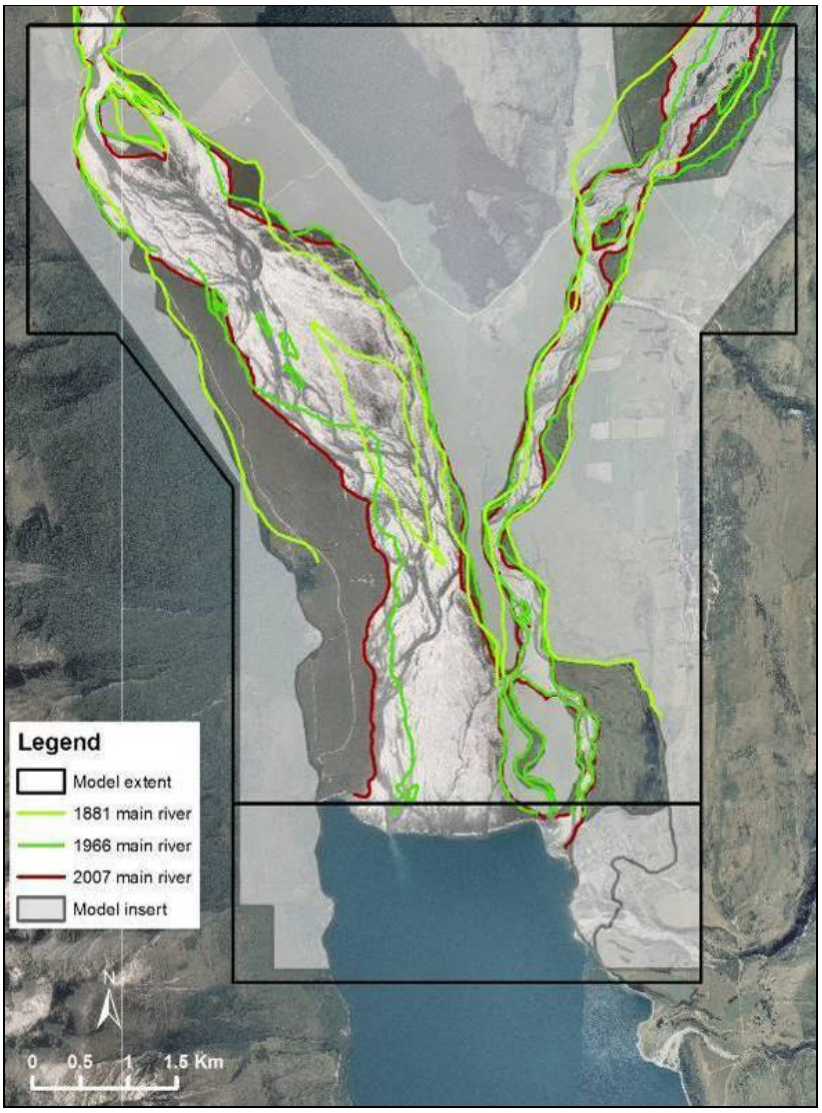

Figure 4.13: Rees-Dart microscale model *final* fixed model boundaries

Once initial model runs were complete, it was decided that the delta would be more likely to prograde in a realistic manner if the fixed boundaries of the braided river channels were limited to the extent of the rivers as observed on historic maps and aerial photographs from 1881 to 2007. Figure 4.13 shows the revised fixed boundaries. These new boundaries (i.e. final model boundary) were created by inserting an additional layer of 75 mm thick shaped polystyrene (and an additional 50 mm layer of polystyrene in the upper reaches) inside the original boundaries. Other temporary boundaries could also be added and removed using thick sheets of flexible plastic.

To measure the changing delta and riverbed profiles, the instantaneous-profile laser scanner (Darboux & Huang, 2003) was mounted on a single rail that ran across the full width of the model. This single rail was attached to a trolley structure with wheels that could be winched upstream from the lake tank along two rails parallel to the 10% slope of the model platform. As the scanner single rail was approximately 1.05 m above the delta profile, the scanner captured a 0.85 to 0.95 m wide strip of the

profile as the stepper motor moved the scanner across the profile in 1 mm increments. The vertical and positional accuracy of the scanned data are approximately ±0.5 mm (Darboux & Huang, 2003).

Experimental flows were monitored by an inline flow meter (providing continuous flow measurements for the Dart flow) and by measuring how long it took to fill a measuring jug (for the smaller Rees flow). Two 2-megapixel webcams (mounted in front of the delta and on the ceiling) also took photographs at a 1-minute interval throughout each experiment. These images were able to be combined to produce time-lapse imagery of the changing delta system.

4.3.2 Assumptions and limitations for use of microscale model

Due to the very small scale of the model, and the vertical distortion, the following assumptions and limitations had to be taken into consideration for both experimental design and for the interpretation of results produced by the model. The assumptions and limitations that need to be considered, when modelling the Rees-Dart delta, include:

1. Deposition of suspended sediment, in the form of a bottomset ahead of the advancing delta, is absent in the model.
2. Turbidity currents are not modelled even though there is substantial evidence for the existence of turbidity currents transporting suspended sediment up to 60^{+} km down the lake (Pickrill & Irwin, 1982), via well-established sub-lacustrine channels (Brodie & Irwin, 1970).
3. Dart/Rees ratios of flow and sediment are constant. For example, it is assumed there will be no sudden increase in sediment supply due to a large landslide in one of the catchments. Climate change modelling (Poyck et al., 2011) also shows that, although there may be an increase in upstream river flows in winter and spring, flows are likely to remain relatively unchanged during the late spring and summer months when flows are usually highest.
4. Fixed polystyrene boundaries (Figure 4.13) cannot be overtopped, thus preventing new flow paths and erosion from extending beyond these limits. Bank erosion within these boundaries was, instead, simulated using temporary plastic barriers; a small section of polystyrene was also removed from the lower west portion of the grassed island, by Glenorchy, to allow for observed flow paths. This was considered appropriate given that avulsions (i.e. diversion of flow from an established channel onto a new course on the adjacent floodplain) are likely to be the main source of floodplain aggradation rather than deposition from overbank flood flows (Slingerland & Smith, 2004).
5. Lake level is constant.
6. The model bathymetry is represented by a flat ‘lake’ bed whereas Lake Wakatipu bathymetry varies with the delta prograding into shallower water near Kinloch and Glenorchy. This may modify the model run time, as would changing the height of the modelled delta.

7. Lateral river mouth bars will not form.

4.3.3 Development of the 1966 Rees-Dart 'base' model

The initial aim of the Rees-Dart microscale model experiments was to produce a 'base' model with Rees and Dart riverbeds and delta configurations that realistically represented the Rees-Dart delta in 1966 (i.e. the first year full aerial photograph coverage of the river delta and upstream river channels was available). By running the model for a longer period of time, the present delta-front location was replicated and estimates for future delta growth produced.

The 1966 Rees-Dart 'base' model (referred to as the 'base' model hereafter) was developed by, firstly, producing an 'equilibrium' model. While regularly removing the sediment accumulating in the lake tank/delta area every 30 to 45 minutes, flow rates for the Dart and Rees Rivers were adjusted so that the Dart flow was approximately 3 to 4 times larger than the Rees flow (a discussion of relative flow rates is given in Section 3.2.3.3). Sediment feed rates were also adjusted to ensure that a consistent braiding pattern occurred in both rivers, while also aiming for a constant sediment feed rate for the Dart River that was within the range of 3 to 7 times greater than that of the Rees River (i.e. within the range I_{Dart}/I_{Rees} ~3 to 7 as described in Section 3.2.5.4).

The final flow and sediment feed rates used for the Rees-Dart microscale model experiments are summarised in Table 4.1. For each Rees-Dart microscale model experiment, the starting 'equilibrium' model also had a slightly different configuration due to the inherent variability associated with braided rivers at all scales. Both of these factors are likely to have some effect on delta growth so need to be considered when interpreting results.

Table 4.1: Flow and sediment feed rates for the Rees-Dart microscale model

	Dart	Rees	Dart/Rees	Dart/Rees (prototype)
Flow (l/min)	1.5 ± 0.1	0.40 ± 0.05	3.3 - 3.8	1.9 - 3.1
Sediment feed rate (g/s)	1.53 ± 0.02	0.235 ± 0.005	6.5	3.1 - 7.2

The development of the 'base' model was an iterative process and, prior to running the simulation scenarios, it was important to ensure that the model was behaving similarly to the prototype. Although the initial Rees-Dart microscale model simulated both the Glenorchy lagoon and the Rees River flow path (along the northern boundary of Glenorchy), some of the other dynamics within the Rees-Dart delta system required additional intervention to produce a representative model configuration. The methodology developed to produce the 'base' model was as follows:

1. The microscale model was set up with plastic barriers representing the 1966 and 2007 Dart River TRB and the small offshore island, as well as an additional plastic barrier separating the

Dart and Rees Rivers upstream of the grassed island (Figure 4.14). The 1966 & 2007 barriers represented the ~1.2 km^2 of eroded farmland (Figure 4.14) and, together with the island, gave a better representation of delta progradation in the Kinloch area. The barrier separating the Rees and Dart Rivers represented the continuous 'tongue' of land that separated the Dart and Rees Rivers all the way to the lake on historic maps from the late 19^{th} century. Without the influence of the Dart River, the Rees riverbed becomes elevated relative to the Dart riverbed resulting in a preference for the Rees River to flow into the Dart River once the barrier is removed (which is consistent with aerial photography and surveyed cross section data).

2. The model was run for ~2 to 3 hours with the flow and sediment feed rates in Table 4.1 to establish a braided river system with a reasonable level of 'equilibrium' (no significant aggradation or degradation occurring) for both rivers. Up to this moment, all accumulated sand at the delta front was regularly removed every ~30 minutes to prevent upstream aggradation due to delta progradation.

3. Once 'equilibrium' was established, and the Glenorchy lagoon had developed, a plastic barrier was inserted between the Rees River and the Glenorchy Lagoon to divert all Rees River sediment and flow along the Rees River rather than allowing sediment to flow into the lagoon. From this time on the delta was allowed to prograde into the lake.

4. As the delta advanced to the approximate 1937 shoreline location (estimated from 1937 aerial photography that only showed the Glenorchy area), the model was stopped, the water level lowered and the delta profile scanned. The processed scan data, showing the delta shoreline location, were then superimposed over the geo-referenced aerial photos to determine whether the modelled delta shoreline had prograded to the approximate position of the 1937 delta shoreline. Note: If either river delta shoreline prograded more quickly than the other, it was possible to run the model for either river independently to get as close a match as possible to the 1937 delta shoreline profile.

5. Once the modelled delta shoreline was at the approximate 1937 delta shoreline location, the plastic barrier separating the Dart and Rees Rivers (upstream of the grassed island) was removed. This allowed the Rees River to flow onto the Dart River (as shown in 1937 aerial photography). The experiment then continued and the model was scanned every 30 minutes to 1 hour until the model delta had prograded to the approximate position of the 1966 delta shoreline. These point sequential scans were then analysed to estimate the model time scale.

At this point the plastic barrier representing the 1966 Dart River TRB, and the small island immediately offshore, were removed and the 'base' model was ready to run the model simulation scenarios.

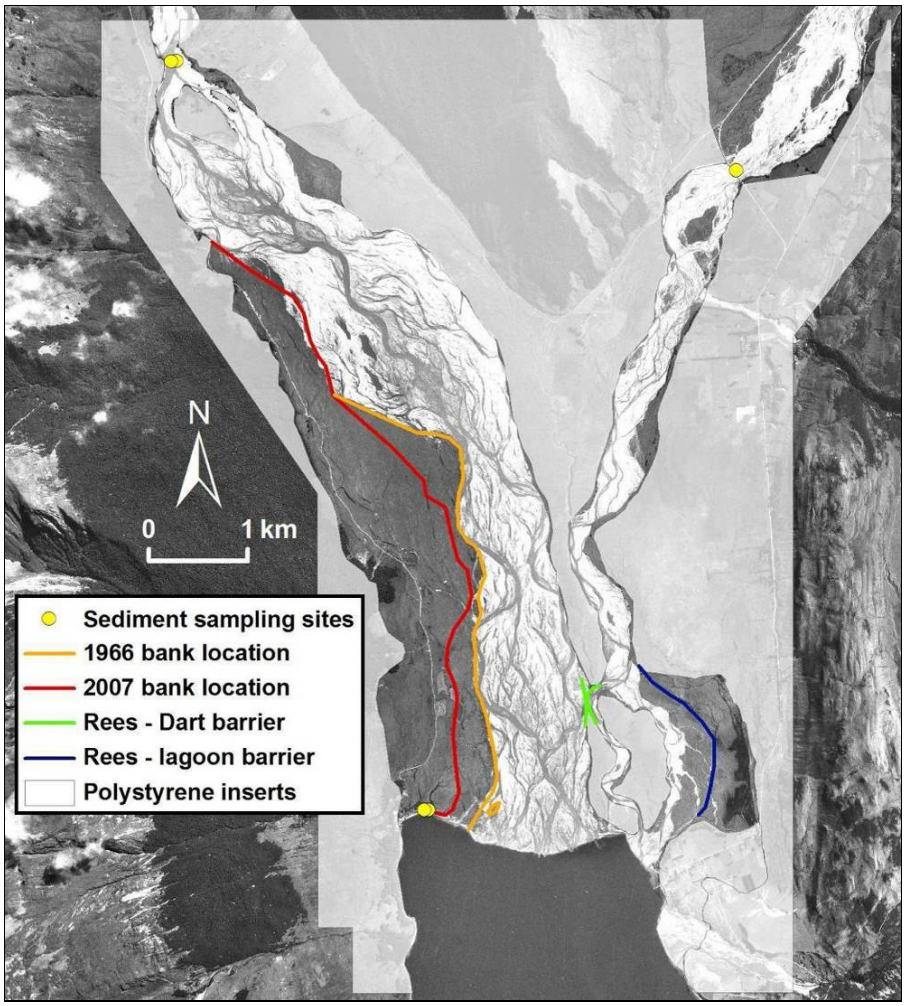

Figure 4.14: A 1966 aerial photograph with sediment sampling sites, bank locations (1966 and 2007), and microscale model polystyrene inserts (and removable plastic barriers)

4.3.4 Experiment methodology

Once historic delta growth was adequately represented, the model time scale was calculated (Section 4.3.4.2). Delta growth, over the future ~120 years, was then simulated. These experiments were repeated three times (Figure 4.17), with the same run parameters, to determine whether the microscale model was able to successfully replicate the advance of the delta shoreline.

Once each experiment had simulated ~120 years of future delta growth, changes were made to assess both the sensitivity of the model to sediment supply, and the effectiveness of the model as a predictive tool.

4.3.4.1 Modelling historic delta growth

For each experiment a 'base' model was developed up to the 1966 shore line. By continuing to run the 'base' model under the same conditions, and scanning regularly, the progress of the model delta shoreline was tracked until it reached the 2007 delta shoreline position.

4.3.4.2 Calculating model time step

The volumetric rate, Qs_p, at which sediment accumulated at the Rees-Dart delta in the 41-year time interval, t_p, was approximately 276 000 m^3/yr. This created an additional delta area, A_p, of 203 000 m^2 along the lake shoreline which is equivalent to a rate of increase in delta area, AR_p, of 4951 m^2/yr, and an average delta depth, d_p, of 60 m. LiDAR data collected in 2011 provided 2011 shoreline data, allowing the rate of increase in delta area, AR_p, to be updated to 5154 m^2/yr for the 1966 to 2011 time interval.

$$AR_p = \frac{A_p}{t_p} \tag{4.1}$$

$$d_p = \frac{Qs_p \times t_p}{A_p} \tag{4.2}$$

Where:
- Qs_p = volumetric rate of delta sediment accumulation (m^3/yr)
- t_p = time interval (years)
- A_p = increase in delta area (m^2)
- AR_p = rate of increase in delta area (m^2/yr)
- d_p = average delta depth (m)

To determine the model time step, t_m, the 1966-2007 increase in model delta area, A_m, was scaled to represent the equivalent prototype increase in delta area, A_p, as defined by geo-referenced aerial photography. The resulting area was divided by the 1966 to 2007 average rate of increase in delta area, AR_p.

$$AR_m = AR_p \quad \Rightarrow \quad t_m = \frac{A_m \times \lambda^2}{A_p} \times t_p \quad or \quad t_m = \frac{A_m \times \lambda^2}{AR_p} \tag{4.3}$$

Where:
- t_m = time interval of the model (hours)
- A_m = increase in delta area of the model (mm^2)
- λ = model horizontal scale (i.e. $length_p/length_m$) = 2000
- AR_m = rate of increase in delta area of the model (m^2/hr)

Analysis of model scan results showed that each hour of experiment run time represents approximately 20.8 ± 1 year of prototype delta growth (Table 4.2).

Table 4.2: Model time step calculations (model scale is 1:2000)

Experiment	Run time t_m (hrs)	Delta area increase A_m x 2000^2 (m^2)	Rate of increase in delta area, AR_p (m^2/yr)	Model time step t_p/t_m (yr/hr)
A	4.0	425 825	5154	20.7
B	4.7	528 595	5154	21.8
C	4.0	409 868	5154	20.0

4.3.4.3 Modelling future delta growth

While modelling future delta growth it was assumed that, up to a total run time of 9.5 hours (i.e. ~120 years of future delta growth), the same sediment supply and flow regimes were maintained and the model configuration remained the same for all experiments (i.e. no further bank erosion took place on the Dart River TRB - or at any other location).

4.3.4.4 Modelling change in sediment supply and potential engineering solutions

At 9.5 hours of model run time, modifications were made to examine potential changes to the Rees-Dart River system and surrounding land in experiments B and C.

For experiment B a plastic barrier, representing a potential river management option utilising the grassed island as a barrier, was inserted upstream of the grassed island to divert all Rees River flow and sediment into the Rees western flow route (Figure 4.19b). Over the past century the advance of Rees River delta has infilled the Glenorchy lagoon and positioned the river and delta adjacent to Glenorchy, increasing the risk of flooding in Glenorchy – especially since ~1989 when the Rees River main channel switched back to diverting the larger portion of the floodwaters along the eastern flow route (Otago Regional Council, 2010). It thus appeared likely to be beneficial to Glenorchy for floodwaters to be conveyed along the western flow route.

For experiment C the Rees River sediment feed rate was increased by 50% to 0.34 g/s. This scenario was included to account for the fact that there are few historic and current sediment yield data available for both the Rees and Dart Rivers, but there is the potential for a relatively sudden and large change in sediment supply to occur, e.g. due to debris flows (McSaveney & Glassey, 2002), or a large landslide (McColl & Davies, 2011).

A M ~8 earthquake on the Alpine Fault, which is less than 30 km from the middle reach of the Dart catchment, has a mean annual occurrence interval of ~200 to 300 years at present with the most recent event occurring ~295 years ago (Rhoades & Van Dissen, 2003). At some stage in the future, this is likely to cause a substantial sediment input to both rivers (but particularly the Dart). In experiment C the additional sediment was added to the Rees River due to its closer proximity, and thus hazard, to Glenorchy.

4.3.5 Model results

4.3.5.1 Development of the 1966 Rees-Dart 'base' model

Using the small flows, fine sediment and relatively steep model platform, a typical braiding patten developed. The Rees-Dart 1966 'base' model was then produced by incorporating temporary plastic barriers to restrict flow paths and divert flow. This resulted in a realistic modelled braided river system of the Rees-Dart delta (Figure 4.15a and Appendix C).

(a) Experiment A at t = 4.0 hrs

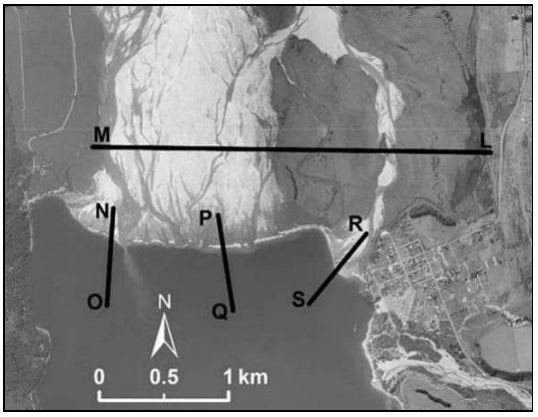

(b) Cross section and delta profile locations

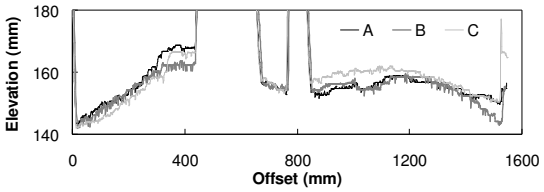

(c) Cross section L-M for experiments A (t=4.0 hrs), B (t=3.2 hrs) & C (t=4.0 hrs)

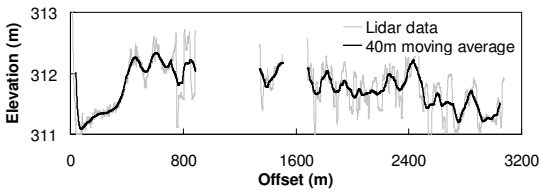

(d) Cross section L-M for 2011 LIDAR data (including moving average over 40 m length)

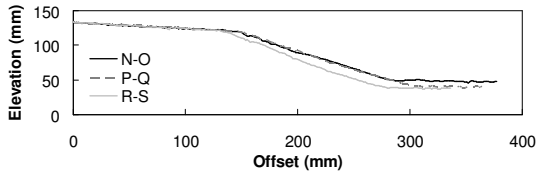

(e) Delta profiles N-O, P-Q and R-S for experiment A at t=4.0 hrs. Note exaggerated riverbed slope and vertical height of delta.

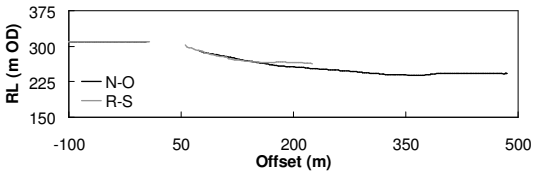

(f) Delta profiles N-O and R-S for 2011 from sonar and LIDAR surveys. Note gap in data near shoreline.

Figure 4.15: Cross sections and delta profiles produced by both the Rees-Dart microscale model and from field measurements

Figures C1 to C6 in Appendix C show the microscale model during Experiment A. These figures show that, as a uniform fine sediment was used in the microscale model, there were occasions when sheet flow (e.g. Figure C1) and exaggerated scour (e.g. Figure C4) occurred because of the hydraulically smooth conditions. However, overall the flow paths were representative of the prototype in 1966 (when compared to 1966 aerial photography), and beyond to the approximate time of the 2007 aerial

photography (Figures 4.15a and b). The modelled delta foreset slope is also shown in Figures C7 to C9. These photographs were taken while the microscale model 'lake' was drained, and they clearly show that no significant delta bottomset was produced.

4.3.5.2 Modelling historic delta growth

The historical analysis of imagery from 1966 and 2007 showed a maximum progradation of the delta shoreline of ~210 m for the Dart River TRB, near Kinloch, and ~120 m for the Rees River at Glenorchy (Figure 4.16a).

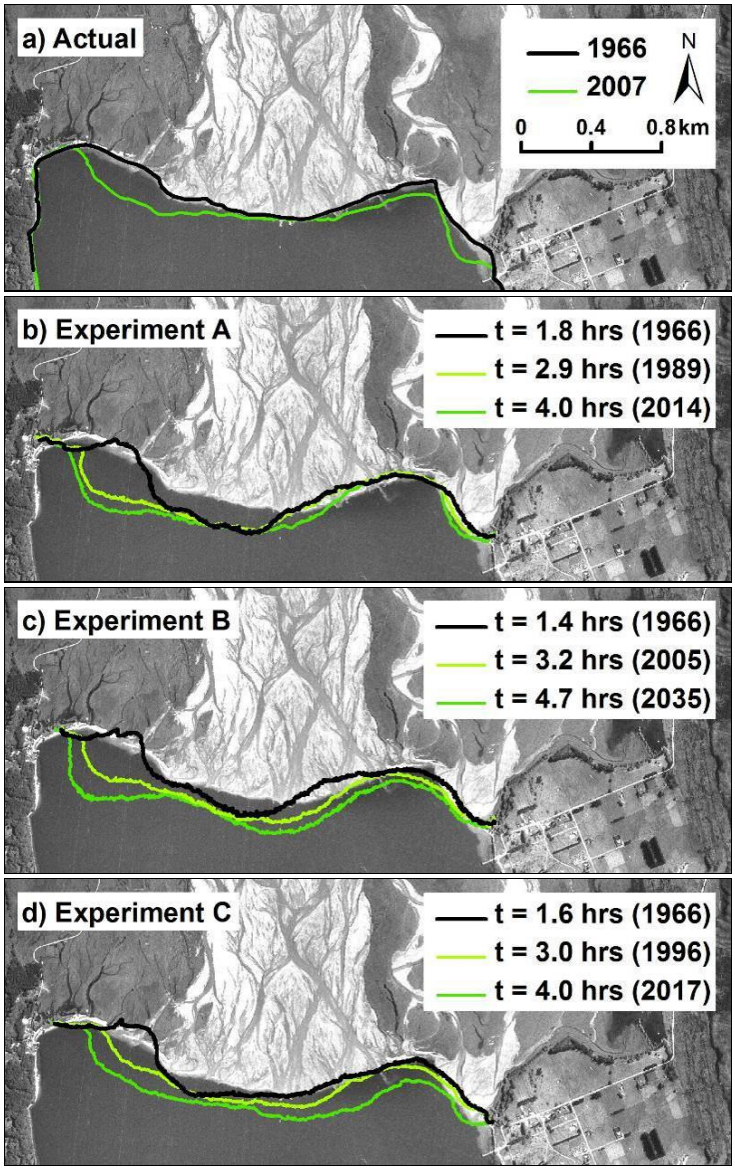

Figure 4.16: Historic Rees-Dart delta shorelines (a) and experimental results (b to d) superimposed on 1966 aerial photography

Model simulations for the same time period (i.e. experiments A, B and C, after 3.2 to 4.7 hours) produced delta progradation in the same areas as observed in the historic imagery (Figures 4.16b to

4.16d). This was particularly true for the Dart delta where delta growth adjacent to Kinloch coincided with the removal of the temporary 1966 river bank plastic barrier in the model and significant bank erosion in the prototype. The historical imagery and experiments also both exhibited negligible delta progradation in the central portion of the Dart delta over this time period.

A comparison of simulated bed levels from each of the three experiments (at t = 3.2 to 4.0 hours) showed similar trends where the Rees River eastern flow route was elevated above the Rees River central and western routes, and the Dart riverbed levels were lower again near the TRB (Figure 4.15c). This showed remarkably good agreement with recently obtained 2011 LIDAR data, extracted for the same cross section (Figure 4.15d).

The simulated deltas had foreset slopes of ~27.5º for the two Dart River delta profiles, and a slightly higher slope of 29.9º for the Rees River delta (Figure 4.15e). This matches maximum prototype Rees-Dart delta foreset slopes of 28º to 29.6º measured during a sonar survey in June 2011 (e.g. Rees delta profile R-S, Figure 4.15f). The prototype delta foreset slopes did, however, vary considerably (to as low as 16º to 18º) which was partly due to the path the survey boat followed, which did not always capture the steepest delta slope. The prototype delta slopes tended to be steeper in areas where the delta was currently advancing, and the prototype delta profiles were also more concave in shape than those in the model.

Other features, such as the Glenorchy Lagoon were also reaslitically developed – as was the elevated 'ridge' extending longitudinally down the central section of the Dart River floodplain (Figure 3.35). Overall the microscale model performed well and historic delta growth was replicated consistently.

4.3.5.3 Modelling future delta growth

Based on the assumption that 1 hour of experiment run time represented 21 years of prototype time, the microscale model was run for 7.3 to 8.1 hours beyond the 1966 Rees-Dart 'base' model (Figure 4.17).

Two of the three experiments (experiments B & C) produced a simulated 2005 to 2017 Dart delta shoreline position near Kinloch very similar to the existing 2007 shoreline, while experiment A showed a more advanced delta shoreline position (Figure 4.17). The experiments therefore show that delta progradation in the Kinloch area is likely to be continuous for the next 45 to 75 years, with an advance of the order of 200 m. Between 1966 and 2007 there was ~210 m of delta progradation in this area, coinciding with significant erosion of farmland along the upstream Dart River TRB; it is therefore likely that further erosion of this farmland will also contribute to delta progradation. If the Dart River TRB continues to be eroded at a similar rate, the access road to Kinloch may need to be relocated or protected.

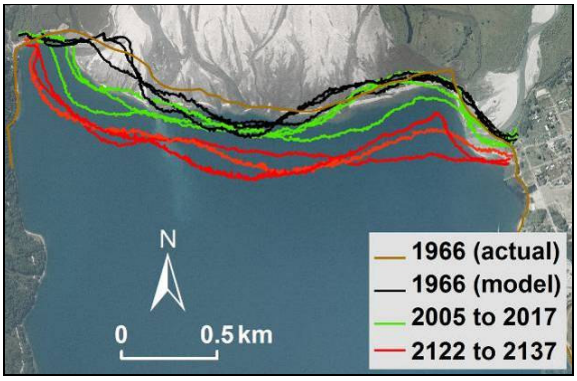

(a) Experiments A, B & C

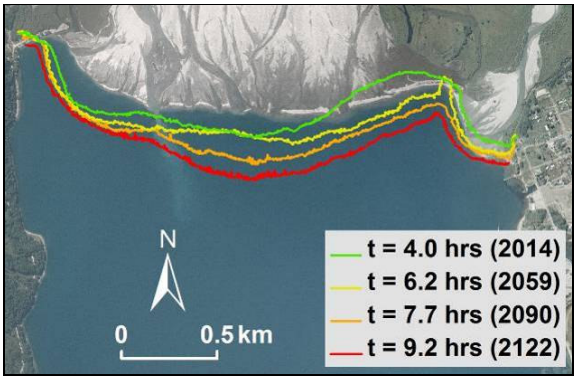

(b) Experiment A

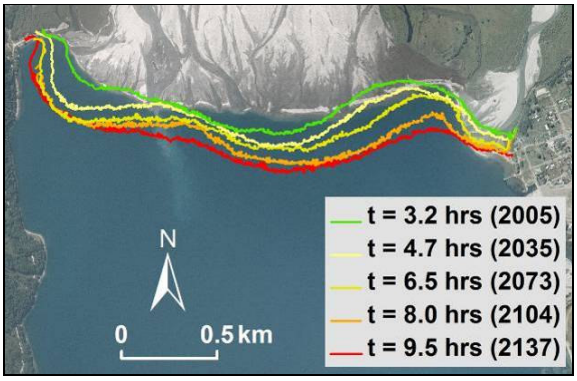

(c) Experiment B

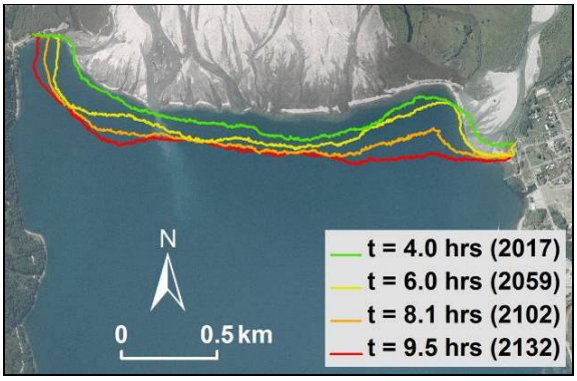

(d) Experiment C

Figure 4.17: Microscale model predictions of delta shoreline locations superimposed on 2007 aerial photography

The model showed that, within the next 50 to 100 years, the Dart River is likely to migrate across the active braidplain and start advancing the delta shoreline in the area between the centre of the braidplain and the grassed island near Glenorchy. As the braidplain and delta aggrade, flood flows use the Rees River central flow route (through the grassed island) into the Rees delta area adjacent to Glenorchy (as observed in the later stages of the modelling); alternatively, the Dart River may overtop the grassed island. Once the area immediately downstream of the grassed island has been filled with sediment, and the delta shoreline is approximately linear, there also is likely to be rapid delta growth along the Glenorchy waterfront due to the shallow shelf immediately offshore from Glenorchy (but just beyond the area of current delta growth simulated for the next ~120 years).

In the experiments, the rate at which the delta shoreline advanced reduced as the experiment run time increased (Figure 4.18). The delta growth curves for the experiments were compared to growth curves derived using a simple numerical model based on

$$\frac{dA_p}{dt} = \frac{Qs_p}{d_p + \frac{A_{topset}}{w_p}\tan\vartheta_{topset}} \qquad \textbf{(4.4)}$$

Where: A_{topset} = area of delta topset (A_{1966} ~2 x 10^6 m^2)

w_p = width of delta shoreline (~2850 m)

$\tan(\theta_{topset})$ = slope of delta topset (~0.002)

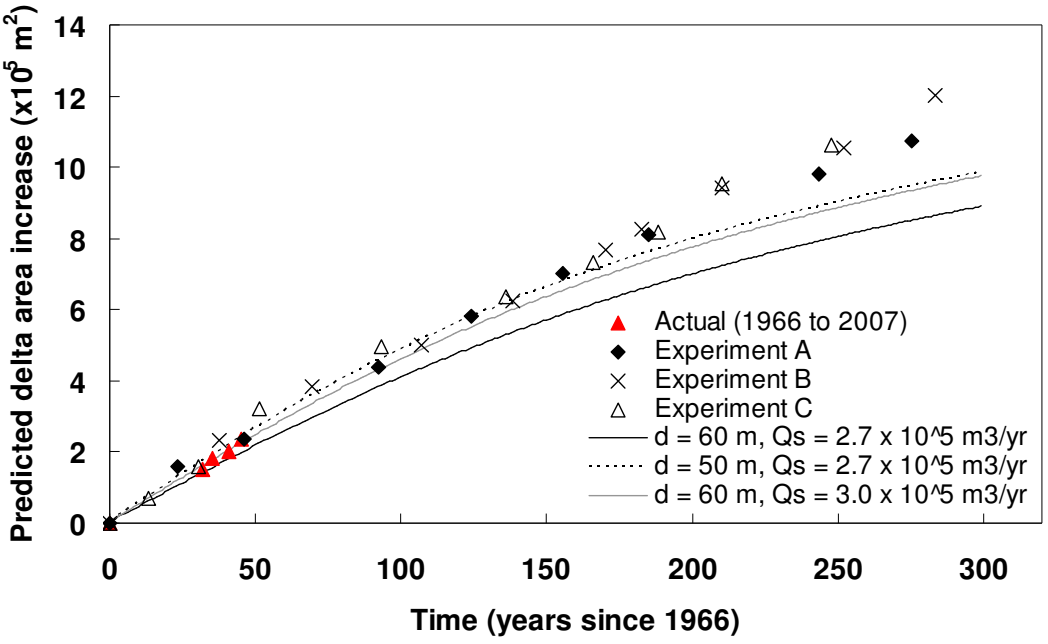

Figure 4.18: Rees-Dart delta area increase since 1966 (determined from aerial photographs, microscale modelling experiments A to C, and Equation 4.4)

Although the use of an estimated delta height, d_p, of 60 m and an annual sediment supply, Qs_p, of 0.27 x 10^6 m^3 in the numerical model indicate that the experiments may be over-estimating the delta growth rate, a relatively small change in these parameters in the numerical model leads to very good agreement for ~175 to 200 years from 1966 (Figure 4.18). Beyond this time the estimated rates of delta growth for the microscale model and from Equation 4.4 diverge, with greater increases in delta area predicted by the microscale model. This difference may be due to the physical constraints of the microscale model (e.g. the delta topset area for the physical model is limited in extent to the area between the sediment feeders and the lake and is therefore likely to start over-estimating delta growth once this whole topset area is aggrading). The many assumptions made for Equation 4.4. may also have resulted in long-term rates of delta growth being under-estimated. For example, the width of delta shoreline, w_D, has been set to a constant value of 2850 m but this is likely to increase over time. An increase in the shoreline length is likely to increase the area of delta topset to be aggraded, resulting in a slower rate of increase in the delta area for the same rate of sediment supply.

The experiments also showed, over the next 120 years (i.e. up to ~2120 to 2140), maximum delta advances of ~300 m in the area to the south of the grassed island, and advances of around 200 m and 100 m in the areas adjacent to Kinloch and Glenorchy, respectively. Assuming that the average delta

area growth rate for the next 120 years is 3900 m^2/yr, and the average delta width is 2850 m, the average rate at which the whole delta advances is approximately 1.4 m/yr. The maximum and minimum simulated rates of delta growth over this time period were 2.5 m/yr and 0.4 m/yr, respectively.

As the delta surface progrades, the upstream riverbed also aggrades to maintain riverbed slopes. Therefore, any upstream flood protection works and engineering structures (e.g. road bridges) will need to take this aggradation into consideration. Given that the riverbed slope in the Dart River is ~0.3%, a delta advance of 200 m at Kinloch will translate into ~0.6 m of aggradation in the entire upstream Dart River TRB riverbed.

4.3.5.4 Modelling change in sediment supply and potential engineering solutions

Where the initial model input parameters and fixed boundaries were continued for 200^+ years into the future (experiment A), the model showed that, after ~120 years (i.e. ~2120 to 2140), most delta growth is likely to occur in the area between the centre of the Dart delta and the Rees delta to the east (Figure 4.19a).

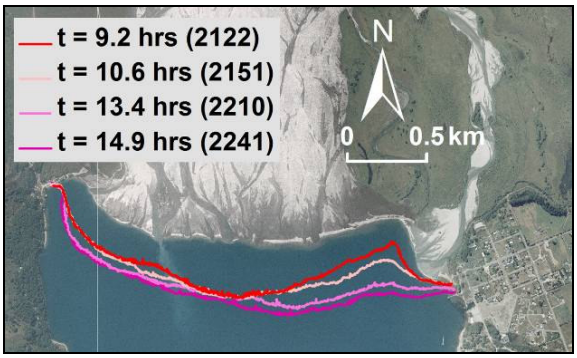

(a) Exp A: no changes.

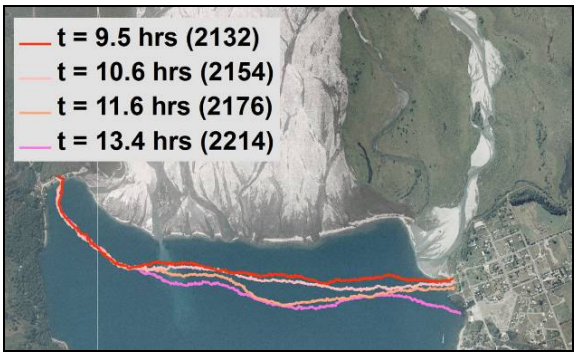

(c) Exp C: Rees sediment +50% at t=9.5hrs.

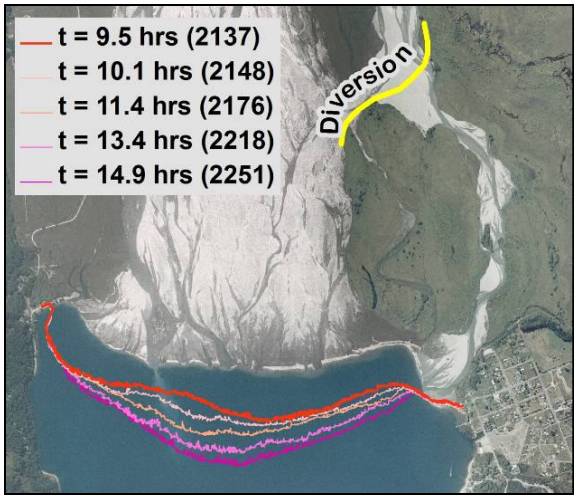

(b) Exp B: Rees diversion at t=9.5hrs

Figure 4.19: Microscale model delta growth with modifications to the river delta system superimposed on 2007 aerial photography

Continued aggradation in this area over the following 80^{+} years (Figure 4.20) is likely to result in aggradation of the active riverbeds and potential overtopping of the grassed island. There would also be a reduction in the differences between the elevated riverbed levels along the Rees River eastern route, which passes flood flows directly along the northern boundary of Glenorchy, and the central and western flow routes, which divert flood flows away from the northern face of Glenorchy.

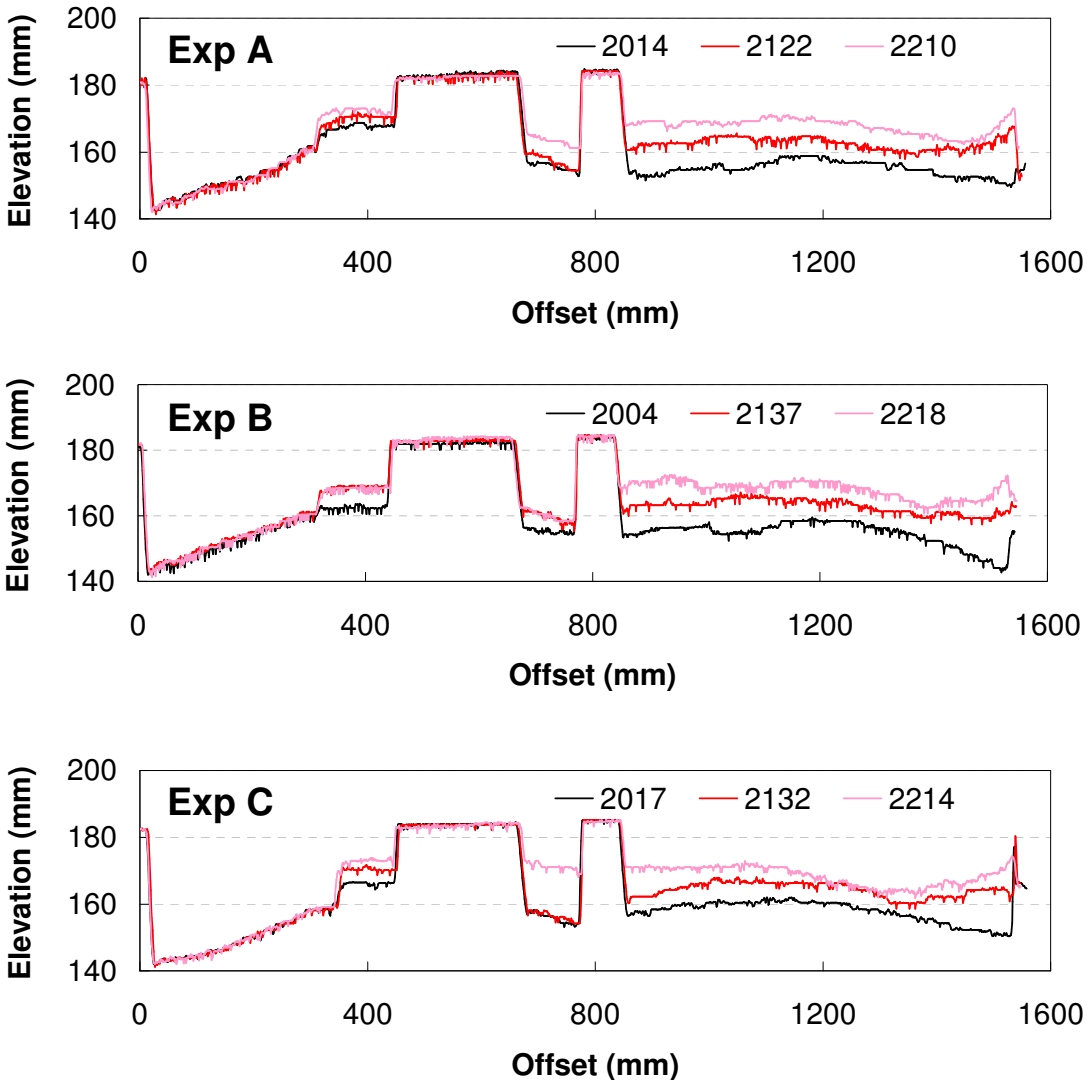

Figure 4.20: **Simulated cross section L-M (see Figure 4.15b) for Experiments A, B and C for current (2000 to 2020), future (2120 to 2140) and modified (2210 to 2220) scenarios**

If, after ~120 years, all Rees River sediment and flow were artificially diverted into the Dart River upstream of the grassed island (experiment B), all delta growth would be focussed on the centre of the Dart delta (Figure 4.19b), with no significant delta growth in the vicinity of the Glenorchy waterfront. Aggradation of the riverbed to the west of the grassed island showed that overtopping of the grassed island was likely to occur. The model showed that by 220 years into the future, the riverbed level along the Rees River western flow route, immediately to the west of the grassed island, would aggrade

to a higher elevation than the Rees River eastern and central flow routes, where aggradation ceased with the implementation of the diversion (Figure 4.20).

If, after ~120 years, the Rees River sediment supply increased by 50% (e.g. to simulate a coseismic landslide in the upstream Rees River catchment, experiment C), then by ~200 years into the future the western half of the Dart delta would produce a similar amount of growth as experiment A (Figures 4.19a and 4.19c). However, greater rates of delta progradation occur between the centre of the Dart delta and Glenorchy – in particular in the area along the Glenorchy waterfront where the delta advanced 150^{+} m in the final 1.8 hours (or 40 years) of experiment C. Upstream of the delta (at cross section L-M) the experiment C riverbed elevations for the Rees central and western flow routes (Figure 4.20) were approaching the riverbed elevations for the eastern flow route; therefore making it more favourable for the delta to prograde in the vicinity of Glenorchy as the river strives to find the shortest path to the lake. By comparison, experiment A showed lower and less aggraded riverbeds in the central and western flow routes, making it easier for Rees River sediment and flow to be diverted away from the Glenorchy shoreline. It is therefore estimated that within 250 years the Glenorchy waterfront could be replaced by the advancing riverbed. Should the current microscale model underestimate the volume of sediment supplied by the Rees River by 50%, this inundation of the Glenorchy waterfront may occur significantly earlier (i.e. in less than 200 years).

Both experiments B and C have greater delta area growth rates between ~120 and 200 years into the future compared to experiment A. For experiment C this is expected due to the increased sediment feed rate for the Rees River, while the increased delta area growth rate for experiment B may be due to erosion of the Rees riverbed. The delta area growth rate over this time period is potentially over-estimated for experiment B relative to the other experiments. This is because delta progradation for experiment B mainly occurs in the centre of the lake where the prototype lake depth is deeper (and hence the delta area growth rate slower for the same sediment input) compared to the shallow areas immediately offshore from Glenorchy (i.e. where experiments A & C prograde). This is not accounted for in the model where the lake depth is constant.

4.3.6 Discussion

The Rees-Dart historic imagery and microscale model both showed significant delta growth in areas where the largest braided river channels deposited sediment along a particular segment of the delta shoreline for several decades. This usually resulted in a pronounced ‘bulge’ or arc in the shoreline. Although there is only limited historic imagery, the model indicated that the Dart River portion of the river delta was likely to produce a prograding ‘bulge’ in the delta shoreline of between 150 to 350 m before migrating across the active braidplain to take advantage of a shorter and steeper path to the lake. It also suggested that the route the Rees River takes to the lake is dependent on the morphology of the channel immediately upstream of the grassed island which, at present, is largely dependent on

aggradation caused by the advancing Rees River portion of the delta. Finally, in ~120 years the Rees-Dart delta will have advanced an average distance of ~165 m (across the entire width of the delta), with actual advances ranging from 40 m to 300 m.

Although there is uncertainty in the timing, it is inevitable that the Rees-Dart delta will eventually overwhelm both Glenorchy and the Dart River TRB as the delta continues to advance. A potential option to temporarily prolong the life of Glenorchy is to 'permanently' divert the Rees River flows (and sediment) into the Dart River upstream of the grassed island – with the grassed island also being maintained as a permanent barrier. Conversely, should there be any major landslide in either catchment (a very likely event given the seismicity of the area), an increased supply of sediment delivery to the delta will accelerate delta progradation.

Several modelling limitations need to be considered. One is that the modelling exercise did not produce an identical starting geometry for each experiment. Variations in initial conditions included both the delta shoreline location and the volume of sediment stored within the model (i.e. the volume of sand stored between the 1966 and 2007 Dart River TRB barriers, and the continuously fluctuating volumes of sediment deposited in, and eroded from, the modelled braided river system). The model was also only scanned at distinct points in time so it was difficult to synchronise the timing of each experiment so that direct comparisons could be made. Nevertheless, it was clear that the patterns of historic delta progradation were replicated in all three experiments. Modifications to the model for experiments B and C also produced results which appeared reasonable. Other limitations included having to add and remove physical barriers to impose known boundaries (e.g. the divide between the Rees and Dart Rivers); the vertical distortion imposed by the model also meant that barrier overtopping was not able to be modelled.

Several lessons were learnt from this set of experiments. These included:

1. The use of a steep, sloping platform meant that the braided river and active floodplain areas needed to be accurately constrained in the model, using physical boundaries, to properly represent the prototype – especially where the dominant flow path was not supposed to be directly down the slope of the platform. Over time the bed, within the constrained boundaries, adjusted so that the active channels migrated across the floodplain.
2. The model allowed some of the historical behaviour of the braided rivers and delta to be 'pieced' together. For instance, the tendency for the Rees riverbed to be elevated relative to the Dart (producing a flow path from the Rees River onto the Dart River floodplain) could be easily observed and explained in the model by inserting a barrier to keep the two channels separate upstream of the lake; this quickly resulted in the two rivers adjusting themselves to produce the elevated Rees River levels. Also, where there was a 'dead' zone (e.g. the lagoon north of Glenorchy), the majority of the sediment still tended to follow the river flow path

downstream to the lake (although more sediment was likely to be directed to the lake in the prototype than in the model, due to bedload material being contained within the more well-defined channel in the prototype, and hence a barrier was used to ensure this).

In spite of the microscale modelling limitations outlined above, the results of this study show that such models are able to provide realistic insights into the future growth of braided, gravel-bed river deltas advancing into deep, low-energy basins. If historic aerial photographs are available, an approximate time scale can also be estimated to enable future delta advances to be estimated – an invaluable tool for planning purposes.

4.3.7 Conclusions

Microscale modelling has proven to be an effective tool for simulating past and future growth of steep, gravel-bed, braided, river deltas entering low-energy basin environments. Successful modelling requires well-defined fixed boundaries and, ideally, good historical aerial photography for the estimation of the model time scale. For the Rees-Dart delta, more work may be required to accurately define the correct ratio of water and sediment feed rates between the two river systems. This is because increasing the sediment feed rate for the Rees River (experiment C) significantly increased the rate of delta progradation in the Glenorchy area. For cases where there is only one braided river feeding the delta this would not be an issue, and microscale modelling would be an even better tool for the prediction of future delta growth.

4.4 Clutha River/Mata-Au microscale model

A 1:1500 scale microscale model of the Clutha River/Mata-Au delta (Figures 4.21 and 4.22) was constructed to examine the braided river delta growth processes of the Clutha River/Mata-Au delta prograding into Lake Dunstan. The model configuration, methodology and results are summarised below.

Figure 4.21: Longitudinal view of the configuration B Clutha River/Mata-Au delta model

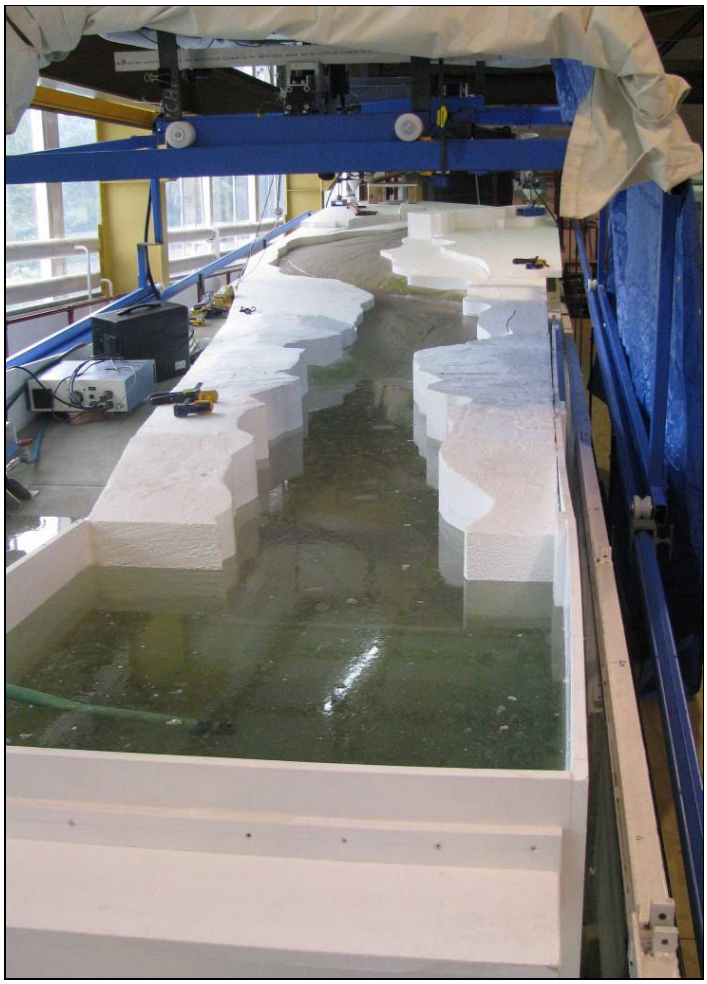

Figure 4.22: Oblique view of the configuration B Clutha River/Mata-Au delta model

4.4.1 Model configuration

Figure 4.23 shows a schematic of the Clutha River/Mata-Au microscale model. The microscale model was constructed on a 2.28 m wide by 9.8 m long platform set to a 10 % slope, as used successfully in the Rees-Dart microscale model as well as other previous microscale models (e.g. Davies et al., 2003).

The design of the platform support was such that the platform slope could be increased or decreased by raising or lowering the level of the upstream platform support, (Figure 4.24a) while simultaneously adjusting the central supports located at the platform mid-point (Figure 4.24b). After the February 2011 earthquake (when the model 'jumped' out of the upstream supports) the upstream platform supports were welded into a fixed position. The lower end of the platform also rested on steel supports (Figure 4.24c).

The downstream end of the platform was attached to a 2.20 m wide by 1.17 m long tank with a base level 0.364 m below the surface of the platform (Figure 4.23). This tank was divided into two compartments with one compartment forming the 'lake' tank with an 0.18 m wide adjustable overflow

weir with a crest level range of 0.64 to 0.76 m above the floor of the 'lake' tank (to simulate a constant post-lake-filling Lake Dunstan water level). The adjustable overflow weir passed the excess water to the other compartment which formed the sump. From the sump, two water pumps recirculated water to the upstream limits of the model (i.e. Clutha River/Mata-Au and Lindis River upstream boundaries) where the water was combined with dry sediment (in a funnel) and fed back into the model. Note: when the model is run as a river without the lake (i.e. pre-lake-filling) water flows between the 'lake' tank and the sump via an opening near the base of the partition between the two tanks.

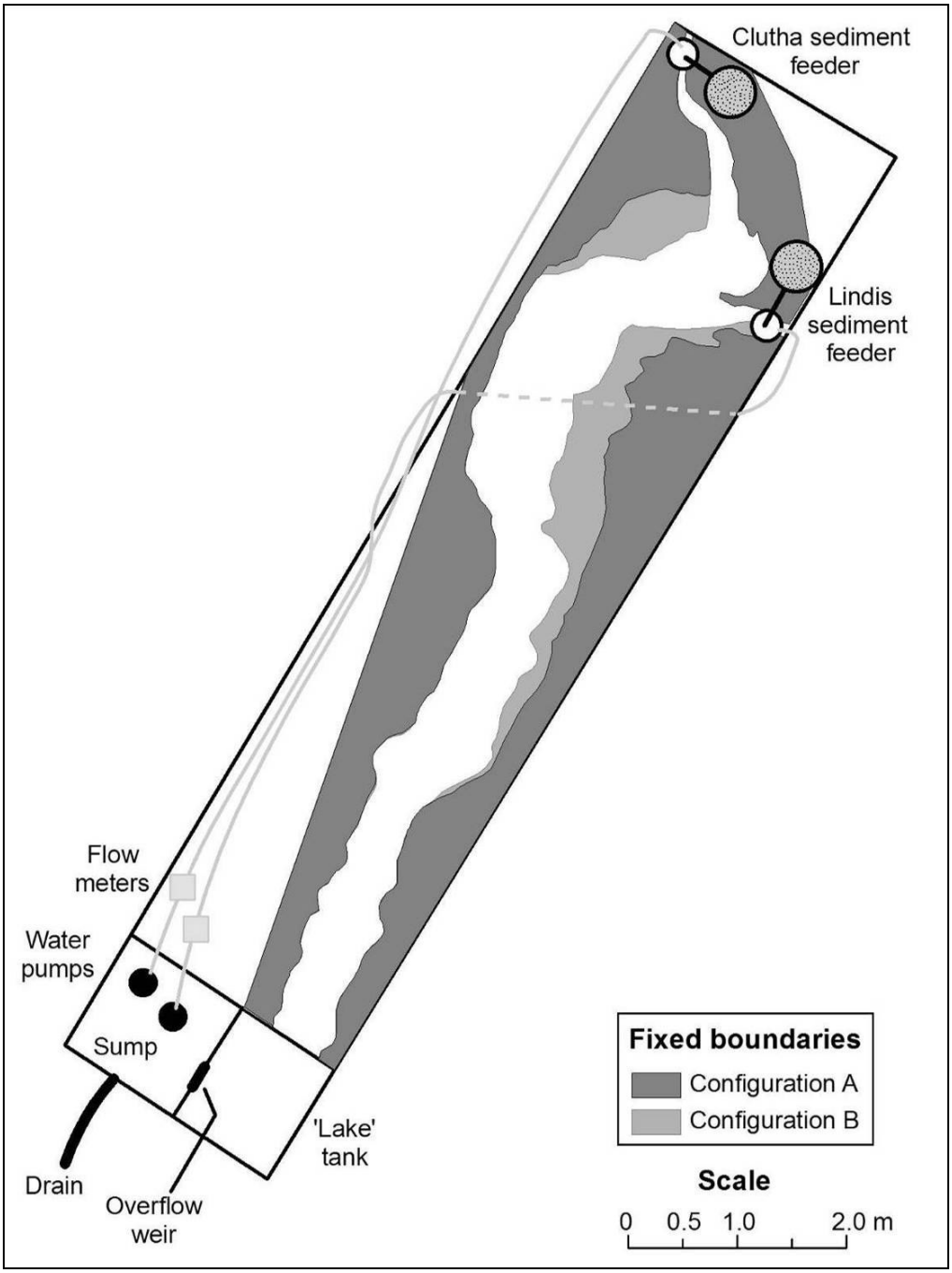

Figure 4.23: Clutha River/Mata-Au microscale model *initial* delta model

(a) Upstream platform support

(b) Adjustable mid-point support

(c) Lower platform support

Figure 4.24: Clutha River/Mata-Au microscale model platform structural supports

High density expanded polystyrene was used to form the fixed boundaries of the river system and lake (as described in Section 4.2.3), and a steady rate of dry sediment was fed into the model by sediment feeders with motorized, rotating, circular tubes.

To measure the changing delta and riverbed profiles, the instantaneous-profile laser scanner (Darboux & Huang, 2003) was mounted on a single rail that ran longitudinally down the microscale model in a downstream direction with the stepper motor at the upstream end of the trolley. This single rail was attached to a trolley structure with two sets of wheels that could be rolled upstream from the lake tank along two rails, or rolled across the model laterally. As the scanner single rail was approximately 1.05 to 1.15 m above the delta profile, the scanner captured a ~0.85 to 0.95 m wide strip of the profile as the stepper motor moved the scanner down the delta profile in 1 mm increments. The vertical and positional accuracy of the scanned data are approximately ±0.5 mm (Darboux & Huang, 2003).

Experimental flows were monitored by inline flow meters that provided continuous flow measurements for both the Clutha River/Mata-Au and Lindis Rivers. Two 2-megapixel webcams (one mounted on the trolley frame in front of the delta and one mounted above the delta) also took photographs at a 1 minute interval throughout each experiment. These images were able to be combined to produce time-lapse imagery of the changing delta system.

4.4.2 Assumptions and limitations for use of microscale model

Due to the very small scale of the model, and the vertical distortion, the following assumptions and limitations had to be taken into consideration for both experimental design and for the interpretation of results produced by the model. The assumptions and limitations that need to be considered, when modelling the Clutha River/Mata-Au delta, include:

1. Deposition of suspended sediment – as a bottomset (ahead of the advancing delta) and in the form of overbank flow deposits – can not be simulated in the model.
2. Clutha River/Mata-Au and Lindis River flows and sediment feed rates are constant. For example, it is assumed there will be no sudden increase in sediment supply due to a large landslide in, for example, the Lindis River catchment. Climate change modelling (Poyck et al., 2011) also shows that, although there may be an increase in upstream river flows in winter and spring, flows are likely to remain relatively unchanged during the late spring and summer months when flows are usually highest.
3. Due to the vertical exaggeration of the model, fixed polystyrene boundaries cannot be overtopped accurately to simulate new flow paths and erosion. Where the river is fixed into a meander pattern the meanders are also unable to migrate longitudinally or laterally. This was considered appropriate in the short-term given the relatively stable Clutha River/Mata-Au meanders upstream of Lake Dunstan.
4. Lake level is constant.
5. The model bathymetry is represented by a flat bed whereas, at the time of the initial filling of Lake Dunstan, the bathymetry included established braided river channels.

4.4.3 Development of the Clutha River/Mata-Au model

4.4.3.1 'Pre-lake-filling' model

The initial aim of the Clutha River/Mata-Au microscale model was to produce a 'pre-lake-filling' model with the Lindis River and Clutha River/Mata-Au realistically represented as they were before Lake Dunstan was formed in 1992/93 (i.e. as shown in 1984 aerial photographs). Once the 'pre-lake-filling' model was established, the water level in the 'lake' tank was raised to represent the post-lake-filling conditions and to simulate the delta formation.

The initial fixed boundaries for the microscale model were derived from 5 m contours created using ArcGIS, and a 25 m DEM of New Zealand generated by Landcare Research (Barringer et al, 2002). The DEM was produced using Land Information New Zealand (LINZ) digital topographic data which are stated as having a planimetric (x,y) accuracy where "90 percent of well-defined points are within ±22 metres", and a vertical (z) accuracy where "90 percent of well-defined points are within ±10 metres" (http://www.nztopoonline.linz.govt.nz/about/data-details/index.html). The Landcare Research

DEM was derived by placing most importance on the generated 25 m cells being consistent with LINZ spot height and 20 m contour information. Although the spatial accuracy of different landforms in the derived DEM varies, most landforms having a RMS error of 5-8 m; valley floors tend to be less accurately represented with RMS errors of ~15 m (Barringer et al, 2002). The fixed polystyrene boundaries representing the model middle and upper reaches of the Clutha River/Mata-Au river system were bounded by the 220 m contour while the lower reaches, in the vicinity of the Bendigo Wildlife Reserve and Lake Dunstan, were bounded by the 205 m contour. This represented the boundary between the moderate to steeply sloping surrounding land and the gently sloping valley floors. These fixed boundaries (referred to as configuration A) are shown in Figure 4.23.

The initial Clutha River/Mata-Au 'pre-lake-filling' model was developed by adjusting flow rates for the Clutha River/Mata-Au and Lindis Rivers so that the Clutha River/Mata-Au flow was approximately 4 times larger than the Lindis River flow (as discussed in Section 3.3.3.5). Sediment feed rates were also adjusted to ensure that the Lindis River bed slope was steeper than that of the Clutha river/Mata-Au, while also aiming for a sediment feed rate for the Clutha River/Mata-Au that was approximately twice that of the Lindis River (also discussed in Section 3.3.3.5).

The flow and sediment feed rates used for the Clutha River/Mata-Au microscale model experiments are summarised in Table 4.3.

Table 4.3: Flow and sediment feed rates for the Clutha River/Mata-Au microscale model

	Clutha River/Mata-Au	Lindis River	Clutha/Lindis	Clutha/Lindis (prototype)
Pre-lake-filling and initial delta experiments				
Flow (l/min)	1.5 ± 0.1	0.37 ± 0.1	4	~3.5
Sediment feed rate (g/s)	1.7 ± 0.01	0.84 ± 0.005	2	~2
Final delta experiments				
Flow (l/min)	1.2 ± 0.1	-	(4.1)	-
Sediment feed rate (g/s)	1.73 ± 0.02	-	(2.0)	-

The development of the 'pre-lake-filling' model was an iterative process. Additional polystyrene inserts were added to improve the model (configuration B, Figure 4.23). These polystyrene inserts were placed inside the original model boundaries with polystyrene inserts up to 0.3 m (i.e. 3 times 0.1 m) high along the Lindis River boundary (due to the steep channel bed). The justification for these additional inserts, along with information about the performance of the 'pre-lake-filling' model, is summarised in Section 4.4.4.1.

4.4.3.2 Initial delta model

To simulate the formation of the Clutha/Mata-Au delta post-lake-filling, model configuration B (Figure 4.23) was used. The water outlet, near the base of the 'lake' tank, was closed and water in the 'lake' tank was raised until water flowed over the adjustable overflow weir (which was set to a crest height of ~0.72 m above the base of the 'lake' tank).

4.4.3.3 Final delta model

To better simulate the meandering main river channel in the prototype, additional polystyrene inserts were added to the model immediately upstream of Lake Dunstan (configuration C, Figure 4.25). As the river flow route was now fully constrained immediately upstream of Lake Dunstan, it was possible to modify the model so that it only required one sediment and flow input (representing the combined Clutha River/Mata-Au and Lindis River sediment and flow contributions) immediately upstream of Lake Dunstan (Figure 4.25). The same relative flow and sediment ratios were maintained although the total quantities were reduced slightly (Table 4.3).

At the same time, an additional barrier/weir was added within the submerged section of the river (~1.8 m downstream of the meandering river exit into the lake) and the area upstream of the barrier was backfilled with sand to a level of 0.69 m above the base of the 'lake' tank. This reduced the model bed slope from 10% to approximately 1%. The lake level was also lowered to 0.692 m above the base of the lake tank to reduce the effect of the exaggerated lake water depths.

The final model configuration is shown in Figure 4.25 and the flow and sediment feed rates are given in Table 4.3.

4.4.4 Model Results

4.4.4.1 'Pre-lake-filling' model

The initial model river flows tended to run straight down the model platform (i.e. following the steep exaggerated slope of the model platform). Excess sand also accumulated at the location of the prototype Lindis River confluence with the Clutha River/Mata-Au due to the less sinuous Clutha River/Mata-Au flow route not eroding the accumulated sediment; the river bed of the Lindis River was also not constrained effectively to allow for the steeper river bed slopes expected in the Lindis River compared to the Clutha River/Mata-Au (i.e. for the higher sediment supply relative to the flow, a steeper river bed slope is required to mobilise the sediment).

As a result, it was decided that the delta would be more likely to prograde in a realistic manner if the fixed boundaries of the braided/meandering river channels were more constrained. Shaped polystyrene inserts, confining the microscale model river to the November 1999 flood extent, were added for this purpose (configuration B, Figure 4.23, 4.25 and 4.26).

With the configuration B polystyrene inserts the river channels were adequately 'trained' to simulate the main river flow paths albeit without the stable meandering channel configuration of the prototype.

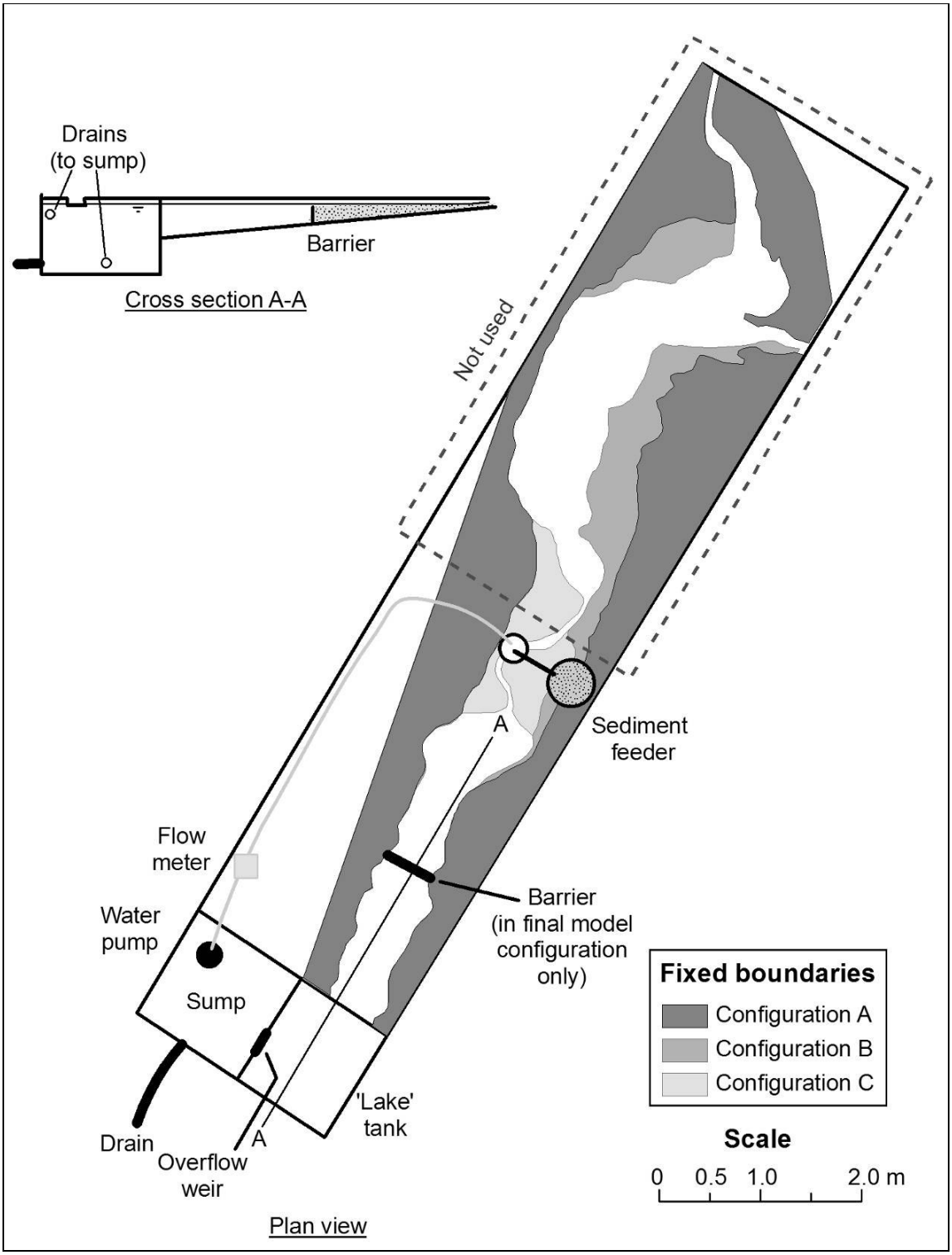

Figure 4.25: Clutha River/Mata-Au microscale model *final* delta model

Figure 4.26: Clutha River/Mata-Au pre-lake-filling (configuration B) microscale model. Looking downstream from top of model (Lindis River feed is lower left corner)

4.4.4.2 Initial delta model

Upon lake filling, the delta formed using configuration B did not properly represent the prototype. Figure 4.27 shows the microscale model delta formation ~1.5 hours after the lake tank was filled.

The vertically-exaggerated, steep model platform (required by very small scale movable bed models to transport sediment) produced rapidly increasing lake water depths (relative to the prototype). Consequently, an abrupt delta transition from the topset to the foreset slope formed, as well as a braided river system that regularly switched channel locations (i.e. it produced a braided river delta similar to those produced by the Rees-Dart microscale model). At no time did a meandering main channel form to feed sediment into the lake at a fixed location (as observed for the Clutha River/Mata-Au delta). This was not unexpected given that the sand was noncohesive and therefore not conducive to the formation of meanders at small-scale flows - especially aggrading bed formations.

4.4.4.3 Final delta model

The final delta model is shown in Figure 4.28 after 2.3 hours of simulated Clutha River/Mata-Au delta growth (i.e. 2.3 hours after the lake was filled). The growth of the simulated delta is also represented in Figure 4.29 by 10 mm contours which have been derived from the microscale model laser scanner data (with the scanner data rescaled and geo-referenced to enable comparisons with the prototype).

These contours identify where there was an accumulated sediment depth of 10+ mm above the initial bed level.

Figure 4.27: Plan view of delta formation for initial delta model (configuration B) ~1.5 hours after the lake tank was filled. River flows from left to right ('lake')

Figure 4.28: Oblique view of delta formation for final delta model (configuration C) after 2.3 hours of delta growth (lake is partially drained to scan delta profile)

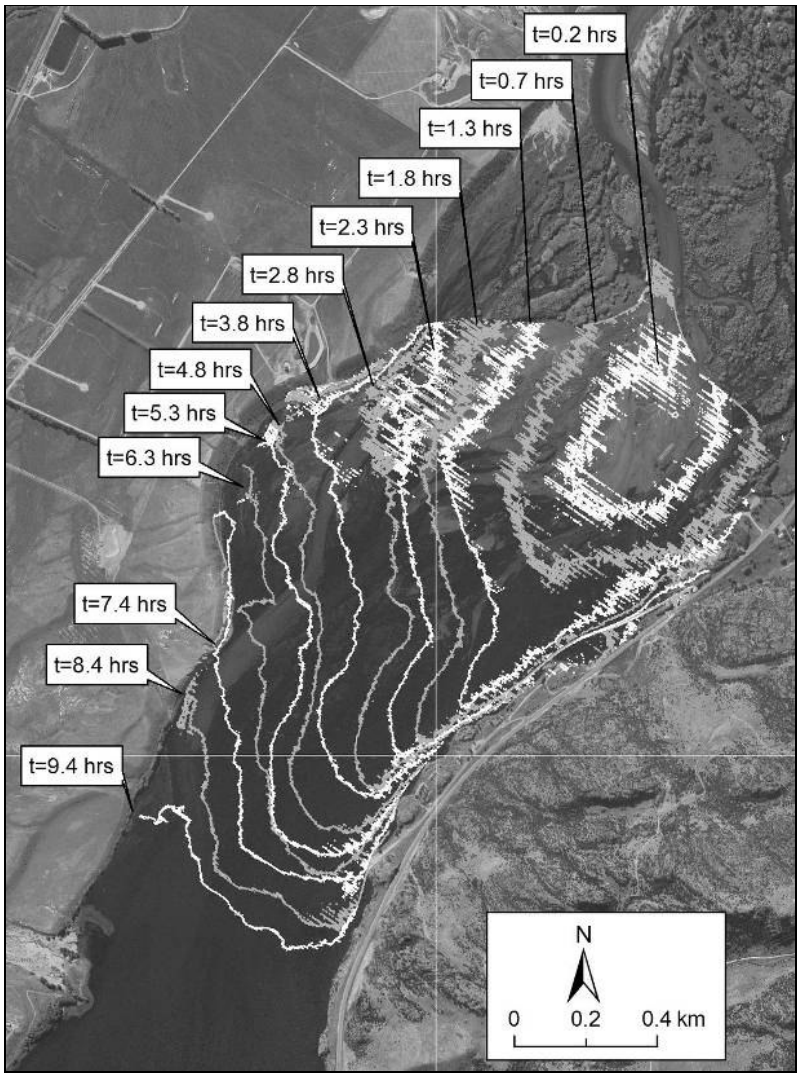

Figure 4.29: Clutha River/Mata-Au microscale model simulated sediment deposition between 0.2 and 9.4 hours of model run time (contours represent 10+ mm of sediment deposition and are located on the delta foreset slope)

Figure 4.30 shows the depths of accumulated sediment after 9.4 hours of delta progradation and Figure 4.31 shows the model cross section profiles over this time for locations equivalent to those for monitored prototype cross sections 71 to 69 (XS71 to XS69).

4.4.5 Discussion

Figures 4.28 and 4.29 show that, for the microscale model, sediment from the Clutha River/Mata-Au was initially deposited immediately downstream of where the river entered the lake. The river flow behaved similarly to a jet with most deposition occurring along the main flow trajectory (i.e. the flow tended to travel in a southerly direction when it exited the confined river channel, then favoured a flow path towards the eastern shore of Lake Dunstan). Like previous fan delta physical models (and prototypes), the sediment laden flow continually adjusted its course, and aggraded based predominantly on the shortest/steepest path across the delta to the fixed downstream boundary (i.e.

lake). As the delta grew, the area where the delta advanced most rapidly was along the eastern lake shoreline in preference to the upstream 'flanks' of the delta.

Figure 4.30 shows that after 9.4 hours of delta progradation, the greatest depth of sediment deposition was still located directly south of where the river exited into the lake. As the delta prograded, rates of sediment deposition tended to be highest near the centre of the lake (i.e. away from the western or eastern shoreline). After 9.4 hours of run time the delta foreset continued to prograde more rapidly between the centre of the lake and the eastern shoreline (compared to near the western shoreline).

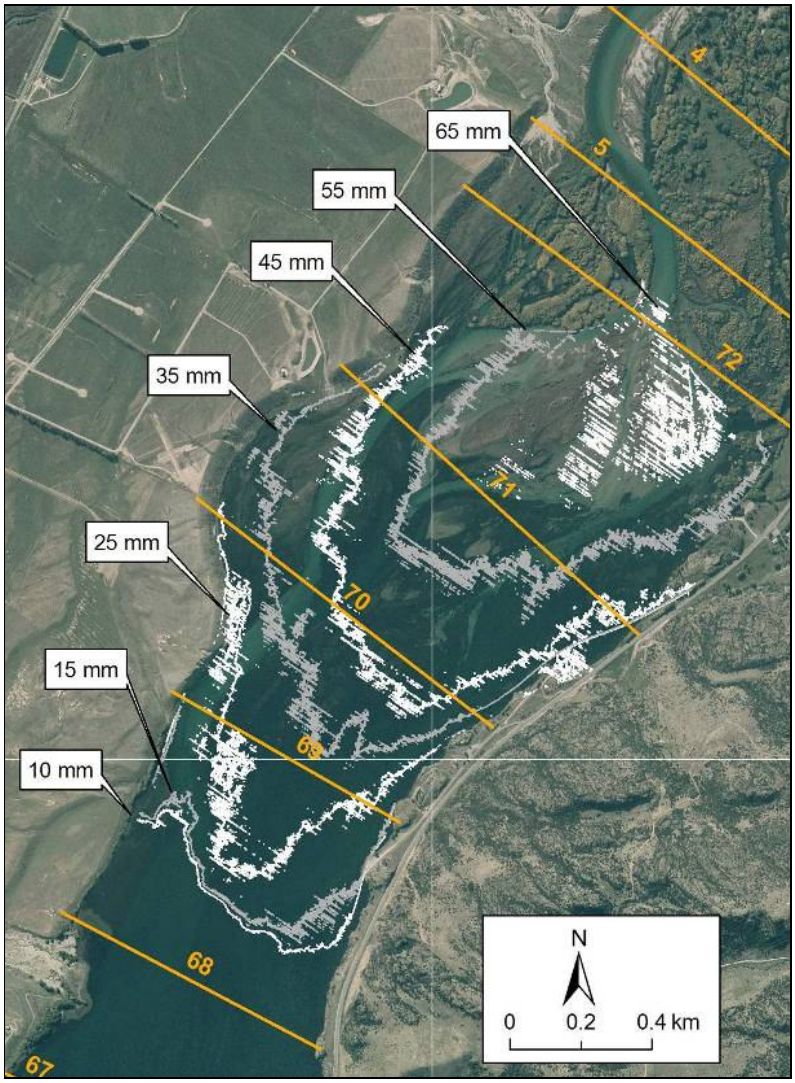

Figure 4.30: Clutha River/Mata-Au microscale model sediment deposition after 9.4 hours of model run time (contours represent depths of sediment deposition)

Model cross section profiles are shown in Figure 4.31 for the same locations as the measured prototype cross sections 71 to 69 (i.e. XS71 to XS69) shown in Figure 4.32 (see Figure 4.30 for cross section locations). Although the horizontal distances in the model have been scaled for comparison with the prototype, no attempt has been made to scale the vertical dimensions.

One of the most obvious differences between the prototype and microscale model delta formations is that the microscale model naturally 'self-adjusts' to a steeper topset gradient resulting in the delta formation rapidly becoming sub-aerial rather than being a predominantly submerged formation like the prototype. This is a good example of a situation where the microscale model requires a steep gradient to transport the 'oversized' sediment particles, but at the same time requires a gently sloping lake bed (i.e. gradually varying water depth) so that sediment is not all 'dumped' immediately as the river exits into the lake.

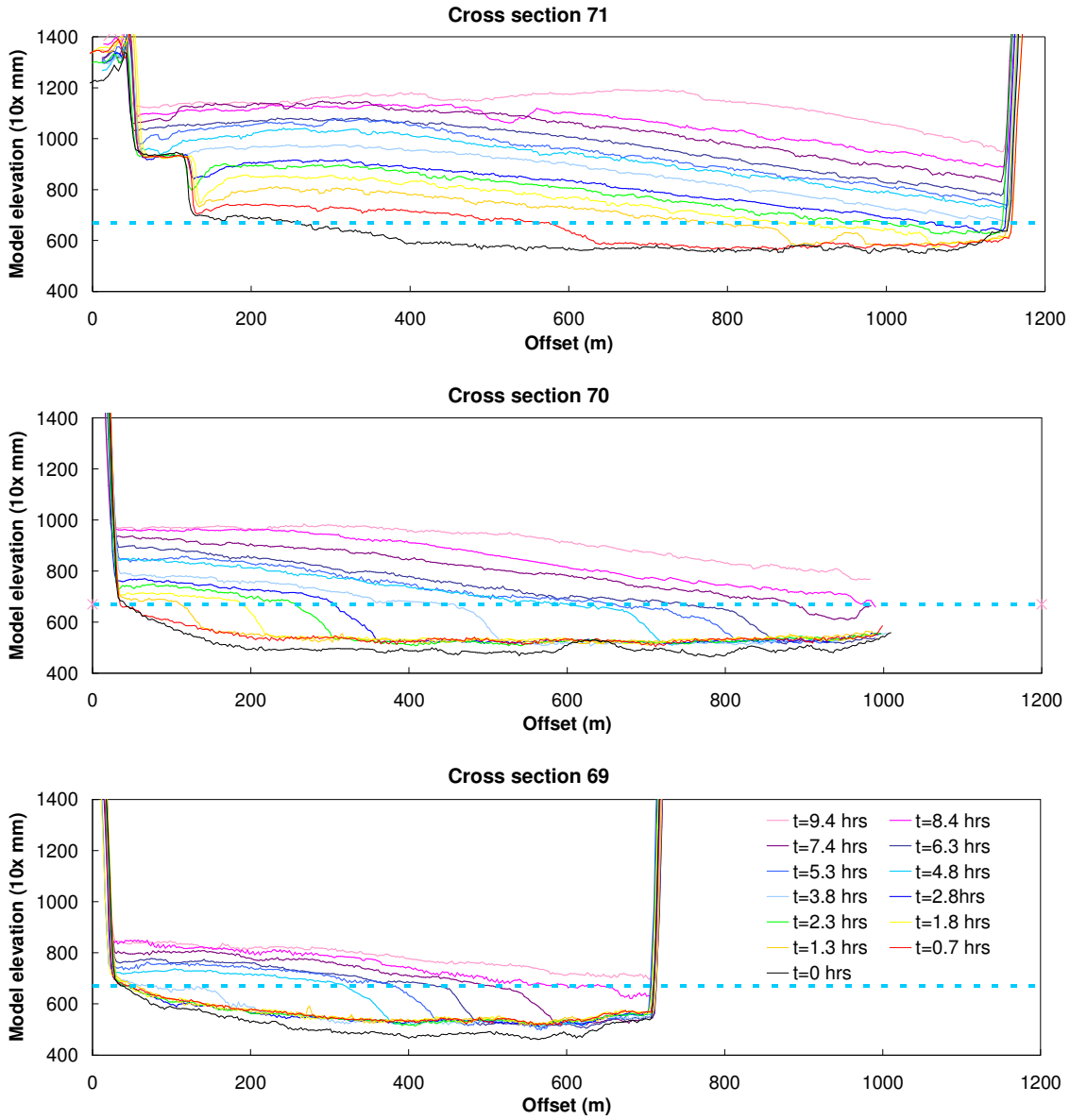

Figure 4.31: Microscale model simulated cross section profiles for XS71 to XS69 between 0 and 9.4 hours of model run time (dashed line is approximate water level). Offset has been scaled to prototype for comparison while vertical scale has been left in measured units.

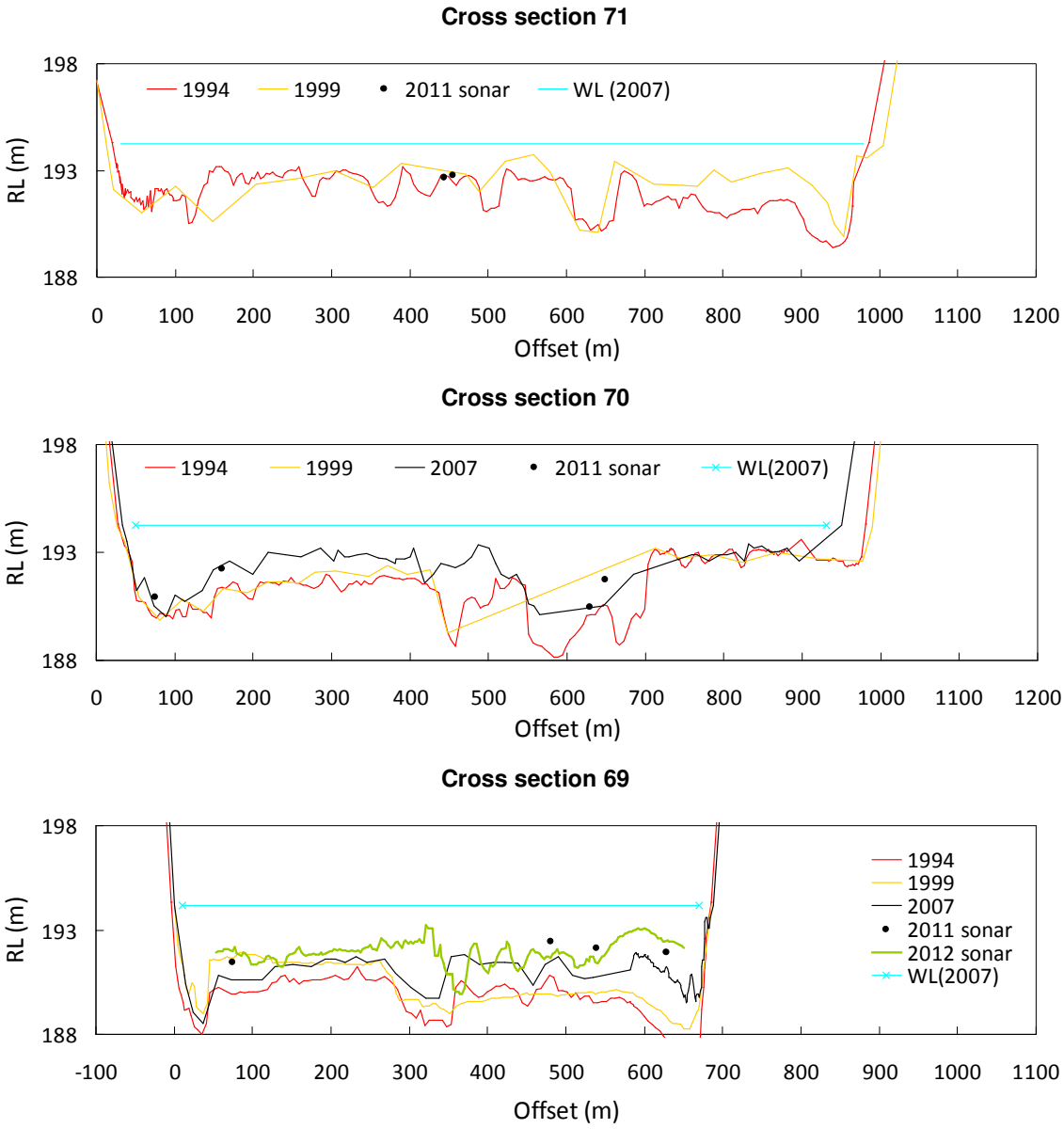

Figure 4.32: Measured prototype cross section profiles for XS71 to XS69 between 1994 and 2012 (light blue line represents 2007 surveyed).

Despite this obvious inadequacy when implementing this type of model, qualitative comparisons between the prototype and modelled cross sections were made. Observations included:

- Cross section 71 (XS71) – in 1994 this section had a naturally higher elevation from an offset of 0 to 700 m (pre-lake-filling this area is observed in aerial photographs to be floodplain). Between 1994 and 1999 the rest of the cross section (excluding main channels) aggraded to a similar level as that at an offset of 0 to 700 m. By comparison, the microscale model showed sediment initially being deposited near the TLB then, over time, it prograded towards the TRB – eventually filling the entire cross section to a similar level after ~2 to 3 hours of model run time (although the lowest bed levels remained adjacent to the TRB).

- Cross section 70 (XS70) – in 1994 this section had a naturally higher elevation from an offset of 700 to 1000 m (pre-lake-filling this area is observed in aerial photographs to be floodplain). Between 1994 and 1999 very little sedimentation occurred at this cross section. However, between 1999 and 2007 most of the rest of the cross section (i.e. between an offset of 150 and 550 m) aggraded to a similar level. By comparison, the microscale model showed sediment starting to be deposited near the TLB after ~1.3 hours of the model run. Over time the delta prograded towards the TRB – eventually filling the entire cross section to a similar level after ~7 to 8 hours of model run time (although the lowest bed level remained adjacent to the TRB).

- Cross section 69 (XS69) – in 1994 this section had a naturally higher elevation from an offset of 50 to 280 m (pre-lake-filling this area is observed in aerial photographs to be floodplain). Between 1994 and 1999 this same area of the cross section aggraded. Between 1999 and 2007 most of the rest of the cross section (i.e. between an offset of 350 and 675 m) aggraded to a similar level. By comparison, the microscale model showed sediment starting to be deposited near the TLB after ~4 hours of the model run. Over time the delta formation prograded towards the TRB – eventually filling the entire cross section to a similar level after ~8 to 9 hours of model run time (although the lowest bed level remained adjacent to the TRB).

- The simulated delta foreset height increased as the lake level increased (i.e. it is higher for cross section 69 compared to 71). Although there are no field comparisons this would appear sensible.

- Over time, both the model and the prototype cross sections have aggraded so that the bed level variations across the profile decrease (i.e. the cross sections become 'flatter').

- The main channels observed in the prototype are not present in the model cross sections. However, during the model simulation it was noted that, once a delta had formed immediately south of the river exit to the lake, there was a preference for the water exiting the confined meandering channel to either travel directly straight ahead or be diverted around the deposited sediment and follow the lake shoreline (particularly along the eastern lake shoreline as shown in Figure 4.28, but also the western shoreline as the model run progressed and sediment filled the full width of the lake).

- Figure 4.30 shows that, as the delta progrades down lake, the largest depths of sediment tend to be deposited in the central portion of lake (or cross section). This may explain the large volume of sediment deposited at cross sections 68 to 66 in Figures B3 and B4 (Appendix B), although it is unknown whether this is derived from bed load, suspended sediment load and/or tributary sediment contributions.

4.4.6 Conclusions

Better field information could potentially determine whether the modelled delta progradation was properly representing bedload deposition. However, this would depend on whether there is a distinct delta foreset slope associated with bedload deposition (which could potentially be used to calibrate the rate of delta growth due to bedload in the microscale model), or whether this foreset slope is 'smothered' by suspended sediment deposition. Further useful information may therefore be gained from additional field data includings sediment sampling to determine particle size distributions at various locations along the lake bed (i.e. to determine whether deposition is mainly bedload and/or suspended sediment load).

Recent developments in microscale modelling, where vegetated microscale models are used to simulate braided and meandering river systems (Tal & Paola, 2010), may also provide more realistic options for simulating the Clutha River/Mata-Au river system upstream of the delta; the rapid rate of delta aggradation in the vicinity of the river mouth may limit the applicability of this methodology though.

Therefore, even though the microscale model was able to visually provide some information on the behaviour of the Clutha River/Mata-Au delta (e.g. likely location for bedload deposition), the complex interaction of bed load, suspended sediment load, established river channels, vegetation and tributary inflows – all within the deposition zone - is likely to be beyond the capabilities of microscale modelling. In particular, given that suspended sediment is likely to provide the most significant sediment contribution (compared to bedload), it will be necessary to establish where this material is deposited - and microscale modelling is unlikely to do this. Therefore, despite microscale models often being able to provide valuable information on the spatial distribution of sediment deposited by gravel-bed rivers, for this scenario the dissimilarity between grain size distribution and/or various other parameters (as discussed earlier in Sections 2.4.1 and 2.4.5) limits the applicability of the Clutha River/Mata-Au microscale model.

5 NUMERICAL MODELLING

5.1 Overview

The complex and dynamic processes of sediment deposition and erosion in braided river systems are, at present, not able to be fully simulated using computational hydraulic models (e.g. Davies & McSaveney, 2006). As well as this gap in our current capability, vast quantities of detailed spatial and temporal data are required by complex braided river numerical models (e.g. sediment sizes, bed roughness coefficients, topography, flow distribution, etc). Therefore, although there are some numerical models available, it is difficult enough to simulate a short braided river reach (e.g. of the order of a kilometre long) without the added complication of a prograding delta and possible backwater effects. One of the main problems encountered when attempting to simulate braided river delta growth is the frequent formation, lateral and longitudinal migration, and abandonment of the confluences and bifurcations within the upstream braided river system (Ashmore & Gardner, 2008). These continual channel confluence modifications, as well as changes in flow and/or sediment supply, cause fluctuating bedload transport rates (Ashmore & Gardner, 2008). Hence, the behaviour of the confluences (and confluence-bifurcation units) will influence how sediment is transported across the delta topset to prograde the delta. At present, there is not enough information to quantify the relationship between braided river confluence morphodynamics and the resulting bedload time series or spatial distribution of bedload (Ashmore & Gardner, 2008).

A summary of the currently available numerical modelling methods, as well as information on previous numerical modelling studies, is provided in Section 2.5. This summary identified that, where simple geometric numerical models have been developed, they tend to simulate width-averaged delta progradation or 3-d delta progradation represented by a regular shape (e.g. cone). This is usually based on the assumption that the model simulation time period is likely to be significantly greater than the time interval for river avulsions. However, this methodology is not likely to be appropriate when considering braided river delta progradation over the decade-to-century timescale. As no numerical model appears to be available to predict decade-to-century timescale braided river delta growth for a delta supplied with sediment from a regularly avulsing braided river system, a simple grid-based sediment routing and deposition model 'DELGROW' is proposed.

The microscale models used in this study (i.e. Rees-Dart River delta and Clutha River/Mata-Au delta) provide information on general trends and spatial distribution of accumulated sediment rather than detailed information regarding sediment transport and fluvial morphodynamics (Kleinhans, 2010). The results of these microscale modelling studies, together with information derived from field studies, can therefore provide valuable information on delta geometry and growth dynamics. In DELGROW, this information has been used to define a set of rules to route sediment over a topographic input grid (i.e.

across a riverbed/delta topset to a delta foreset/lakebed). These sediment-routing and deposition rules transport and deposit sediment based on the bed slope between adjacent cells; with rules varying between cells identified as riverbed/delta topset and delta foreset. Simulated channel switching is based solely on the assumption that the river follows the shortest, steepest path to the lake bed with the transition from topset to foreset occurring at the shoreline.

Section 5.2 describes the DELGROW numerical model, together with the assumptions made, while Section 5.3 applies the developed numerical model to the Rees-Dart River delta. Conclusions are summarised in Section 5.4.

5.2 Model description

The DELGROW model developed in this study simulates braided river delta growth using square cells (in a rectangular grid) to represent the topography and bathymetry of the river-delta system. Figure 5.1 shows a flow chart summarising the main processes included in the model. These processes are:

- Input data - Two grids are read into the model to define the delta topography (i.e. riverbed/delta topset, delta foreset and lakebed elevations) and delta composition (i.e. each cell is allocated a number according to whether it is located on the riverbed/delta topset, delta foreset or lakebed). The sediment input (representing total sediment supply to each channel for each time step) is defined by either a constant value or a time series.

- Calculate the sediment/flow path - The cell with the lowest elevation (within the pre-defined input cell range) is identified as the 'start' cell at the upstream input location. The path to the lakebed is then determined by following the steepest topographic path downstream to the lakebed.

- Deposit sediment - Sediment is deposited over the sediment/flow path cells according to a set of rules (e.g. more sediment is deposited in foreset cells compared to topset cells, and no sediment is deposited on a topset cell if the bed slope to the adjacent downstream cell is greater than a predetermined slope). There are also rules defining when deposition leads to a foreset cell becoming a topset cell, and when a lakebed cell becomes a foreset cell. The model was initially developed for one sediment input but can easily be modified to incorporate several sediment inputs.

The DELGROW model assumptions, input grids, and other parameters are described in more detail below. The Fortran code for DELGROW is provided in Appendix D. This code also includes the calculation of a grid that determines how many times each grid cell is part of the sediment/flow path between the upstream limit of the model and the downstream lakebed. This may also have useful applications but is excluded from Figure 5.1 for clarity.

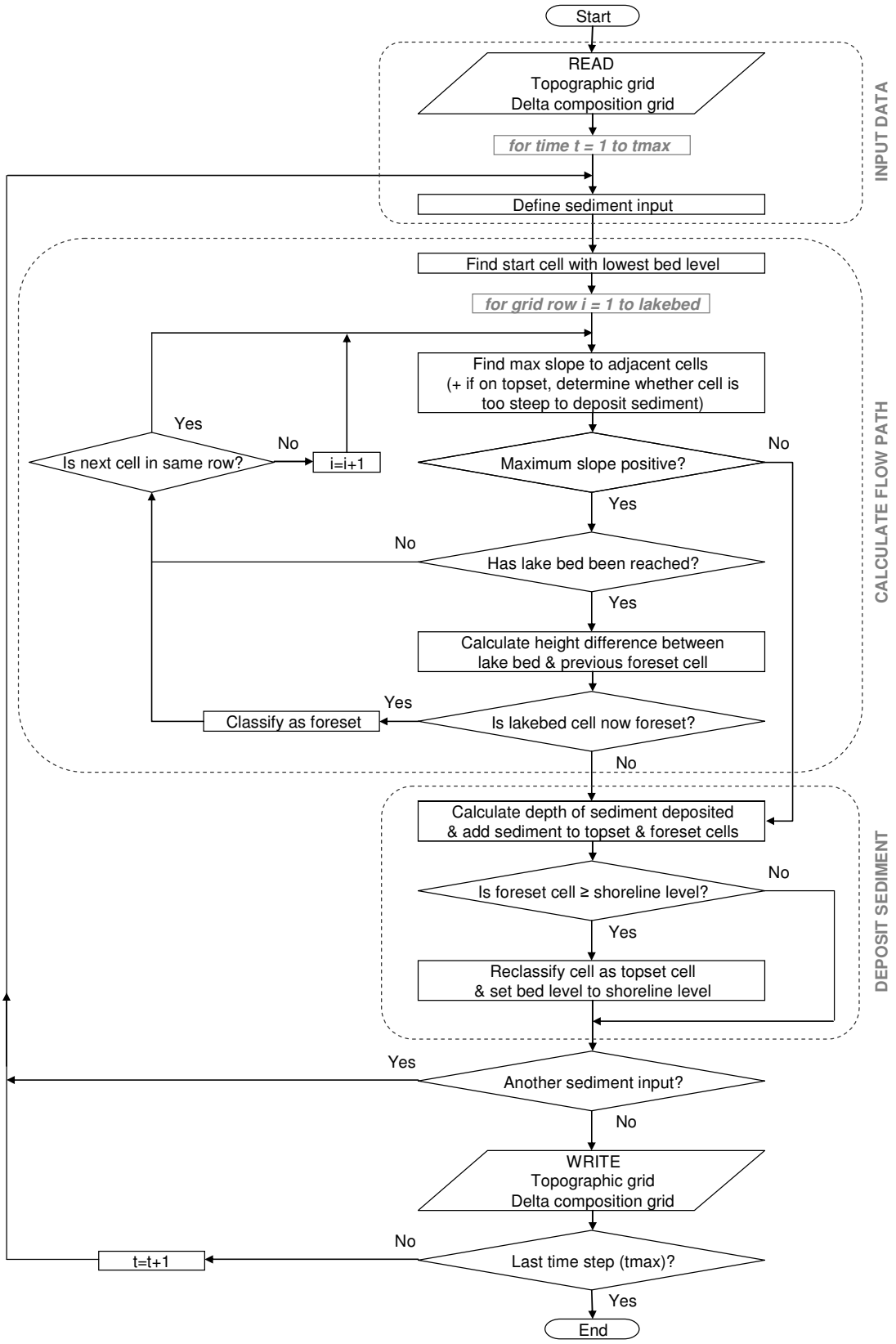

Figure 5.1: Flow chart for DELGROW numerical model

5.2.1 Assumptions

Many assumptions have been made in the development of DELGROW, which has been specifically developed to simulate delta progradation over the decade-to-century time scale. Assumptions include:

1. Mass is conserved with all sediment being deposited on the riverbed (or topset) and foreset.
2. Only bedload deposition is modelled.
3. The delta foreset has a linear slope. This is based on the assumption that sediment transport (for coarse-grained deltas with a steep, submerged foreset slope prograding into a low wave energy receiving basin) is likely to be dominanted by gravity-driven avalanche processes such as grain flows (Swenson et al., 2000).
4. Temporary storage of sediment on the topset or upper foreset slopes is not simulated.
5. Lake level (i.e. base level) remains constant, and represents the transition from topset (or riverbed) to foreset.
6. Climate change is not specifically considered. However, should expected changes in sediment input (due to climate change) be quantified, this scenario could be simulated.
7. Lake currents, wave dynamics, biological feedbacks, suspended sediment transport, aeolian transport, sediment loading (i.e consolidation of rapidly deposited sediment) and tectonic effects (i.e. subsidence) were considered less important than bedload processes.
8. Many of the factors that affect delta and channel morphology (e.g. sediment grain size distribution, turbidity currents) will be accounted for by the parameters chosen to represent riverbed and delta geometry (e.g. topset and foreset slopes) and sediment feed rates. For example, if the long-term average rate of sediment delivered to the delta is determined using the methodology in Section 3.2.5.3, then the volume of sediment removed from the delta by turbidity currents will already be accounted for.
9. River mouth bars are not simulated.

5.2.2 Input grids and parameters

Two grid maps and several other model parameters need to be defined to successfully use DELGROW to simulate decade-to-century timescale delta progradation. The two grids required by DELGROW are:

1. A ‘topographical’ grid that provides the elevation data for the riverbed/topset and floodplain as well as the bathymetry for the submerged delta and lakebed.
2. A ‘delta composition’ grid that covers the same extent as the ‘topographical’ grid. This grid contains a value from 1 to 3 depending on the location of the cell (i.e. ‘1’ = riverbed/topset and floodplain, ‘2’ = delta foreset and ‘3’ = lakebed)

The other parameters that need to be defined in DELGROW are summarised in Table 5.1.

Table 5.1: Description of parameters used in the DELGROW numerical model

Parameter	Description	Units
Numrows	Number of model grid rows	-
Numcols	Number of model grid columns	-
Del_t	Model run time step	Weeks (or days, months)
Tmax	Number of time steps Del_t	-
T_write	Number of time steps Del_t between writing output	-
Cellx	Cell size (assuming a square so both sides are equal)	m
jmin	Lowest column number for range of cells in row 1 that sediment can be fed into	-
jmax	Highest column number for range of cells in row 1 that sediment can be fed into	-
S_tset	Riverbed/topset slope	m/m
delS_tset	Maximum increase in slope before sediment not deposited (used to determine threshold topset slope)	m/m
S_fset	Foreset slope	m/m
RL_top_fore	Elevation of transition from topset to foreset (and shoreline)	m relative to a datum
VSed_in	Sediment input to model (input to one cell at each time step)	m^3/week (or day, month)

At each time step sediment is fed into a grid cell in the first row of the rectangular grid (i.e. at the upstream limit of the model). The sediment input cell selected by the model has the lowest riverbed level within the specified range of 'active riverbed' cells, and as such can change for each time step. More than one sediment input can also be fed into the river system at each time step (including a different range of 'active riverbed' cells to represent a second river), although the sediment from each input will be routed through the model sequentially rather than simultaneously. This means that if there are two sediment inputs, the first sediment input will be routed through the existing grid, and deposited in the appropriate cells, before the second sediment input is routed through the newly modified grid.

The sediment entering the upstream model boundary follows the steepest path across the 'active riverbed' areas to the delta, then down the delta foreset to the lakebed. If all destination cells were to have the same slope the preference would be to travel to the cell directly downstream (i.e. cell 3, Figure 5.2). The preferred path to the lakebed (from most to least favoured) is cell 3, 4, 2, 1 and lastly 5 - although this could easily be modified.

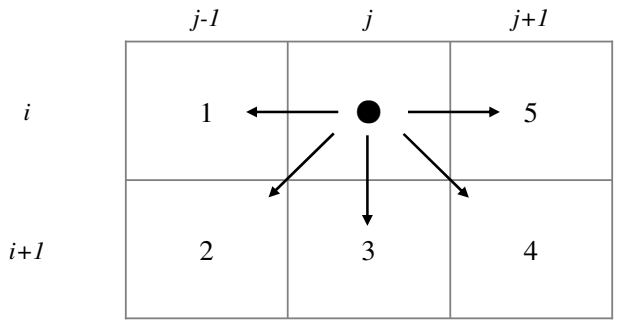

Figure 5.2: Possible destination cells for sediment passing over the topographic grid

At each time step (and for each sediment input, if there are more than one), the cells along the steepest path to the lakebed are identified, as well as any cells along the riverbed (but not foreset) that have a slope to their destination cell that is greater than some specified slope. This slope is intended to represent a threshold riverbed slope for which sediment will not be deposited in the cell. Conversely, when the sediment/flow path passes through a stationary body of water (e.g. a lagoon), or the bed level in all adjacent cells is higher, sediment will be deposited in the cells along the sediment/flow path that are upstream of (and also include) that cell - rather than sediment being transported further downstream.

Once the sediment path to the lakebed (or 'dead end') has been established, sediment is deposited in the delta topset cells (i.e. riverbed cells with a downstream bed slope less than the threshold slope) and foreset cells passed through along that route. At this stage no temporary (or permanent) steepening of the delta foreset, or localised storage of sediment on the topset, is incorporated into the model. To 'evenly' distribute the sediment, the number of riverbed (or topset) cells, n_t, and foreset cells, n_f, along the path to the lakebed need to be determined – excluding any topset cells with slopes above the threshold slope assumed to prevent sediment deposition. Horizontal delta progradation distance, Δx, is shown on Figure 5.3. Equations 5.1 is used to calculate Δx, and Equations 5.2a and 5.2b are used to calculate the depth of sediment added to each cell on the topset and foreset (i.e. Δz_t and Δz_f, respectively).

$$\Delta x = \frac{V_{Sed}}{(\alpha \times A \times n_t) + (\beta \times A \times n_f)} \quad \textbf{(5.1)}$$

Where:

Δx = horizontal distance of delta advance (m)

V_{Sed} = volume of sediment (m^3)

α = riverbed (or topset) slope (m/m)

β = foreset slope (m/m)

n_t = number of riverbed (or topset) cells along path

n_f = number of foreset cells along path

A = Grid cell size (m^2)

The depth of sediment, Δz, added to each riverbed (or topset) and foreset cell is then calculated to be

$$\Delta z_t = \alpha \times \Delta x \qquad \text{(a)}$$
$$\Delta z_f = \beta \times \Delta x \qquad \text{(b)} \qquad \textbf{(5.2)}$$

Where: Δz_t = Depth of sediment added to riverbed or topset (m)
Δz_f = Depth of sediment added to foreset (m)

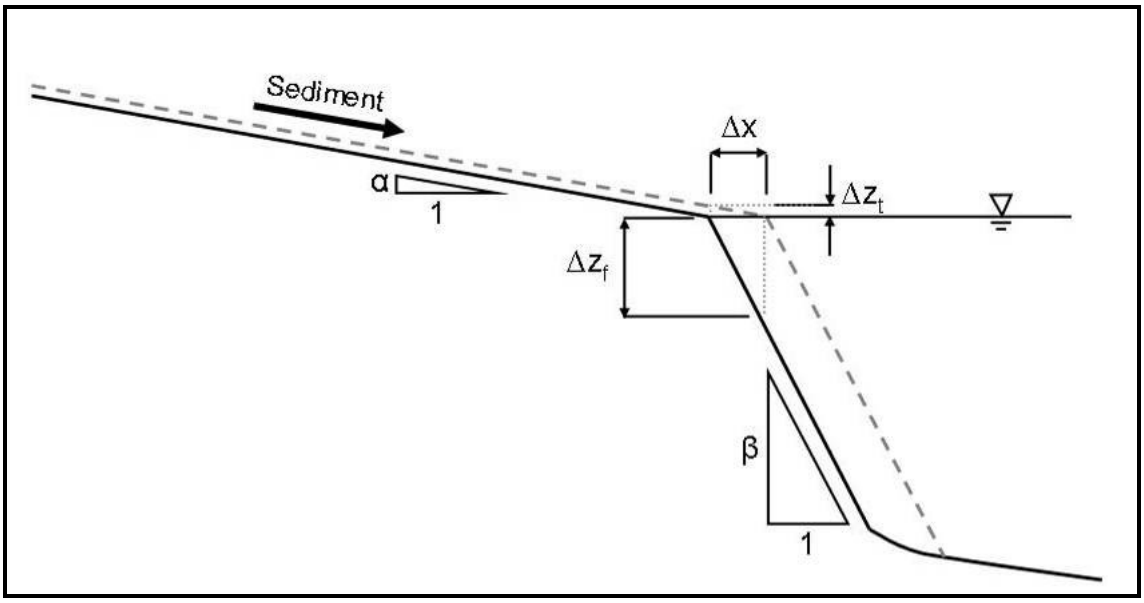

Figure 5.3: Schematic of delta progradation

When using DELGROW it should be noted that:

- The delta foreset slope initially maintains the same profile (as sediment is evenly distributed over the slope), but new cells incorporated into the foreset slope from the lake bed will have an average foreset slope (as specified in the model to be the representative foreset slope).
- Channel switching (i.e. a new route from the upstream model limit to the lake bed) can occur at any time step, as well as at each new sediment input within each time step. Channel switching is based only on the steepest slope between adjacent cells – starting from the cell with the lowest riverbed level within the 'active' riverbed at the model upstream limit.
- When an active riverbed cell level exceeds a river bank or island cell level, the barrier (i.e. bank or island) will be overtopped. However, for the model runs completed in this study active river bank boundaries have been set high and potential bank erosion and overtopping was not simulated. This numerical model will not necessarily simulate overtopping of banks accurately as river banks may fail (and rivers are likely to avulse) prior to the riverbed level exceeding the bank levels.

- The model time step chosen should not be too large (such that sediment accumulation at each time step is excessive), but also not too small (so that incremental increases in sediment are potentially rounded to zero). The time step can be adjusted if required.

5.3 Application of numerical model to Rees-Dart delta

To test the DELGROW model, 250 years of future delta progradation was predicted for the Rees-Dart river delta described previously in Section 3.2. A description of the model grids, model scenarios, and model results are given below together with a comparison to future delta progradation predicted in Section 4.3 by the Rees-Dart microscale model. Numerical modelling of historic delta progradation was not undertaken since there was only very limited (and recent) spatial and temporal data available for the topographic grid.

5.3.1 Topographic grid generation

A 50 m topographic grid of the Rees-Dart river delta system was generated in ArcGIS by using the 'Topo to Raster' interpolation method. The following point data was used to produce the topographic raster grid:

- LiDAR data of both the Rees and Dart Rivers and adjacent floodplains (described in Section 3.2.5.5). The high resolution LiDAR raster grid was resampled, using a bilinear interpolation resampling algorithm, to generate a 5 m raster grid. This 5 m grid was then converted into a series of points; points with elevations less than 309.5 m asl were removed to ensure any water level readings were discarded.
- A digitised 309.5 m shoreline (contour derived from LiDAR data).
- Sonar data from the June 2011 survey, supplemented by November 2007 sonar for the delta and lake bed levels further offshore (sonar data are described in section 3.2.5.2).

Figure 5.4a shows the location of the points used to generate the 50 m model topographic grid. Modifications made to the 50 m topographic grid, shown in Figure 5.4b, included:

- Raising river bank levels to ensure that sediment remained within the channels. This was required because of the averaging of the LiDAR bed levels over the 50 m cell size (i.e. river bank levees were often underestimated).
- Lowering some river bed cells near the lake shoreline and in some of the narrower reaches of the Rees river bed. This was required because of the averaging of the LiDAR bed levels over the 50 m cell size (i.e. grid cells that included mouth bars or river banks were elevated in places 'blocking' sediment routes to the delta foreset).

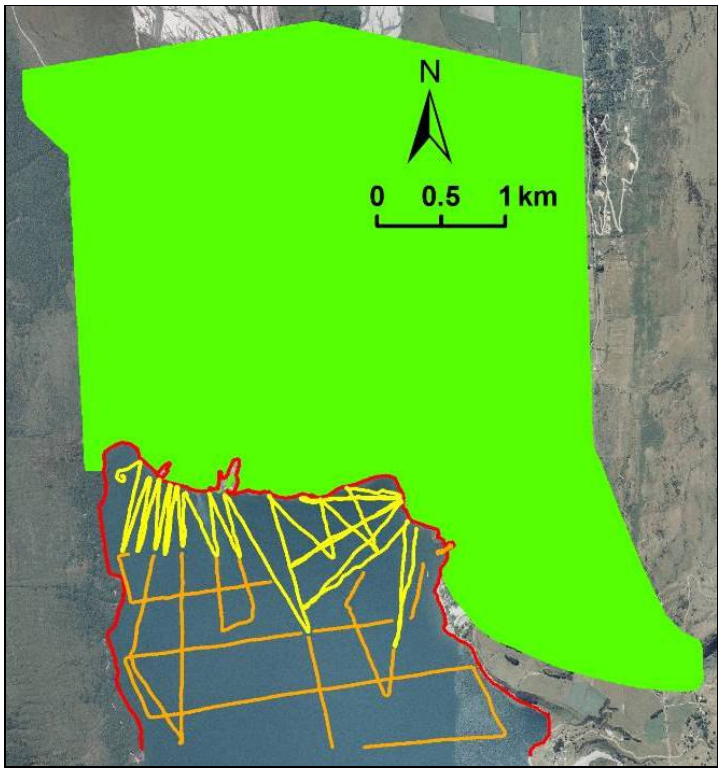

(a) Input data points for topographic grid (green = LiDAR, red = 309.5 m contour, yellow = 2011 sonar, orange = 2007 sonar data)

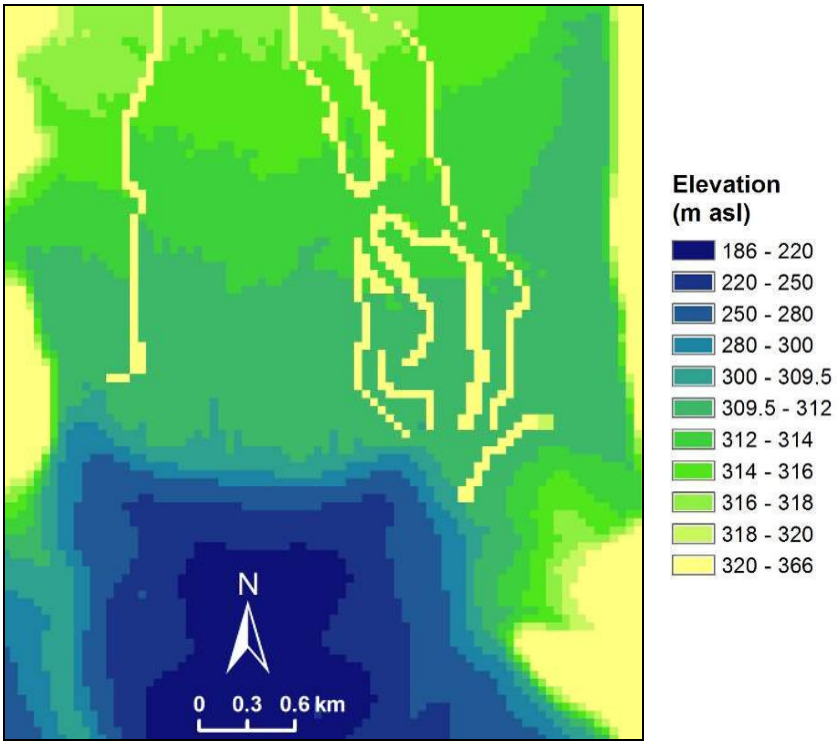

(b) Topographic model grid with barriers inserted and river mouth bars removed

Figure 5.4: (a) Input data points for topographic model grid and (b) topographic model grid (including modifications)

5.3.2 Run parameters

A summary of the DELGROW run parameters for the Rees-Dart delta model are summarised in Table 5.2. These parameters are described previously in Section 5.2.2 and Table 5.1.

Table 5.2: Summary of parameters used in the Rees-Dart DELGROW model

Parameter	Value	Units
Numrows	92	-
Numcols	81	-
Del_t	1	week
Tmax	13000 (250 years)	weeks
T_write	520 (10 years)	weeks
Cellx	50	m
jmin	Dart = 21 Rees = 42	-
Jmax	Dart = 37 Rees = 45	-
S_tset (α)	Dart = 0.0028 Rees = 0.0024	m/m
delS_tset	Dart = 0.0002 Rees = 0.0002	m/m
S_fset (β)	0.24	m/m
RL_top_fore	309.5	m asl
VSed_in	See Section 5.3.2 and Table 5.3	m^3/week

5.3.3 Scenarios

Initially the numerical model was run for 250 years using the same Dart/Rees sediment ratio as used in the Rees-Dart microscale model (i.e. 6.5). The sediment input rate was determined by dividing the estimated total annual sediment volume (derived in Section 3.2.5.3) between the Dart and Rees Rivers and then feeding it into the model as a constant weekly rate. This initial model scenario (Run 1, R1) represented the best estimate of future delta progradation using the currently available information on Rees-Dart delta sedimentation rates. For this model (and all model simulations for the Rees-Dart delta) there were two sediment inputs for the Dart River, and one for the Rees. Sediment inputs to the Dart River were equal in magnitude (i.e. half of the total Dart River sediment input). The start of the run is assumed to be 2011 (i.e. t = 0 is the year 2011).

Additional model scenarios, summarised in Table 5.3, simulated the effects of decreasing the Dart/Rees sediment ratio (Run 2, R2), increasing the delta foreset slope (Run 3, R3), and increasing

the threshold slope for no sediment deposition on the topset/increase in delS_tset (Run 4, R4). Another model scenario (Run 5, R5) was also completed to see if there was a significant difference to delta progradation if the priority assigned to each downstream cell was changed (i.e. if path the model chooses changes when there are more than one cell with the lowest elevation).

Table 5.3: Rees-Dart DELGROW numerical model scenarios

Run	Description	Time (years)	Sediment volume (x 10^6 m^3/yr)			Sediment ratio (Dart/Rees)
			Total	Dart River	Rees River	
1	'Base' case	0 – 250	0.270	0.234	0.036	6.5
2	Dart/Rees sediment ratio decreased	0 – 250	0.270	0.204	0.066	3.1
3	Delta foreset slope (β) changed from 0.24 (~13.5º) to 0.36 (~20º)	0 – 250	0.270	0.234	0.036	6.5
4	Threshold slope for no topset sediment deposition increased (delS_tset = 0.0005)	0 – 250	0.270	0.234	0.036	6.5
5	Preferred path to the lakebed (from most to least favoured) is changed to cell 3, 2, 4, 5 and 1 (see Figure 5.2)	0 – 250	0.270	0.234	0.036	6.5
6	Rees sediment input increased by 50%	0 – 120 120 – 250	0.270 0.288	0.234 0.234	0.036 0.054	6.5 4.3
7	Dart sediment input increased by 50%	0 – 120 120 – 250	0.270 0.387	0.234 0.351	0.036 0.036	6.5 9.8
8	Rees sediment diverted into Dart upstream of grassed island	0 – 120 120 – 250	0.270	0.234	0.036	6.5
9	Dart River sediment input varies over a 50 year cycle	0 – 10 10 – 20 20 – 50	0.166 0.686 0.166	0.130 0.650 0.130	0.036 0.036 0.036	4.2 20.8 4.2
10	Topset length reduced by 1 km (i.e. sediment input moved 1km downstream)	0 – 250	0.270	0.234	0.036	6.5

After 120 years of future delta growth (simulated by the 'base' model up to the year ~2120), the 'base' model was modified to: increase the Rees sediment input by 50% (Run 6, R6), increase the Dart River sediment input by 50% (Run 7, R7), and divert all the Rees River sediment into the Dart River upstream of the grassed island (Run 8, R8). Previously both Run 6 and Run 8 were also simulated

using the Rees-Dart microscale model (Experiments C and B, respectively) so have been chosen partially for comparative purposes.

Lastly, two model scenarios simulated the input of a large 'slug' of sediment to the Dart River (Run 9), and a decrease in the topset length/area by moving the sediment input location 1 km downstream (Run 10). For Run 9 the Dart River sediment input varied over a 50 year cycle (Figure 5.5), rather than maintaining a constant sediment supply of 0.234 x 10^6 m^3/yr. Dart River sediment inputs were increased for years 10 to 19 (inclusive), but also decreased in magnitude for the first 10 years and for years 20 to 50; this meant that the total sediment volume input into the model over each 50 year cycle still remained the same as for Run 1 for each 50 year cycle.

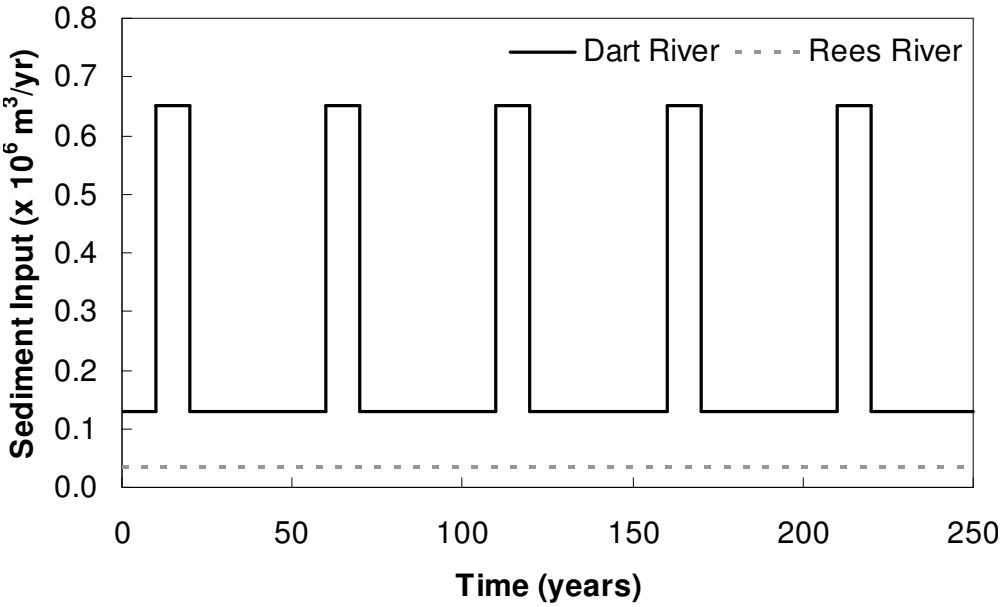

Figure 5.5: Run 9 sediment feed rates for the Dart and Rees Rivers

5.3.4 Results

The DELGROW model results are shown below for the model scenarios and sediment feed rates specified in Table 5.3. Sediment depth has been calculated by subtracting the topographic grid at the start of the simulation from the topographic grid at the specified times (e.g. after 50 years of simulated future delta growth). Shoreline positions are also represented by the 309.5 m asl contour, although this only provides a fairly coarse shoreline as it is derived from the 50 m model grid. Comparisons with the Rees-Dart microscale model are also shown where possible.

Depths of deposited sediment are shown in Figures 5.6a to h for Run 1 at 10, 20, 50, 100, 150, 200 and 250 years beyond 2011. This model represents the 'base' model (or model most representative of the prototype) from which the other model scenarios are compared. Figure 5.6h also shows shoreline advance for Run 1 over this 250 year time period. Comparisons with microscale model experiments are also made in Figure 5.7 (i.e. Run 1 compared to microscale model Experiment A).

Runs 2 to 5 were compared to Run 1 by subtracting the Run 1 topographic grids from the Run 2 to 5 topographic grids at 10, 50, 100, 150 and 250 years beyond 2011 (Figures 5.8 to 5.11). The Run 1 shoreline position is also compared to the Run 2 to 5 shoreline positions in Figures 5.8f to 5.11f.

As Runs 6 to 8 have the same profile as Run 1 up to 120 years beyond 2011 (i.e. up to 2131), Figures 5.12a, 5.14a and 5.15a compare the Run 6 to 8 topographic grids and the Run 1 topographic grid for 200 years beyond 2011 (i.e. for 80 years after the modification to Run 1 occurred). Figures 5.12b, 5.14b, and 5.15b also compare Run 6 to 8 shoreline positions to the Run 1 shoreline. When comparing a 50% increase in sediment supply to the Rees River (Figure 5.12a and b), versus a 50% increase to the Dart River (Figures 5.13a and b), it should be noted that increasing the sediment input of the Dart River by 50% (Run 7) is a much greater increase in the total sediment supply compared to a 50% increase in the Rees River sediment input (Run 6). Comparisons with microscale model experiments are also made in Figure 5.13 (Run 6 compared to microscale model Experiment C) and Figure 5.16 (Run 8 compared to microscale model Experiment B).

Figure 5.17a compares the Run 9 scenario (where the Dart River sediment supply fluctuates as shown in Figure 5.5) with Run 1 by subtracting the modelled topographic grids. The modelled shoreline positions comparing Run 9 to Run 1 are also shown on Figure 5.17b for 250 years beyond 2011.

Run 10 (where the topset upstream length is reduced by 1 km) was compared to Run 1 by subtracting the Run 1 topographic grids from the Run 10 topographic grids at 10, 50, 100, 150 and 250 years beyond 2011 (Figures 5.18a to e). The Run 1 shoreline position is also compared to the Run 10 shoreline position in Figure 5.18f.

The modelled increase in delta area for the next 250 years was also quantified in arcGIS by calculating the area of the delta that had a level greater than or equal to 309.5 m (i.e. foreset-topset transition which represents the water level). Figure 5.19 compares Run 1 and the various other simulations that modified the sediment supply and delta configuration (i.e. Runs 2 to 10).

Lastly, Figure 5.20 shows measured delta area increases for the Rees-Dart delta (derived from geo-referenced aerial photos), together with microscale modelling, numerical modelling and Equation 4.4 estimates of future delta progradation.

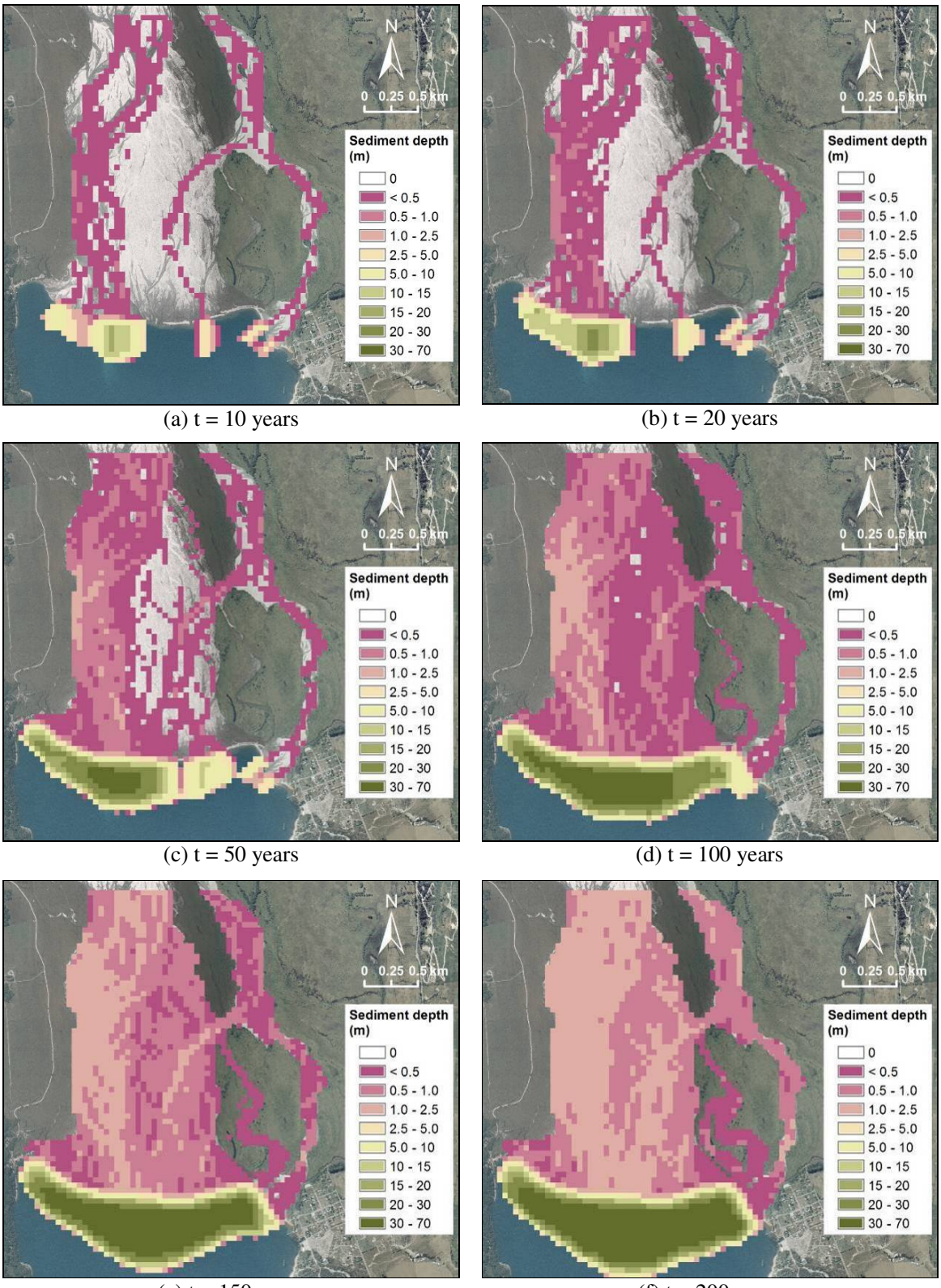

(a) t = 10 years (b) t = 20 years

(c) t = 50 years (d) t = 100 years

(e) t = 150 years (f) t = 200 years

Figure 5.6: (a to g) Run 1 (R1, base model) sediment deposition from 10 to 250 years into the future, and (h) shoreline progradation over this time period

(*continued next page*)

(Figure 5.6 continued)

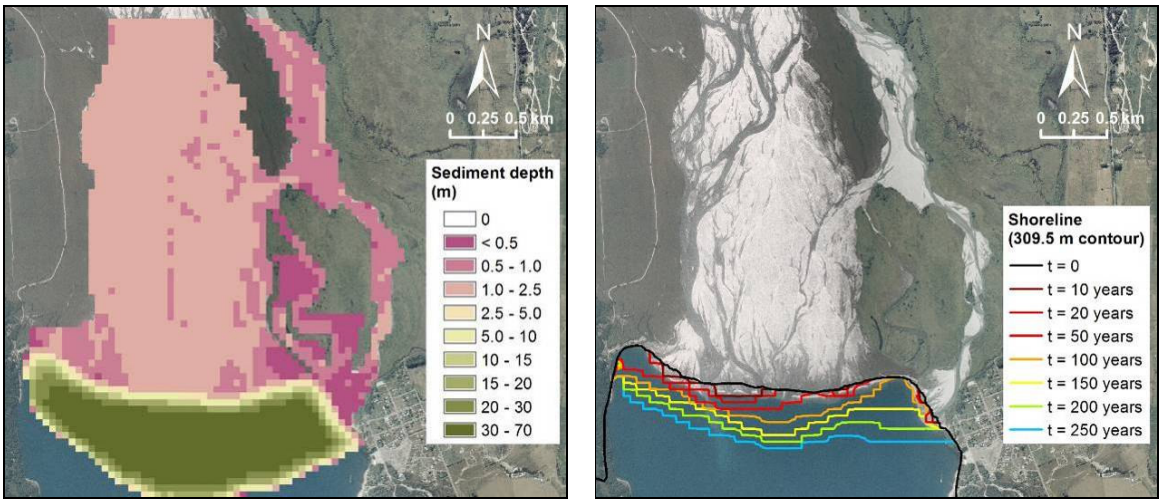

(g) t = 250 years (h) t = 0 to 250 years

Figure 5.6 *(continued)*: (a to g) Run 1 (R1, base model) sediment deposition from 10 to 250 years into the future, and (h) shoreline progradation over this time period

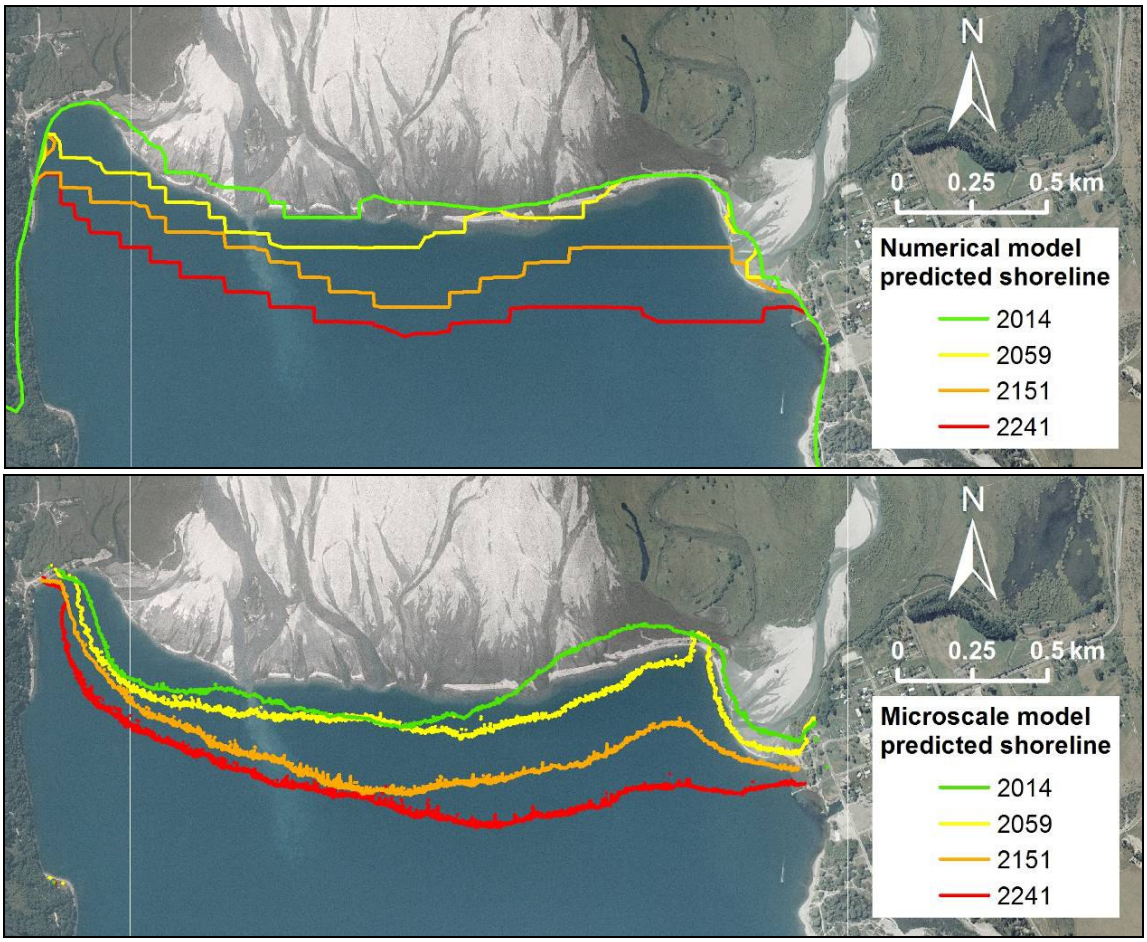

Figure 5.7: Run 1 (R1, base model) shoreline locations for the next 250 years predicted by numerical model (top) and microscale model (bottom)

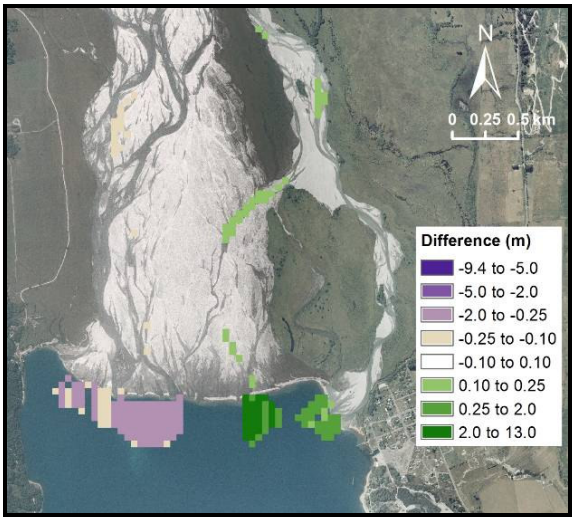

(a) t = 10 years

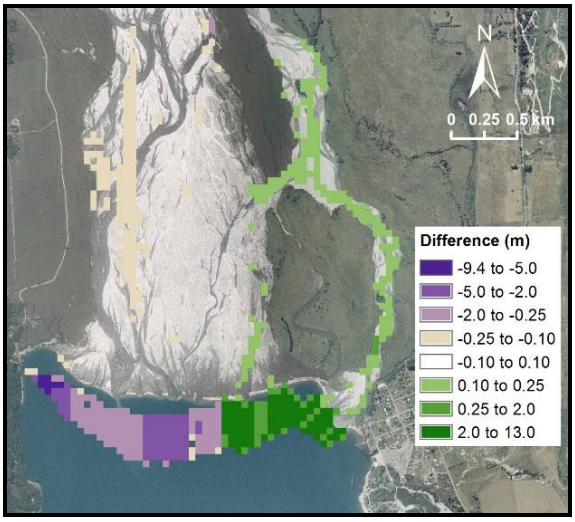

(b) t = 50 years

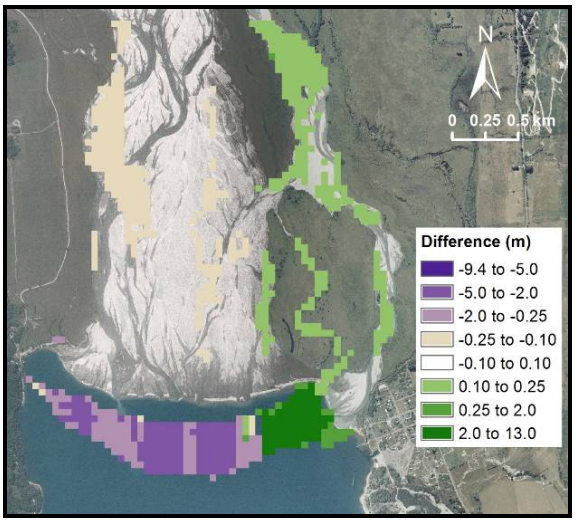

(c) t = 100 years

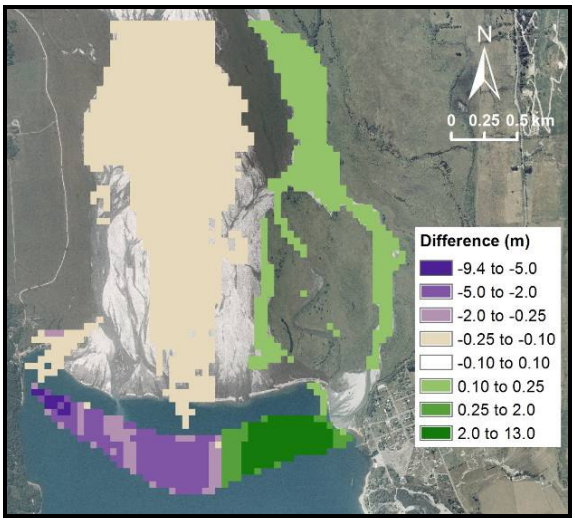

(d) t = 150 years

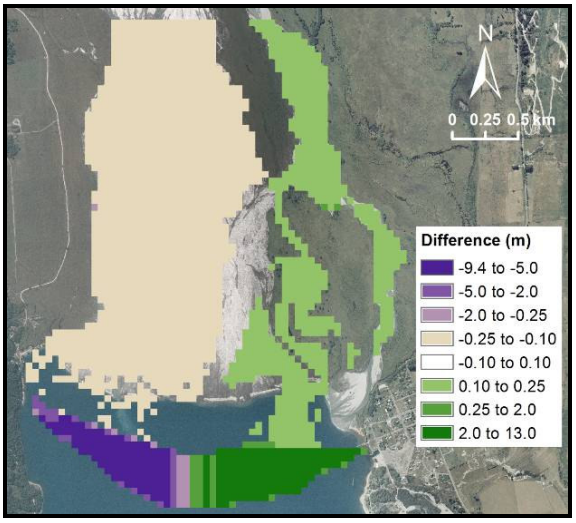

(e) t = 250 years

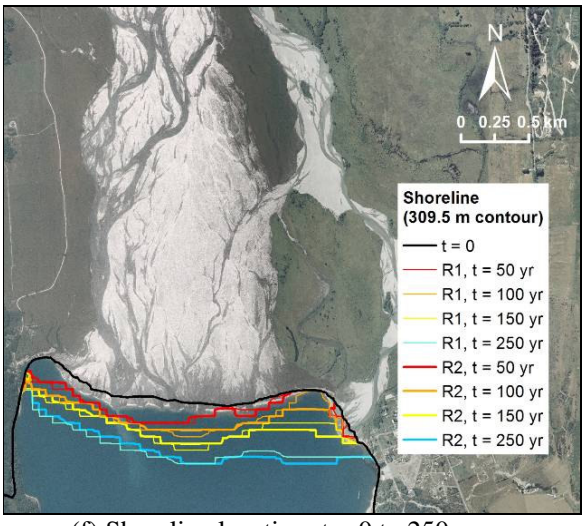

(f) Shoreline location: t = 0 to 250 years

Figure 5.8: (a to e) Difference in elevation between Run 2 (R2, Dart/Rees sediment ratio decreased to 3.1) and Run 1 (R1, base model) from 10 to 250 years into the future, and (f) shoreline comparison for this time period

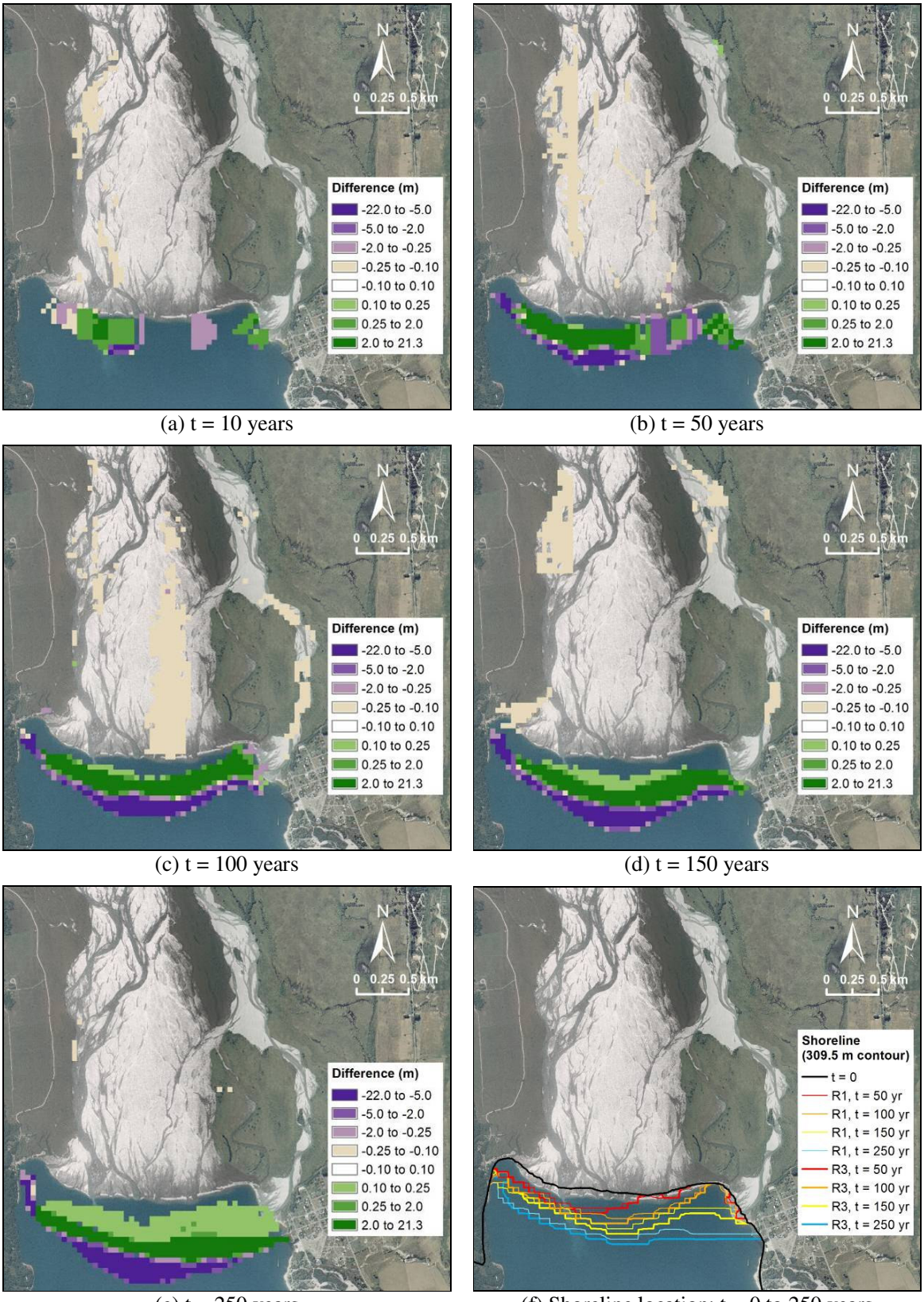

(a) t = 10 years (b) t = 50 years

(c) t = 100 years (d) t = 150 years

(e) t = 250 years (f) Shoreline location: t = 0 to 250 years

Figure 5.9: (a to e) Difference in elevation between Run 3 (R3, delta foreset slope increased to 0.36 m/m) and Run 1 (R1, base model) from 10 to 250 years into the future, and (f) shoreline comparison over this time period

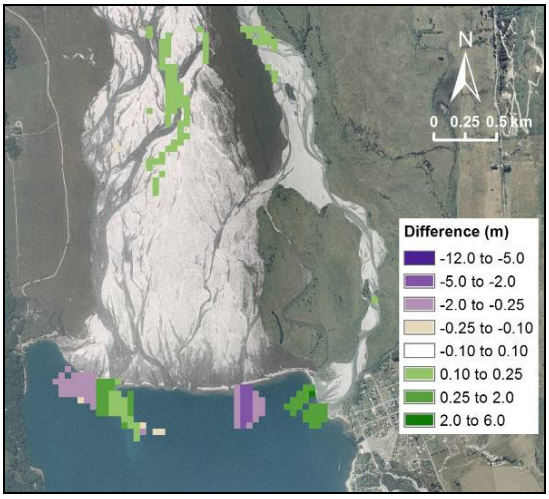

(a) t = 10 years

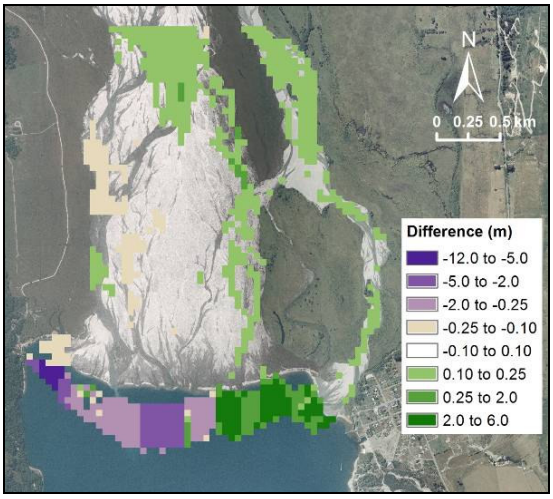

(b) t = 50 years

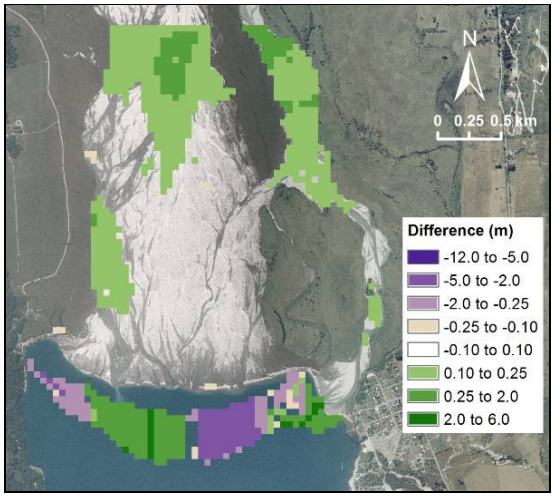

(c) t = 100 years

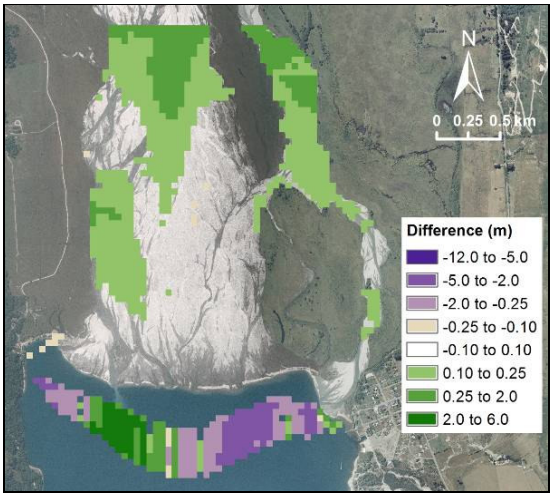

(d) t = 150 years

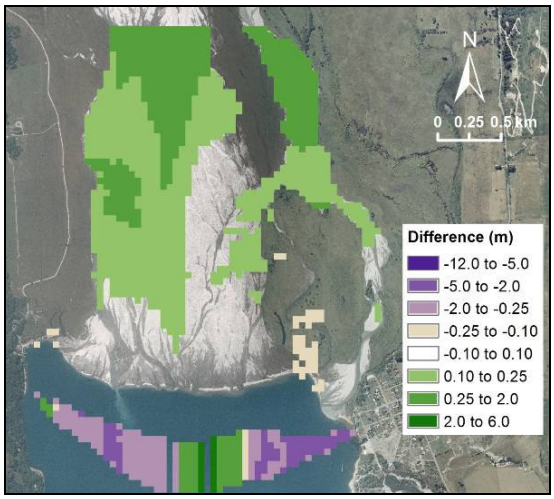

(e) t = 250 years

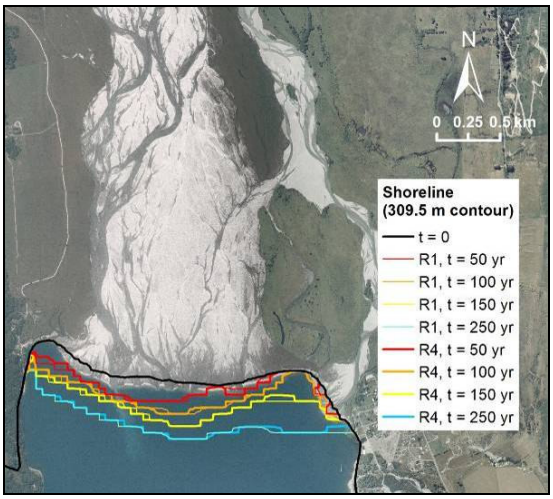

(f) Shoreline location: t = 0 to 250 years

Figure 5.10: (a to e) Difference in elevation between Run 4 (R4, threshold slope for no topset sediment deposition, delS_tset = 0.0005) and Run 1 (R1, base model) from 10 to 250 years into the future, and (f) shoreline comparison over this time period

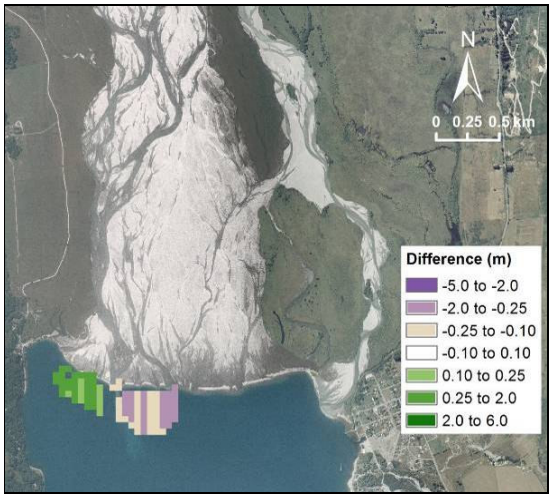

(a) t = 10 years

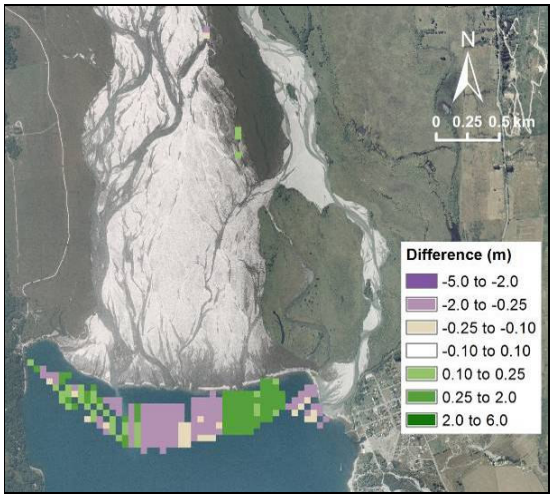

(b) t = 50 years

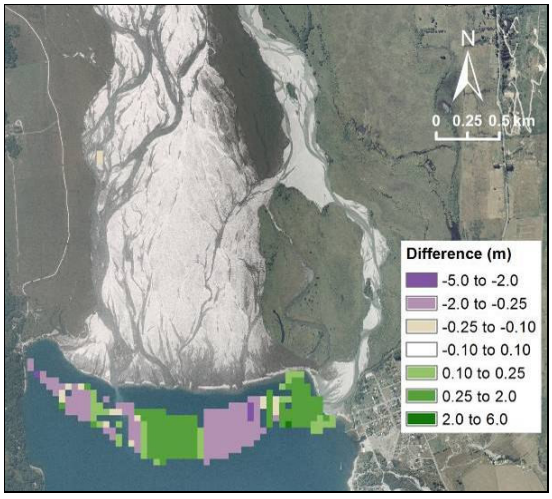

(c) t = 100 years

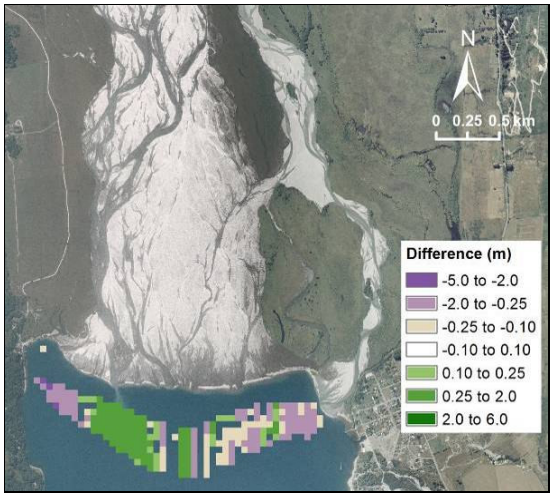

(d) t = 150 years

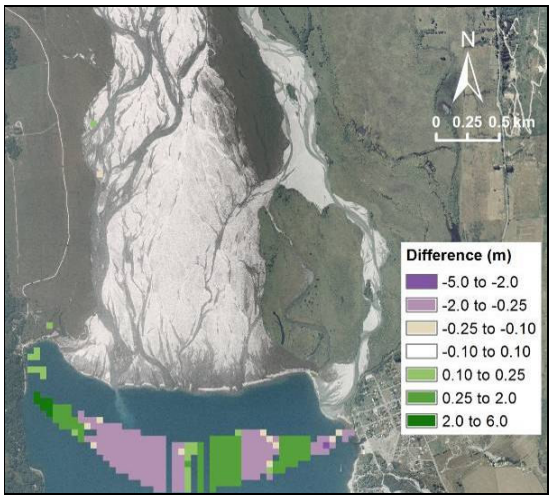

(e) t = 250 years

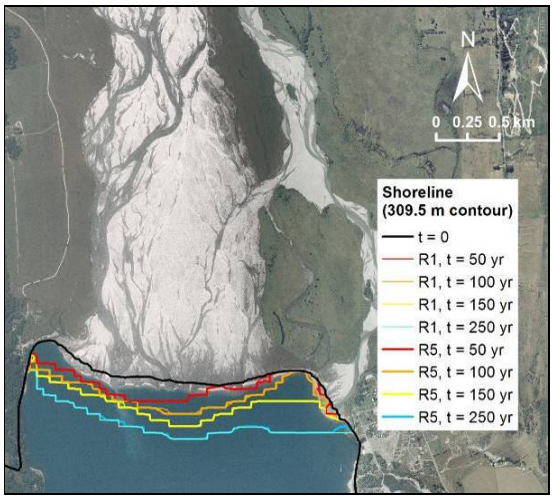

(f) Shoreline location: t = 0 to 250 years

Figure 5.11: (a to e) Difference in elevation between Run 5 (R5, path preference changed as described in Table 5.3) and Run 1 (R1, base model) from 10 to 250 years into the future, and (f) shoreline comparison over this time period

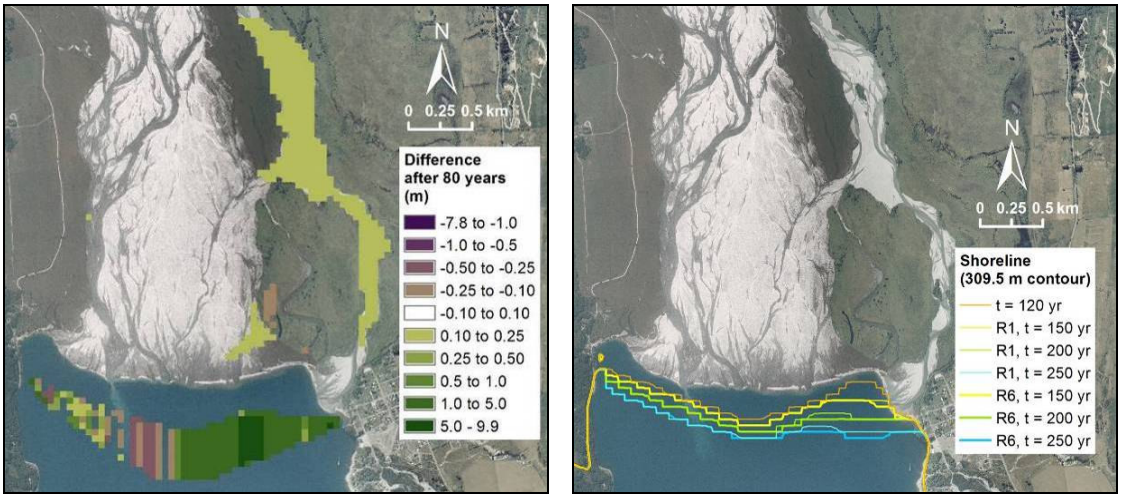

(a) t = 200 years (80 years of increased sediment) (b) Shoreline between t=120 and 250 years

Figure 5.12: (a) Difference in elevation between Run 6 (R6, Rees River sediment input increased by 50% after 120 years) and Run 1 (R1, base model) after 200 years, and (b) shoreline comparison after 120, 150, 200 and 250 years

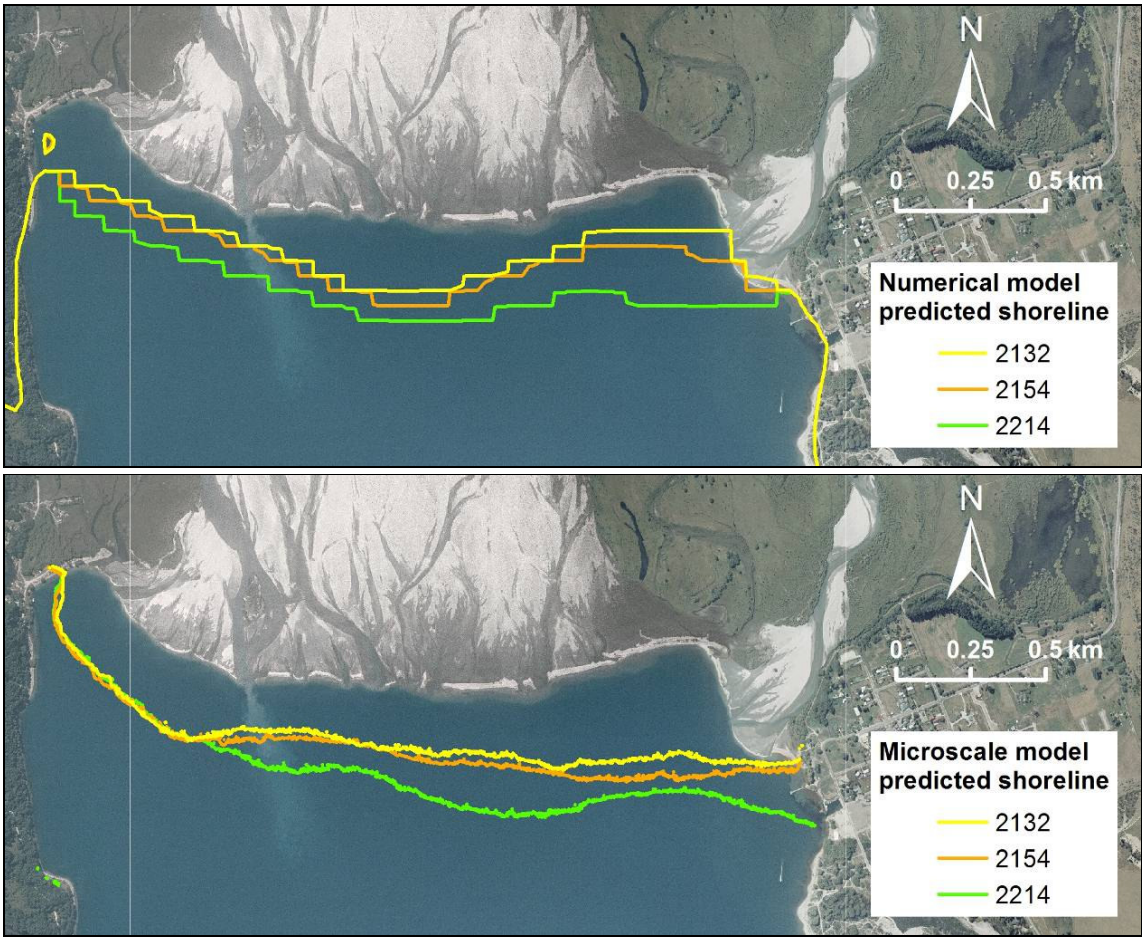

Figure 5.13: Shoreline locations predicted for 120 to 250 years into the future by (top) numerical model Run 6 (R6, Rees River sediment input increased by 50% after 120 years), and (bottom) microscale model Experiment C

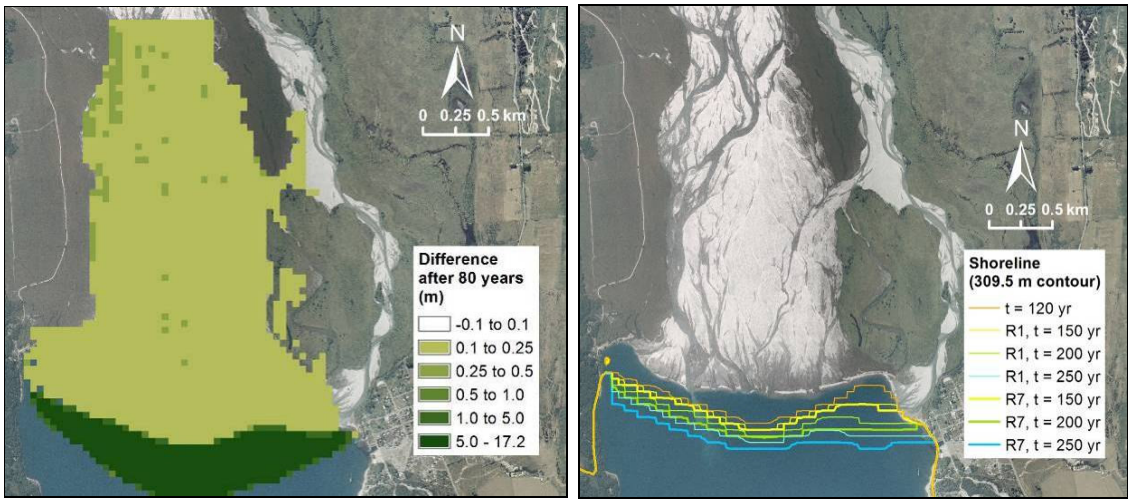

(a) t = 200 yr (80 yrs of increased sediment) (b) Shoreline between t=120 and 250 yrs

Figure 5.14: (a) Difference in elevation between Run 7 (R7, Dart River sediment input increased by 50% after 120 years) and Run 1 (R1, base model) after 200 years, and (b) shoreline comparison after 120, 150, 200 and 250 years

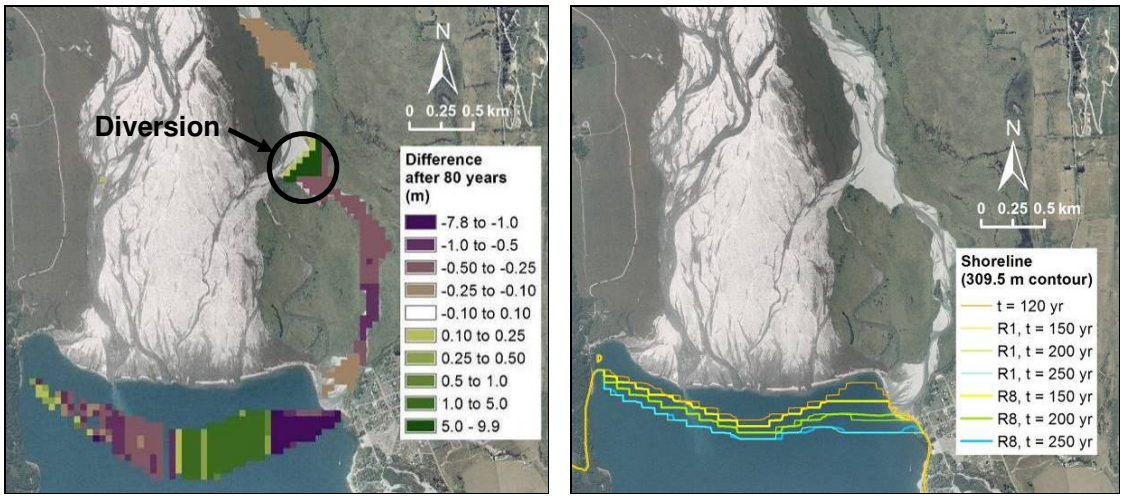

(a) t = 200 yr (80 yrs of increased sediment) (b) Shoreline between t=120 and 250 yrs

Figure 5.15: (a) Difference in elevation between Run 8 (R8, Rees River sediment diverted into the Dart River after 120 years) and Run 1 (R1, base model) after 200 years, and (b) shoreline comparison after 120, 150, 200 and 250 years

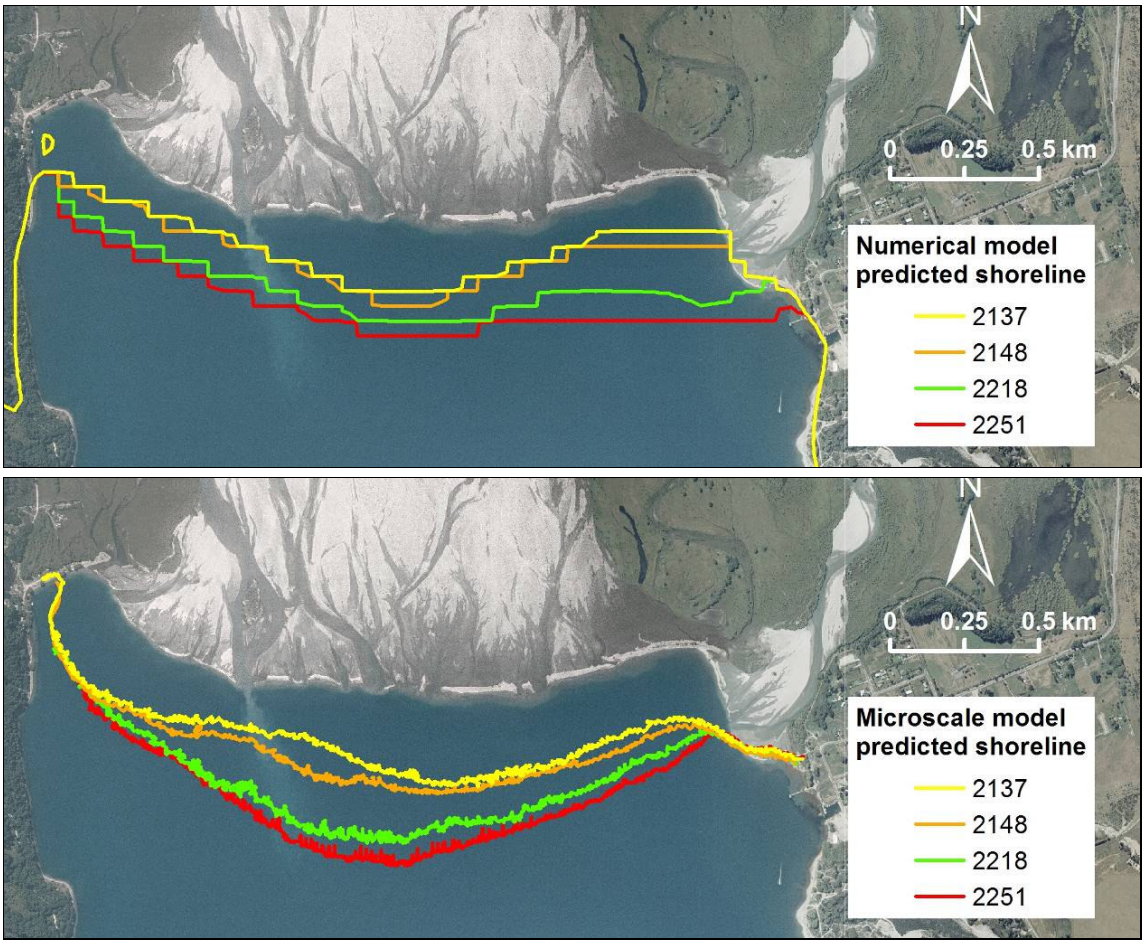

Figure 5.16: **Shoreline locations predicted for 120 to 250 years into the future by (top) numerical model Run 8 (R8, Rees River sediment diverted into the Dart River after 120 years), and (bottom) microscale model Experiment B**

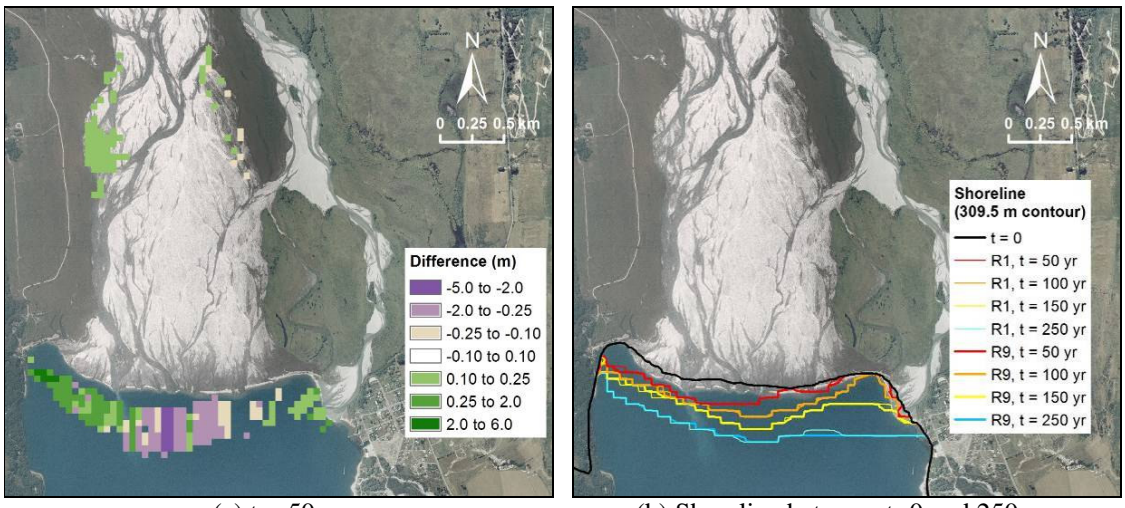

(a) t = 50 yr (b) Shoreline between t=0 and 250 yrs

Figure 5.17: **(a) Difference in elevation between Run 9 (R9, Dart River sediment input fluctuating over 50 year cycle) and Run 1 (R1, base model) after 50 years, and (b) shoreline comparison after 50, 100, 150 and 250 years**

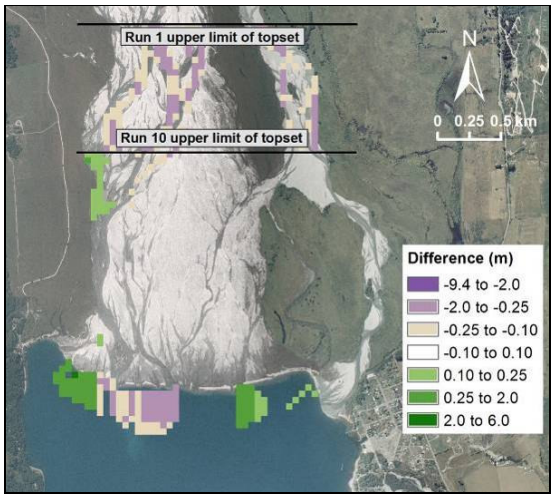

(a) t = 10 years

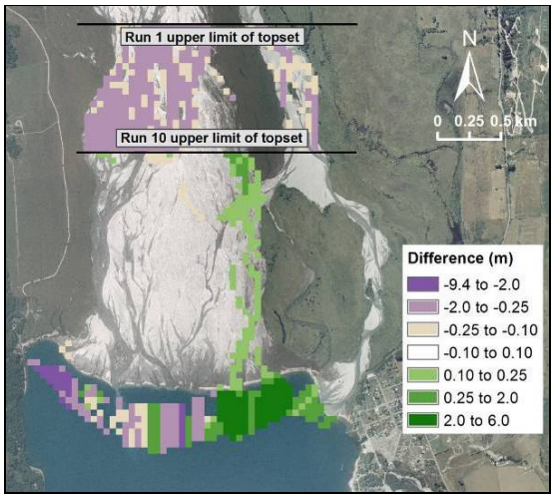

(b) t = 50 years

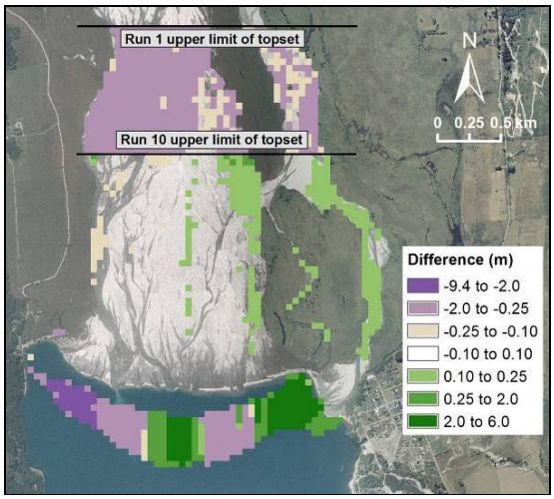

(c) t = 100 years

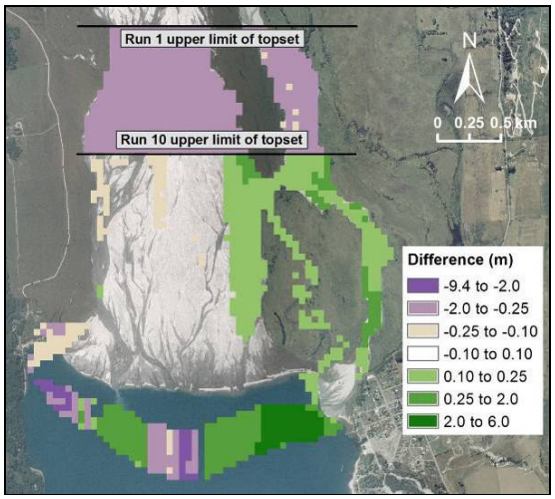

(d) t = 150 years

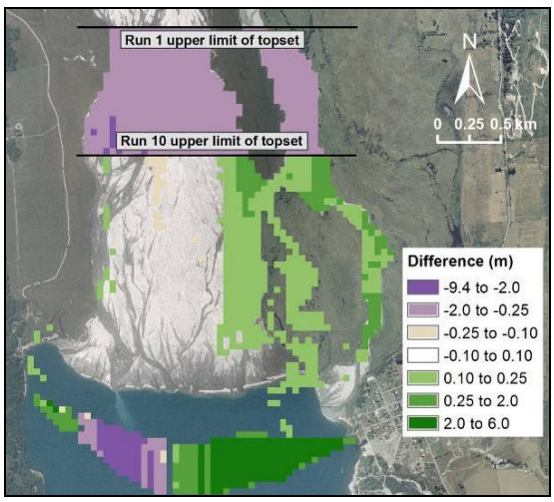

(e) t = 250 years

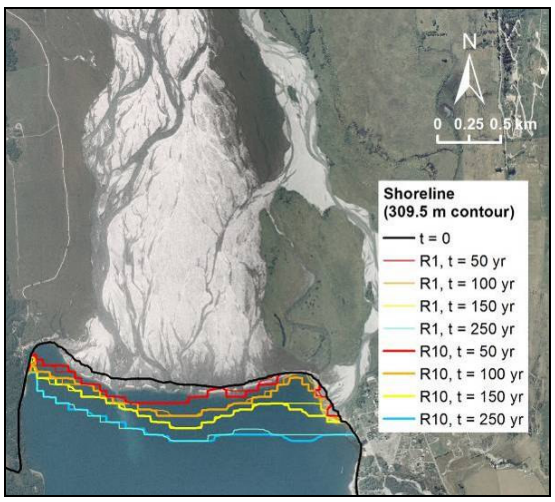

(f) Shoreline location: t = 0 to 250 years

Figure 5.18: (a to e) Difference in elevation between Run 10 (R10, delta topset length decreased by 1 km) and Run 1 (R1, base model) from 10 to 250 years into the future, and (f) shoreline comparison over this time period

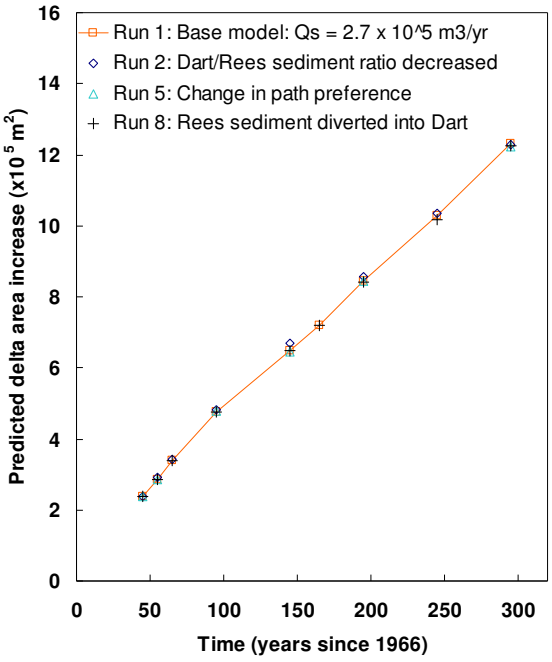

(a) Changes due to modified sediment paths

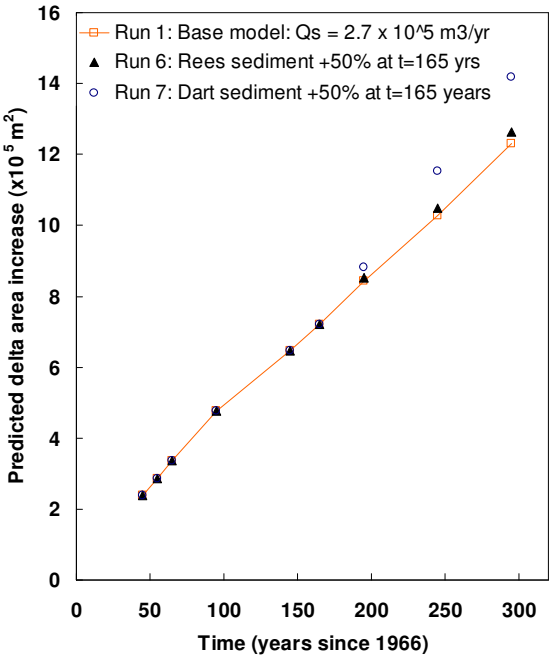

(b) Changes due to increased sediment supply

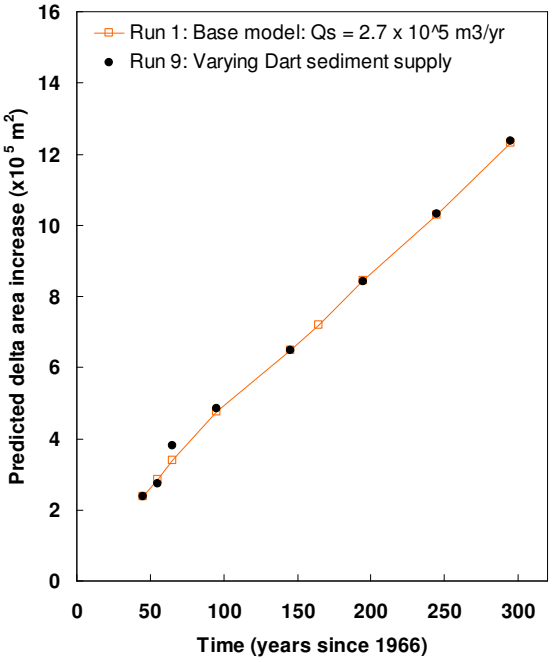

(c) Changes due to varying temporal sediment supply (50 yr cycle)

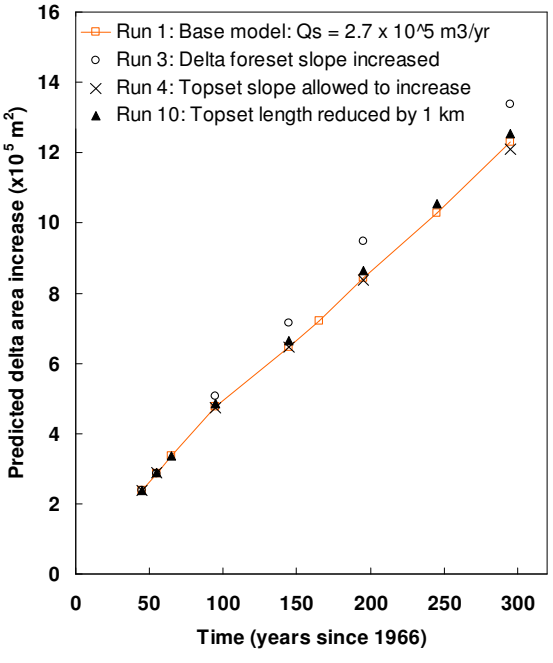

(d) Changes due to varying delta geometry

Figure 5.19: Comparison of increased delta area over time for Run 1 compared to various changes in sediment characteristics and delta configurations

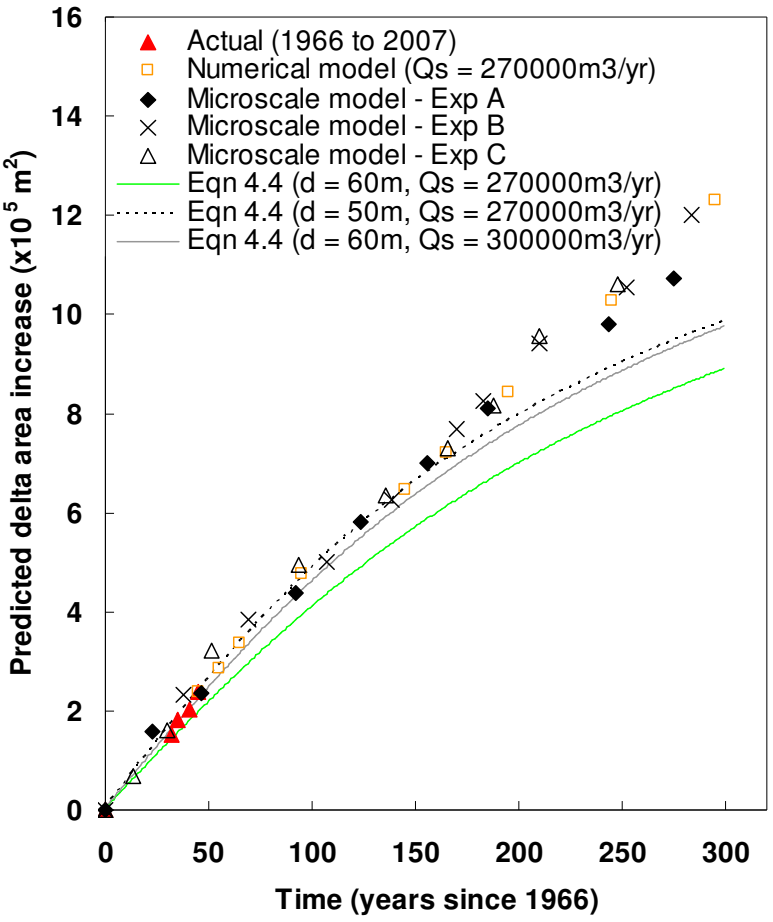

Figure 5.20: Measured Rees-Dart delta area increase compared to simulated results from the numerical model (Run 1), microscale model and Equation 4.4

5.3.5 Discussion

Run 1 (Figure 5.6) shows the Dart River remaining near the TRB and in the vicinity of Kinloch for the next ~50 years before migrating across the riverbed to the east, and closer to Glenorchy. The latest LiDAR data (Figure 3.35) shows that this part of the Dart floodplain currently has the lowest bed levels, and is the obvious path for the Dart River to follow. However, as the delta advances in the vicinity of Kinloch, and the adjacent upstream floodplain/topset aggrades, it is likely that the current area of lower bed levels will fill and the sediment flow path will migrate across the floodplain to find any other areas with lower bed levels. Once any low areas are filled, sediment will be distributed more evenly over the delta forest and topset, and will behave similarly to 1-d width-averaged numerical models – except DELGROW is still able to take into consideration barriers (e.g. islands) and the convergence of multiple deltas. Run 1 shows that DELGROW successfully simulates these processes, including the migration of the Dart River to the east, and the Rees River alternating routes around the grassed island and contributing sediment to both the Rees River delta and the Dart River delta. Run 1

also shows that aggradation of the Rees River, in the vicinity of Glenorchy, appears to be of the order of 0.5 m over this time period, and that within 250 years the shoreline is likely to have reached the existing Glenorchy jetty (Figure 5.7). Uniform depths of topset aggradation along both the Dart and Rees Rivers, also suggests that the chosen topset slopes and threshold slopes for the Dart and Rees Rivers are appropriate.

Comparisons between Run 1 and microscale model Experiment A (Figures 5.7 and 5.20), show remarkably good agreement 150 to 250 years into the future, despite the difference in the existing (~2011) shoreline positions represented by the two simulation methods. This can largely be explained by the fact that the preference for both the numerical model and microscale model is for the braided gravel-bed topset slope to be uniform. Both of these modelling methods initially use the supplied sediment to try and eliminate any irregularities (e.g. low points), before continuing to advance and deposit sediment in a more evenly-distributed manner (similarly to that of a simple 1-d width-averaged geometric model but with the advantage of being able to account for barriers and complicated river and delta configurations). The close agreement between the DELGROW and microscale modelling results also confirms that the microscale model time scale was scaled correctly.

Changing the Dart/Rees sediment input ratio from 6.5 (Run 1) to 3.1 (Run 2) produced less sediment deposition in the vicinity of Kinloch, to the west, and more near Glenorchy (Figure 5.8). This occurs due to the increased sediment input to the Rees River, and decreased sediment input to the Dart River. However, changes to aggradation on the riverbed\topset were fairly minor (~ ±0.3 m over the next 250 years); the delta shoreline was also not significantly different (i.e. ±50 m or one grid cell) between Run 1 and Run 2 (Figure 5.8f) and there were negligible changes to total increase in delta area (Figure 5.19a).

At present DELGROW uses an average delta foreset slope to simulate the entire width of the delta. When the value assigned to the foreset slope is increased from 0.24 to 0.36 m/m (Run 3), the depth of sediment deposition at the shoreline increased, and the depth of sediment deposited further offshore decreased (Figures 5.9a to e). After 250 years the shoreline had advanced by up to an additional ~100 m for the steeper foreset slope (Figure 5.9f), and the delta area had increased by ~100 000 m^2 (Figure 5.19d).This pattern of sediment distribution is what would be intuitively expected for an increased foreset slope. Figure 5.21 shows the simulated delta foreset profiles (along the centre of the Dart River after 250 years of model simulation) for delta foreset slopes of 0.24 m/m (Run 1) and 0.36 m/m (Run 3). Changes to riverbed/delta topset levels are relatively negligible for the increased foreset slope.

When using DELGROW it is important to select a realistic topset slope so that the topset can maintain a constant slope. When the 'threshold slope' between adjacent riverbed/delta topset cells is increased, so that sediment will be more readily deposited (Run 4), additional sediment is deposited on the riverbed/delta topset cells in the upper reaches of the Rees and Dart Rivers (Figures 5.10a to e). This

results in steepening of the topset slope, and the distribution of sediment delivered to the foreset also varies (most likely due to the increased riverbed levels in the upper Dart River redistributing some of the sediment supplied to the river). Changes to the shoreline, compared to Run 1, are still relatively minor (Figure 5.10f and 5.19d).

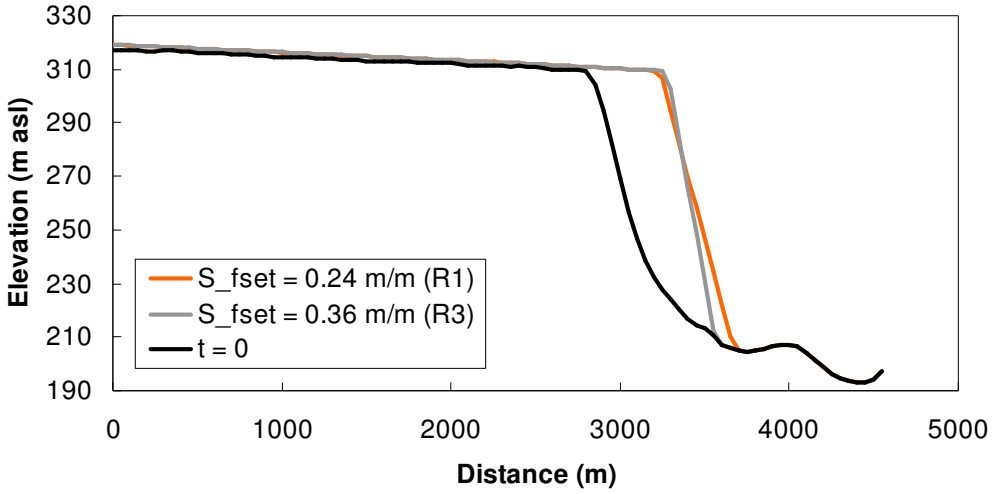

Figure 5.21: Comparison of delta profiles at t = 250 years for foreset slopes of 0.24 m/m (Run 1) and 0.36 m/m (Run 3). The initial grid at t = 0 is also shown in black

Changing the flow/sediment path preference (when all downstream cells have the same riverbed elevation) appeared to have no significant effect on riverbed/delta topset aggradation in Run 5 (Figures 5.11a to e). Changes to the shoreline (when compared to Run 1) were also minor (Figure 5.11f and 5.19a).

Run 6 increased the Rees River sediment input by 50% between 120 and 250 years into the future. This had a relatively minor impact on riverbed aggradation (Figures 5.12a to e), shoreline position (Figure 5.12f), and the total increase in delta area (Figure 5.19b). A comparison with the Rees-Dart microscale model (Experiment C, Figures 5.13 and 5.20) showed that, despite the different initial shoreline positions representing the existing (~ 2011) shoreline, advances in the shoreline were generally in the same area (i.e. in the eastern portion of the Rees-Dart delta where the additional sediment was being directed) and they both produced similar rates of increase in delta area. The more significant shoreline advances adjacent to Glenorchy, observed in the microscale model, may be due to limitations in one or both modelling methods. For example, the routing of sediment around and through the grassed island may be inadequately represented by the fixed boundaries imposed in each model, or the longitudinal vertical exaggeration of the microscale model may produce a less meandering, or widely distributed, sediment distribution at the shoreline. The microscale model also has a constant lakebed elevation while the numerical model incorporates the lake bathymetry shown in Figure 5.4.

Run 7 increased the Dart River sediment input by 50% (which increases the combined Dart and Rees sediment rate by 43%) between 120 and 250 years into the future. Figure 5.14b shows that after 130 years of increased sediment input, the shoreline had advanced by at least 50 m more than Run 1 (and the total delta area had increased by ~190 000 m^2 more than Run 1, Figure 5.19b). This implies that the increased Dart River sediment input was able to impact the entire delta shoreline. However it should be noted that increasing the sediment input of the Dart River by 50% is a much greater increase in sediment supply to the delta overall compared to a 50% increase in the Rees River sediment input (Run 6).

After 120 years, Run 8 diverted all Rees River sediment into the Dart River upstream of the grassed island. After 250 years (i.e. 130 years after diversion) there was very little difference to the shoreline, or increased area of delta progradation, when compared to Run 1 (Figures 5.15b and 5.19a). There was also no apparent difference to the shoreline after 150 years (i.e. 30 years after diversion commenced). However, it should be remembered that the grid resolution is 50 m so some shoreline differences are likely to be hidden. Figure 5.15a shows that riverbed and foreset levels in the Rees River (in the reach downstream of the diversion) are 1^+ m lower after 80 years of diversion, due to all sediment being diverted away from the Rees River.

A comparison of the Run 8 DELGROW model simulation and the Rees-Dart microscale model (Experiment B) shoreline locations (Figure 5.16) does not show a particularly good comparison between the two modelling methods in the vicinity of Glenorchy – although the total increases in delta area over time are very comparable (Figures 5.19a and 5.20). It is difficult to ascertain if this is due to the initial topography and shoreline at the time of the diversion (which would tend to favour aggradation near Glenorchy for the numerical model, and aggradation near the centre of the Dart riverbed for the microscale model, as these are the areas less prograded at the start of the diversion), or whether it is due to reasons like those mentioned above with regard to the differences with Run 6.

Run 9 examined the impact of varying the sediment supply to the Dart River to simulate a ‘slug’ of sediment being transported along the river system to the delta. This could occur as a result of a large flood, or other events within the upstream catchment (e.g. a landslide). For this scenario it was assumed that the same volume of sediment was supplied to the Dart River as was supplied by the Dart River in the base model (over any 50 year period); the difference being that there is a 10 year period where the sediment supply is increased significantly, and the sediment supply is reduced over the other 40 years (to conserved sediment volumes). Figures 5.17a and 5.19c show that after the first 50 year cycle (i.e. after the same volume of sediment has been input for both Run 9 and Run 1), changes in predicted riverbed elevations were relatively negligible (< 0.25 m) and the increase in delta area was comparable – even though, immediately after the period of high sediment input, there was temporarily an increased rate of delta area for Run 9 compared to Run 1. Over 250 years of model simulation time there are very small differences in shoreline positions (Figure 5.17b) or the total increase in delta area

(Figure 5.19c). This shows that the model is able to successfully redistribute sediment by avulsing across the riverbed - as would be expected with an active braided gravel-bed river system.

Despite the Run 9 model scenario producing negligible differences with the changing sediment supply regime, it should be noted that it is unknown whether the varying sediment supply rates are realistic. At present there is little information available on sediment supply rates for historic flood events, and future sediment supply rates can also not be predicted precisely. DELGROW can also not accurately predict whether a large sediment input event will lead to the active river channels potentially eroding the river banks and/or avulsing and finding a new flow route outside of the active riverbed. Further information on sub-aerial braided river behaviour and the feedbacks between sediment supply, flood flows, increasing lake levels and avulsion, could therefore allow the model to potentially be developed further to better simulate smaller time periods (e.g. month-to-year), and examine the effects of individual floods where avulsions have occurred.

Run 10 reduced the topset area by moving the sediment input locations (and hence the cells sediment is able to be deposited in) 1 km further downstream. Compared to Run 1, this resulted in additional topset aggradation in the Rees River and eastern portion of the Dart River, as well as along the river reach through the grassed island; some delta shoreline advance occurred downstream of these areas (i.e. near Glenorchy and the grassed island) but less delta progradation occurred in other areas. After 250 years the delta area increased by a relatively small area of ~23 000 m^2 (Figure 5.19d). Moving the sediment input locations downstream not only decreased the topset area but also changed the number of potential sediment flow paths. For example, Run 10 sediment can also pass down the eastern side of the Dart River without having to first aggrade the riverbed to the height of the elevated central portion of the Dart riverbed (as shown in Figure 3.35). It is therefore likely that a reduced topset area will have less influence on delta progradation and topset aggradation than the topography if the riverbed has significant topographic features.

Changing riverbed (or topset) slopes, both along and across the riverbed, have not been simulated by DELGROW but could be considered in future work (e.g. allowing for the change in slope that occurs for the Rees River when it travels along the more steeper western route around the grassed island onto the Dart riverbed, versus the more gently sloping riverbed of the Rees River). The threshold slope between cells, determining whether deposition will occur, could also be investigated to potentially improve the routing of flood events (e.g. incorporate sediment deposition and remobilisation).

Better quality, higher density sonar data or 3-d multibeam sonar (bathymetric) swath data may also allow a better simulation of delta foreset and lakebed deposition, and improved estimates of the volumes of sediment delivered to the delta. For example, a better understanding of the volumes of sediment retained on the delta foreset and topset, rather than removed from the delta by other

processes such as turbidity currents, is likely to improve estimates of delta progradation – especially if this could be determined for individual flood events.

5.4 Conclusions

The DELGROW numerical model developed as part of this study provides an effective tool for estimating braided gravel-bed river delta growth over the decade-to-century time scale when a braided river system enters a deep, low-energy body of water (e.g. a lake). Unlike simple 1-d width-averaged geometric models, DELGROW takes into consideration barriers (e.g. islands) as well as relatively complex converging braided river delta configurations. By changing the sediment supply, or modifying the river-delta system, the response of the river-delta system to various scenarios can be assessed both temporally and spatially. However, it would not be possible to reliably predict locations of bank erosion, or channel avulsions diverting flows and sediment outside the existing active braided channel system.

For the Rees-Dart delta, DELGROW calculated similar rates of increase in delta area as both the microscale model and Equation 4.4 over the next 150+ years (Figure 5.20) – based on the same sediment input rates. By modifying the delta geometry and the sediment characteristics (i.e. input volume, mobility and flow paths), it was observed that the greatest increases in delta area occurred when the volume of sediment input was increased or the delta foreset slope was steepened (Figures 5.19b ad 5.19d, respectively). It was also noted that delta area increased significantly as the delta foreset height (water depth) decreased (Figure 5.20, Eqn 4.4 results). These are results you would intuitively expect as a steeper foreset slope or shallower water depth require less 'filling', and a more rapid delivery of sediment to the delta will increase delta progradation.

Successful operation of the DELGROW model requires a known sediment supply rate, as well as information on the braided river and topset topography, and submerged delta foreset and lakebed bathymetry. The threshold slope can also be adjusted to ensure that the topset slope maintains a steady slope. The accuracy of the delta progradation simulated by DELGROW will be dependent on the extent of initial riverbed irregularities, and the frequency of channel avulsions. This is because DELGROW will initially use the supplied sediment to try and eliminate any irregularities, before continuing to advance and deposit sediment in a more uniform and evenly-distributed manner (similarly to that of a simple 1-d width-averaged geometric model but with the advantage of being able to account for barriers and complicated river and delta configurations). As more detailed data are acquired for braided gravel-bed rivers and deltas it will be possible to provide a more comprehensive assessment of DELGROW. DELGROW could potentially be enhanced to account for processes that often occur during individual flood events (e.g. channel avulsions beyond the active braided channel system and feedbacks between delta progradation and channel avulsions). A more sophisticated

method could also be developed to distribute the sediment across the riverbed/ delta topset and the delta foreset.

It should also be noted that, as this is a simple rule-based model rather than a high-resolution physics-based model, care must be taken when choosing the size of the model grid. The model grid size should be approximately equal to the active width of the main river channel during a flood event, since the flow route to the lakebed is only one cell wide for each sediment input. The model output should also be assessed carefully to make sure it is realistic and, where possible, historic data or physical modelling should be used in conjunction with the numerical model to provide further confidence in the scenarios modelled.

6 CONCLUSIONS AND FUTURE RESEARCH

Despite a growing interest in braided gravel-bed rivers and deltas there are still many physical processes that are not well understood - for example, how upstream aggradation and downstream backwater effects influence channel switching. As a result, the laterally-varying supply of sediment to the downstream braided gravel-bed river delta is usually difficult to predict, along with other aspects of delta growth over the decade-to-century timescale.

The relative isolation of many braided gravel-bed deltas also means that there is usually very little spatial and temporal field data to enable the growth dynamics of these systems to be studied in detail. This is complicated by the fact that a large portion of deltas are usually submerged, and most of the processes shaping both the braided gravel-bed rivers and deltas occur during flood events when it is generally most difficult to obtain useful field data. Fortunately, advances in airborne and terrestrial laser scanning (Section 2.3.1) and sonar technology (e.g. 3-d bathymetric swath mapping combining multibeam sonar and sidescan sonar) will make data-intensive field studies progressively more practical and feasible in the future. For example, it is now feasible to obtain data before and after individual flood events – although it is still difficult to obtain data *during* a flood event.

Other methods of studying braided gravel-bed river deltas include analysing historical field data and physical modelling (e.g. microscale models). In this study field data and physical microscale models have been used to simulate braided gravel-bed river delta growth over the decade-to-century timescale. The Rees-Dart microscale model was proven to be an effective tool for simulating past and future growth of a steep, gravel-bed, braided, river delta entering a deep, low-energy basin. However, successful modelling required well-defined fixed boundaries and good historical aerial photography (for the estimation of the model time scale and sediment supply rates). The Clutha delta (i.e. a complex gravel-bed river delta where the receiving basin was shallow) did appear to be beyond the capabilities of microscale modelling. For this type of gravel-bed river delta the interaction of bed load, suspended sediment load, established river channels, vegetation and/or tributary inflows are all likely to have some influence on delta deposition. In particular, microscale modelling did not appear to be suitable for situations where fine sediment (able to be transported as bedload or suspended sediment) provided a significant proportion of the deposited sediment. Therefore, despite microscale models often being able to provide valuable information on the spatial distribution of sediment deposited by gravel-bed rivers, the dissimilarity between grain size distribution and/or various other parameters (as discussed earlier in Sections 2.4.1 and 2.4.5) can limit the applicability of microscale modelling for some delta configurations.

The DELGROW numerical model developed as part of this study also provides an effective tool for estimating braided gravel-bed river delta growth over the decade-to-century time scale when a braided

river system enters a deep, low-energy body of water (e.g. a deep lake). DELGROW requires a known sediment supply rate, as well as information on the braided river topography, submerged delta foreset, and lakebed bathymetry. Unlike simple 1-d width-averaged geometric models, DELGROW takes into consideration barriers (e.g. islands) as well as relatively complex converging braided river delta configurations. By changing the sediment supply, or modifying the river system, the response of the river system to various scenarios can also be assessed both temporally and spatially. Modelling showed that the greatest increases in delta area occurred when the model sediment input increased or the delta foreset slope was steepened; delta area also increased significantly as the delta foreset height decreased (based on Equation 4.4).

The complex behaviour of a braided gravel-bed river entering a shallow body of water (e.g. Clutha River/Mata-Au delta) has not been simulated using DELGROW due to the limited field data and microscale modelling data available to calibrate or validate any model. It is therefore unknown whether this type of simple numerical model would be applicable for braided gravel-bed river deltas entering shallow lakes.

In summary, both microscale models and DELGROW appear to realistically simulate decade-to-century timescale growth of braided gravel-bed river deltas entering a deep, low-energy, receiving basin. Both of these modelling methods initially use the supplied sediment to try and eliminate any irregularities (e.g. low points), before continuing to advance and deposit sediment in a more evenly-distributed manner, whilst taking into consideration irregularities due to barriers, and asymmetric sediment sources such as merging deltas. The close agreement between the DELGROW and microscale modelling results also confirms that the microscale model time scale was scaled correctly for the Rees-Dart delta.

Unfortuately it is not possible to reliably predict locations of bank erosion, or channel avulsions diverting flows and sediment outside the existing active braided channel system, using either microscale models or DELGROW so the use of fixed boundaries must be carefully considered. Further work (and more field data) is also required to determine whether similar models can be applied effectively to braided gravel-bed river deltas forming in shallow receiving basins (e.g. a ‘drowned’ river channel).

Recent technological advances have led to improvements in flow measurement (e.g. Acoustic Doppler Current Profilers, ADCP), bed morphology (multi-beam echo sampling) and digital elevation models (e.g. Sambrook Smith et al., 2006). Ground penetrating radar (GPR) has also become an invaluable tool for studying subsurface stratigraphy in deltas and other coarse-grained deposits (Bristow et al., 2003; Jol et al., 2003; Sambrook Smith et al., 2006). As technology becomes more cost-efficient, it is expected these tools will become more widely used in braided gravel-bed river delta research. For instance, greater temporal and spatial availability of detailed digital elevation models would enable a

more detailed analysis of changes in delta profiles – especially if the data can be acquired immediately before and after flood events (e.g. Williams et al., 2011). Such data could be used to provide better estimates of sediment supply rates (i.e. to improve microscale and numerical model predictions), as well as provide information for future research on braided gravel-bed river and delta processes such as channel avulsions, bank erosion and backwater effects. Improved spatial and temporal data for the submerged delta area could also provide valuable information for future research on the behaviour of delta foreset slopes exposed to turbidity currents and various slope failure mechanisms.

Better field information for gravel-bed river deltas entering shallow receiving basins (e.g. Clutha River/Mata-Au) would allow a better assessment of whether microscale models can adequately simulate delta growth (most likely bedload deposition only) for shallow receiving basins; additional field studies may need to include sediment sampling to determine particle size distributions at various locations along the lake bed (i.e. to determine whether deposition is mainly bedload and/or suspended sediment load).

As more accurate and higher resolution data are acquired for braided gravel-bed rivers and deltas it will be possible to provide a more comprehensive assessment of the simple numerical model, DELGROW, developed as part of this study. DELGROW could potentially be enhanced to account for processes that often occur during individual flood events (e.g. channel avulsions beyond the active braided channel system and feedbacks between delta progradation and channel avulsions). A more sophisticated method could also be developed to distribute the sediment across the riverbed/ delta topset and the delta foreset.

With increased data acquisition, and further research on braided gravel-bed river delta growth dynamics (e.g. braided channel bank erosion, backwater effects, etc), it will be possible for the physically-based complex 2-d and 3-d numerical models to become more robust. However, even with numerical modelling improvements, the simulation of hydrodynamic and geomorphic processes will still include some potential sources of errors (e.g. human error) as well as continuing to require large volumes of detailed spatial and temporal data. The use of simple rule-based numerical models (e.g. DELGROW) may still provide the only solution when limited input data is available, and an indicative or relatively coarse solution is adequate. DELGROW could also be made more user-friendly so that it could be used by scientific and engineering personnel employed by local authorities, research institutes and/or engineering consultancies.

7 REFERENCES

Aqualinc. (2009). *Report No. 1 - Feasibility study summary report - Tarras Water supply (http://water.tarrasnz.com/documents/design)*.

ASCE Committee on Hydraulic Research. (1942). *Hydraulic models*. New York: American Society of Civil Engineers.

Ashmore, P. (1991a). Channel morphology and bed load pulses in braided, gravel-bed streams. *Geografiska Annaler. Series A, Physical Geography, 73*(1), 37-52.

Ashmore, P., Bertoldi, W., & Gardner, J. T. (2011). Active width of gravel-bed braided rivers. *Earth Surface Processes and Landforms, 36*(11), 1510-1521.

Ashmore, P., & Gardner, J. T. (2008). Unconfined confluences in braided rivers. In S. P. Rice, A. G. Roy & B. L. Rhoads (Eds.), *River confluences, tributaries and the fluvial network* (pp. 119-147). Chichester, England ; Hoboken, NJ: Wiley.

Ashmore, P., & Parker, G. (1983). Confluence scour in coarse braided streams. *Water Resour. Res., 19*(2), 392-402.

Ashmore, P. E. (1982). Laboratory modelling of gravel braided stream morphology. *Earth Surface Processes and Landforms, 7*(3), 201-225.

Ashmore, P. E. (1988). Bed load transport in braided gravel-bed stream models. *Earth Surface Processes and Landforms, 13*(8), 677-695.

Ashmore, P. E. (1991b). How do gravel-bed rivers braid? *Canadian Journal of Earth Sciences, 28*(3), 326-341.

Ashworth, P. J. (1996). Mid-channel bar growth and its relationship to local flow strength and direction. *Earth Surface Processes and Landforms, 21*(2), 103-123.

Ashworth, P. J., Best, J. L., & Jones, M. (2004). Relationship between sediment supply and avulsion frequency in braided rivers. *Geology, 32*(1), 21-24.

Ashworth, P. J., Best, J. L., & Jones, M. A. (2007). The relationship between channel avulsion, flow occupancy and aggradation in braided rivers: insights from an experimental model. *Sedimentology, 54*(3), 497-513.

Ashworth, P. J., & Ferguson, R. I. (1986). Interrelationships of channel processes, changes and sediments in a proglacial braided river. *Geografiska Annaler. Series A, Physical Geography, 68*(4), 361-371.

Axelsson, V. (1967). The Laitaure Delta: A study of deltaic morphology and processes. *Geografiska Annaler. Series A, Physical Geography, 49*(1), 1-127.

Bagnold, R. A. (1980). An empirical correlation of bedload transport rates in flumes and natural rivers. *Proceedings of the Royal Society of London A, 372*(1751), 453-473.

Bagnold, R. A. (1986). Transport of solids by natural water flow: evidence for a worldwide correlation. *Proceedings of the Royal Society of London A, 405*(1829), 369-374.

Barrell, D. J. A., Riddolls, B. W., Riddolls, P. M., & Thomson, R. (1994). *Surficial geology of the Wakatipu Basin, Central Otago, New Zealand* (No. 94/39): Institute of Geological & Nuclear Sciences Ltd.

Bates, C. C. (1953). Rational theory of delta formation. *American Association of Petroleum Geologists Bulletin, 37*(9), 211-262.

Beavan, J., Denys, P., Denham, M., Hager, B., Herring, T., & Molnar, P. (2010). Distribution of present-day vertical deformation across the Southern Alps, New Zealand, from 10 years of GPS data. *Geophysical Research Letters, 37*(16).

Bertoldi, W., Ashmore, P., & Tubino, M. (2009a). A method for estimating the mean bed load flux in braided rivers. *Geomorphology, 103*(3), 330-340.

Bertoldi, W., Zanoni, L., & Tubino, M. (2009b). Planform dynamics of braided streams. *Earth Surface Processes and Landforms, 34*(4), 547-557.

Bertoldi, W., Zanoni, L., & Tubino, M. (2010). Assessment of morphological changes induced by flow and flood pulses in a gravel bed braided river: The Tagliamento River (Italy). *Geomorphology, 114*(3), 348-360.

Best, J. L., & Bristow, C. S. (Eds.). (1993). *Braided rivers*. London: Geological Society.

Bishop, G., & Forsyth, J. (1988). *Vanishing ice : an introduction to glaciers based on a study of the Dart Glacier*. Dunedin, N.Z.: John McIndoe and New Zealand Geological Survey, DSIR.

Bolla Pittaluga, M., Repetto, R., & Tubino, M. (2003). Channel bifurcation in braided rivers: Equilibrium configurations and stability. *Water Resour. Res., 39*(3), 1046.

Brasington, J., & Richards, K. (2007). Reduced-complexity, physically-based geomorphological modelling for catchment and river management. *Geomorphology, 90*(3–4), 171-177.

Brasington, J., Rumsby, B. T., & McVey, R. A. (2000). Monitoring and modelling morphological change in a braided gravel-bed river using high resolution GPS-based survey. *Earth Surface Processes and Landforms, 25*(9), 973-990.

Bridge, J. (2009). Numerical modelling of alluvial deposits: Recent developments. *Analogue and Numerical Modelling of Sedimentary Systems : From Understanding to Prediction (Special Publication 40 of the IAS)*, 97-138. Retrieved from http://canterbury.eblib.com.au/patron/FullRecord.aspx?p=416355

Bristow, C. S., Jol, H. M., & Geological Society of London. (2003). *Ground penetrating radar in sediments*. London: Geological Society.

Brodie, J. W., & Irwin, J. (1970). Morphology and sedimentation in Lake Wakatipu, New Zealand. *New Zealand Journal of Marine and Freshwater Resources, 4*(4), 479-496.

Bryant, M., Falk, P., & Paola, C. (1995). Experimental study of avulsion frequency and rate of deposition. *Geology, 23*(4), 365-368.

Capart, H., Bellal, M., & Young, D.-L. (2007). Self-similar evolution of semi-infinite alluvial channels with moving boundaries. *Journal of Sedimentary Research, 77*(1), 13-22.

Cazanacli, D., Paola, C., & Parker, G. (2002). Experimental steep, braided flow: Application to flooding risk on fans. *Journal of Hydraulic Engineering, 128*(3), 322-330.

Celoria, F. (1966). Delta as a geographical concept in Greek literature. [Notes & Correspondence]. *Isis, 57*(3), 385-388.

Chang, H. H. (1982). Fluvial hydraulics of deltas and alluvial fans. *Journal of the Hydraulics Division, ASCE, 108*(HY11), 1282-1295.

Chanson, H. (2004). The hydraulics of open channel flow [electronic resource]: an introduction ; basic principles, sediment motion, hydraulic modelling, design of hydraulic structures.

Church, M., Wolcott, J. F., & Fletcher, W. K. (1991). A test of equal mobility in fluvial sediment transport: behavior of the sand fraction. *Water Resour. Res., 27*(11), 2941-2951.

Clarke, L., Quine, T. A., & Nicholas, A. (2010). An experimental investigation of autogenic behaviour during alluvial fan evolution. *Geomorphology, 115*(3–4), 278-285.

Clausen, B., & Plew, D. (2004). How high are bed-moving flows in New Zealand rivers? *Journal of Hydrology (NZ), 43*(1), 19-37.

Colella, A., & Prior, D. B. (Eds.). (1990). *Coarse-grained deltas*. Oxford ; Boston: Blackwell Scientific Publications.

Coleman, J. M. (1976). *Deltas: processes of deposition & models for exploration*. Champaign, Ill.: Continuing Education Publication Co.

Coleman, J. M. (1988). Dynamic changes and processes in the Mississippi River delta. *Geological Society of America Bulletin, 100*(7), 999-1015.

Coleman, J. M., & Wright, L. D. (1975). Modern river deltas: variability of processes and sand bodies. In M. L. Broussard, Houston Geological Society. Research and Study Group. & Gulf-Coast Association of Geological Societies. (Eds.), *Deltas: models for exploration* (pp. 99-149). [Houston, Tex.]: Houston Geological Society.

Connell, S. D. (2010). *Fluvial sedimentation in continental half-graben basins.* Unpublished PhD thesis, The University of New Mexico, New Mexico.

Coulthard, T. J., Kirkby, M. J., & Macklin, M. G. (2000). Modelling geomorphic response to environmental change in an upland catchment. *Hydrological Processes, 14*(11-12), 2031-2045.

Coulthard, T. J., Macklin, M. G., & Kirkby, M. J. (2002). A cellular model of Holocene upland river basin and alluvial fan evolution. *Earth Surface Processes and Landforms, 27*(3), 269-288.

Credner, G. R. (1878). *Die deltas, ihre morphologie, geographische verbreitung und entstehungs-bedingungen*. Gotha: J. Perthes.

Crosato, A., & Saleh, M. S. (2011). Numerical study on the effects of floodplain vegetation on river planform style. *Earth Surface Processes and Landforms, 36*(6), 711-720.

Cui, Y., Parker, G., Pizzuto, J., & Lisle, T. E. (2003). Sediment pulses in mountain rivers: 2. Comparison between experiments and numerical predictions. *Water Resources Research, 39*(9), 41-411.

Dan, S., Walstra, D.-J. R., Stive, M. J. F., & Panin, N. (2011). Processes controlling the development of a river mouth spit. *Marine Geology, 280*(1–4), 116-129.

Darboux, F., & Huang, C.-h. (2003). An instantaneous-profile laser scanner to measure soil surface microtopography. *Soil Science Society of America Journal, 67*(1), 92-99.

Davies, G. H. (1922). *A complete guide to the scenic beauties of Lake Wakatipu, New Zealand : the Switzerland of the Southern hemisphere.* Dunedin: Coulls, Somerville, Wilkie, printers.

Davies, T. R. (2007). *Shotover river sediment management: microscale modelling*. Department of Geological Sciences, University of Canterbury, NZ: Prepared for Otago Regional Council, Dunedin, NZ.

Davies, T. R., & Lee, A. L. (1988). Physical hydraulic modelling of width reduction and bed level change in braided rivers. *Journal of Hydrology (NZ), 27*(2), 113-127.

Davies, T. R., & McSaveney, M. J. (2006). Geomorphic constraints on the management of bedload-dominated rivers. *Journal of Hydrology (NZ), 45*(2), 111-130.

Davies, T. R. H. (1987). Problems of bed-load transport in braided gravel-bed rivers. In C. R. Thorne, J. C. Bathurst & R. D. Hey (Eds.), *Sediment transport in gravel-bed rivers* (pp. 793-828). Chichester, UK: John Wiley & Sons.

Davies, T. R. H., & Korup, O. (2007). Persistent alluvial fanhead trenching resulting from large, infrequent sediment inputs. *Earth Surface Processes and Landforms, 32*(5), 725-742.

Davies, T. R. H., McSaveney, M. J., & Clarkson, P. J. (2003). Anthropic aggradation of the Waiho River, Westland, New Zealand: microscale modelling. *Earth Surface Processes and Landforms, 28*(2), 209-218.

Department of Conservation. (1992). *Bendigo wildlife area management strategy*: Report for ECNZ Ltd.

Deverell, W. (Cartographer). (1904). *Lake Wakatipu and Surrounding Country, Middle Island New Zealand*.

Devgun, M. S., & Bowler, J. M. (1999). *Clutha River catchment hydrological overview*: Contact Energy Ltd.

Eaton, B. C., & Lapointe, M. F. (2001). Effects of large floods on sediment transport and reach morphology in the cobble-bed Sainte Marguerite River. *Geomorphology, 40*(3–4), 291-309.

Edmonds, D. A. (2009). *The growth and evolution of river-dominated deltas and their distributary networks.* Unpublished PhD thesis, The Pennsylvania State University, Pennsylvania.

Edmonds, D. A., & Slingerland, R. L. (2007). Mechanics of river mouth bar formation: Implications for the morphodynamics of delta distributary networks. *J. Geophys. Res., 112*(F2), F02034.

Egozi, R., & Ashmore, P. (2009). Experimental analysis of braided channel pattern response to increased discharge. *J. Geophys. Res., 114*(F2), F02012.

Elliot, T. (1986). Deltas. In H. G. Reading (Ed.), *Sedimentary environments and facies* (2nd. ed., pp. 113-154). Oxford: Blackwood Scientific.

Fagherazzi, S., & Overeem, I. (2007). Models of deltaic and inner continental shelf landform evolution. *Annual Review of Earth and Planetary Sciences, 35*, 685-715.

Fahnestock, R. K. (1963). Morphology and hydrology of a glacial stream - White River, Mount Rainier, Washington. *U.S. Geological Survey Professional Paper, 422-A*, 70pp.

Ferguson, R. (1987). Hydraulic and sedimentary controls of channel pattern. In K. Richards (Ed.), *River channels: environment and process* (pp. 129-158). Oxford: Blackwell.

Ferguson, R. I., Ashmore, P. E., Ashworth, P. J., Paola, C., & Prestegaard, K. L. (1992). Measurements in a braided river chute and lobe: 1. Flow pattern, sediment transport, and channel change. *Water Resour. Res., 28*(7), 1877-1886.

Fielding, C. R. (2010). Planform and facies variability in asymmetric deltas: Facies analysis and depositional architecture of the Turonian Ferron Sandstone in the Western Henry Mountains, south-central Utah, U.S.A. *Journal of Sedimentary Research, 80*(5), 455-479.

Freestone, H. J., & Payne, D. (2000). *Clutha hydro lakes operating regimes*: Report for Contact Energy Ltd., Opus International Consultants, Wellington.

Gaines, R. A., & Maynord, S. T. (2001). Microscale loose-bed hydraulic models. *Journal of Hydraulic Engineering, 127*(5), 335-338.

Gaines, R. A., & Smith, R. H. (2002). Micro-scale loose-bed physical models. In T. L. Wahl, American Society of Civil Engineers, International Association for Hydraulic Research & Environmental and Water Resources Institute (U.S.) (Eds.), *Hydraulic measurements & experimental methods, 2002* (pp. CD-ROM). Reston, Va.: ASCE.

Galloway, W. E. (1975). Process framework for describing the morphologic and stratigraphic evolution of deltaic depositional systems. In M. L. Broussard, Houston Geological Society. Research and Study Group. & Gulf-Coast Association of Geological Societies. (Eds.), *Deltas: models for exploration* (pp. 87-98). [Houston, Tex.]: Houston Geological Society.

Gao, S. (2007). Modeling the growth limit of the Changjiang Delta. *Geomorphology, 85*(3–4), 225-236.

Geleynse, N., Storms, J. E. A., Walstra, D.-J. R., Jagers, H. R. A., Wang, Z. B., & Stive, M. J. F. (2011). Controls on river delta formation; insights from numerical modelling. *Earth and Planetary Science Letters, 302*(1–2), 217-226.

Gerber, T. P., Pratson, L. F., Wolinsky, M. A., Steel, R., Mohr, J., Swenson, J. B., et al. (2008). Clinoform progradation by turbidity currents: Modeling and experiments. *Journal of Sedimentary Research, 78*(3), 220-238.

Gilbert, G. K. (1885). The topographic features of lake shores *U.S. Geological Survey Annual Report no. 5* (pp. 75-123).

Gilbert, G. K. (1890). Lake Bonneville *Monograph - U.S. Geological Survey, Report M 0001* (pp. 438).

Gilbert, R. (1973). *Observations of lacustrine sedimentation at Lillooet Lake, British Columbia.* Unpublished PhD thesis, The University of British Columbia, Vancouver, Canada.

Gilbert, R. (1975). Sedimentation in Lillooet Lake, British Columbia. *Canadian Journal of Earth Sciences, 12*(10), 1697-1711.

Gilvear, D. J. (2004). Patterns of channel adjustment to impoundment of the upper River Spey, Scotland (1942–2000). *River Research and Applications, 20*(2), 151-165.

Girardclos, S., Schmidt, O. T., Sturm, M., Ariztegui, D., Pugin, A., & Anselmetti, F. S. (2007). The 1996 AD delta collapse and large turbidite in Lake Brienz. *Marine Geology, 241*(1–4), 137-154.

Goff, J. R., & Ashmore, P. (1994). Gravel transport and morphological change in braided Sunwapta River, Alberta, Canada. *Earth Surface Processes and Landforms, 19*(3), 195-212.

Gomez, B., & Church, M. (1989). An assessment of bed load sediment transport formulae for gravel bed rivers. *Water Resour. Res., 25*(6), 1161-1186.

Graf, W. H. (1971). *Hydraulics of sediment transport*: New York : McGraw-Hill.

Grant, G. E. (1997). Critical flow constrains flow hydraulics in mobile-bed streams: A new hypothesis. *Water Resour. Res., 33*(2), 349-358.

Hajek, E. A., & Wolinsky, M. A. (2011). Simplified process modeling of river avulsion and alluvial architecture: Connecting models and field data. *Sedimentary Geology*(accepted manuscript).

Heath, R. A. (1975). Surface oscillations of Lake Wakatipu, New Zealand. *New Zealand Journal of Marine and Freshwater Resources, 9*(2), 223-238.

Hey, R. D., & Thorne, C. R. (1986). Stable channels with mobile gravel beds. *Journal of Hydraulic Engineering, 112*(8), 671-689.

Hickin, E. J. (1989). Contemporary Squamish River sediment flux to Howe Island, British Columbia. *Canadian Journal of Earth Sciences, 26*( ), 1953-1963.

Hicks, D. M., Duncan, M. J., Walsh, J. M., Westaway, R. M., & Lane, S. N. (2002). New views of the morphodynamcis of large braided rivers from high-resolution topographic surveys and time-lapse video *The structure, function and management implications of fluvial systems (Proceedings of an international symposium held at Alice Springs, Australia, September 2002)* (IAHS Red Publ. no. 276 ed., Vol. IAHS Publ. 276, pp. 373-380): IAHS Publ. 276.

Hicks, D. M., Shankar, U., McKerchar, A. I., Basher, L., Lynn, I., Page, M., et al. (2011). Suspended sediment yields from New Zealand rivers *Journal of Hydrology (NZ), 50*(1), 81-142.

Hicks, D. M., Walsh, J. M., & Duncan, M. J. (2000). *Clutha River sediment budget. Report prepared for Contact Energy Ltd.* Christchurch: NIWA.

Hodge, R., Richards, K., & Brasington, J. (2007). A physically-based bedload transport model developed for 3-D reach-scale cellular modelling. *Geomorphology, 90*(3–4), 244-262.

Hoey, T. B., & Sutherland, A. J. (1991). Channel morphology and bedload pulses in braided rivers: a laboratory study. *Earth Surface Processes and Landforms, 16*(5), 447-462.

Hong, L. B., & Davies, T. R. H. (1979). A study of stream braiding: Summary. *Geological Society of America Bulletin, 90*(12), 1094-1095.

Hooke, R. L. (1967). Processes on arid-region alluvial fans. *The Journal of Geology, 75*(4), 438-460.

Hooke, R. L. (1968a). Model geology: Prototype and laboratory streams: Discussion. *Geological Society of America Bulletin, 79*(3), 391-394.

Hooke, R. L. (1968b). Steady-state relationships on arid-region alluvial fans in closed basins. *American Journal of Science, 266*(8), 609-629.

Hoyal, D. C. J. D., & Sheets, B. A. (2009). Morphodynamic evolution of experimental cohesive deltas. *J. Geophys. Res., 114*(F2), F02009.

Irwin, J. (1980). Sublacustrine channels in Lake Wanaka. *New Zealand Journal of Marine and Freshwater Research, 14*(1), 87-92.

Jerolmack, D. J., & Paola, C. (2010). Shredding of environmental signals by sediment transport. *Geophys. Res. Lett., 37*(19).

Johnston, W. A. (1921). *Sedimentation of the Fraser river delta*. Ottawa: T. Mulvey, printer.

Jol, H. M., Lawton, D. C., & Smith, D. G. (2003). Ground penetrating radar: 2-D and 3-D subsurface imaging of a coastal barrier spit, Long Beach, WA, USA. *Geomorphology, 53*(1-2), 165-181.

Jopling, A. V. (1965). Hydraulic factors controlling the shape of laminae in laboratory deltas. *Journal of Sedimentary Petrology, 35*(4), 777-791.

Jowett, I. G., & Hicks, D. M. (1981). Surface, suspended and bedload sediment - Clutha river system. *Journal of Hydrology (NZ), 20*(2), 121-130.

Kenyon, P. M., & Turcotte, D. L. (1985). Morphology of a delta prograding by bulk sediment transport. *Geological Society of America Bulletin, 96*(11), 1457-1465.

Kim, W., Connell, S. D., Steel, E., Smith, G. A., & Paola, C. (2011). Mass-balance control on the interaction of axial and transverse channel systems. *Geology, 39*(7), 611-614.

Kim, W., & Muto, T. (2007). Autogenic response of alluvial-bedrock transition to base-level variation: Experiment and theory. *Journal of Geophysical Research, 112*(F3), F03S14.

Kim, W., & Paola, C. (2007). Long-period cyclic sedimentation with constant tectonic forcing in an experimental relay ramp. *Geology, 35*(4), 331-334.

Kim, W., Paola, C., Swenson, J. B., & Voller, V. R. (2006). Shoreline response to autogenic processes of sediment storage and release in the fluvial system. *Journal of Geophysical Research, 111*(F4), F04013.

Kleinhans, M. (2010). Sorting out river channel patterns. *Progress in Physical Geography, 34*(3), 287.

Kleinhans, M. G. (2005a). Autogenic cyclicity of foreset sorting in experimental Gilbert-type deltas. *Sedimentary Geology, 181*(3-4), 215-224.

Kleinhans, M. G. (2005b). Grain-size sorting in grainflows at the lee side of deltas. *Sedimentology, 52*(2), 291-311.

Kleinhans, M. G., Ferguson, R. I., Lane, S. N., & Hardy, R. J. (2013). Splitting rivers at their seams: bifurcations and avulsion. *Earth Surface Processes and Landforms, 38*(1), 47-61.

Kleinhans, M. G., & van den Berg, J. H. (2011). River channel and bar patterns explained and predicted by an empirical and a physics-based method. *Earth Surface Processes and Landforms, 36*(6), 721-738.

Knighton, D. (1998). *Fluvial forms and processes: A new perspective*: London: Arnold; New York: J. Wiley.

Komar, P. D. (1973). Computer models of delta growth due to sediment input from rivers and longshore transport. *Geological Society of America Bulletin, 84*(7), 2217-2226.

Koss, J. E., Ethridge, F. G., & Schumm, S. A. (1994). An experimental study of the effects of base-level change on fluvial, coastal plain and shelf systems. *Journal of Sedimentary Research, 64*(2b), 90-98.

Kostaschuk, R. A. (1985). River mouth processes in a fjord-delta, British Columbia, Canada. *Marine Geology, 69*(1-2), 1-23.

Kostic, S., & Parker, G. (2003a). Progradational sand-mud deltas in lakes and reservoirs; Part 1, Theory and numerical modeling. *Journal of Hydraulic Research, 41*(2), 127-140.

Kostic, S., & Parker, G. (2003b). Progradational sand-mud deltas in lakes and reservoirs; Part 2, Experimental and numerical simulation. *Journal of Hydraulic Research, 41*(2), 141-152.

Kostic, S., Parker, G., & Marr, J. G. (2002). Role of turbidity currents in setting the foreset slope of clinoforms prograding into standing fresh water. *Journal of Sedimentary Research, 72*(3), 353-362.

Kubo, Y. s., Syvitski, J. P. M., Hutton, E. W. H., & Paola, C. (2005). Advance and application of the stratigraphic simulation model 2D-SedFlux: From tank experiment to geological scale simulation. *Sedimentary Geology, 178*(3-4), 187-195.

Lai, S. Y. J., & Capart, H. (2007). Two-diffusion description of hyperpycnal deltas. *Journal of Geophysical Research, 112*(F3), F03005.

Lai, S. Y. J., & Capart, H. (2009). Reservoir infill by hyperpycnal deltas over bedrock. *Geophys. Res. Lett., 36*(8), L08402.

Landward Management Ltd. (2009). *LINZ Annual Report: Unalienated crown land weed control, Otago Region, Financial Year 2008-2009*.

Lane, S. N., Westaway, R. M., & Murray Hicks, D. (2003). Estimation of erosion and deposition volumes in a large, gravel-bed, braided river using synoptic remote sensing. *Earth Surface Processes and Landforms, 28*(3), 249-271.

Le Blanc, R. J. (1975). Significant studies of modern and ancient deltaic sediments. In M. L. Broussard, Houston Geological Society. Research and Study Group. & Gulf-Coast Association of Geological Societies. (Eds.), *Deltas: models for exploration* (pp. 13-86). [Houston, Tex.]: Houston Geological Society.

Legleiter, C. J. (2011). Remote measurement of river morphology via fusion of LiDAR topography and spectrally based bathymetry. *Earth Surface Processes and Landforms*.

Leopold, L. B., & Maddock, T. (1953). The hydraulic geometry of stream channels and some physiographic implications. *U.S. Geological Survey Professional Paper, 252*.

Leopold, L. B., & Wolman, M. G. (1957). River channel patterns: Braided, meandering and straight. *U.S. Geological Survey Professional Paper, 282-B*.

Lesser, G. R., Roelvink, J. A., van Kester, J. A. T. M., & Stelling, G. S. (2004). Development and validation of a three-dimensional morphological model. *Coastal Engineering, 51*(8-9), 883-915.

Lindsay, J. F., Prior, D. B., & Coleman, J. M. (1984). Distributary-mouth development and role of submarine landslides in delta growth, South Pass, Mississippi Delta. *American Association of Petroleum Geologists -- Bulletin, 68*(11), 1732-1743.

Malverti, L., Lajeunesse, E., & Métivier, F. (2008). Small is beautiful: Upscaling from microscale laminar to natural turbulent rivers. *J. Geophys. Res., 113*(F4), F04004.

Martin, Y., & Church, M. (2000). Re-examination of Bagnold's empirical bedload -formulae. *Earth Surface Processes and Landforms, 25*(9), 1011-1024.

Max, D. W., Gordon, D. C., & Gaines, R. A. (2002). Operation and calibration procedures for micro-models. In T. L. Wahl, American Society of Civil Engineers, International Association for Hydraulic Research & Environmental and Water Resources Institute (U.S.) (Eds.), *Hydraulic measurements & experimental methods, 2002* (pp. CD-ROM). Reston, Va.: ASCE.

Maynord, S. T. (2006). Evaluation of the micromodel: an extremely small-scale movable bed model. *Journal of Hydraulic Engineering, 132*(4), 343-353.

McColl, S. T., & Davies, T. R. (2011). Evidence for a rock-avalanche origin for 'The Hillocks' "moraine", Otago, New Zealand. *Geomorphology, 127*(3-4), 216-224.

McKenzie, D. (1973). *Road to Routeburn : the story of Kinloch, Lake Wakatipu* Dunedin: John McIndoe Ltd.

McMillan, H. K., & Brasington, J. (2007). Reduced complexity strategies for modelling urban floodplain inundation. *Geomorphology, 90*(3–4), 226-243.

McSaveney, M. J., & Glassey, P. J. (2002). *The fatal Cleft Peak debris flow of 3 January 2002, Upper Rees Valley, West Otago*. Institute of Geological & Nuclear Sciences, Lower Hutt, NZ.

Meyer, R. J. (1980). *All aboard : The ships and trains that served Lake Wakatipu* (2nd ed.): New Zealand Railway and Locomotive Society, Wellington.

Milana, J. P., & Tietze, K.-W. (2002). Three-dimensional analogue modelling of an alluvial basin margin affected by hydrological cycles: processes and resulting depositional sequences. *Basin Research, 14*(3), 237-264.

Ministry of Works and Development. (1976). *Clutha Power Development: Siltation of hydro-electric lakes*. Wellington: Ministry of Works and Development.

Ministry of Works and Development. (1977a). *Clutha Valley Development: environmental impact report on design and construction proposals*. Wellington: Ministry of Works and Development.

Ministry of Works and Development. (1977b). *Shotover River catchment report on sediment sources survey and feasibility of control 1975*. Wellington: Ministry of Works and Development.

Mojzisek, J. (2005). *Precipitation variability in the South Island of New Zealand.* Unpublished Dissertation/Thesis, University of Otago. Department of Geography.

Moreton, D. J., Ashworth, P. J., & Best, J. L. (2002). The physical scale modelling of braided alluvial architecture and estimation of subsurface permeability. *Basin Research, 14*(3), 265-285.

Mosley, M. P. (1976). An experimental study of channel confluences. *The Journal of Geology, 84*(5), 535-562.

Mosley, M. P. (1982). Analysis of the effect of changing discharge on channel morphology and instream uses in a braided river, Ohau River, New Zealand. *Water Resour. Res., 18*(4), 800-812.

Mosley, M. P. (1983). Response of braided rivers to changing discharge. *Journal of Hydrology (NZ), 22*(1), 18-67.

Mosley, M. P. (1984). Response of the Ohau river and delta to lake level lowering. *Earth Surface Processes and Landforms, 9*(2), 181-187.

Mosley, M. P., & Zimpfer, G. L. (1978). Hardware models in geomorphology. *Progress in Physical Geography, 2*(3), 438-461.

Muir & Moodie Dunedin. (1904). *The Cold lakes of the South Island : Wakatipu and Wanaka*. Dunedin: Muir & Moodie.

Murray, A. B., & Paola, C. (1994). A cellular model of braided rivers. *Nature, 371*(Sep 1), 54-57.

Murray, A. B., & Paola, C. (1997). Properties of a cellular braided-stream model. *Earth Surface Processes and Landforms, 22*(11), 1001-1025.

Muto, T. (2001). Shoreline autoretreat substantiated in flume experiments. *Journal of Sedimentary Research, 71*(2), 246-254.

Muto, T., & Swenson, J. B. (2005). Large-scale fluvial grade as a nonequilibrium state in linked depositional systems: Theory and experiment. *J. Geophys. Res., 110*(F3), F03002.

Nemec, W. (1990). Aspects of sediment movement on steep delta slopes. In A. Colella & D. B. Prior (Eds.), *Coarse-grained deltas* (Vol. 10, pp. 29-73). Oxford: Blackwell Scientific Publications.

Nemec, W., & Steel, R. J. (Eds.). (1988). *Fan deltas : sedimentology and tectonic settings*. Glasgow: Blackie.

Nicholas, A. P. (2009). Reduced-complexity flow routing models for sinuous single-thread channels: intercomparison with a physically-based shallow-water equation model. *Earth Surface Processes and Landforms, 34*(5), 641-653.

Novak, P., & Cabelka, J. (1981). *Models in hydraulic engineering : physical principles and design applications*. Boston: Pitman.

Olariu, C., & Bhattacharya, J. P. (2006). Terminal distributary channels and delta front architecture of river-dominated delta systems. *Journal of Sedimentary Research, 76*(2), 212-233.

Opus. (2000). *Clutha hydro lakes cross-sections: survey and analysis, volume 1. Contact Energy study brief CLU#10.* Wellington: Opus.

Orton, G. J., & Reading, H. G. (1993). Variability of deltaic processes in terms of sediment supply, with particular emphasis on grain size. *Sedimentology, 40*(3), 475-512.

Otago Catchment Board. (1985). Rees River flood protection: G. Thomson and Lake County Council, extends proposal E.84/198.

Otago Catchment Board. (1987). Rees River - Bank protection - G. Thomson and Queenstown Lakes District Council.

Otago Regional Council. (1990). Rees River - Bank protection - G. Thomson.

Otago Regional Council. (1999). Floodbank at Glenorchy: Application for special assistance.

Otago Regional Council. (2002). *Otago Regional Council staff recommending report 2002/428, Contact Energy application 2001.383 - 2001.399 and 2002.416*. Dunedin, NZ.

Otago Regional Council. (2007). *The water resources of the Cardrona River*: Otago Regional Council, Dunedin, NZ.

Otago Regional Council. (2008a). *Channel morphology and sedimentation in the Rees River*: Otago Regional Council, Dunedin, NZ.

Otago Regional Council. (2008b). *Management flows for aquatic ecosystems in the Lindis River*: Otago Regional Council, Dunedin, NZ.

Otago Regional Council. (2010). *Natural hazards at Glenorchy*: Otago Regional Council, Dunedin, NZ.

Overeem, I., Syvitski, J. P. M., & Hutton, E. W. H. (2005). Three-dimensional numerical modeling of deltas. In J. P. Bhattacharya & L. Giosan (Eds.), *River Deltas: Concepts, Models and Examples, SEPM Special Publication* (Vol. 83, pp. 13-30). Tulsa, OK: SEPM.

Paine, D. P., & Kiser, J. D. (2012). Aerial Photography and Image Interpretation Available from http://canterbury.eblib.com.au/patron/FullRecord.aspx?p=817321

Paine, S. (2009). *Bendigo Wildlife Reserve: Assessment of cross-sections and sediment management*: Report for Contact Energy Ltd., Opus International Consultants, Wellington.

Paola, C. (1976). Incoherent structure: Turbulence as a metaphor for stream braiding. In P. J. Ashworth, S. J. Bennett, J. L. Best & S. J. McLelland (Eds.), *Coherent flow structures in open channel* (pp. 705-723). Chichester: Wiley.

Paola, C. (2000). Quantitative models of sedimentary basin filling. *Sedimentology, 47*(s1), 121-178.

Paola, C., Straub, K., Mohrig, D., & Reinhardt, L. (2009). The "unreasonable effectiveness" of stratigraphic and geomorphic experiments. *Earth-Science Reviews, 97*(1-4), 1-43.

Papatheodorou, G., & Ferentinos, G. (1997). Submarine and coastal sediment failure triggered by the 1995, Ms = 6.1 R Aegion earthquake, Gulf of Corinth, Greece. *Marine Geology, 137*(3–4), 287-304.

Parker, G. (1976). On the cause and characteristic scales of meandering and braiding in rivers. *Journal of Fluid Mechanics, 76*(3), 457-480.

Parker, G. (1979). Hydraulic geometry of active gravel rivers. *Journal of the Hydraulics Division, ASCE, 105*(HY9), 1185-1201.

Parker, G. (2005). 1D sediment transport morphodynamics with applications to rivers and turbidity currents *Chapter 34:Morphodynamics of rivers ending in 1D deltas* *http://hydrolab.illinois.edu/people/parkerg//morphodynamics_e-book.htm*.

Parker, G., Paola, C., Whipple, K. X., & Mohrig, D. (1998). Alluvial fans formed by channelized fluvial and sheet flow. I: Theory. *Journal of Hydraulic Engineering, 124*(10), 985-995.

Passalacqua, P., Porté-Agel, F., Foufoula-Georgiou, E., & Paola, C. (2006). Application of dynamic subgrid-scale concepts from large-eddy simulation to modeling landscape evolution. *Water Resour. Res., 42*(6), W06D11.

Peakall, J., Ashworth, P., & Best, J. (1996). Physical modelling of geomorphology: Principles, applications, and unresolved issues. In B. Rhoads & C. Thorn (Eds.), *The scientific nature of geomorphology* (pp. 221-253). Chichester ; New York: Wiley.

Peakall, J., & Warburton, J. (1996). Surface tension in small hydraulic river models - the significance of the Weber number. *Journal of Hydrology (NZ), 35*(2), 199-212.

Pelpola, C. P., & Hickin, E. J. (2004). Long-term bed load transport rate based on aerial-photo and ground penetrating radar surveys of fan-delta growth, Coast Mountains, British Columbia. *Geomorphology, 57*(3-4), 169-181.

Pickrill, R. A. (1987). *Sedimentation problems and management implications in hydro-electric storage lakes of South Island, New Zealand.* Paper presented at the 8th Australasian Conference on Coastal and Ocean Engineering, Launceston.

Pickrill, R. A., & Irwin, J. (1982). Predominant headwater inflow and its control of lake-river interactions in Lake Wakatipu. *New Zealand Journal of Marine and Freshwater Research, 16*(2), 201-213.

Pickrill, R. A., & Irwin, J. (1983). Sedimentation in a deep glacier-fed lake - Lake Tekapo, New Zealand. *Sedimentology, 30*, 63-75.

Pickup, G., & Higgins, R. J. (1979). Estimating sediment transport in a braided gravel channel - the Kawerong River, Bougainville, Papua New Guinea. *Journal of Hydrology, 40*(3-4), 283-297.

Postma, G. (1990). Depositional architecture and facies of river and fan deltas: a synthesis. In A. Colella & D. B. Prior (Eds.), *Coarse-grained deltas* (Vol. 10, pp. 13-28). Oxford: Blackwell Scientific Publications.

Postma, G., Babic, L., Zupanic, J., & Roe, S.-L. (1988). Delta-front failure and associated bottomset deformation in a marine, gravelly Gilbert-type fan delta. In W. Nemec & R. J. Steel (Eds.), *Fan Deltas: Sedimentology and Tectonic Settings* (pp. 91-102). Glasgow: Blackie and Son Ltd.

Postma, G., Kleinhans, M. G., Meijer, P. T., & Eggenhuisen, J. T. (2008). Sediment transport in analogue flume models compared with real-world sedimentary systems: a new look at scaling evolution of sedimentary systems in a flume. *Sedimentology, 55*(6), 1541-1557.

Poyck, S., Hendrikx, J., McMillan, H., Hreinsson, E. O., & Woods, R. (2011). Combined snow and streamflow modelling to estimate impacts of climate change on water resources in the Clutha River, New Zealand *Journal of Hydrology (NZ), 50*(2), 293-312.

Prior, D. B., & Bornhold, B. D. (1988). Submarine morphology and processes of fjord fan deltas and related high-gradient systems: modern examples from British Columbia. In W. Nemec & R. J. Steel (Eds.), *Fan Deltas: Sedimentology and Tectonic Settings* (pp. 125-143). Glasgow: Blackie and Son Ltd.

Reitz, M. D., Jerolmack, D. J., & Swenson, J. B. (2010). Flooding and flow path selection on alluvial fans and deltas. *Geophys. Res. Lett., 37*(6), L06401.

Rhoades, D. A., & Van Dissen, R. J. (2003). Estimates of the time-varying hazard of rupture of the Alpine Fault, New Zealand, allowing for uncertainties. *New Zealand Journal of Geology and Geophysics, 46*, 479-488.

Richardson, W. R., & Thorne, C. R. (2001). Multiple thread flow and channel bifurcation in a braided river: Brahmaputra-Jamuna River, Bangladesh. *Geomorphology, 38*(3-4), 185-196.

Robert, A. (2003). *River processes: An introduction to fluvial dynamics*: London: Arnold.

Rojas, E., & Le Roux, J. P. (2005). Sedimentary processes on a Gilbert-type delta in Lake Llanquihue, southern Chile. [Article]. *Revista Geologica De Chile, 32*(1), 19-31.

Rosatti, G. (2002). Validation of the physical modeling approach for braided rivers. *Water Resour. Res., 38*(12), 1295.

Sambrook Smith, G., Best, J., Bristow, C., & Petts, G. (2006). Braided rivers : Where have we come in 10 years? Progress and future needs. In G. H. Sambrook Smith, J. L. Best, C. S. Bristow & G. E. Petts (Eds.), *Braided rivers : process, deposits, ecology, and management* (pp. 1-10). Malden, Mass: Blackwell Pub.

Schumm, S. A., Mosley, M. P., & Weaver, W. E. (1987). *Experimental fluvial geomorphology*: New York: Wiley.

Schwab, J. W. (1999) Tsunamis on Troitsa Lake. *Extension Note 35, Forest Sciences* (pp. 4): Forest Service, Smithers, BC.

Seybold, H., Andrade (Jr), J. S., & Herrmann, H. J. (2007). Modeling river delta formation. *Proceedings of the National Academy of Sciences, 104*(43), 16804-16809.

Seybold, H. J., Molnar, P., Singer, H. M., Andrade, J. S., Jr., Herrmann, H. J., & Kinzelbach, W. (2009). Simulation of birdfoot delta formation with application to the Mississippi Delta. *Journal of Geophysical Research, 114*(F3), F03012.

Sheets, B. A., Hickson, T. A., & Paola, C. (2002). Assembling the stratigraphic record: depositional patterns and time-scales in an experimental alluvial basin. *Basin Research, 14*(3), 287-301.

Slingerland, R., & Smith, N. D. (2004). River avulsions and their deposits. [Review]. *Annual Review of Earth and Planetary Sciences, 32*, 257-285.

Smith, A. L. (1909). Delta experiments. *Bulletin of the American Geographical Society, 41*(12), 729-742.

Smith, M., Vericat, D., & Gibbins, C. (2011). Through-water terrestrial laser scanning of gravel beds at the patch scale. *Earth Surface Processes and Landforms*.

Sohn, Y. K., Kim, S. B., Hwang, I. G., Bahk, J. J., Choe, M. Y., & Chough, S. K. (1997). Characteristics and depositional processes of large-scale gravelly Gilbert-type foresets in the Miocene Doumsan fan delta, Pohang Basin, SE Korea. *Journal of Sedimentary Research, 67*(1), 130-141.

Southard, J. B., Smith, N. D., & Kuhnle, R. A. (1984). Chutes and lobes: Newly identified elements of braiding in shallow gravelly streams. In E. H. Koster & R. J. Steel (Eds.), *Sedimentology of gravels and conglomerates* (pp. 51-59). Calgary, Canada: Canadian Society of Petroleum Geologists Memoir 10.

Srinivasan, M. S., McDowell, R. W., Hunt, C., & Stevenson, P. (2007). Selecting curve numbers for predicting storm flow in Otago catchments. *Journal of Hydrology (NZ), 46*(2), 91-104.

Stewart, R. E. (1992). *Flood management and the Bendigo Wildlife Area*: Report for ECNZ Ltd., Works Consultancy Services.

Storms, J. E. A. (2003). Event-based stratigraphic simulation of wave-dominated shallow-marine environments. *Marine Geology, 199*(1–2), 83-100.

Suggate, R. P. (1990). Late Pliocene and Quaternary glaciations of New Zealand. *Quaternary Science Reviews, 9*, 175-197.

Sun, T., Paola, C., Parker, G., & Meakin, P. (2002). Fluvial fan deltas: Linking channel processes with large-scale morphodynamics. *Water Resour. Res., 38*(8), 261-2610.

Swenson, J. B., Paola, C., Pratson, L., Voller, V. R., & Murray, A. B. (2005). Fluvial and marine controls on combined subaerial and subaqueous delta progradation: Morphodynamic modeling of compound-clinoform development. *Journal of Geophysical Research, 110*(F2), F02013.

Swenson, J. B., Voller, V. R., Paola, C., Parker, G., & Marr, J. G. (2000). Fluvio-deltaic sedimentation: A generalized Stefan problem. *European Journal of Applied Mathematics, 11*(5), 433-452.

Syvitski, J. P. M., & Daughney, S. (1992). Delta2: Delta progradation and basin filling. *Computers & Geosciences, 18*(7), 839-897.

Syvitski, J. P. M., & Farrow, G. E. (1983). Structures and processes in bayhead deltas: Knight and Bute inlet, British Columbia. *Sedimentary Geology, 36*(2-4), 217-244.

Syvitski, J. P. M., & Hutton, E. W. H. (2001). 2D SEDFLUX 1.0C: An advanced process-response numerical model for the fill of marine sedimentary basins. *Computers & Geosciences, 27*(6), 731-753.

Syvitski, J. P. M., Smith, J. N., Calabrese, E. A., & Boudreau, B. P. (1988). Basin sedimentation and the growth of prograding deltas. *Journal of Geophysical Research, 93*(C6), 6895-6908.

Tal, M., & Paola, C. (2010). Effects of vegetation on channel morphodynamics: Results and insights from laboratory experiments. *Earth Surface Processes and Landforms, 35*(9), 1014-1028.

Thompson, S. M. (1985). Transport of gravel by flows up to 500 m3/s, Ohau River, Otago, New Zealand. *Journal of Hydraulic Research, 23*(3), 285-303.

Tippett, J. M., & Kamp, P. J. J. (1993). Fission track analysis of the late Cenozoic vertical kinematics of continental Pacific crust, South Island, New Zealand. *J. Geophys. Res., 98*(B9), 16119-16148.

Tomer, A., Muto, T., & Kim, W. (2011). Autogenic hiatus in fluviodeltaic successions: geometrical modeling and physical experiments. *Journal of Sedimentary Research, 81*(3), 207-217.

Toniolo, H., & Schultz, J. (2005). Experiments on sediment trap efficiency in reservoirs. *Lakes & Reservoirs: Research & Management, 10*(1), 13-24.

Turnbull, I. M., & Forsyth, P. J. (1988). *Queenstown - a geological guide*: Geological Society of New Zealand, c/o PO Box 30-368, Lower Hutt.

URS. (2007). *Glenorchy area geomorphology and geo-hazard assessment*: Prepared for Otago Regional Council, Dunedin, NZ.

van Dijk, M., Kleinhans, M. G., Postma, G., & Kraal, E. (2012). Contrasting morphodynamics in alluvial fans and fan deltas: effect of the downstream boundary. *Sedimentology, 59*(7), 2125-2145.

van Dijk, M., Postma, G., & Kleinhans, M. G. (2009). Autocyclic behaviour of fan deltas: an analogue experimental study. *Sedimentology, 56*(5), 1569-1589.

van Maren, D. S. (2004). *Morphodynamics of a cyclic prograding delta: The Red River, Vietnam.* Unpublished PhD thesis, Utrecht University, Utrecht, Netherlands.

Voller, V. R. (2010). A model of sedimentary delta growth: a novel application of numerical heat transfer methods. *International Journal of Numerical Methods for Heat & Fluid Flow, 20*(5), 570-586.

Voller, V. R., Swenson, J. B., & Paola, C. (2004). An analytical solution for a Stefan problem with variable latent heat. *International Journal of Heat and Mass Transfer, 47*(24), 5387-5390.

Warburton, J. (1994). Channel change in relation to meltwater flooding, Bas Glacier d'Arolla, Switzerland. *Geomorphology, 11*(2), 141-149.

Warburton, J. (1996). A brief review of hydraulic modelling of braided gravel-bed rivers in New Zealand. *Journal of Hydrology (NZ), 35*(2), 157-173.

Warburton, J., & Davies, T. (1994). Variability of bedload transport and channel morphology in a braided river hydraulic model. *Earth Surface Processes and Landforms, 19*(5), 403-421.

Warburton, J., Davies, T. R., Griffiths, G. A., Hoey, T. B., & Young, W. J. (1996). Future prospects for the use of hydraulic models in the management of New Zealand braided gravel-bed rivers. *Journal of Hydrology (NZ), 35*(2), 287-302.

Waugh, J. R., Harding, S. J., & Freestone, H. J. (2000). *Flood history in the Clutha catchment*: Report for Contact Energy Ltd., Opus International Consultants, Wellington.

Webby, M. G., Apirumanekul, C., Labaznova, G., & Belleville, R. (2009). *Lake Dunstan sedimentation and backwater analysis for July 2007 bed*. Wellington: Opus International Consultants.

Webby, M. G., & Waugh, J. R. (2006). Hydraulic behaviour of the outlet of Lake Wakatipu, Central Otago, New Zealand. *Journal of Hydrology (NZ), 45*(1), 29-40.

Westaway, R. M., Lane, S. N., & Hicks, D. M. (2003). Remote survey of large-scale braided, gravel-bed rivers using digital photogrammetry and image analysis. *International Journal of Remote Sensing, 24*(4), 795-815.

Whipple, Kelin X., Parker, G., Paola, C., & Mohrig, D. (1998). Channel dynamics, sediment transport, and the slope of alluvial fans: Experimental study. *The Journal of Geology, 106*(6), 677-694.

Wilcock, P. R. (2001). The flow, the bed, and the transport: Interaction in flume and field. In M. P. Mosley (Ed.), *Gravel-bed rivers V* (pp. 183-219). Wellington: New Zealand Hydrological Society.

Wild, M., Cochrane, T., Davies, T. R., Hicks, D. M., Painter, D., & Palmer, G. (2008). Recent sedimentation rates for the Rees-Dart braided river delta. In J. Schmidt, T. Cochrane, C. Phillips, S. Elliot, T. R. Davies & L. Basher (Eds.), *Sediment Dynamics in Changing Environments* (IAHS Red Books Publ. 325 ed., pp. 312-315): Wallingford : IAHS Press, c2008.

Williams, R., Brasington, J., Vericat, D., Hicks, M., Labrosse, F., & Neal, M. (2011). Chapter twenty - Monitoring braided river change using terrestrial laser scanning and optical bathymetric mapping *Developments in Earth Surface Processes* (Vol. 15, pp. 507-532): Elsevier.

Wolfram, S. (1984). Cellular automata as models of complexity. *Nature, 311*, 419-424.

Wolfram, S. (2002). A new kind of science, http://www.wolframscience.com/nksonline/section-11.2, p 638-642.

Wright, L. D. (1977). Sediment transport and deposition at river mouths: A synthesis. *Geological Society of America Bulletin, 88*(6), 857-868.

Yalin, M. S. (1971). *Theory of hydraulic models*. London: MacMillan.

Young, W. J., & Davies, T. R. H. (1990). Prediction of bedload transport rates in braided rivers: a hydraulic model study. *Journal of Hydrology (NZ), 29*(2), 75-92.

Young, W. J., & Warburton, J. (1996). Principles and practice of hydraulic modelling of braided gravel-bed rivers. *Journal of Hydrology (NZ), 35*(2), 175-198.

Zarn, B., & Davies, T. R. H. (1994). The significance of processes on alluvial fans to hazard assessment. *Zeitschrift für Geomorphologie, 38*(4), 487-500.

APPENDIX A: HYDROMETRIC DATA

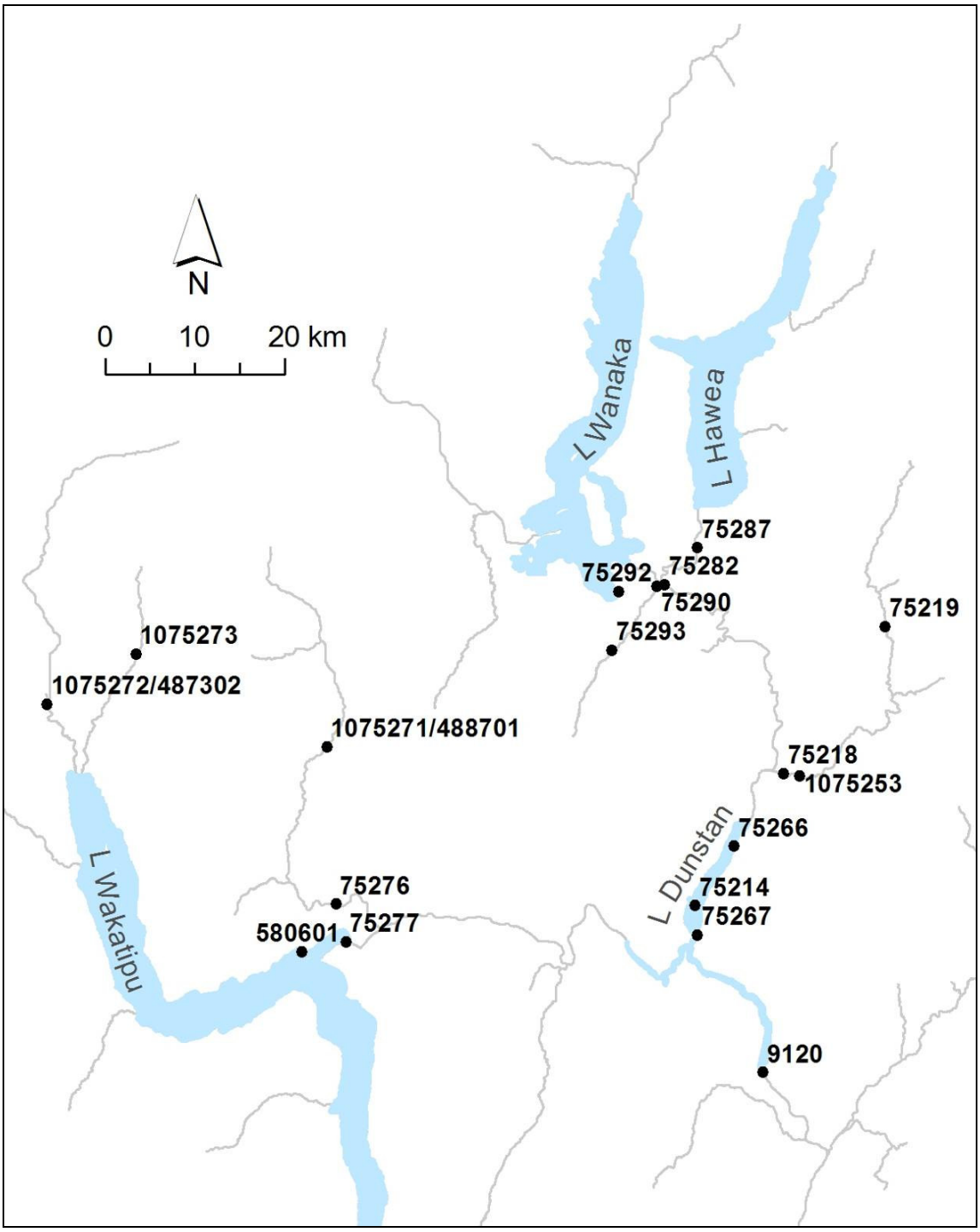

Figure A1: Hydrometric recorder location map (see Tables A1 and A2 for details)

Note: There are other hydrometric sites within this region but they have been omitted for clarity

Table A1: Flow recorder site information

Site name	Site No.	Start of record	End of record	Source
Clutha at Clyde PS Inflows	9120	22 Apr 1992	-	Contact
Clutha at Lowburn	75214	15 Nov 1965	16 Jan 1992	NIWA
Lindis at Crossing Br	75218	14 Nov 1972	25 May 1977	NIWA
Lindis at Lindis Peak	75219	24 Sep 1976	-	ORC, Contact
L Dunstan (Clutha Arm) at Crippletown	75266	30 Aug 1993	-	Contact
L Dunstan at Cromwell	75267	29 Aug 1993	-	Contact
Shotover at Bowens Peak	75276	1 May 2007	-	NIWA, Contact
L Wakatipu at Willow Place	75277	28 Nov 1962	-	Contact, NIWA, QLDC and M-co.
Clutha at Cardrona Confluence	75282	10 Apr 1992	-	Contact
Hawea at Camphill Br	75287	6 Mar 1968	-	NIWA, Contact
Cardrona at Albert-town	75290	28 Sep 1978	9 Jan 2002	NIWA
L Wanaka at Roys Bay	75292	1 Feb 1933	-	Contact, NIWA, QLDC and M-co.
Cardrona at Mt Barker	75293	23 Feb 2001	-	NIWA, ORC
Lindis at Ardgour Rd	1075253	9 Nov 2005	-	ORC
Shotover at Peats Hut	1075271	12 Dec 1996	-	ORC
Dart at The Hillocks	1075272	12 Jun 1996	-	ORC
Rees at Invincible	1075273	18 Sep 2009	25 Mar 2011	ReesScan Project

Table A2: Rainfall recorder site information

Site name	Site No.	Start of record	End of record	Source
Dart Rainfall at The Hillocks	487302	21 Aug 1997	-	ORC
Shotover Rainfall at Peats Hut	488701	19 Dec 1996	-	ORC
Queenstown rainfall	580601	3 Jan 1890	-	Met Service/NIWA

APPENDIX B: CLUTHA RIVER CROSS SECTION DATA

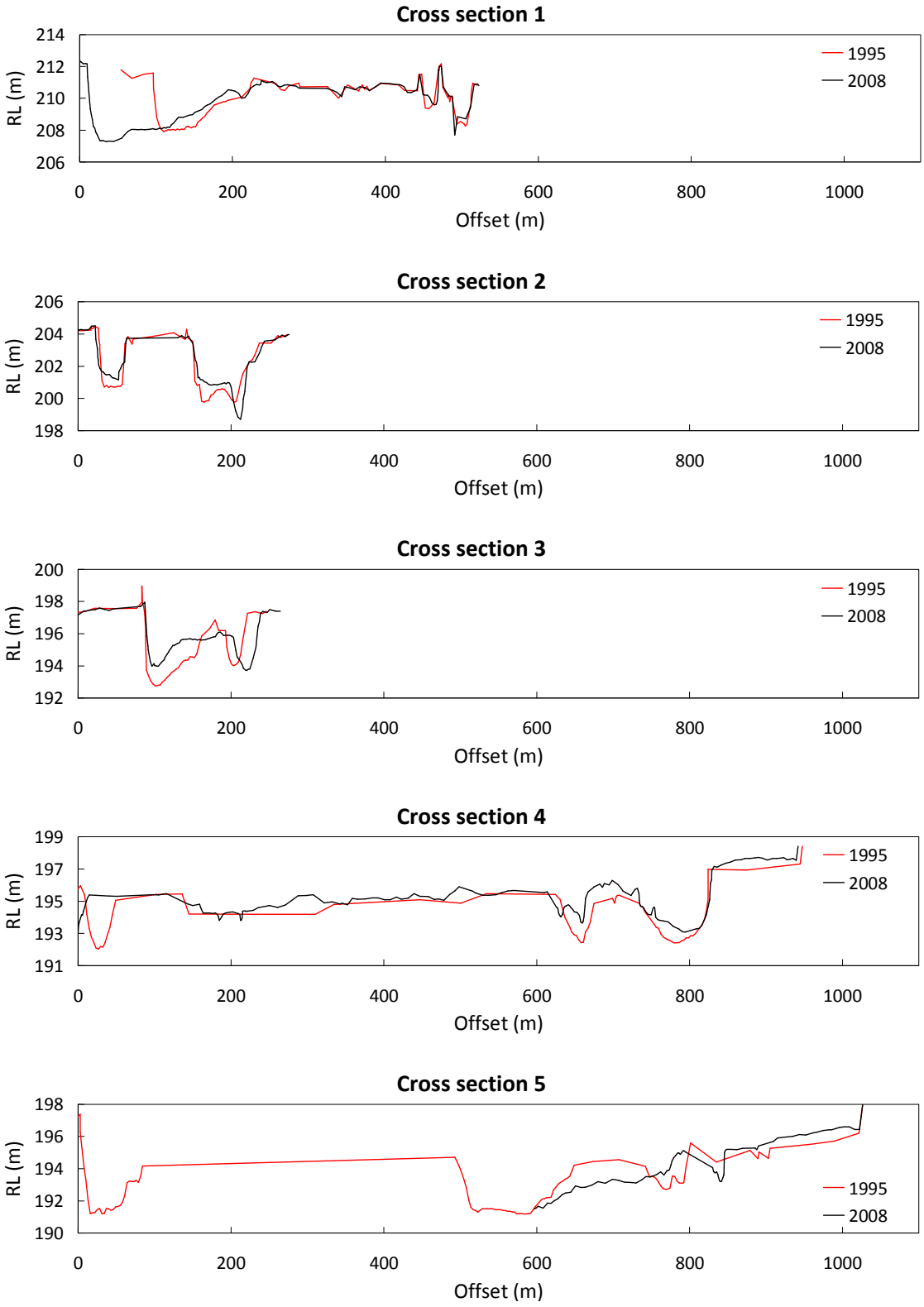

Figure B1: Clutha River/Mata-Au cross sections in 1995 and 2008 (looking downstream)

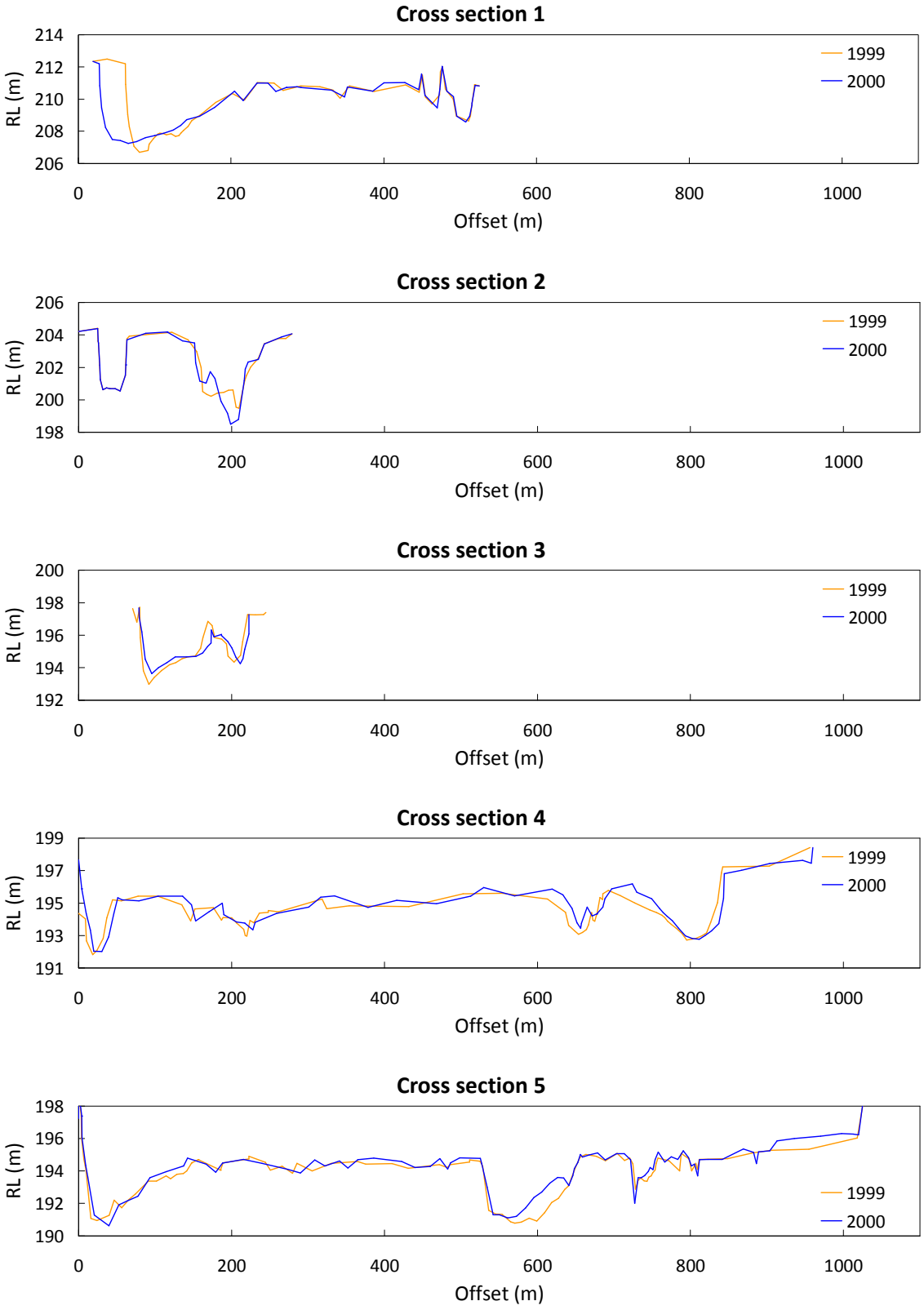

Figure B2: **Clutha River/Mata-Au cross sections in 1999 and 2000, capturing November 1999 flood (looking downstream)**

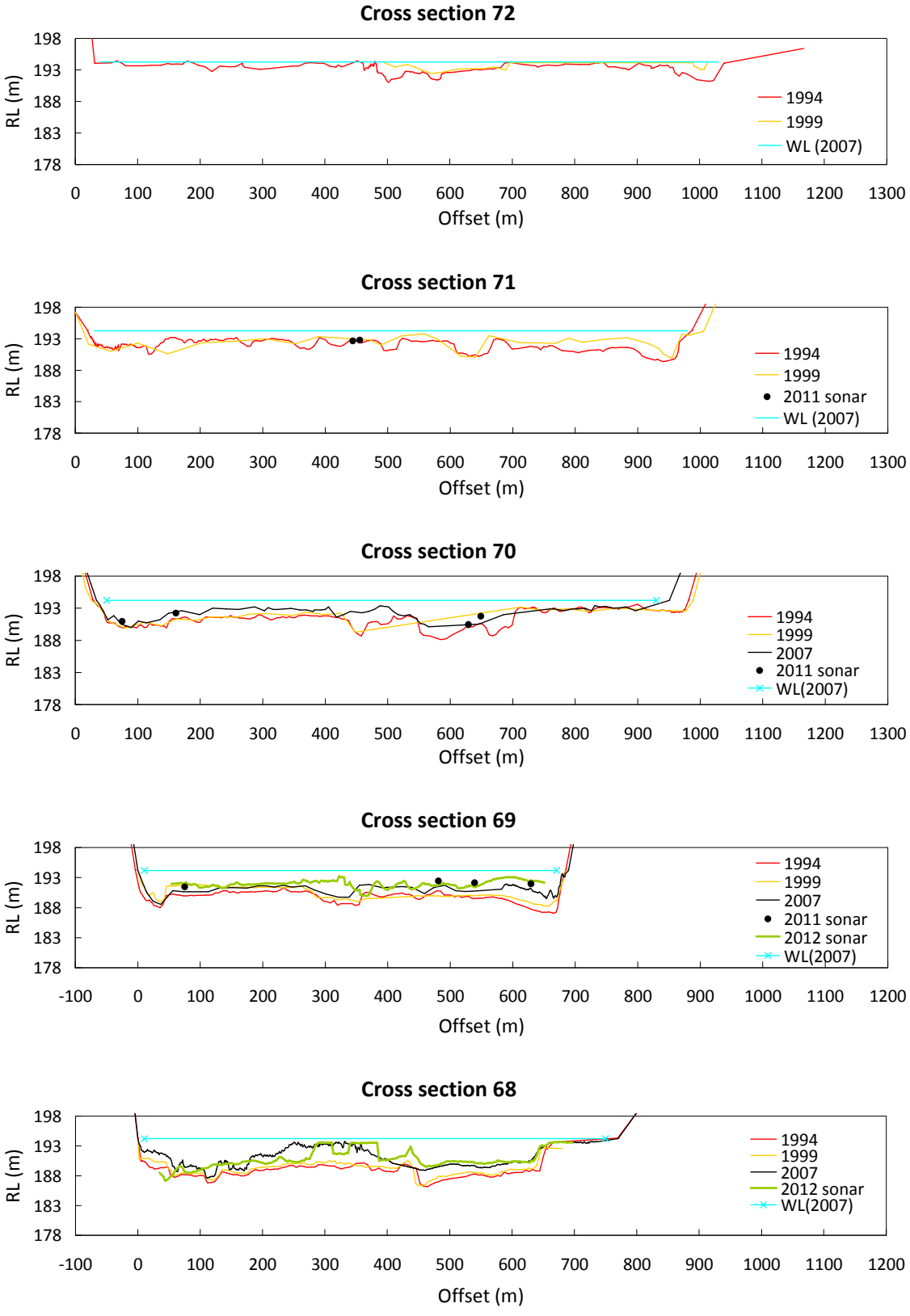

Figure B3: Lake Dunstan cross sections 72 to 68 in April 1994, September 1999, July 2007 and September 2012 (looking down lake)

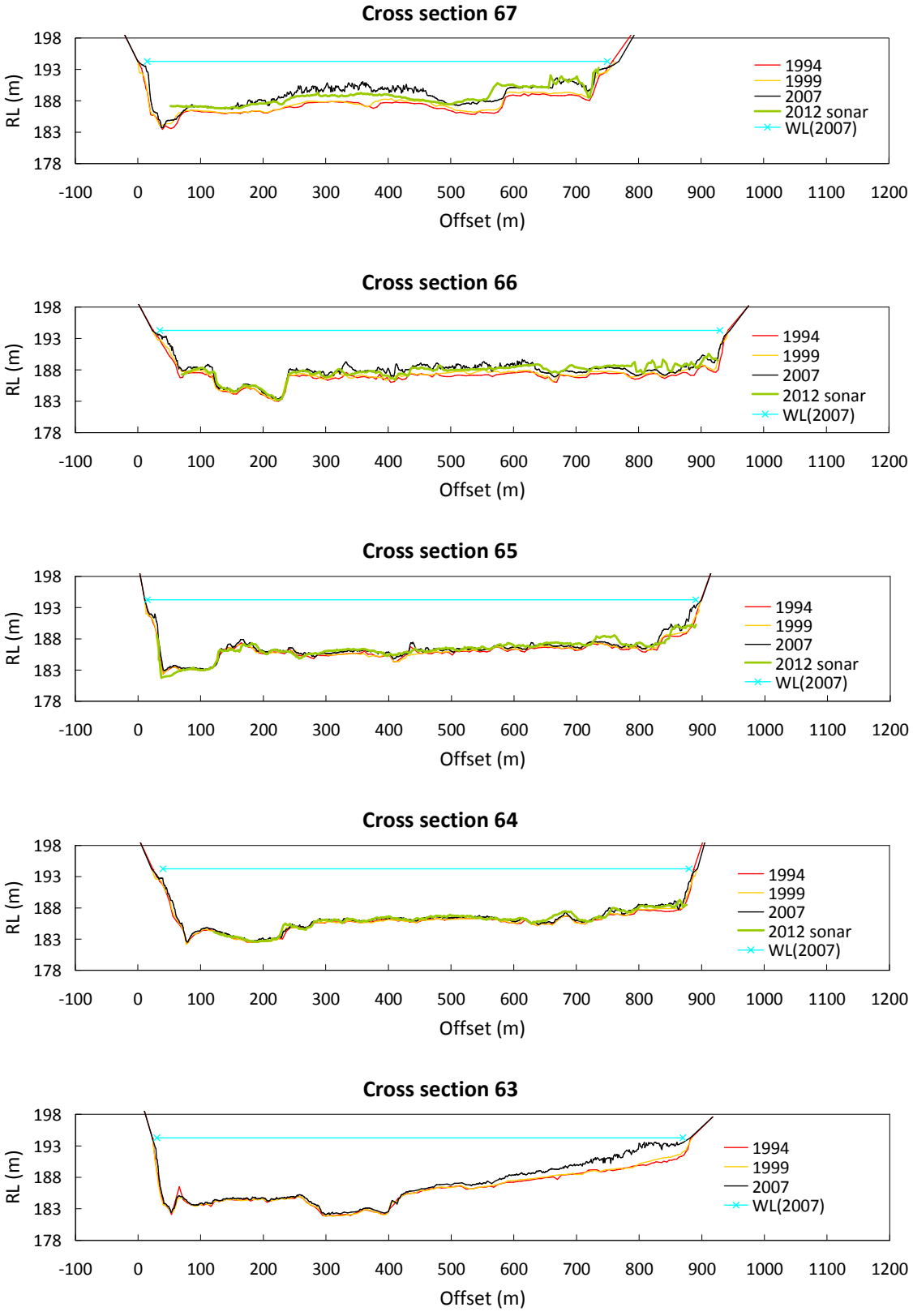

Figure B4: Lake Dunstan cross sections 67 to 63 in April 1994, September 1999, July 2007 and September 2012 (looking down lake)

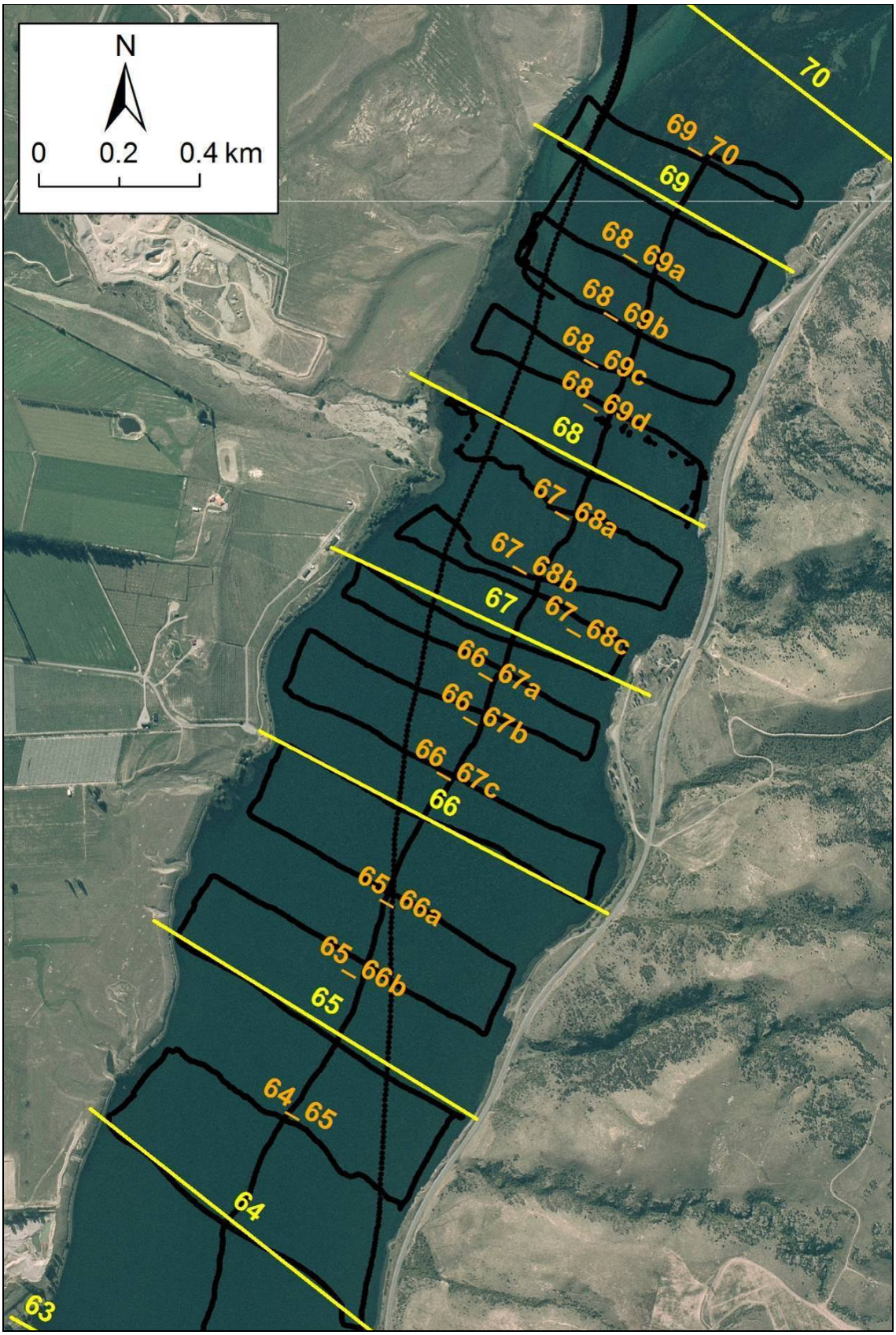

Figure B5: Lake Dunstan September 2012 sonar data cross section locations

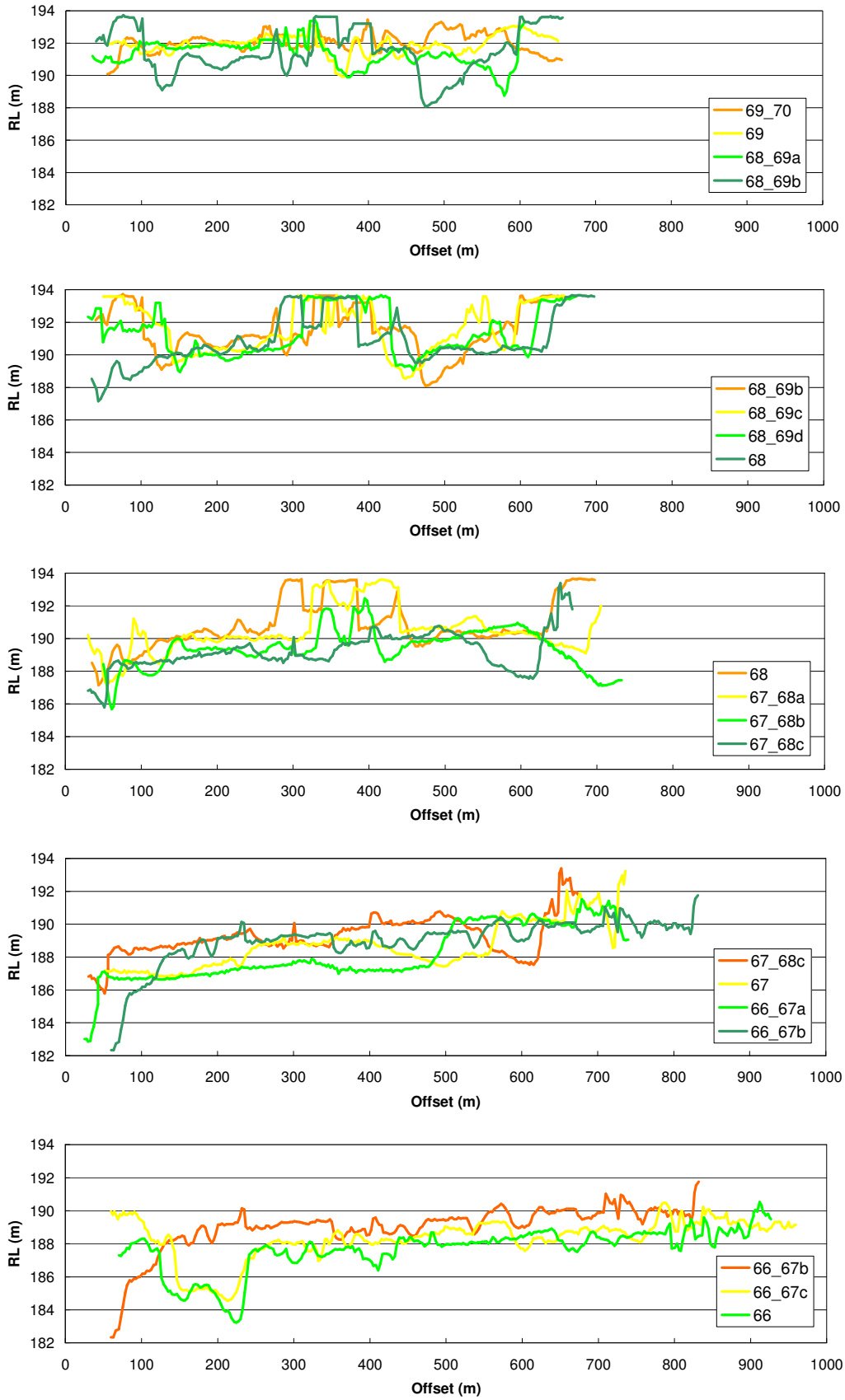

Figure B6: **Lake Dunstan cross sections derived from September 2012 sonar data, looking downlake (see Figure B5 for locations)**

Table B1: Summary of 1995 to 2008 cross section 1 (BXS1) to 5 (BXS5) data

Cross section	Distance from Clyde dam (km)	Cross section (m)			Average bed level (m asl)					Average change in bed level (m)		Average change in cross section area (m^2/yr)	
		Start	End	Width	1995	1997	1999	2000	2008	1995 to 2008	1999 to 2008	1995 to 2008	1999 to 2000
1-BXS1	43.6	21	521	500	210.34	210.05	210.06	209.79	209.78	-0.56	-0.27	-21.61	-133.46
2-BXS2	40.2	23	274	251	202.43	202.28	202.47	202.40	202.48	0.05	-0.07	0.98	-17.54
3-BXS3	36.5	71	244	173	195.30	195.25	195.28	195.35	195.52	0.22	0.08	2.97	13.17
4-BXS4	35.6	114	849	735	194.63	194.65	194.72	194.87	195.01	0.38	0.15	21.39	110.45
5-BXS5	35.1	8	881	873	193.78	193.91	193.81	193.98	-	-	0.18	-	153.44

Table B2: Summary of 1995 to 2008 cross section 1 (BXS1) to 5 (BXS5) thalweg levels

Cross section	Distance from Clyde dam (km)	Thalweg level (m asl)				
		1995	1997	1999	2000	2008
1-BXS1	43.6	207.92	207.58	206.69	207.25	207.28
2-BXS2	40.2	199.77	199.32	199.49	198.51	198.70
3-BXS3	36.5	192.75	192.92	192.97	193.64	193.72
4-BXS4	35.6	192.42	192.63	192.73	192.78	193.08
5-BXS5	35.1	191.18	190.77	190.79	191.11	191.50

Table B3: Summary of 1994 to 2007 cross section 72 (XS72) to 60 (XS60) data

Cross section	Dist from Clyde dam (km)	Cross section			Average bed level (m asl)				Average change in bed level (m)				Total change in cross section area (m^2)				Volume of sediment ($x10^3$ m^3)	
		Start (m)	End (m)	Width (m)	1994	1999	2007	Mod 2007	1994 to 1999	1999 to 2007	1994 to 2007	Mod 1994 to 2007	1994 to 1999	1999 to 2007	1994 to 2007	Mod 1994 to 2007	1994 to 2007	Mod 1994 to 2007
XS72	34.8	30	1030	1000	193.3		194.3 [a]	194.3 [a]			0.92	0.92			919	919	893	590
XS71	34.2	15	980	965	191.9	192.3	193.8 [a]	192.8 [a]	0.45	1.40	1.85	0.90	435	1352	1787	870	672	436
XS70	33.6	30	940	910	191.3	191.7	192.2	192.2	0.42	0.48	0.90	0.90	381	438	819	819	366	366
XS69	33.2	0	680	680	189.7	190.3	191.0	191.0	0.59	0.66	1.25	1.25	402	448	850	850	764	550
XS68	32.5	0	660	660	188.7	189.2	190.9	189.9	0.44	1.66	2.11	1.16	293	1098	1391	762	599	334
XS67	32.1	12	760	748	187.3	187.6	188.9	188.3	0.28	1.34	1.62	0.92	211	1003	1214	692	546	335
XS66	31.5	50	920	870	186.8	187.0	187.8	187.5	0.26	0.74	1.00	0.68	227	646	872	588	367	286
XS65	31.0	30	890	860	185.9	186.0	186.4	186.4	0.09	0.38	0.47	0.47	76	328	405	405	200	200
XS64	30.4	50	880	830	185.6	185.6	186.0	186.0	0.00	0.39	0.39	0.39	2	325	327	327	249	140
XS63	29.9	30	880	850	186.1	186.0	186.9	186.4	-0.04	0.87	0.83	0.30	-33	736	703	252	237	119
XS62	29.4	50	760	710	184.3	184.3	184.6	184.6	0.00	0.28	0.28	0.28	2	198	200	200	83	83
XS61	28.8	50	700	650	182.6	182.6	182.8	182.8	0.00	0.15	0.14	0.14	-3	97	94	94	36	36
XS60	28.3	50	750	700	181.6	181.5	181.7	181.7	-0.12	0.16	0.04	0.04	-83	112	29	29		
Total volume of sediment ($x10^3$ m^3) =																	5013	3475

[a] assumed level from Webby et al. (2009)

APPENDIX C: REES-DART MICROSCALE MODEL PHOTOS

Figure C1: Rees-Dart microscale model – Experiment A at t~0.8 hours

Figure C2: Rees-Dart microscale model – Experiment A at t~5.5 hours

Figure C3: Rees-Dart microscale model – Experiment A at t~6.8hours

Figure C4: Rees-Dart microscale model – Experiment A at t~8.1 hours

Figure C5: Rees-Dart microscale model – Experiment A at t~9.2 hours

Figure C6: Rees-Dart microscale model – Experiment A at t~14.4 hours

Figure C7: Rees-Dart microscale model – Experiment C at t~14.9 hours (View 1)

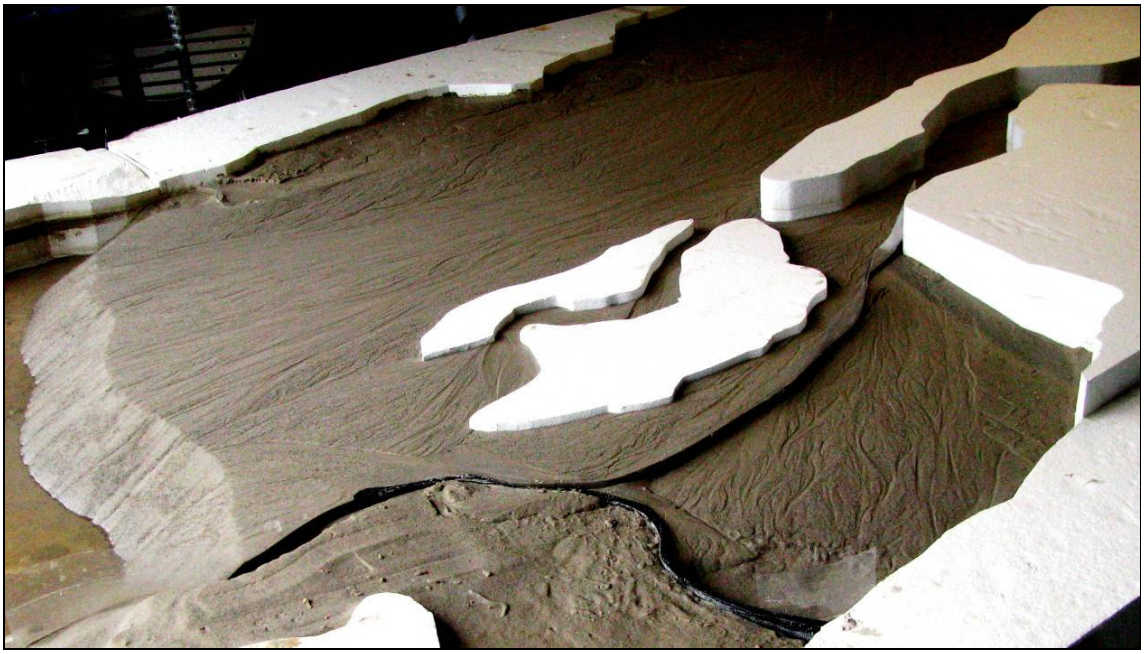

Figure C8: Rees-Dart microscale model – Experiment C at t~14.9 hours (View 2)

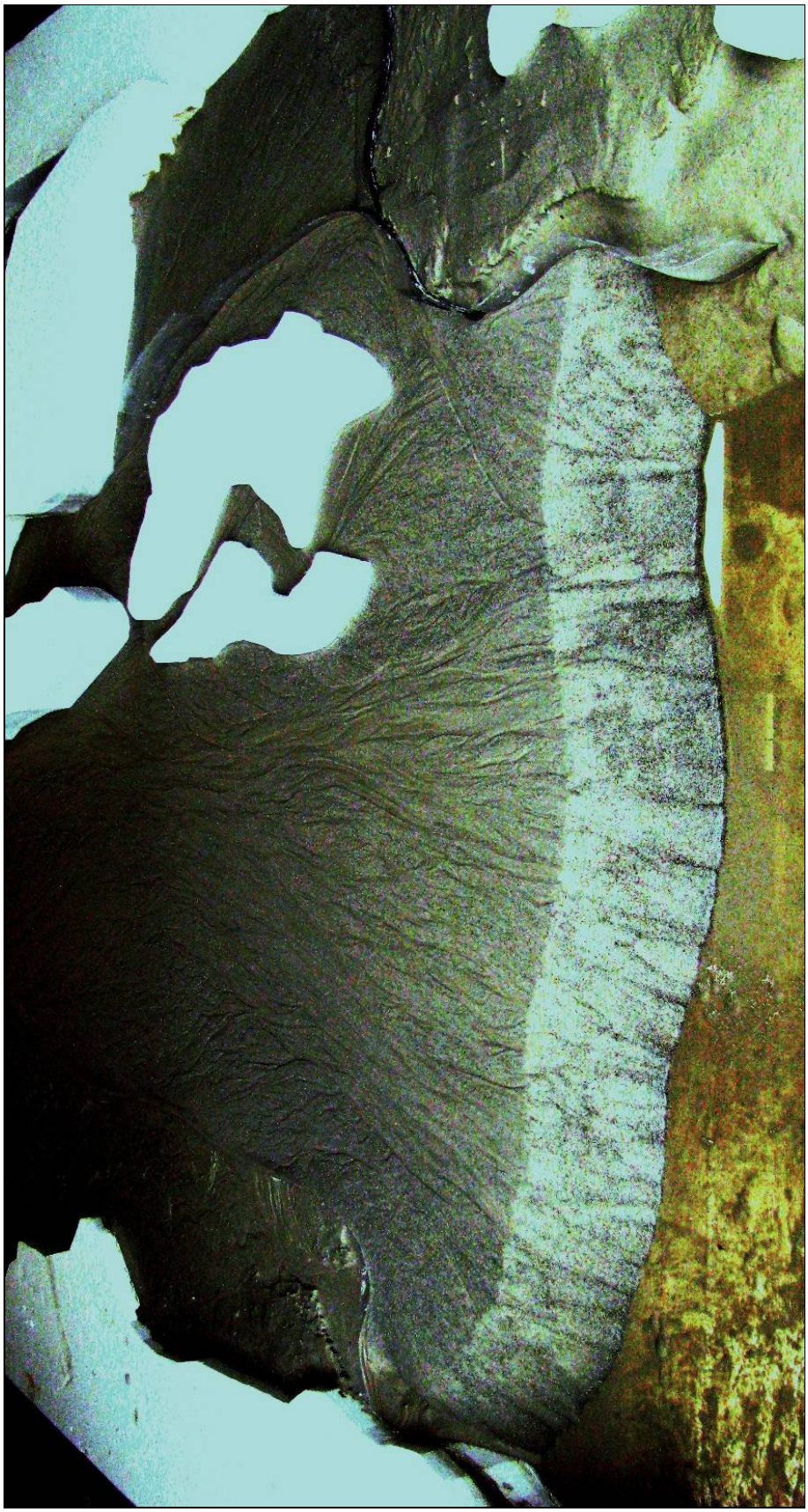

Figure C9: Rees-Dart microscale model – Experiment C at t~14.9 hours (View 3)

APPENDIX D: DELGROW CODE

Code for one sediment input location (Delgrow_simple.f90)

```
! ----------------------------------------------------------------------
      PROGRAM Delgrow
!     This program simulates delta progradation for a braided gravel-bed
!     river delta
! ----------------------------------------------------------------------
!
      IMPLICIT NONE
!
      INTEGER :: i, j, t
      INTEGER :: numrows, numcols   ! number of rows and columns of grid
      REAL :: cellx, celly          ! size of grid cells (m)
      REAL :: Axy                   ! area of cell (m2)
!
      REAL :: del_t           ! time step (weeks, days, months)
      INTEGER :: tmax         ! total number of time steps
      INTEGER :: t_write      ! number of time steps between writing output
      INTEGER :: count        ! counts # time steps between writing output
!
      INTEGER :: jmin, jmax   ! cell range for inputting sediment to row 1
      INTEGER :: j_start      ! start cell (in row 1 between jmin & jmax)
      INTEGER :: i_max, j_max ! next cell (i_max, j_max) along steepest
                              ! path to lake bed
      REAL :: d_coeff         ! '1'=adjacent cell, 'sqrt(2)'=diagonal cell
!
      REAL :: S_1, S_2, S_3, S_4, S_5, S_max    ! slope from current cell
                                                ! to adjacent cells (m/m)
!
      REAL :: Vsed_in               ! volume of sediment input (m3)
      REAL :: S_tset, delS_tset     ! topset slope and max slope increase
      REAL :: S_fset                ! foreset slope (m/m)
      REAL :: S_tset_max            ! threshold topset slope (m/m)
      INTEGER :: Tset_tot, Fset_tot ! number of topset and foreset cells
                                    ! along steepest path to lake
      REAL :: del_x                 ! 'shoreline' advance for time step (m)
      REAL :: del_zt                ! delta topset cell height increase (m)
      REAL :: del_zf                ! delta foreset height increase (m)
      REAL :: delz_f_to_lk          ! Diff between foreset cell & adjacent
                                    ! lakebed cell (m)
!
      REAL :: RL_top_fore     ! transition from topset to foreset (m asl)
      REAL :: delz_max        ! maximum elevation difference before lakebed
                              ! is included in foreset (m)
!
      REAL, DIMENSION(:,:), ALLOCATABLE :: gTOPO
      INTEGER, DIMENSION(:,:), ALLOCATABLE :: gPATH
      INTEGER, DIMENSION(:,:), ALLOCATABLE :: gPATH_T
      INTEGER, DIMENSION(:,:), ALLOCATABLE :: gDEL
!     INTEGER, DIMENSION (:), ALLOCATABLE :: gQSED
!
! gTOPO = grid of RL for each cell
! gPATH = grid of steepest path (9=cells along path,0=cells not along path)
! gPATH_T = sum of times sediment passes through cells of steepest path
! gDEL = grid identifying parts of delta (1=topset, 2=foreset, 3=lake bed)
! gQSED = time series of monthly Qsed (m3/month)
!
! Formatting variables
      CHARACTER(LEN=30) :: rowfmt1,rowfmt2,rowfmt3, rowfmt4
```

```
      CHARACTER(LEN=30) :: fname1,fname2,fname3, fname4
!
! ---------------------------------------------------------------------
!     Values to be specified
! ---------------------------------------------------------------------
!
      numrows = 92            ! number of grid rows
      numcols = 81            ! number of grid columns
      tmax = 13000            ! number of time steps
      t_write = 520           ! # time steps between writing output files
      del_t = 1               ! time step
      cellx = 50              ! cell width in x-dir (m)
      jmin = 21               ! minimum cell # in first row for sed input
      jmax = 37               ! maximum cell # in first row for sed input
      S_tset = 0.0028         ! topset average slope (m/m)
      delS_tset = 0.0002      ! S_tset + delS_tset = max slope of topset in
                              ! upper input cells
      S_fset = 0.24           ! foreset average slope (m/m)
      RL_top_fore = 309.5     ! Transition from topset to foreset (m asl)
!
! ---------------------------------------------------------------------
!     Calculate parameters
! ---------------------------------------------------------------------
!
      celly = cellx                ! cell width in y-dir - square grid(m)
      Axy = cellx * celly          ! cell area (m2)
      delz_max = S_fset*celly      ! Max diff before lakebed=foreset (m)
      S_tset_max = S_tset + delS_tset     ! max topset slope (m/m)
!
! ---------------------------------------------------------------------
!     Initialise variables
! ---------------------------------------------------------------------
!
      count = 0         ! increases by 1 each time step until count=t_write
      del_x = 0         ! 'shoreline' advance for time step (m)
      del_zt = 0        ! delta topset cell increase (m)
      del_zf = 0        ! delta foreset cell increase (m)
      d_coeff=1         ! '1'=adjacent cell, 'sqrt(2)'=diagonal cell
!
! ---------------------------------------------------------------------
! ---------------------------------------------------------------------
!     Define, allocate & open grid files
! ---------------------------------------------------------------------
! ---------------------------------------------------------------------

      OPEN (UNIT=4,FILE="Modgrid.txt")          ! Input initial gTOPO
      OPEN (UNIT=5,FILE="Delcomp.txt")          ! Input initial gDEL
!
!     OPEN (UNIT=3,FILE="Qsed.txt")
!     (Input sediment time series if using time series rather than
!     constant value gQSED)
!
      ALLOCATE(gTOPO(numrows,numcols))
      ALLOCATE(gPATH(numrows,numcols))
      ALLOCATE(gPATH_T(numrows,numcols))
      ALLOCATE(gDEL(numrows,numcols))
!     ALLOCATE(gQSED(tmax))
!
! ---------------------------------------------------------------------
!     Read in initial topographic grid (gTOPO) with average RLs for each
!     cell
! ---------------------------------------------------------------------
```

```
!
      DO i=1,numrows
          READ (4,*) (gTOPO(i,j),j=1,numcols)
      END DO
      CLOSE(4)
! ---------------------------------------------------------------------
!     Read in initial delta composition grid (gDEL) where 1=topset,
!     2=foreset, 3=lake bed
! ---------------------------------------------------------------------
!
      DO i=1,numrows
          READ (5,*) (gDEL(i,j),j=1,numcols)
      END DO
      CLOSE(5)
!
! ---------------------------------------------------------------------
!     Read in Qsed time series (if using a varying sediment input)
! ---------------------------------------------------------------------
!
!      DO t=1,tmax
!          READ (3,*) gQSED(t)
!      END DO
!     CLOSE(3)
!
! ---------------------------------------------------------------------
!     Generate grid (gPATH_T) set initially to zeros for each cell
! ---------------------------------------------------------------------
!
      DO i=1,numrows
            DO j=1,numcols
                  gPATH_T(i,j) = 0
            END DO
      END DO
!
! ---------------------------------------------------------------------
! ---------------------------------------------------------------------
! ---------------------------------------------------------------------
!     Start model at t=1 and run until final time step (tmax)
! ---------------------------------------------------------------------
! ---------------------------------------------------------------------
! ---------------------------------------------------------------------
!
      start_t: DO t=1,tmax
            Print *, "t=", t
!
! ---------------------------------------------------------------------
! ---------------------------------------------------------------------
!     SEDIMENT INPUT
! ---------------------------------------------------------------------
! ---------------------------------------------------------------------
!
!           ** if using a time series of sediment input **
!           Vsed_in = gQSED(t) * del_t
!
            Vsed_in = 3.25/7.5 * 5192 * del_t   ! m3/week
!
! ---------------------------------------------------------------------
!     Generate path grid (gPATH) set initially to zeros for each cell
! ---------------------------------------------------------------------
!
      DO i=1,numrows
            DO j=1,numcols
```

```
                  gPATH(i,j) = 0
            END DO
      END DO
!
!
! ------------------------------------------------------------------------
!     Find lowest RL in gTOPO at upstream limit = start point
! ------------------------------------------------------------------------
!
      j_start=jmin
!
      DO j=jmin,jmax
            IF (gTOPO(1,j) .LE. gTOPO(1,j_start)) THEN
                  j_start = j
                  print *, j_start
            ENDIF
      END DO
!
! ------------------------------------------------------------------------
!     Follow lowest RL to lake bed
! ------------------------------------------------------------------------
!
      j=j_start
      print *, j
!
      gPATH(1,j) = 9
      S_max = 0
!
      main_1: DO i=1,numrows-1
!
      print *, "i=" ,i
!
!     Determine which adjacent cell (on same row or next row d/s) has
!     steepest slope
!
10    CONTINUE
!
!     Cell 1 (i,j-1)
      S_1 = (gTOPO(i,j)-gTOPO(i,j-1))/cellx
!     Cell 2 (i+1,j-1)
      S_2 = (gTOPO(i,j)-gTOPO(i+1,j-1))/(SQRT((cellx**2)+(celly**2)))
!     Cell 3 (i+1,j)
      S_3 = (gTOPO(i,j)-gTOPO(i+1,j))/celly
!     Cell 4 (i+1,j+1)
      S_4 = (gTOPO(i,j)-gTOPO(i+1,j+1))/(SQRT((cellx**2)+(celly**2)))
!     Cell 5 (i,j+1)
      S_5 = (gTOPO(i,j)-gTOPO(i,j+1))/cellx
!
!     Check adjacent cells on same row first then replace slope with any
!     steeper options from next row (i.e. if same slope then pref given
!     to next row)
!
      IF (S_1 .GE. S_5) THEN
            S_max = S_1
            i_max = i
            j_max = j-1
            d_coeff=1
      ELSE
            S_max = S_5
            i_max = i
            j_max = j+1
            d_coeff=1
```

```
      END IF
!
      IF (S_2 .GE. S_max) THEN
            S_max = S_2
            i_max = i+1
            j_max = j-1
            d_coeff=SQRT((1.0**2)+(1.0**2))
      END IF
!
      IF (S_4 .GE. S_max) THEN
            S_max = S_4
            i_max = i+1
            j_max = j+1
            d_coeff=SQRT((1.0**2)+(1.0**2))
      END IF
!
      IF (S_3 .GE. S_max) THEN
            S_max = S_3
            i_max = i+1
            j_max = j
            d_coeff=1
      END IF
!
! ---------------------------------------------------------------------
!     If both origin and receiving cells are on topset, & slope is
!     greater than max specified slope, then path grid = 7
!     (i.e. will not add sediment to this cell)
! ---------------------------------------------------------------------
!
      IF(i .LE. 50) THEN
            IF (gDEL(i,j) .EQ. 1) THEN
                  IF (gDEL(i_max,j_max) .EQ. 1) THEN
                        IF (S_max .GT. S_tset_max) THEN
                              gPATH(i,j)=7
                        END IF
                  END IF
            END IF
      END IF
!
! ---------------------------------------------------------------------
!     Terminate program if all d/s cells have a higher elevation than
!     origin cell and add sediment to u/s cells just as if it had
!     reached the lake bed
! ---------------------------------------------------------------------
!
      IF (S_max .LE. 0.0) THEN
            gPATH(i_max,j_max)=8
            GOTO 20
      END IF
!
! ---------------------------------------------------------------------
!     If path reaches lake bed then set end cell = 8 and exit loop
!     FIRST - check that lake bed cell is not now part of foreset (which
!     occurs when the lowest foreset cell has aggraded to 'delz_max'.
!     Then, the gDEL cell changes from '3' to '2' and additional loop is
!     done to reach next lake bed cell
! ---------------------------------------------------------------------
!
      IF (gDEL(i_max,j_max) .EQ. 3) THEN
            delz_f_to_lk = gTOPO(i,j) - gTOPO(i_max,j_max)
            delz_max=S_fset*celly*d_coeff
            IF(delz_f_to_lk .GE. delz_max) THEN
```

```
                  gDEL(i_max,j_max)=2
            ELSE
                  gPATH(i_max,j_max)=8
            END IF
      END IF
!
20    IF (gPATH(i_max,j_max) .EQ. 8) GOTO 30
!
! ---------------------------------------------------------------------
!     Label the destination cell with steepest slope with a '9' in gPATH
!     array
! ---------------------------------------------------------------------
!
      gPATH(i_max,j_max) = 9
      j=j_max
!
      IF(i_max .EQ. i) GOTO 10
!
END DO main_1
!
! ---------------------------------------------------------------------
!     Sum number of topset and foreset cells along path
! ---------------------------------------------------------------------
!
30    Tset_tot = 0
      Fset_tot = 0

      DO i=1,numrows
            DO j=1,numcols
                  IF (gPATH(i,j) .EQ. 9) THEN
                        IF (gDEL(i,j) .EQ. 1) THEN
                              Tset_tot = Tset_tot + 1
                        ELSE IF (gDEL(i,j) .EQ. 2) THEN
                              Fset_tot = Fset_tot + 1
                        END IF
                  END IF
            END DO
      END DO
!
! ---------------------------------------------------------------------
!     Determine delz to be added to topset and foreset
! ---------------------------------------------------------------------
!
      del_x = Vsed_in /((S_tset*Axy*Tset_tot)+(S_fset*Axy*Fset_tot))
      del_zt = S_tset*del_x
      del_zf = S_fset*del_x
!
! ---------------------------------------------------------------------
!     Add delz to topset and foreset
! ---------------------------------------------------------------------
!
      DO i=1,numrows
            DO j=1,numcols
              IF (gPATH(i,j) .EQ. 9 .AND. gDEL(i,j) .EQ. 1) THEN
                gTOPO(i,j)= gTOPO(i,j) + del_zt
              ELSE IF (gPATH(i,j) .EQ. 9 .AND. gDEL(i,j) .EQ. 2) THEN
                gTOPO(i,j)= gTOPO(i,j) + del_zf
              END IF
            END DO
      END DO
!
! ---------------------------------------------------------------------
```

```
!     If new foreset level is greater than water level (i.e. RL_top_fore)
!     then set: gDEL(i,j) = 1 and gTOPO(i,j)=RL_top_fore
! ---------------------------------------------------------------------
!
      DO i=1,numrows
        DO j=1,numcols
          IF(gDEL(i,j) .EQ. 2) THEN
            IF(gTOPO(i,j) .GE. RL_top_fore) THEN
                  gDEL(i,j)=1
                  gTOPO(i,j)=RL_top_fore
            END IF
          END IF
        END DO
      END DO
!
! ---------------------------------------------------------------------
!     Accumulate gPATH cells so know where river has been ....
! ---------------------------------------------------------------------
!
      DO i=1,numrows
            DO j=1,numcols
                  IF(gPATH(i,j) .GT. 0) THEN
                        gPATH_T(i,j) = gPATH_T(i,j)+1
                  END IF
            END DO
      END DO
!
      count = count + 1
      IF (count .NE. t_write) GOTO 500
!
! ---------------------------------------------------------------------
!     Write to output file modified topographic grid (gTOPO)
! ---------------------------------------------------------------------
!
      WRITE(rowfmt1,'(A,I5,A)') '(',numcols,'(1X,F8.2))'
      WRITE(fname1,'(a,I5.5,a)') 'Topo',t,'.txt'
      OPEN (UNIT=6,FILE=fname1)
!
!     To add header (so data can be imported to ArcGIS)
      WRITE(6,*) "ncols         ", numcols
      WRITE(6,*) "nrows         ", numrows
      WRITE(6,*) "xllcorner     1232140"        ! to be determined
      WRITE(6,*) "yllcorner     5021780"        ! to be determined
      WRITE(6,*) "cellsize      ", cellx
      WRITE(6,*) "NODATA_value  -9999"
!
      DO i=1,numrows
          WRITE(UNIT=6,FMT=rowfmt1) (gTOPO(i,j), j=1,numcols)
      END DO
      CLOSE(6)
!
! ---------------------------------------------------------------------
!     Write to output file modified path grid (gPATH)
! ---------------------------------------------------------------------
!
      WRITE(rowfmt2,'(A,I5,A)') '(',numcols,'(1X,I2))'
      WRITE(fname2,'(a,I5.5,a)') 'Path',t,'.txt'
      OPEN (UNIT=7,FILE=fname2)
      DO i=1,numrows
          WRITE(7,FMT=rowfmt2) (gPATH(i,j), j=1,numcols)
      END DO
      CLOSE(7)
```

```
!
! ---------------------------------------------------------------------
!     Write to output file total cell count for path grid (gPATH_T)
! ---------------------------------------------------------------------
!
      WRITE(rowfmt4,'(A,I5,A)') '(',numcols,'(1X,I4))'
      WRITE(fname4,'(a,I5.5,a)') 'Pathtot',t,'.txt'
      OPEN (UNIT=9,FILE=fname4)
!
      WRITE(9,*) "ncols         ", numcols
      WRITE(9,*) "nrows         ", numrows
      WRITE(9,*) "xllcorner     1232140"        ! to be determined
      WRITE(9,*) "yllcorner     5021780"        ! to be determined
      WRITE(9,*) "cellsize      ", cellx
      WRITE(9,*) "NODATA_value  -9999"
!
      DO i=1,numrows
          WRITE(9,FMT=rowfmt4) (gPATH_T(i,j), j=1,numcols)
      END DO
      CLOSE(9)
!
! ---------------------------------------------------------------------
!     Write to output file modified delta composition (gDEL)
! ---------------------------------------------------------------------
!
      WRITE(rowfmt3,'(A,I5,A)') '(',numcols,'(1X,I1))'
      WRITE(fname3,'(a,I5.5,a)') 'Del',t,'.txt'
      OPEN (UNIT=8,FILE=fname3)
      DO i=1,numrows
          WRITE(8,FMT=rowfmt3) (gDEL(i,j), j=1,numcols)
      END DO
      CLOSE(8)
!
      count = 0
!
500   END DO start_t
! ---------------------------------------------------------------------
!     End
! ---------------------------------------------------------------------
!
      END Delgrow
```